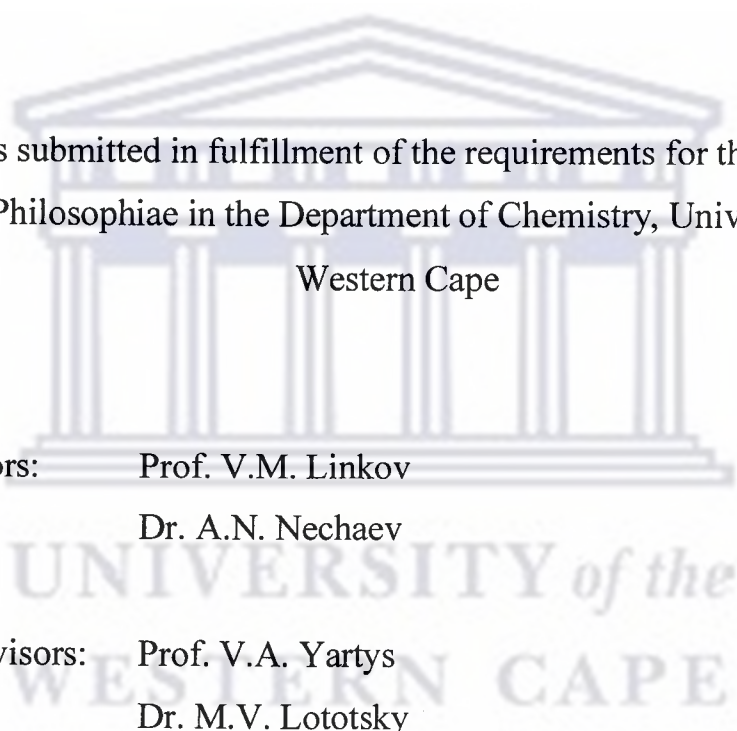


**PALLADIUM SURFACE-MODIFIED RARE EARTH
METAL-BASED AB₅-TYPE HYDRIDE-FORMING MATERIALS**

MARIO WILLIAMS



A thesis submitted in fulfillment of the requirements for the degree of
Doctor Philosophiae in the Department of Chemistry, University of the
Western Cape

Supervisors: Prof. V.M. Linkov

Dr. A.N. Nechaev

Co-supervisors: Prof. V.A. Yartys

Dr. M.V. Lototsky

November 2008

Student Number: 2438658

DECLARATION

I declare that "*Palladium Surface-Modified Rare Earth Metal-Based AB₅-Type Hydride-Forming Materials*" is my own work, that it has not been submitted before for any degree or examination in any other university, and that all the sources I have used or quoted have been indicated and acknowledged as complete references.

Mario Williams

November 2008

Signed.....



UNIVERSITY *of the*
WESTERN CAPE

SYNOPSIS

**PALLADIUM SURFACE-MODIFIED RARE EARTH METAL-BASED
AB₅-TYPE HYDRIDE-FORMING MATERIALS**

Mario Williams, November 2008

PhD Thesis, Department of Chemistry, University of the Western Cape.

Composite hydrogen sorption materials exhibiting rapid hydrogenation kinetics at ambient temperature, easy activation after handling in non-inert environments, sorption stability after long-term air exposure, and exceptional surface catalytic activity towards hydrogen dissociation were sought as key elements in separation / purification / storage of high-purity hydrogen. Technologically-flexible AB₅-type alloys were identified as substrate materials in the preparation of composite hydrogen sorption materials, using palladium as a unique catalytic mantle. The research undertaken dealt with development of new surface engineering solutions, based on electroless plating, in the surface modification of AB₅-type alloys using Pd-based catalytic layers.

Pd electroless plating resulted in removal of the mixed RE₂NiO₄ phase detected on the parent alloy surface and in the formation of discontinuous Pd layers. Morphology and kinetics of hydrogenation (k) of the surface-modified materials were found to depend strongly on the type of reducing agent, sodium hypophosphite (NaH₂PO₂) or hydrazine (N₂H₄), used in preparation of the Pd coating (high-load; $k_{\text{NaH}_2\text{PO}_2} = 0.19 \text{ h}^{-1}$; $k_{\text{N}_2\text{H}_4} = 5.9 \times 10^{-2} \text{ h}^{-1}$). Improvements were credited to promotion of the hydrogen spillover phenomenon. An interrelation between morphological features and hydrogenation properties of surface-modified materials was detailed.

Inadequacies in Pd-P electroless plating on AB₅-type alloys (i.e. discontinuous layers; inhomogeneity; poor adhesion) were circumvented by employment of a novel pre-treatment method, in which γ -aminopropyltriethoxysilane (γ -APTES) was used to increase the affinity of (hydr)oxidized alloy surfaces towards immobilization of Pd nuclei in electroless plating. Subsequent Pd-P plating resulted in deposition of continuous Pd-P layers and significant improvements in Pd surface density; hydrogen sorption stability; Pd²⁺/Pd⁰ conversion; and kinetics of hydrogenation of the non-activated material under mild conditions ($k = 1.3 \text{ h}^{-1}$) compared to that prepared without the pre-treatment step ($k = 1.9 \times 10^{-1} \text{ h}^{-1}$). The attractiveness of the γ -APTES pre-treatment in facilitating a change in the Pd-P layer morphology from discontinuous to continuous and subsequent improvement of hydrogen sorption properties of hydride-forming alloys was demonstrated.

An attempt was made to pre-oxidize the alloy surface in H₂O₂ solution prior to functionalization to promote maximum coverage by γ -APTES molecules, and in that way promote deposition of continuous Pd-P layers. The pre-oxidation step in the functionalization process facilitated deposition of high-density Pd-P continuous layers (Pd total loading = 1.35 wt. %), resulting in improved kinetics of hydrogenation ($k = 2.0 \text{ h}^{-1}$) compared to that prepared without the pre-oxidation step ($k = 1.3 \text{ h}^{-1}$).

Pre-complexation of Pd cations using aqueous solutions of γ -APTES, prior to electroless plating on AB₅-type alloys, yielded dense coatings resulting in improved kinetics of hydrogenation ($k = 1.1 \text{ h}^{-1}$), compared to that prepared using the standard sensitization / activation technique ($k = 0.19 \text{ h}^{-1}$).

An approach was adopted in which γ -APTES layers were used to immobilize Pd²⁺ and Pt⁴⁺ precursor ions on the alloy surface from dilute salt solutions. Increases in rate constants were observed with increases in PdCl₂ and PtCl₄ concentration.

An approach was used in which Pd mixed-metal coatings (e.g. Pd-Ni-P, Pd-Cu-P, Pd-Ag, Pd-Pt) were deposited on AB₅-type alloys in both sequential and co-deposition modes of electroless plating. AB₅-type alloys surface-modified with co-deposited Pd-Ni-P ($k = 6.6 \times 10^{-2} \text{ h}^{-1}$) and sequentially-deposited Pt-Pd coatings ($k = 1.9 \times 10^{-1} \text{ h}^{-1}$) were characterised by significantly improved kinetics of hydrogenation under standard experimental conditions, compared to alloys surface-modified using pure Pd-P coatings ($k = 3.7 \times 10^{-2} \text{ h}^{-1}$) and pure Pd coatings ($k = 3.7 \times 10^{-3} \text{ h}^{-1}$). A synergistic effect between the Pd-Ni-P coating and the AB₅-type alloy, and enhanced catalysis of hydrogen transport by Pt layers at the interface were credited for the improvements.

It was observed that the introduction of a Pt interfacial layer between the AB₅-type alloy surface and Pd-P layer enhanced the hydrogenation rate compared to that prepared without the introduction of the Pt interfacial layer.

A novel approach was taken to enhance the kinetics of hydrogenation by depositing Pd-P layers onto AB₅-type alloys after fluorination treatment and generation of a high-surface area LaF₃ shell. Pd-P particles were observed to plug micro-cavities of the LaF₃ layer after γ -APTES functionalization of the fluorinated alloy. In the process, continuous Pd-P surface layers were prepared on the AB₅-type alloy surface, manifesting in superior kinetics of hydrogenation ($k = 3.6 \text{ h}^{-1}$). The fluorinated AB₅-type alloy plugged with Pd-P layers, after γ -APTES functionalization, exhibit the best Pd-P surface density and the kinetics of hydrogenation in the study. The significant enhancements were a direct result of the promotion of the hydrogen spillover phenomenon.

Knowledge gained from the project is expected to allow the directed design of new classes of high-efficiency; robust; recyclable hybrid hydrogen sorption materials based on hydride-forming alloys and Pd surface catalysts, as key elements of envisaged hydrogen separation / purification / storage systems.

**PALLADIUM SURFACE-MODIFIED RARE EARTH
METAL-BASED AB₅ HYDRIDE-FORMING MATERIALS**

MARIO WILLIAMS

KEYWORDS

Hydrogen Separation / Purification / Storage

Electroless Plating

Palladium

Encapsulation

Functionalization

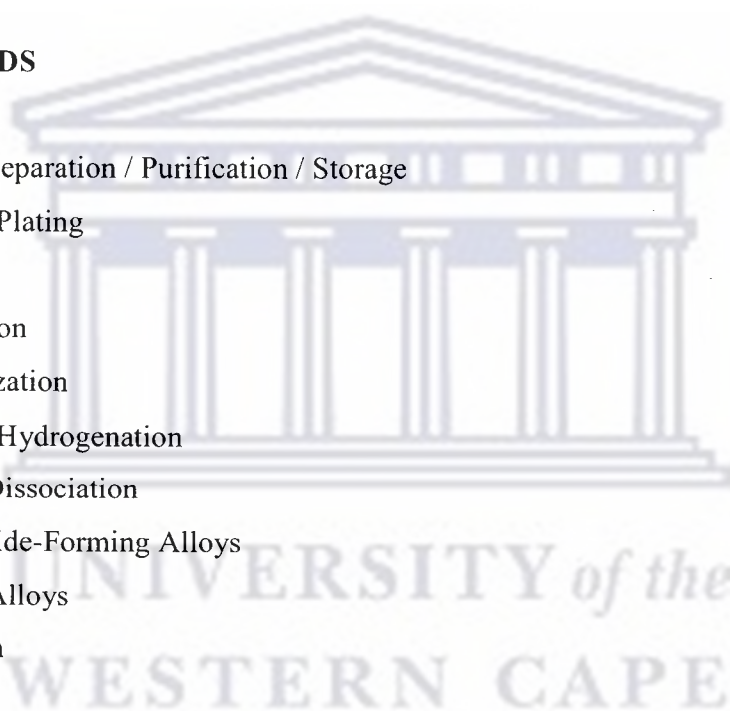
Kinetics of Hydrogenation

Hydrogen Dissociation

Metal Hydride-Forming Alloys

AB₅-Type Alloys

Fluorination



ACKNOWLEDGEMENTS

Almighty God for the many opportunities he has provided me.

Greatest thanks and gratitude to my parents, Mr. I. Williams and Mrs. P. Williams, for always supporting me in achieving my goals. Thanks for always believing that I would “pick the fruit” someday.

Prof. V. Linkov (*South African Institute for Advanced Materials Chemistry*) for his support and allowing me to conduct the research.

Huge thanks and gratitude to Dr. A. Nechaev (*Shubnikov Institute of Crystallography, Russian Academy of Science, Moscow, Russia*), Dr. M. Lototsky (*South African Institute for Advanced Materials Chemistry*), and Prof. V. Yartys (*Institute for Energy Technology, Kjeller, Norway*) for their guidance and supervision.

Prof. J. Solberg (*Norwegian University of Science and Technology, Trondheim, Norway*) for allowing me to conduct the research.

Dr. B. Bladergroen (*South African Institute for Advanced Materials Chemistry*) for his contribution to the project.

Dr. R. Denys (*Physico-Mechanical Institute, National Academy of Sciences, Lviv, Ukraine*) and Dr. J. Mæhlen (*Institute for Energy Technology, Kjeller, Norway*) for their assistance with the crystallography.

Mr. A. Josephs (*University of the Western Cape*), Mr. T. Nilson and Dr. Y. Yu (*Norwegian University of Science and Technology, Trondheim, Norway*) for their assistance with the electron microscopy.

Acknowledgements

Dr. C. Pineda-Vargas (*Materials Research Group, iThemba Labs*) for assistance and guidance with the nuclear microprobe.

Ms. E. Khataibe (*Shubnikov Institute of Crystallography, Russian Academy of Science, Moscow, Russia*) for collaboration and contribution to our parallel studies.

Mrs. B. Rodgers, Mr. I. Sprinceana, Mr. L. Jansen van Vuuren, Ms. S. Adams, Ms. M. Orffer (*South African Institute for Advanced Materials Chemistry*), Mr. J. Baartnes, and Mr. P. Ulseth (*Norwegian University of Science and Technology, Trondheim, Norway*) for their administrative and technical assistance.

Ms. S. Mbana (*Cape Peninsula University of Technology*) and Mr. G. Maduna (*University of the Western Cape*) for their assistance.

Dr. Q. Li (*Guangzhou Research Institute of Non-Ferrous Metals, Guangzhou, China*) for the collaboration in the preparation of the AB₅-type alloys.

ASPECT[®] (*Moscow, Russia*) for generously supplying Trumem[®] membranes.

The financial assistance of the *National Research Foundation (NRF)* towards this research is hereby acknowledged. Opinions expressed and conclusions arrived at are those of the author and are not necessarily to be attributed to the *NRF*.

The financial assistance of the *Black Research Academic Development Program (BRAD)*, sponsored by the *Electricity Supply Commission (ESKOM)* and the *NRF*, towards this research is hereby acknowledged.

The work was supported by the South African – Norwegian Program of Research Co-operation (2007-2010), Project #180344.

TABLE OF CONTENTS

Declaration	i
Synopsis	ii
Keywords	iii
Acknowledgements	iv

CHAPTER 1. BACKGROUND AND RATIONALE OF THE STUDY

1.1. HYDROGEN PRODUCTION	1
1.2. PROBLEMS IN TECHNOLOGIES ASSOCIATED WITH HYDROGEN SEPARATION AND PURIFICATION	2
1.3. PROBLEMS IN TECHNOLOGIES ASSOCIATED WITH HYDROGEN STORAGE	4
1.4. NEW MATERIALS FOR HYDROGEN SEPARATION / PURIFICATION / STORAGE BASED ON METAL HYDRIDE-FORMING ALLOYS AND PALLADIUM	6
1.5. RATIONALE TO THE STUDY	7

CHAPTER 2. LITERATURE REVIEW

2.1. STATE-OF-ART IN HYDROGEN SORPTION MEDIA	10
2.2. METAL HYDRIDE-FORMING ALLOYS	16
2.3. MECHANISM OF HYDROGEN SORPTION IN AB ₅ -TYPE METAL ALLOYS	22

Table of Contents

2.4.	LIMITATIONS OF HYDROGEN SORPTION USING AB ₅ -TYPE ALLOYS	24
2.4.1.	<i>Surface poisoning and deactivation of AB₅-type alloys</i>	25
2.4.2.	<i>Decrepitation of the hydrogenation / dehydrogenation rate</i>	28
2.4.3.	<i>Activation and incubation periods</i>	29
2.5.	STATE-OF-ART IN METAL HYDRIDE-FORMING ALLOY SURFACE MODIFICATION	30
2.5.1.	<i>Fluorination treatment</i>	31
2.5.2.	<i>Encapsulation using metal layers</i>	31
2.5.3.	<i>Potassium borohydride treatment</i>	32
2.5.4.	<i>Alkaline solution treatment</i>	33
2.5.5.	<i>Hydrochloric acid treatment</i>	33
2.5.6.	<i>Yttrium oxide surface film deposition</i>	34
2.5.7.	<i>Ni-containing weak acid treatment</i>	34
2.5.8.	<i>Plasma immersion and ion implantation</i>	35
2.5.9.	<i>Conclusions from review of surface modification techniques</i>	35
2.6.	SCIENTIFIC REQUIREMENTS IN THE SEPARATION / PURIFICATION / STORAGE OF HYDROGEN USING PALLADIUM-BASED COMPOSITE MATERIALS	36
2.7.	INCREASE OF SURFACE POISONING RESISTANCE BY FLUORINATION	36
2.8.	METAL LAYER ENCAPSULATION IN THE PROMOTION OF HYDROGEN SORPTION	39

Table of Contents

2.9	PLATINUM GROUP METAL ENCAPSULATION IN THE PROMOTION OF HYDROGEN SORPTION	40
2.10.	PALLADIUM IN THE SORPTION OF HYDROGEN	42
2.11.	MECHANISM OF HYDROGEN SORPTION THROUGH PALLADIUM-BASED LAYERS	45
2.12.	APPLICATION OF PALLADIUM MIXED-METAL LAYERS IN HYDROGEN SORPTION TECHNOLOGY	47
	<i>2.11.1. Hydrogen sorption properties of palladium mixed-metal layers</i>	48
	<i>2.12.2. Conclusions from review of palladium mixed-metal layers in hydrogen sorption technology</i>	52
2.13.	ENHANCING HYDROGEN SORPTION KINETICS AND POISONING RESISTANCE BY SURFACE DEPOSITION OF PALLADIUM AND PALLADIUM-BASED MIXED METAL COATINGS	53
2.14.	METHODS OF METAL SURFACE LAYER DEPOSITION	54
	<i>2.14.1. Sputter deposition</i>	54
	<i>2.14.2. Mechanochemical deposition</i>	55
	<i>2.14.3. Chemical vapour deposition</i>	56
	<i>2.14.4. Electrolytic plating</i>	56
	<i>2.14.5. Electroless plating</i>	57
	<i>2.14.6. Conclusions of review of methods of surface layer deposition</i>	57
2.15.	MECHANISM OF ELECTROLESS PLATING	58
	<i>2.15.1. Surface sensitization and activation</i>	59
	<i>2.15.2. Film growth by decomposition of the reducing agent</i>	61

Table of Contents

2.16.	CONCLUSIONS OF THE LITERATURE REVIEW	63
2.17.	EXPERIMENTAL TASKS	65
2.18.	RESEARCH AREA AND HYPOTHESIS	68
2.19.	RESEARCH FRAMEWORK AND DESIGN	69
2.20.	DELIMITATIONS OF THE STUDY	70
 CHAPTER 3. METHODOLOGY		
3.1.	SELECTION OF THE AB ₅ -TYPE HYDRIDE-FORMING ALLOY PARENT MATERIAL	72
3.2.	ENCAPSULATION OF AB ₅ -TYPE HYDRIDE-FORMING ALLOYS USING ELECTROLESS PLATING	73
3.3.	SURFACE FLUORINATION OF AB ₅ -TYPE METAL HYDRIDE-FORMING ALLOYS	80
3.4.	MATERIALS CHARACTERIZATION	81
3.4.1.	<i>Elemental analysis of surface-modified AB₅-type alloys</i>	82
3.4.2.	<i>Evaluation of surface morphology and crystallinity</i>	86
3.4.3.	<i>Direct study of surface and structure morphology using electron microscopy</i>	89
3.4.4.	<i>Evaluation of surface elemental dispersion on surface-modified AB₅-type alloys</i>	92
3.4.5.	<i>Evaluation of surface chemical composition using x-ray studies</i>	94
3.4.6.	<i>Determination of specific surface area by nitrogen physisorption</i>	95

Table of Contents

3.4.7. <i>Construction of Pressure-Composition isotherms of the parent AB₅-type hydride-forming alloy</i>	97
3.4.8. <i>Evaluation of dynamics in hydrogen absorption using surface-modified AB₅-type hydride-forming alloys</i>	99
3.5. LIMITATIONS IN THE CHARACTERIZATION OF SURFACE-MODIFIED AB ₅ -TYPE HYDRIDE-FORMING ALLOYS	102
3.6. CONCLUSIONS OF THE METHODOLOGY	103
 CHAPTER 4. RESULTS AND DISCUSSION	
4.1. SELECTION OF THE PARENT AB ₅ -TYPE METAL HYDRIDE-FORMING ALLOY	104
4.1.1. <i>Morphology and crystallinity of the mischmetal AB₅-type alloys</i>	104
4.1.2. <i>Comparison of chemical composition of mischmetal AB₅ – type alloys</i>	107
4.1.3. <i>Thermodynamic evaluation of the AB₅-type hydride-forming alloys</i>	111
4.1.4. <i>Construction of pressure-composition isotherms for the parent AB₅-type alloy</i>	114
4.1.5. <i>Crystallinity of the AB₅-type alloy parent material</i>	119
4.1.6. <i>Summary</i>	122
4.2. AB ₅ -TYPE ALLOYS SURFACE-MODIFIED USING THE ELECTROLESS PLATING OF PALLADIUM: MORPHOLOGY AND HYDROGEN SORPTION STUDIES	122

Table of Contents

4.2.1	<i>Palladium surface-modified AB₅-type alloys: retrospectives in synthetic approaches</i>	123
4.2.2.	<i>Influence of the reducing agent on the morphology and kinetic properties of surface-modified AB₅-type alloys</i>	124
4.2.3.	<i>Influence of preparation variables of palladium electroless plating baths on elemental composition, surface morphology, and kinetic properties of surface-modified AB₅-type alloys</i>	139
4.2.4.	<i>Summary</i>	156
4.3.	SURFACE FUNCTIONALIZATION IN PALLADIUM ELECTROLESS PLATING ON AB₅-TYPE ALLOYS USING AMINOSILANES	158
4.3.1.	<i>Chemical conjunction between metal layers and substrate surfaces using aminosilanes</i>	158
4.3.2.	<i>Methodological approach in surface functionalization of AB₅-type hydride-forming alloys using γ-aminopropyltriethoxysilane</i>	162
4.3.3.	<i>Structural and kinetic characterization of surface-modified AB₅-type alloys functionalized using γ-aminopropyltriethoxysilane</i>	165
4.3.4.	<i>Morphology and kinetics of surface-modified AB₅-type alloys after pre-complexation of palladium nuclei with γ-aminopropyltriethoxysilane</i>	189
4.3.5.	<i>Immobilization of palladium(II) and platinum(IV) ions from dilute solution onto γ-aminopropyltriethoxysilane functionalized AB₅-type alloys</i>	196
4.3.6.	<i>Summary</i>	202

Table of Contents

4.4.	AB ₅ -TYPE ALLOYS SURFACE-MODIFIED USING THE ELECTROLESS PLATING OF PALLADIUM MIXED-METAL LAYERS	204
4.4.1.	<i>Characterization of morphological and kinetic properties of AB₅-type alloys surface-modified using palladium mixed-metal coatings</i>	205
4.4.2.	<i>Summary</i>	235
4.5.	INTRODUCTION OF A PLATINUM INTERFACIAL LAYER USING LIXIVIATION FOR ENHANCEMENT OF HYDROGEN TRANSPORT	237
4.5.1.	<i>Methodology in the introduction of a platinum interfacial layer</i>	238
4.5.2.	<i>Characterization of morphological and kinetic properties of AB₅-type alloys surface-modified using platinum interfacial layers</i>	239
4.5.3.	<i>Summary</i>	243
4.6.	PALLADIUM SURFACE MODIFICATION OF FLUORINATED AB ₅ -TYPE HYDRIDE-FORMING ALLOYS	243
4.6.1.	<i>Surface fluorination of AB₅-type alloys using wet treatment in fluoride-containing solutions</i>	245
4.6.2.	<i>Electroless plating of palladium on fluorinated AB₅-type alloys</i>	249
4.6.3.	<i>Electroless plating of palladium on fluorinated AB₅-type alloys after surface pre-treatment in γ-aminopropyltriethoxysilane</i>	253
4.6.4.	<i>Summary</i>	259

Table of Contents

CHAPTER 5. CONCLUSIONS AND RECOMMENDATIONS	261
---	-----

REFERENCES	276
-------------------	-----



UNIVERSITY *of the*
WESTERN CAPE

**PALLADIUM SURFACE-MODIFIED RARE EARTH
METAL-BASED AB₅-TYPE HYDRIDE-FORMING MATERIALS**

MARIO WILLIAMS

A thesis submitted in fulfillment of the requirements for the degree of
Doctor Philosophiae in the Department of Chemistry, University of the
Western Cape

Supervisors: Prof. V.M. Linkov

Dr. A.N. Nechaev

Co-supervisors: Prof. V.A. Yartys

Dr. M.V. Lototsky

November 2008

Student Number: 2438658

Examination Copy

LIST OF ABBREVIATIONS

PEMFC	Polymer Electrolyte Fuel Cell
PGM	Platinum Group Metal
PSA	Pressure-Swing Adsorption
PCT	Pressure-Composition-Temperature Isotherms
ΔH	Enthalpy
ΔS	Entropy
k	Rate constant
t_0	Characteristic time of hydrogenation
n	Morphological dimensionality of growth
CVD	Chemical Vapour Deposition
EDS	Energy-Dispersive X-ray Spectroscopy
AAS	Atomic Absorption Spectroscopy
XRD	X-ray Diffractometry
SR-XRD	Synchrotron Radiation X-ray Diffractometry
FESEM	Field Emission Scanning Electron Microscopy
PIXE	Particle-Induced X-ray Emission Spectroscopy
SXPS	Scanning X-ray Photoelectron Spectroscopy
γ -APTES	γ -aminopropyltriethoxysilane

CHAPTER 1**BACKGROUND AND RATIONALE OF THE STUDY****1.1. HYDROGEN PRODUCTION**

Driven by mounting standards of living and a growing population, South African energy consumption is expected to increase dramatically within the next decade. The increased demand for more energy will require enormous growth in the capacity for energy generation, more secure and diversified energy sources, and a successful strategy to reduce greenhouse gas emissions. The wellbeing of the South African economy depends on reliable and affordable supplies of energy; whilst environmental wellbeing, from improving urban air quality to abating the risk of global warming, requires energy resources that emit less greenhouse gases compared to petrochemicals. Amongst the various alternative energy strategies, building an energy infrastructure that utilises hydrogen as the primary energy carrier may enable a non-polluting energy security in the future, when it is produced using renewable energy sources (e.g. water electrolysis). Hydrogen has been acknowledged as a key element in the future generation of energy and will be essential in increasing and maintaining economic growth. The significance of hydrogen as a future energy source is due to its large abundance and an energy density that is three times greater than that of an average hydrocarbon fuel.

Roughly 80% of hydrogen is produced by natural gas reforming, partial oxidation of light alcohols, and autothermal reforming. In addition, a number of alternative technologies exist in which hydrogen can be generated from starting materials such as coal; biomass; and water, including electrolysis, fossil fuel processing, and coal gasification. However, most of these technologies produce a hydrogen product which is of poor purity. Purification is achievable considering equipment costs are extremely high and the process is therefore mostly economically unfeasible.

Introducing hydrogen as a universal environment-friendly energy carrier demands efficient technologies facilitating separation of high-purity hydrogen (i.e. 99.999% H₂) from industrial streams (e.g. products of coal gasification, process gases of refineries), purification, storage in a compact and safe way, and delivery of hydrogen to a consumer at high pressure. Availability of high-purity hydrogen is directly connected to the development of efficient methods for hydrogen separation, purification and storage. Separation and storage of high-purity hydrogen from gaseous mixtures plays a vital role in the realisation of the hydrogen economy. For this reason many research institutions pay particular interest in developing separation and storage of hydrogen for industrial and automotive applications. The high-purity hydrogen prepared may be used in energy-generating devices such as the polymer electrolyte fuel cell (PEMFC). Due to the presence of platinum group metals at the PEMFC electrodes, and the resultant ease at which these electrodes are poisoned by trace quantities of gaseous species such as carbon monoxide, it is imperative that the hydrogen fuel be of the highest purity. It is acknowledged that the energy-generating capacity of the PEMFC is significantly limited by the purity of the hydrogen fuel, and for this reason notable developments should be made into improving the separation media which produce high-purity hydrogen from impure feed streams.

1.2. PROBLEMS IN TECHNOLOGIES ASSOCIATED WITH HYDROGEN SEPARATION AND PURIFICATION

It is suitable for the hydrogen sorption system (i.e. separation, purification, storage, compression, delivery) to operate at low temperature (< 100 °C) with the sorption media exhibiting good mechanical strength. It is also desirable that the system should operate at moderate pressures, demonstrate low heat losses, and could be regenerated if charged with hydrogen contaminated with impurities such as oxygen, water vapour, sulphur, methane, carbon dioxide and carbon monoxide.

The separation of the gaseous products is the most costly step in chemical processes, where high temperature, high pressure and aggressive environments limit the use of

more conventional separation techniques. The four most widely-used hydrogen separation techniques include adsorption, membrane filtration, cryogenic distillation, and absorption. Generally, a technology known as pressure-swing adsorption (PSA) is used in the large-scale separation of hydrogen from product gas streams. PSA entails the separation of a gas species from a mixture under pressure according to the molecular characteristics of that species and its affinity for an adsorbent bed. Problems associated with the use of PSA to separate hydrogen from product mixtures derived from industrial processes such as coal gasification include: high cost of operation; low hydrogen specificity of adsorbent beds; low mechanical stability of adsorbent beds; large size of PSA reactors resulting in inadequate rapid gas transfer; high operational costs due to compression and cooling of gases.

Where high-purity hydrogen is required dense Pd membranes present a technology for separating the product from gaseous mixtures. Unfortunately, these membranes suffer from poor thermo-mechanical stabilities at high temperature, are costly, suffer from hydrogen embrittlement after repeated thermal cycling in hydrogen especially in “start-up-shutdown” processes, and are easily poisoned by aggressive surface adsorbates (e.g. H₂S, CO, CO₂, O₂, H₂O) over extended operation. Also, although regeneration of poisoned membranes is achievable, the high temperature and long heating periods necessary to achieve this make it an uneconomical and energy-demanding practice. As a consequence, Pd and Pd-alloy membranes may be ineffective in gas separation from product gas mixtures.

Cryogenic distillation has been widely used to separate hydrogen isotopes (i.e. protium, deuterium, and tritium) from hydrogenous feed streams. Unfortunately, cryogenic distillation processes are generally not applied for the separation of high-purity H₂ from reformer gases derived from industrial processes such as coal gasification and require huge energy inputs in their operation making the process economically unfeasible.

An attractive avenue in the separation of hydrogen from impure hydrogenous feed streams is absorption processes. Absorptive materials interact with hydrogen by physical-chemical processes, thereby providing an attractive method of separating / purifying hydrogen. Binary (e.g. Pd, Mg) and intermetallic (e.g. LaNi₅, FeTi) hydride-forming materials in particular are of significant interest. These materials are characterised by their interactions with atomic hydrogen; minimal energy expenditure; and simplicity in operation. For these reasons alternative separation / purification media, based on absorptive materials, are sought to effectively separate and purify hydrogen from hydrogenous product gas mixtures containing aggressive components.

1.3. PROBLEMS IN TECHNOLOGIES ASSOCIATED WITH HYDROGEN STORAGE

One of the largest stumbling blocks towards the widespread use of hydrogen as an energy carrier is the effective storage thereof. Subsequent to the separation and purification of hydrogen it is necessary to store the product in a manner which maintains its high-purity, allows for fast rates of storage and discharge, allows for efficient transport of hydrogen, and does not require large amounts of energy in its operation. For these reasons, effective storage and delivery of hydrogen are key elements within the hydrogen economy. In addition, hydrogen storage is a “critical path” technology that will facilitate the commercialization of the PEMFC.

Three technologies are currently available for the storage of hydrogen: compressed; liquefied; and solid-state hydrogen storage. Compressed hydrogen storage entails the compression and storage of hydrogen in high strength stainless steel cylinders. These high-pressure cylinders are usually filled to a maximum operating pressure of ~20 MPa, amounting to ~4.0 wt. % hydrogen, which is well below the 6.0 wt. % target generally accepted for vehicular applications. An increase of the storage capacity would require the production of significantly larger cylinders and an undesirable increase in the weight of the cylinder. Also, safety issues associated when using

compressed hydrogen cylinders for vehicular applications are still a primary concern and the energy essential to compress the hydrogen is economically unfeasible.

The storage of liquefied hydrogen requires high-efficiency cryogenic containers. As hydrogen has a critical temperature of $-241\text{ }^{\circ}\text{C}$, large amounts of energy ($\sim 15\text{ kWh/kg}$) are required to liquefy hydrogen and limit boil-off. The high cost of liquefying hydrogen, the safety issues involved in storing liquid hydrogen at cryogenic temperatures, and losses due to boil-off have limited the use of liquefied hydrogen.

Solid-state storage, in which the hydrogen is absorbed into a solid material, holds considerable promise for meeting the hydrogen economy targets, but no completely satisfactory material has yet been identified. Solid-state storage refers to the storage of hydrogen in metal hydride-forming materials, chemically binding materials, and high-surface area nanostructured materials. This method of hydrogen storage offers perhaps the best opportunities for meeting the requirements for onboard storage. An attractive feature of solid-state storage is that the absorption of hydrogen using many of these materials is reversible, thereby reducing operational costs.

The material requirements for effective solid-state hydrogen storage include the following: appropriate thermodynamics; fast kinetics (quick uptake and release); high storage capacity (specific capacity to be determined by usage); effective heat transfer; high gravimetric and volumetric densities (lightweight and space efficient); long cycle lifetime for hydrogen sorption; high mechanical strength and durability; safety under normal use and acceptable risk under abnormal conditions. Future focus will be on solid-state materials that enable the storage of hydrogen at low pressure. Hydrogen storage under these conditions may be achieved by adsorption on high-surface area materials like carbon nanotubes; absorption into metal hydride-forming materials such as magnesium or intermetallic alloys; and hydrogen binding in chemical compounds such as sodium borohydride. In particular, metal hydride-

forming materials have the potential for reversible on-board hydrogen storage and release at low temperatures and pressures.

1.4. NEW MATERIALS FOR HYDROGEN SEPARATION / PURIFICATION / STORAGE BASED ON METAL HYDRIDE-FORMING ALLOYS AND PALLADIUM

Combining intermetallic alloys with suitable catalytic “dopants” will potentially introduce enhanced kinetic and hydrogenation properties which address the abovementioned material issues, and thus new classes of composite hydrogen sorption materials can be developed for application in hydrogen separation, purification, and storage. For example, an intermetallic alloy substrate material could be selected because of its thermodynamic properties and the mantle could be chosen for its catalytic activity towards important surface processes involving hydrogen. The combination of these functional materials in a layered fashion could open up completely new routes for optimizing the overall performance of sorption materials.

Engineering solutions are required to promote improvements in current technologies to meet the hydrogen sorption requirements. These solutions require investments in fundamental research to develop and examine new materials and obtain an atomic-level understanding of the physical and chemical processes involved in hydrogen uptake and release. The knowledge gained from this research will allow the tailored design and synthesis of new materials that will meet the requirements for efficient hydrogen separation / purification / storage. These materials will potentially be based on platinum group metals (PGM's) and metal hydride-forming alloys due to the unique properties of PGM's in hydrogen separation and the reversible hydrogen sorption properties of metal hydride-forming alloys.

1.5. RATIONALE TO THE STUDY

Programs are currently in place to develop advanced technologies which will facilitate the transition to a local hydrogen economy and the use of the abundance of coal (the coal gasification product gas is processed by carbon sequestration and desulphurization units to remove pollutants) and PGM resources in South Africa to produce, store, deliver, and utilize affordable hydrogen in an environmentally compliant manner.

As was previously established, separation; purification; and storage of hydrogen play vital roles in the efficiency of hydrogen production technologies. There are a few mechanisms which can be used in the separation of hydrogen: adsorption, membrane filtration, cryogenic distillation, and absorption. Of the available mechanisms, absorption processes have the biggest potential for the separation / purification / storage of high-purity hydrogen from gaseous mixture derived from industrial processes such as the coal gasification. In addition, the preparation of high-purity hydrogen through absorption can be achieved through a large variety of available materials, including carbon-based nanomaterials; zeolites; metal organic frameworks; alanates; complex borohydrides; glass microspheres; metal hydride-forming intermetallic alloys; and many others. These materials and their advantages, disadvantages, potential usage, and suitability for the production of hydrogen of high-purity will be further reviewed in Chapter 2. As a result of the various disadvantages of these materials it became necessary to improve their absorption properties and make them suitable for long-term application in integrated hydrogen separation / purification / storage systems.

Based on technological requirements of long-term sorption stability; fast reaction rates; superior dynamics of activation, and improved kinetic properties in the absorption of hydrogen it became necessary to develop scientific approaches for the preparation of advanced composite materials, based on metal hydride-forming alloys, for the effective production of high-purity hydrogen from contaminated feeds. From a

materials science standpoint the fabrication of hydrogen sorbent composite materials; addition of deoxidisers; and surface modification are of greatest importance in terms of efficient hydrogen separation / purification / storage systems and delivery thereof. Of particular interest is the effect of PGM catalysts on the performance of hydrogen sorbent materials. These scientific approaches can result in breakthrough hydrogen technologies and can be implemented as key elements in the greater scheme of the envisaged hydrogen economy.

Sustainable economic and social development through the realization of advanced hydrogen production technologies using PGM's, especially Pd, as hydrogenation catalysts are key components of hydrogen separation / purification / storage systems. These technologies will facilitate the use and diversification of PGM resources in South Africa to produce affordable hydrogen in an environmentally compliant manner. Ideally, new innovative materials based on the unique properties of PGM's should be developed to increase the demand for these politically-sensitive metals in research and development.

The ultimate scientific goal of the project is to successfully develop methodological approaches for the preparation of surface-modified hydrogen sorption materials that meet hydrogenation/dehydrogenation targets considered to be requirements for practical commercial applications. These requirements include improved kinetics of hydrogenation; rapid hydrogen uptake and release rates, and stable operation under ambient conditions of temperature and pressure. These targets are achievable through surface-modification using nano-engineering. Nano-scale architectures will be incorporated onto these materials to increase specific surface area, surface catalysis, and sorption stability. Research on surface-modified materials may also provide insight into the mechanisms responsible for potential improvements in kinetics when catalysts are added to these materials. Similarly, improvements in the lifetimes of sorption materials may be possible upon examination of the mechanisms for associated degradation processes and sensitivity to impurities. This knowledge is

expected to allow the directed design of new, higher-efficiency, reusable hydrogen sorption materials.

The research undertaken in the development of advanced materials will also provide an understanding of the relationship between the morphological features of the PGM surface-modified hydrogen sorbents and the corresponding behaviour in hydrogenation / dehydrogenation.

To improve the chances for a wider application of metal-hydride forming alloys in the existing and future hydrogen industry, the following objectives, in order of priority, will need to be addressed: (a) improving resistance to surface deactivation by impurities; (b) improving the ease of alloy activation; (c) improving kinetics of hydrogen sorption.

The abovementioned objectives can be addressed by nano-engineering the desired moieties onto the surface of the chosen alloy, and through the development and manufacture of composite hydride-forming materials and subsequent study of their hydrogen sorption potential for numerous applications. The nano-engineering of these composite materials can be built upon a layer-by-layer approach.

The development of modified materials based on modern technological advancements in metal hydride chemistry holds great potential. Successful implementation of the developed technology will facilitate transfer to novel processes in hydrogen-generating technologies to yield high-purity hydrogen as a non-polluting energy carrier of the future.

CHAPTER 2

LITERATURE REVIEW

The literature review focuses on a discussion of hydrogen sorption materials, metal hydride-forming alloys and the hydrogenation properties thereof, the identification of limitations in their application, and the envisaged surface modifications of these materials for the purposes of enhanced hydrogen separation / purification / storage properties. The problem areas will be introduced, detailed experimental tasks for the study will be formulated and a hypothesis of the study postulated.

2.1. STATE-OF-ART IN HYDROGEN SORPTION MEDIA

It was previously discussed in Chapter 1 that a key objective in the progress towards utilization of hydrogen as a sustainable energy carrier of the future is the development of sorption media with attractive characteristics such as rapid hydrogen uptake and release kinetics, poisoning resistance, and cycle stability. Materials which interact with molecular or atomic hydrogen by physical-chemical processes were identified as attractive media for processing high-purity hydrogen. These materials include carbon nanomaterials, fullerenes, activated carbon, ammonia, methanol, spongy iron, alumino and silico-based alloys, liquid (organic) hydrides, zeolites, metal organic frameworks, alanates, complex borohydrides, aluminohydrides, ammonium salts, imidazolium ionic liquids, phosphonium borate, glass microspheres, and metal hydride-forming alloys [1].

Carbon nanomaterials include graphitic nanofibres, nanotubes, aerogels, carbon black, and carbon molecular sieves. These materials interact with hydrogen through physisorption and dissociative chemisorption of hydrogen molecules. Under ambient conditions ($T = 20\text{ }^{\circ}\text{C}$, $P_{\text{H}_2} = 1.0\text{ bar}$) these materials are known to exhibit insignificant hydrogen absorption rates and capacities ($\leq 1.0\text{ wt. \% H}_2$). Other disadvantages of carbon nanomaterials include ease of poisoning, the need for high

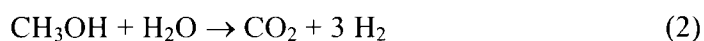
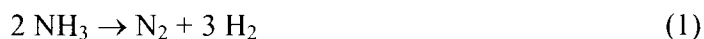
pressure hydrogen feeds, the requirement of exceptionally large surface areas, and fragility of the materials [1-5].

Reversible hydrogenation-dehydrogenation on fullerenes is attractive as a hydrogen sorption technology as a result of high levels of interaction with hydrogen ($C_{60} + 24H_2 \rightarrow C_{60}H_{48}$) and hydrogen weight capacities (6.3 wt. %). However, the high temperatures (400 - 450 °C) required to bring about dehydrogenation of these materials is unattractive for many applications where reduction of operational costs is of paramount importance [1,6]. Also, hydrogenation of fullerenes is only initiated at high hydrogen pressures ($P_{H_2} = 50 - 85$ MPa), although the use of intermetallic compounds as catalysts is known to reduce the required pressure ($P_{H_2} = 1.0 - 3.0$ MPa) [7]. Also, incremental increases in dehydrogenation temperature may result in formation of carbide species of the fullerenes. Importantly, the fraction of reversibly exchangeable hydrogen in these systems still remains below the quantity required for practical applications [6].

Low-density activated carbon is known to adsorb hydrogen at cryogenic temperature and moderate hydrogen pressure ($P_{H_2} \sim 40$ bars) by the condensation of hydrogen in micropores [8,9]. Dehydrogenation is associated with a decrease in the hydrogen pressure ($P_{H_2} \sim 2.0$ bars). Hydrogen sorption capacity of the activated carbon is about 2.0 - 3.3 wt. % at -196 °C. However, a large energy input is necessary to maintain the cryogenic state required for hydrogen absorption, and once achieved, it is necessary to maintain the material under cryogenic conditions [1].

Hydrogen storage and transportation using ammonia and methanol is attractive due to high hydrogen volume densities (109 g/L for liquefied ammonia at $T = 15$ °C; and 99 g/L for CH_3OH at $T = 20$ °C) [1]. The volume density of hydrogen in liquefied ammonia is more than 40% greater than in liquefied H_2 . Ammonia forms hydrogen bonds, unlike H_2 or CH_4 , which can be broken with the release of nitrogen and hydrogen [10]. The dissociation of ammonia is carried out at high temperature ($T = 800-900$ °C) using iron as a catalyst. The process of hydrogen generation from

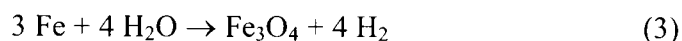
CH₃OH requires moderate temperature (i.e. 300 - 400 °C) in the presence of a zinc-chromium catalyst. Hydrogen is obtained by the following catalysed reactions for ammonia and methanol:



A major limitation in the use of ammonia and methanol as hydrogen storage media is their irreversibility in hydrogen storage. This irreversibility, as well as large power inputs for hydrogen liberation, restricts a wider implementation of ammonia and methanol as hydrogen storage media. Also, hydrogen generation from methanol requires the use of hydrogen reformers which have slow yield rates and are costly. Large-scale methanol steam reforming also leads to the generation of large quantities of CO and CO₂, which may add to the environmental burden. [11]. Although ammonia is not a greenhouse gas it quickly forms hydrogen bonds to water vapour and returns to the ground in alkaline rain; is toxic; and releases heat on contact with water [12].

Organic hydride systems exhibiting reversible hydrogenation / dehydrogenation action include benzene-cyclohexane and naphthalene-decalin [13]. The hydrogenation-dehydrogenation processes occur at T = 200–400 °C and P_{H₂} = 10–100 bar in the presence of metal catalysts (e.g. Pt, Pd, Mo₂O₃). Hydrogen sorption in organic hydrides is very efficient in weight and volume sorption capacities (5.0-7.0 wt. % and 70-100 g/L H volume density) [14]. Also, large quantities of hydrogen (5.0 mol of H₂ per 1.0 mol of decalin) can be produced and can be sorbed in 1.0 mol of naphthalene. However, the energy input necessary to heat the sorption system to the reaction temperature is large and should only be used where a vast amount of waste heat is available. Generally, organic hydride systems were found to be lacking in terms of catalyst requirements, as well as the pressure and temperature excursions required for charging and discharging [14].

Hydrogen can be generated by high-temperature reaction of water vapour with spongy iron which has previously been reduced using a fuel gas [15]. The reaction takes place at $T = 550 - 600$ °C:



The process is somewhat reversible because the starting iron can be recovered by reducing Fe_3O_4 using CO. In addition, the hydrogen is not chemically bound to the spongy iron [16]. Disadvantages include low efficiency in terms of economic and environmental considerations.

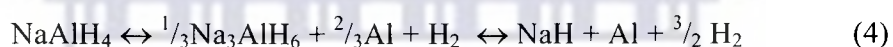
Reaction of aluminium or silicon alloys with alkaline solutions at room temperature can also be used in hydrogen generation [16]. By appropriate selection of the alloying components, as well as design features and operating conditions of the hydrogen-generating reactor, it is possible to attain fast reaction kinetics under soft conditions and to easily control hydrogen generation. Hydrogen can be generated, although the technology is not appropriate for reversible H_2 sorption [1].

Zeolites can potentially be employed as hydrogen sorption media as the diameter of their channels can be controlled by exploiting ion-exchange properties to modify the valence state and the size of the exchangeable cations. Reversible hydrogen sorption is achievable at moderate temperature ($T = 20-200$ °C) and pressure ($P_{\text{H}_2} = 25-100$ bar) [17]. In doing so, hydrogen molecules are transported into the framework of the zeolite, and when cooled to below room temperature the hydrogen becomes trapped within the zeolite. Subsequent heating of the zeolites leads to the discharge of hydrogen. However, the maximum sorption capacity (less than $10 \text{ cm}^3/\text{g}$; 1.0-1.8 wt. %) is too low to compete with other sorption systems [18].

Metal organic frameworks (e.g. $\text{Zn}_4\text{O}[\text{O}_2\text{C}-\text{C}_6\text{H}_4-\text{CO}_2]_3$) have similar microporous structure to zeolites and show promise as potential hydrogen sorption materials as a result of their tuneable pore size and functionality. These materials have large specific

surface areas (i.e. 2500–3000 m²/g) and can absorb up to 7.5 wt.% H₂ at -196°C and P_{H₂} = 20 bar, or up to 1.0 wt.% H at the room temperature and P_{H₂} = 20 bar [18]. However, the materials are extremely expensive and require cryogenic temperatures in their operation.

Alanes are salt-like complex hydrides based on coordination compounds where absorbed hydrogen combines as ligands. These materials demonstrate high potential for application as hydrogen sorption materials as a result of their large hydrogen weight capacities (e.g. 7.4 wt. % H₂ for NaAlH₄). Alanes can absorb and release hydrogen reversibly when catalyzed with titanium dopants. Alanes, such as NaAlH₄, generally exhibit two-stage desorption of hydrogen [19-22]:



Under mild pressure, the first reaction becomes thermodynamically favoured at temperatures above 33 °C and can release 3.7 wt% H₂, while the second reaction takes place above 110 °C and can release 1.8 wt% H₂. Disadvantageous is the slow kinetics and uptake in hydrogen absorption-desorption, the decay of hydrogen sorption capacity with prolonged cycling, the extremely high chemical reactivity with O₂ and water vapour, difficulty in synthesis, and high cost [23].

Complex borohydrides, aluminohydrides, and ammonium salts have been investigated for use as hydrogen sorption media as a result of their theoretical hydrogen capacities of about 8.5 wt.%. Representative materials include: amine boranes, boron hydride ammoniates, hydrazine-borane complexes, and ammonium octahydrotriborates or tetrahydroborates. Of these, borohydrides have been extensively investigated as hydrogen sorption media. Potential borohydrides which have high gravimetric and volumetric hydrogen densities include LiBH₄, NaBH₄, Mg(BH₄)₂, and Ca(BH₄)₂ [24]. Use of these materials as hydrogen sorption media is not favourable as a result of the extremely high toxicity of diborane which is produced during side reactions in the hydrolysis and thermolysis of borohydrides.

Also, the hydrogenated borohydrides are known to decompose with the loss of large quantities of hydrogen; and the temperatures and pressures required to initiate hydrogenation of borohydrides are impractical.

Imidazolium ionic liquids, including alkyl(aryl)-3-methylimidazolium N-bis(trifluoromethanesulphonyl)imide salts, possess almost negligible volatility (10^{-8} bar), thermal / chemical stability, inflammability, and can reversibly absorb 6-12 hydrogen atoms when catalysed with PGM's [25]. However, hydrogen has a very low solubility in imidazolium ionic liquids and hydrogenation is a very slow process [26].

Non-metal phosphonium borate presents an alternative medium for reversible hydrogen sorption. Favourably, the hydrogenation can be conducted at room temperature using low hydrogen pressures ($P_{H_2} = 1.0$ bar) and dehydrogenated at merely 100°C in toluene. Hydrogen absorption occurs via interaction with the Lewis acidic centres at the borane side followed by intramolecular proton migration to the phosphine side. However, the hydrogen absorption capacity is only 0.25 wt. % and still considerably insufficient for practical application of phosphonium borate [27].

Hollow glass microspheres can be utilized for controlled sorption and release of hydrogen. Unfortunately, the release of hydrogen from the hollow glass microspheres is exceptionally slow and impractical for application in sorption systems [28]. Importantly, hydrogen sorption and delivery using hollow glass microspheres is an irreversible process.

Binary and intermetallic hydrides have been intensely investigated as a result of their potential application as hydrogen sorption media and potentially hold more hydrogen (e.g. 6.5 H atoms/ cm^3 for MgH_2) than compressed hydrogen cylinders (0.99 H atoms/ cm^3) and liquefied hydrogen (4.2 H atoms/ cm^3) [29-31]. Metal hydrides are simply metals or metal alloys into which dissociated hydrogen atoms have been incorporated into the crystal structure of the metal and that exhibit metal-hydrogen bonding [32]. These materials are capable of selectively absorbing and releasing pure hydrogen without compromising their structure. The reversibility of these materials

also guarantees that expulsion of high-purity hydrogen can simply be achieved under the stimulus of an applied energy greater than the heat of formation for the metal hydride. Intermetallic hydrides or metal hydride-forming alloys are of particular interest due to their reversible nature, reasonable kinetics in hydrogenation, and high hydrogen selectivity [32].

From the classes of hydrogen sorption materials under consideration, metal hydride-forming alloys have the greatest practical potential in hydrogen separation / purification / storage systems. Favourably, the thermodynamic features of the reversible interaction between hydrogen and metal hydride-forming alloys allows for absorption at low pressure and temperature while releasing high pressure H₂ at elevated temperatures. Such a feature allows for the development of fairly simple heat-driven separation / purification / storage units. This feature demonstrates the technological flexibility of metal hydride-forming alloys and illustrates their potential benefit as an alternative technology in hydrogen processing [33].

2.2. METAL HYDRIDE-FORMING ALLOYS

Metal hydride-forming alloys are considered the best solid-state hydrogen sorption media available and also present an effective technology in separating hydrogen from gas mixtures for the production of high-purity hydrogen [34]. These materials find numerous applications in industry, including [35]: hydrogen storage for vehicular and stationary applications, electrodes in nickel metal hydride batteries, electrodes in water electrolyzers and fuel cells, hydrogen compressors, catalysis of electrochemical / chemical processes using hydrogen as a reactant, metallurgical processing, heat pumps, separation of hydrogen isotopes, hydrogen getters, and hydrogen sensors.

Metal hydride-forming alloys are obtained by combining an element forming a stable hydride with an element forming a non-stable hydride [31]. The hydride-forming ability of metal alloys can generally be given as follows, where M = metal alloy, ΔH = heat of formation [36]:



The reaction is noted as being of a reversible nature with the forward direction associated with the charging of hydrogen (exothermic) and the reverse direction associated with the discharge of hydrogen (endothermic). The heat is the enthalpy of the reaction (heat of formation, ΔH) and is indicative of the metal-hydrogen bond strength in the metal hydride system. Heat energy is evolved upon formation of the metal hydride; therefore a quantity of energy greater than ΔH can be used to discharge hydrogen from the metal hydride [31]. In doing so, high-purity hydrogen can be released, leaving the material in its original chemical state.

As the stability of the metal hydride is largely dependent on the equilibrium pressure at a fixed temperature, the thermodynamic properties of the metal hydride can be illustrated by construction of pressure-composition (PCT) isotherms (Figure 2.1) [37]. When the hydrogen content (H/M) within the metal alloy is low ($<\alpha_{\max}$) a single-phase solid solution (α -phase) is formed. An increase in the H/M within the metal alloy beyond α_{\max} facilitates the formation of a mixed-phase where both α - and β -phases are present, with the β -phase corresponding to a pure metal hydride. This region occurs as a plateau region at the equilibrium pressure (P_{eq}). Beyond β_{\min} only a single phase metal hydride (β -phase) is observed.

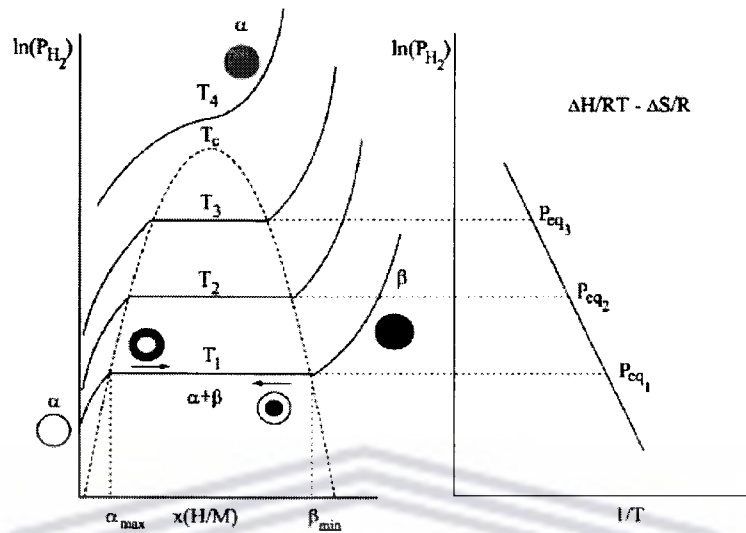


Figure 2.1. General pressure-composition isotherms of a typical hydrogen sorption alloy

The general classes of metal hydride-forming alloys and their hydrogen absorption properties of interest are given in Table 2.1 [32].

UNIVERSITY of the
WESTERN CAPE

Table 2.1. Hydriding properties of metal hydride-forming materials

Alloy	Maximum hydrogen absorption		Absorption kinetics	Hydride stability	Cycling stability	Poisoning resistance	Material Cost
	Molar ratio (H/M)	Maximum weight %					
Haucke-type AB ₅ (e.g. LaNi ₅)	1 - 1.5	1.4 - 1.9	Express kinetics, no activation required	Relative stability	Degradation after 300-400 cycles	Resistance to H ₂ O and O ₂ , poisoned by CO and H ₂ S	Quite expensive
AB (e.g. FeTi)	1	1.8	Reasonable kinetics, activation required	Fairly stable	-	Poor resistance	Cost-effective
Laves-type AB ₂ (e.g. ZrV ₂)	1 - 2	1.5 - 2	Fast kinetics, activation not always required	Stable	-	No poisoning	Quite expensive
Mg and Mg-based compounds (e.g. Mg ₂ Ni)	1.3 - 2	3.5 - 6.7	Slow kinetics, difficult activation required	Highly stable	Reduction in desorption rate with cycling	Poor resistance	Cost-effective
AB ₃ (e.g. VFe ₃) and A ₂ B ₇ (e.g. Th ₂ Fe ₇)	1.4 and 0.67	1.6	-	Stable	-	-	Cost-effective

The diverse usage of the different classes of metal hydride-forming alloys, in industrial applications, can further be illustrated in Figure 2.2.

AB₅-, AB₂- and AB-type metal hydride-forming alloys offer the best options for room-temperature hydrogen sorption, with the AB-type alloys (e.g. TiFe) offering the

best combination of reasonable capacity; lowest raw material cost; availability and accessibility of these metals in the South African region. In terms of hydrogen separation and purification the AB and AB₅ classes are the most promising metal hydride-forming alloys. Sandrock *et al.* have stated that AB alloys are the most suitable in the separation of H₂ from gas streams containing small amounts of CO [38]. However, it is not suitable where large quantities of gaseous impurities are present. For this reason it is difficult to use AB compounds to separate hydrogen from industrial streams derived from coal gasification, which contains an appreciable quantity of CO ~ 22.5 vol. %. Also, hydriding is difficult to initiate in Ti, the hydriding component of FeTi, because the *d*-electrons are almost totally involved in metallic bonding, where these electrons are necessary for bonding with hydrogen atoms during hydrogenation [32].

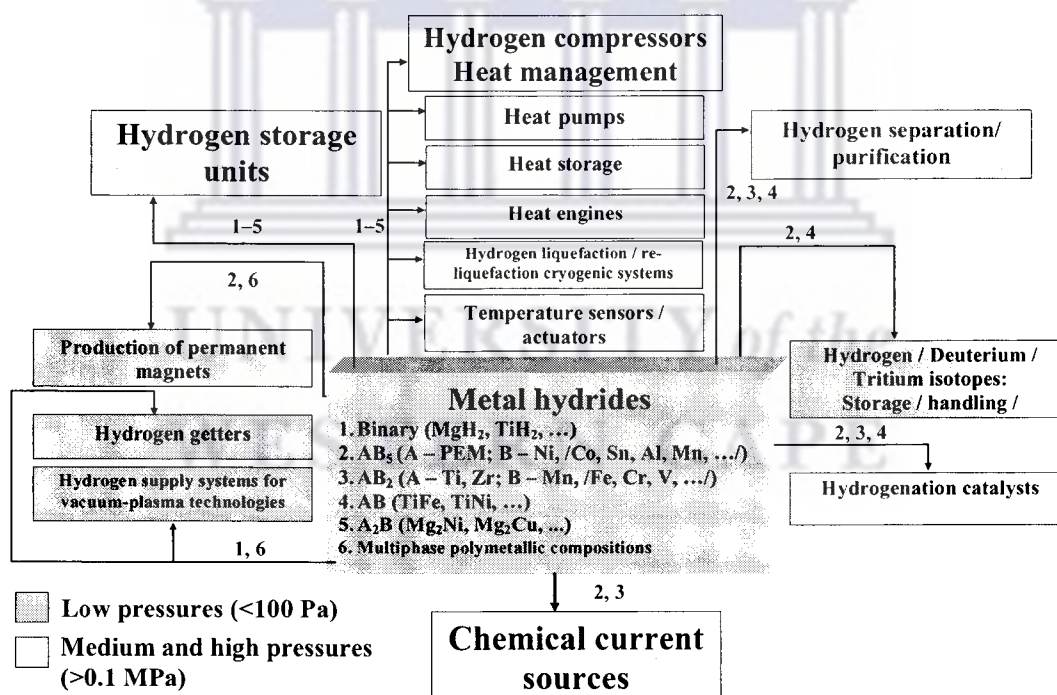


Figure 2.2. Flow diagram illustrating industrial applications of metal hydride-forming materials

AB₅-type alloys show greater promise for gas separation and purification applications. The “A” component has a strong affinity towards hydrogen and is a rare earth metal like La or a mischmetal (i.e. mixture of rare earth metals, mainly lanthanum, cerium, neodymium and praseodymium) while the “B” component absorbs little hydrogen and is a transition metal such as Ni (sometimes with additions of Al, Co, or Mn). AB₅-type alloys exhibit hydrogen absorption rates nearly an order of magnitude faster than that of AB-type alloys, with good absorption kinetics. AB₅-type alloys are also applicable in gas separation-purification over a wide temperature and pressure range ($T = 0\text{-}200\text{ }^{\circ}\text{C}$; $P_{\text{H}_2} = 1\text{-}200\text{ bars}$). Of the AB₅-type alloys available LaNi₅ receives the most attention due to an attractive working temperature and pressure, activation-free operation, relative hydride stability, express kinetics of hydrogenation, and reasonable poisoning resistance [31]. The material consists of a La-based core with Ni clusters dispersed on the surface. The La component may act to induce Ni to become a hydrogen-binding element [32]. Interaction between hydrogen and the LaNi₅ surface may therefore occur on the Ni active surface sites which have the capacity to catalyse the hydrogen dissociation process. The LaNi₅-type alloy generally has a hexagonal CaCu₅-type crystal structure, with three octahedral and three tetrahedral sites per elemental unit cell [39,40]. The alloy readily forms the hydride phase LaNi₅H _{γ} ($\gamma \approx 6$) upon hydrogen absorption [34]. The LaNi₅ alloy is able to form hydrides without decomposing into separate components upon hydrogenation (i.e. disproportionation) [41].

It is important to note that although AB₅-type metal hydride-forming alloys do not exhibit the largest hydrogen sorption capacities (~1.4 wt. %) for practical application in sorption systems, their thermodynamic and kinetic properties make them ideal substrates for the development of new surface modification techniques. Also, although the AB₅-type alloys exhibit the best kinetic properties of the available metal hydride-forming alloys they are deficient of the kinetics properties required for practical application in hydrogen sorption systems. The ability of this alloy to absorb

hydrogen at moderate temperatures and pressures makes the surface modification of AB₅-type alloy materials worth investigating.

2.3. MECHANISM OF HYDROGEN SORPTION IN AB₅-TYPE METAL ALLOYS

Hydrogen absorption follows Sieverts' law at low hydrogen concentration as follows [42]:

$$\sqrt{\frac{p}{p^0}} = K_S x \quad (6)$$

where p = pressure of hydrogen, p^0 = standard pressure, K_S = Sieverts' constant, which is dependent on temperature (T) as follows:

$$\ln K_S = -\frac{\Delta S_s}{R} + \frac{\Delta H_s}{RT} \quad (7)$$

where S_s and H_s = solution entropy and enthalpy of hydrogen in the metal, respectively, R = gas constant (8.314472 J.K⁻¹.mol⁻¹; 0.082057459 L.atm.K⁻¹.mol⁻¹).

The general mechanism involved in the absorption and desorption of hydrogen by AB₅-type alloys can be illustrated in Figure 2.3.

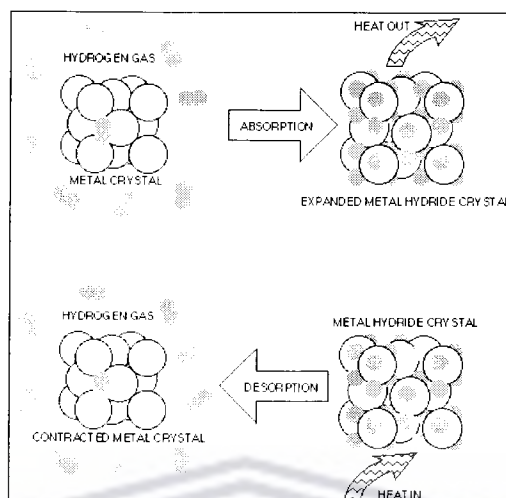


Figure 2.3. Mechanism for hydrogen absorption and desorption in AB_5 -type alloys

The reaction between the AB_5 -type alloy and hydrogen gas consists of several reactions proceeding on the surface and in the bulk material. As hydrogen molecules approach the alloy surface weak Van der Waals forces begin to act upon the hydrogen molecules, drawing them closer. The molecules are then physically bound to the surface (i.e. physisorption) where they dissociate to form hydrogen atoms (H) which are subsequently chemically bound to the surface (chemisorption). At this point the dissociation energy for molecular hydrogen ($432 \text{ kJ}\cdot\text{mol}^{-1}$) is exceeded by the chemisorption energy ($500 - 600 \text{ kJ}\cdot\text{mol}^{-1}$). The hydrogen atoms then diffuse into the crystal lattice of the alloy. Generally, AB_5 -type alloys absorb hydrogen into the free tetrahedral interstitial sites of the crystalline lattice and undergo several mass transfer steps [32,43]. The hydrogen atoms, whilst absorbed into the free tetrahedral interstitial sites of the metal, are surprisingly mobile even at room temperature [44]. The hydrogen atoms force the nearest-neighbour metal atoms further apart from each other causing a lattice expansion and. In doing so, changes in the crystal structure of the host metal are observed and are manifested as changes in the lattice parameters (a_0) and increases in the unit cell volume. Generally, the distance between the hydrogen atoms is maintained at more than 2.0 \AA [45].

During desorption hydrogen atoms migrate to the surface of the metal hydride, under stimulus of energy greater than the heat of formation, recombine to form hydrogen molecules and leave the alloy surface in the gaseous state. The alloy atoms contract to form the original crystal structure, as a result of the reversibility characteristics of the AB₅-type alloy material.

2.4. LIMITATIONS OF HYDROGEN SORPTION USING AB₅-TYPE ALLOYS

Generally, surface poisoning seems to be the biggest shortcoming in the separation / purification / storage of hydrogen from gaseous mixtures containing aggressive components using AB₅-type hydride-forming alloys [46]. AB₅-type alloy materials also exhibit low rates of hydrogen absorption. This shortcoming stems from the observation of rare earth metal oxide and hydroxide formation on the surface after short-term exposure of the alloy to air [47,48]. As a result, the surface catalytic sites are deactivated and hydrogen absorption can no longer be initiated at reasonable rates. Complete losses of hydrogenation capacity have been reported after less than 100 hours exposure to air. Longer exposure to air also increases the difficulty involved in thermal activating the alloy under hydrogen pressure [49].

Another common feature in absorption using AB₅-type materials is the observation of an incubation period in which hydrogen absorption rates are insignificant [49]. This incubation period may increase considerably with increasing exposure to air.

To be considered for applications such as onboard hydrogen storage or hydrogen separation / purification long-term hydrogen sorption stabilities are required, and are achievable using surface nano-engineering.

2.4.1. Surface poisoning and deactivation of AB₅-type alloys

Sorption capacity is determined by the bulk properties of the metal hydride-forming alloy (i.e. structure, electronic band structure), whereas the kinetics of hydrogen absorption depend strongly on the surface structure and the chemical state thereof.

Poisoning of metal hydride-forming alloy materials is observed by a rapid loss in the H₂ sorption capacity and a large decrease in the overall kinetic properties of the material. AB₅-type alloys are also prone to surface poisoning by electrophilic molecules which affect the rate-controlling processes in hydrogenation/dehydrogenation. The influence of gaseous mixtures containing hydrogen and impurities are presented in Table 2.2.

Table 2.2. Influence of contaminants on hydrogen sorption properties of AB₅-type hydride-forming alloys (T = 20-100°C, P = 0.001-50 atm) [34]

<i>Gas accompanying hydrogen</i>	<i>Behaviour on AB₅-type alloy surface</i>	<i>Number of cycles prior to loss of hydrogen sorption capacity</i>
Ar, He, N ₂ , CH ₄ , C ₂ H ₆	Inert, leading to loss in adsorption kinetics due to surface blanketing	>1000
CO ₂ , NH ₃	Chemisorption without poisoning; reduction in adsorption-desorption kinetics without significant loss in capacity	~1000
C ₂ H ₄ , C ₂ H ₂ , C ₃ H ₆	Catalytic conversion	~1000
O ₂ , H ₂ O	Surface oxidation leading to irreversible capacity loss	~100
CO, SO ₂ , H ₂ S, CH ₃ SH	Surface poisoning and rapid loss of hydrogen capacity with cycling; irreversible adsorption onto active surface sites	1-2

The susceptibility of AB₅-type alloys to surface contamination by aggressive gases, especially CO; H₂S; H₂O; and O₂, is a major problem and can be illustrated in Figure 2.4 [50]. These poisoning species form stable surface films (i.e. oxides, sulphides, carboxides, etc.) which inhibit the process of molecular hydrogen dissociation (H₂→2H). This is because hydrogen absorption/desorption kinetics on AB₅-type alloys is highly dependent on the surface chemical integrity, which is degraded by poisoning species [51]. These surface films are known to increase the activation energy for the dissociation of H₂ molecules with the result that this surface process becomes the rate-limiting step in the separation / purification / storage of H₂ using surface-contaminated alloys. By limiting the dissociation of hydrogen molecules the poisons also markedly decrease the hydrogen sticking coefficient on the alloy, which determines whether the hydrogen molecules interact with the surface [41]. When the sticking coefficient approaches zero the surface is completely deactivated and can no longer interact with hydrogen. Similarly, absorbed hydrogen cannot be desorbed from the alloy after the sticking coefficient approaches zero.

CO and H₂S typically form chemically-bonded surface monolayers; H₂O forms physical bonds, while O₂ forms stable surface oxide films by the oxidation of the most electropositive surface components, typically the rare earth metals in the “A”-component [34,38,41]. In addition, hydrogen exhibits a very low degree of solubility and diffusivity through these surface films [52]. CO and H₂S, two of the most common poisons in industrial hydrogen mixed gases, exhibit identical poisoning of AB₅-type alloys and reduce the surface reactivity by large orders of magnitudes [53]. Miniscule amounts of CO and H₂S in gas mixtures results in a significant suppression of the hydrogen sorption properties of AB₅-type alloys. Increasing the CO concentration in the feed gas leads to an associated increase in the rate of oxidation of the alloy components and a decrease in rate of hydrogenation of the alloy [54,55]. Sandrock *et al.* have observed rapid losses in hydrogen sorption capacity and kinetics when cycling AB₅-type alloys in H₂S-containing H₂ gas streams [51]. A similar observation was made by Bratanich *et al.* where as little as 0.03 vol. % CO in H₂

rapidly passivated AB₅-type alloy surfaces [54]. The presence of as little as 1.0 vol. % O₂ in hydrogen results in a reduction in the hydrogen sorption properties of the alloy [41]. Oxygen is also known to deactivate the surface of AB₅-type alloys with a 50% loss in the hydrogen absorption capacity being observed after 50 cycles in hydrogen containing 0.5% O₂ [41]. Exposure of LaNi₅ with H₂O (as water vapour) and is also associated with the occurrence of surface oxidation [54]. Surface oxidation renders Ni sites inactive towards catalysis of H₂ surface dissociation processes due to the formation of stable lanthanum trioxide and sesquioxide films, which act as a hydrogen diffusion barrier due to the poor diffusivity and solubility of hydrogen through these layers. NiO layers are also formed upon exposure of LaNi₅ to water vapour and CO. The stable NiO layer formed inhibits any further surface reactions as NiO is non-catalytic towards the dissociation of H₂. The negative influence of surface poisoning species on the hydrogenation rate of AB₅-type alloys can be observed in Figure 2.4.

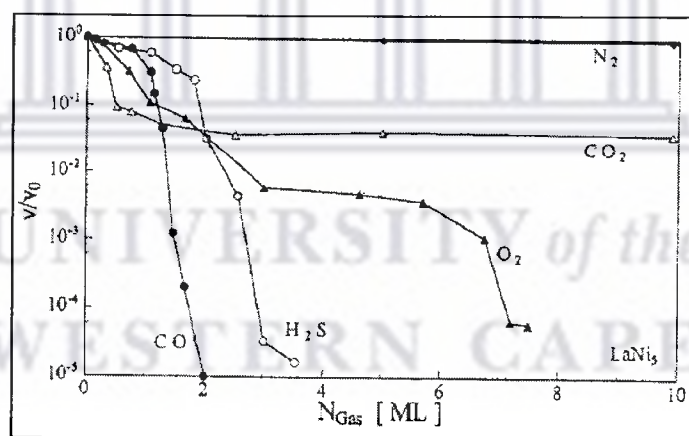


Figure 2.4. Rate of H₂ absorption by LaNi₅ as a function of the pre-exposure to poisoning gases, V/V_0 - relative reaction rate of hydrogen with LaNi₅, N_{Gas} [ML] - monolayers of poisoning gas [50]

Medium to long-term exposure of the AB₅-type alloy materials to air has also been well-documented as having a deactivating effect on the AB₅-type alloy surface. Air contains quantities of O₂, water vapour, and trace quantities of CO, all of which have detrimental effects on the long term sorption stability and surface chemical state of

the alloys. Similar poisoning of the AB₅-type alloy surface was observed by Willey *et al.* after exposure to air for 150 minutes. The effect of air exposure on an AB₅-type metal hydride alloy can be illustrated as Figure 2.5. Prior to surface passivation by contaminants the rate-determining step in H₂ sorption on AB₅-type alloys is both absorption of hydrogen in the bulk material and the surface reactions. After surface contamination of AB₅-type alloy the rate-determining step is surface processes alone.

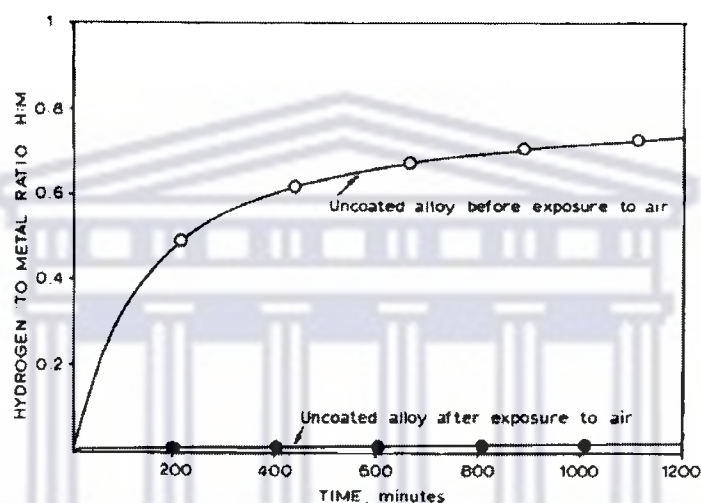


Figure 2.5. Hydrogen absorption characteristics of AB₅-type alloys before and after air exposure [56]

Large-scale commercial application of AB₅-type alloys in the separation, purification, and storage of hydrogen has not as yet been achieved due to ineffective surface poisoning resistance of the alloy towards gaseous impurities in hydrogen feed streams [57]. It has been recognized that these hydrogen technologies will not be practical on AB₅-type alloys unless they can be made more resistant to surface impurities.

2.4.2. Decrepitation of the hydrogenation / dehydrogenation rate

The principle causes for loss of hydrogenation rate and capacity of the AB₅-type alloys with repeated cycling are gradual oxidation of the alloy surface; rapid oxidation of new surfaces formed after initial activation; hindrance of hydrogen

dissociation; and obstruction of hydrogen diffusion from the surface of the alloy to the bulk material [58]. The latter is a result of the temperature dependence of hydrogen diffusion, where the exothermic nature of hydrogenation process governs the temperature of the alloy material, which in turn will determine the rate of diffusion of hydrogen atoms through the core material [59].

Also, high temperature regeneration of metal hydride-forming alloys, after cycling in contaminated hydrogen, is limited in that the maximum hydrogen sorption performance is never again achievable due to imperfect reversible facilitated by the contaminating species.

2.4.3. Activation and incubation periods

Another serious problem encountered with these materials is that they do not readily absorb hydrogen under ambient conditions and have to be thermally activated prior to hydrogenation [60]. The activation process is usually complicated, involving repeated annealing at high temperature and/or pressure.

In practice it is very difficult to avoid surface contamination of the sample during synthesis of the material and handling. The obvious solution is to maintain ultra-high vacuum conditions, but this is very expensive and may be limited to laboratory-scale samples. To restore good hydrogen sorption properties some kind of activation procedure has to be applied. Unfavourably, this requires repeated heating in hydrogen to pulverize the alloy and generate fresh surfaces for reaction.

Generally, a period of incubation may be observed at the onset of hydrogen absorption by metal hydride-forming materials [61]. The incubation period is due to the presence of an oxide layer that has to be disintegrated, through repeated activation cycles, before significant hydrogen absorption commences [62]. It has also been stated that the incubation period can be shortened and the rate of hydrogen absorbed increased with increasing specific surface area and temperature.

2.5. STATE-OF-ART IN METAL HYDRIDE-FORMING ALLOY SURFACE MODIFICATION

For AB₅-type alloys to be considered suitable media in the separation of hydrogen from contaminated gas feeds the reaction kinetics should satisfy the sorption requirements of the gas separation system and should demonstrate superior poisoning resistance in contaminated hydrogen. These problems can be addressed using surface engineering as they are non-intrinsic and can be avoided.

Previous attempts to address the dilemma of oxide formation, poisoning, and low rate of absorption have been focussed on the modification of the bulk material using additional elemental components, or varying ratios of elements present in the metal hydride-forming alloy. However, such actions increase the complexity of the alloy preparation [48]. To simplify the problem, special attention was given to addressing the surface chemistry of the alloys. Promising surface modifications include the introduction of protective layers, such as those produced using encapsulation [63-67], fluorination treatment [68-74], potassium borohydride treatment [75,76], alkaline solution treatment (e.g. LiOH; NaOH; KOH; NH₃OH) [74,77-80]; HCl acid treatment [81-84]; Y₂O₃ surface film deposition [85]; Ni-containing weak acid treatment [86]; plasma immersion and ion implantation [87]; combined alkaline solution treatment and encapsulation [88,89]; combined treatment with potassium borohydride and alkaline solutions [79,90-93]; combined fluorination and HCl acid treatment [81]. These approaches have been well-documented by numerous sources [51,68,94-96]. It should be noted that no research works pertaining to combination coatings of fluorination and encapsulated metal layers could be found in literature, where metal hydride-forming alloys surface-modified using these techniques have the potential to produce high-purity hydrogen in rapid time.

The abovementioned methods all have their advantages and disadvantages which will be further discussed in the subsequent Sections 2.5.1 – 2.5.9.

2.5.1. Fluorination treatment

The poisoning resistance of fluoride layers is well-understood and developed and leads to tolerance to many types of surface poisons. The benefit of fluorination is that the mechanical stability and sorption stability of fluorinated materials, under extreme process conditions and large pressure range, can be dramatically increased. Surface treatment by deposition of a fluoride layer facilitates the generation of a Ni-rich sublayer, by removal of surface oxide layers, which increase the catalytic activity of the AB₅-type alloy surface towards the hydrogen dissociation reaction. Typically, surface fluorides are formed with rare earth metals in AB₅-type alloys (i.e. REF₃).

The advantages of fluorination in the surface treatment of metal hydride-forming alloys include: enrichment of the electrocatalytic Ni sublayers; improvement in hydriding ability of the alloy; improvement of the cycle lifetime [68]; increasing of specific surface area [71]; simplicity; moderate cost of starting materials; increases gas selectivity. Disadvantageous are the various safety issues associated with fluorine [64]; unavailability of detailed mechanisms for improvement of performance of the hydride-forming alloy [69,74]; incubation periods still present after fluorination [70]; quantities of nickel are removed as (NiF₄)²⁻ [71]; fluorination effect varies with a variation in the chemical composition of the alloy surface [74].

2.5.2. Encapsulation using metal layers

Encapsulation involves enveloping the surface of a substrate material with a layer which may act to promote the catalytic properties and surface chemical stability of the substrate material. The encapsulating layer may be polymeric; graphitic; ceramic; or metallic in nature, although metallic layers are most often used where the substrate is a metal hydride-forming alloy.

Metals which can be used to encapsulate metal hydride-forming alloys to alleviate the deterioration of their active surfaces by retarding surface oxide formation and

promoting the reaction kinetics include Pd, Co, Ni, Cu, Au, Ag, Pt, Ir, V, Nb, Ti, Pd alloys, Co alloys, Au alloys, Ag alloys, Pt alloys, Ir alloys, V alloys, Nb alloys, Ti alloys, and combinations thereof [48]. However, few of these options have the ability of simultaneously promoting the hydrogen dissociation process, enhancing poisoning resistance, eliminating incubation periods, and increasing the kinetic rate of hydrogen absorption.

Advantageous are the high hydrogen selectivity attained using this technique; significant improvement in hydrogenation performance; prevention of oxidation; improvement of thermal and electrical conduction; improvement of cycle lifetime and discharge rate; improvement of hydrogen dissociation rate; and simplicity [63,65]. Disadvantageous is the requirement of high concentrations of metals which do not participate in hydrogen storage [64].

2.5.3. Potassium borohydride treatment

KBH_4 surface treatment is known to improve the activation behaviour, cyclic stability, and electrochemical performances of metal hydride-forming alloys through the reduction of surface nickel oxides. The treatment of the alloy surface is typically conducted by immersion in dilute solutions of potassium borohydride [75]. The KBH_4 treatment can also be conducted in concentrated alkaline solution. The KBH_4 treatment is known to generate smaller alloy particles, thereby facilitating an increase in specific surface area.

Advantageous are the improvements in reaction kinetics and cycle lifetime; dissolution of surface oxide layers; increases in catalytic activity [76]; improved activation and increased specific surface area [91]. Disadvantageous is the dissolution of Al and Mn components in mischmetal hydride-forming alloys which may lead to losses in hydrogen absorption capacity and the retention thereof [92].

2.5.4. Alkaline solution treatment

Surface pretreatment of AB₅-type alloys in concentrated solutions of KOH, LiOH, and NaOH have been known to improve the hydrogenation rate and electrochemical activity [75]. The enhanced performances of alloy materials after surface treatment in alkaline solutions have been credited to the removal of passivating oxides on the surface of the parent alloy to expose a Ni-rich sublayer, thereby restoring the initial catalytic activity of the alloy. Small additions of reducing agent to the alkaline solution have been known to further increase the electrochemical properties of the alloy material. It was also suggested by Chen [91] that pre-treatment of mischmetal alloys in alkaline solution acts to remove Al and Mn from the surface and promote Ni and Co concentration at the surface of the alloy. Also, quantities of K, Li, and Na atoms are known to be impregnated into the surface layer after alkaline treatment. The impregnation of these atoms is linked to changes in the electronic properties of the AB₅-type alloy and subsequent enhancements in the hydrogenation rate.

Advantageous are the increase in the hydrogenation rate and lowering of the activation energy required to initiate hydrogenation [77]; increase in cycle lifetime [78]; increase in specific surface area by formation of a porous surface with enriched Ni and Co atoms [80]. Disadvantageous are the incorporation of alien Li, K, and Na atoms into the surface structure [77]; dissolution of Al leading to loss of durability [78]; generation of Mn oxides and rare earth metal hydroxides which inhibit H₂ dissociation as a result of low reactivities towards hydrogen [74].

2.5.5. Hydrochloric acid treatment

HCl treatment facilitated improvements in the electrochemical characteristics of the AB₅-type alloy by increasing the Ni and Co concentration, and reactivity, at the surface of the alloy [84]. The improvements were a result of the leaching of surface Mn and rare earth metals into solution and the subsequent increase in the specific surface area of the alloy material.

Advantageous are the increase in the specific surface area of the alloy with acid treatment; Ni and Co surface enrichment; enhanced electrochemical activity. Disadvantageous are the partial dissolution of elements at the surface; partial oxidation of the surface elements with the newly-formed surface layer exhibiting non-uniformity in thickness [83]; inability to protect the surface from poisoning after long term exposure to air [82].

2.5.6. Yttrium oxide surface film deposition

The addition of Y_2O_3 layers to the surface of metal hydride-forming alloys is known to increase the oxidation resistance and cycle lifetime of the alloy [85]. This is achieved by prevention of the dissolution of Al, Mn, and Co in solution and suppression of the formation of hydroxides of the rare earth metals at the surface.

Advantageous are the prevention of dissolution of constituents of the alloy surface; suppression of hydroxide formation in rare earth metals; increased cycle lifetime. Disadvantageous is the decrease in the hydrogenation / dehydrogenation and electrocatalytic properties of the hydride-forming alloy.

2.5.7. Ni-containing weak acid treatment

Treatment of AB_5 -type alloys in Ni-containing weak acids (e.g. $NiSO_4 + C_6H_8O_7$) is known to increase the concentration of Ni, Mn, and Co at the surface of the alloy. Advantageous is the promotion of the presence of a Ni-rich surface layer. Disadvantageous is the limited knowledge of this technique and its influence on the hydrogenation characteristics, activation kinetics, and surface poisoning. Also, this technique does not increase the resistance towards degradation in air and strong electrolytes [86].

2.5.8. Plasma immersion and ion implantation

Surface treatment of metal hydride-forming alloys by plasma immersion entails applying a plasma to the alloy surface and in such a way implanting ions (e.g. B^+ , N_2^+ , H^+) into the surface structure [87]. In doing so, the corrosion resistance of metal hydride-forming alloys is promoted. However, analytical difficulties are encountered when studying hydrogenation properties of hydride-forming alloys surface-modified using plasma immersions and ion implantation, as hydrogen is included into the surface structure and the alloy composition upon surface treatment.

2.5.9. Conclusions from review of surface modification techniques

Of the surface modification techniques described, encapsulation and fluorination are the most attractive as they have the ability to simultaneously protect the catalytically active surface sites of the alloy against deactivation and improve the activation kinetics in hydrogenation. Encapsulation provides phenomenal selectivity towards hydrogen and surface catalysis of the hydrogen dissociation process. Fluorination is attractive because of the large improvement in the surface Ni content and large increase in specific surface area provided by the fluoride shell. No known attempts were made to study the influence of the combination of encapsulation and fluorination on the hydrogenation performances of hydrogen sorption alloys. Separately these surface modification techniques provide notable improvements in the performance of the alloy material, but combined these techniques may have the ability to produce high-performance materials, based on hydride-forming metal alloys, for the separation / purification / storage of hydrogen from impure feed streams. The incubation periods observed in fluoride-coated hydride-forming metal alloys can be suppressed by deposition of metal layers which act as excellent hydrogen dissociation catalysts. Also, the amount of precious metals used in the encapsulation of the alloy surface can be reduced by deposition of low-cost fluoride layers on the surface of the alloy, which also provide a measure of surface protection against poisoning.

The fluorination and encapsulation techniques in the surface treatment of metal hydride-forming alloys are further discussed in Sections 2.7 and 2.8.

2.6. SCIENTIFIC REQUIREMENTS IN SEPARATION / PURIFICATION / STORAGE OF HYDROGEN USING PALLADIUM-BASED COMPOSITE MATERIALS

Ideal hydrogen separation / purification / storage materials for the production and delivery of high-purity hydrogen should exhibit the following characteristics: high rates of reaction; high selectivity; superior kinetic properties in hydrogenation / dehydrogenation; acceptable cost; mechanical stability; high durability; employment through large temperature and pressure ranges; high resistance towards aggressive gaseous species.

Currently, AB₅-type metal hydride-forming do not exhibit all these ideal properties in inert and non-inert environments. The envisaged composite Pd-AB₅-type alloy materials have the potential to satisfy all the abovementioned requirements for application in hydrogen separation / purification / storage systems. This is a direct result of the combination of enhanced catalytic activity, potentially modified hydrogenation mechanism, and the hydrogen selectivity which may be encountered upon surface modification using fluorination and encapsulation.

2.7. INCREASE OF SURFACE POISONING RESISTANCE BY FLUORINATION

Fluorination of metal hydride-forming alloys has been reported to improve performances in activation, reaction kinetics, durability, and poisoning resistance at the gas-solid interface of the alloy, albeit with a decrease in the electrical conductivity [49,69]. The increase in the poisoning resistance of AB₅-type alloys is due to an increase in the activation kinetics in the absorption of hydrogen. Activation times of AB₅-type compounds have also been known to decrease by up to two orders of

magnitude with fluorination [97]. The fluoride layer is highly stable and can withstand repeated hydrogenation cycles at high temperature and ultra-high vacuum.

Fluorination produces a fresh reactive catalytic Ni sublayer which is protected from passivation and the formation of catalytically-inactive NiO [98]. Fluorine ionically bonds to inorganic surfaces by substituting hydroxyl groups (-OH) [99]. Micro-cavities within the fluoride layer facilitate facile penetration of H₂ molecules whereas other gaseous species are impeded from penetration through the layer [94]. Fluorination also reduces the binding energy of undesired gaseous species and creates a diffusion barrier which is lower for H₂ molecules than for other gas molecules [95]. The influence of fluoride layers on the poisoning resistance of AB₅-type materials can be illustrated in Figure 2.6 [57]. It was observed in Figure 2.6 (a) that repeated cycling in hydrogen contaminated with CO results in the subsequent decrease in the absorption rate and hydrogenation kinetics of the unfluorinated LaNi₅ alloy. In comparison, significantly slower degradation in the absorption rate and hydrogenation kinetics were observed with repeated cycling of the fluorinated LaNi₅ alloy in hydrogen contaminated with CO. The fluoride layer is, however, not infinitely selective towards H₂, as miniscule amounts of poisoning species may still have the ability to penetrate through micro-cavities in the layer [33,68]. The fluoride layer may merely decrease the rate of surface poisoning. As a result, it is accepted that fluorination alone cannot provide the high level of poisoning tolerance required for separation / purification / storage systems based on metal hydride-forming alloys.

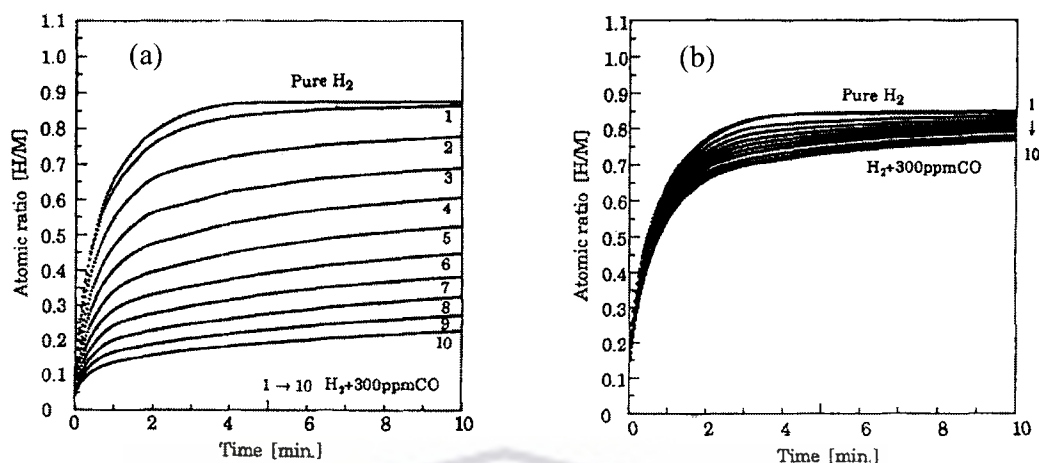
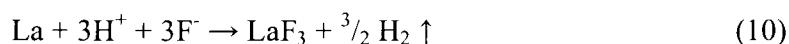
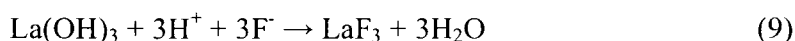
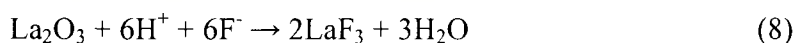


Figure 2.6. Influence of fluorination on poisoning tolerance of LaNi_5 towards hydrogen contaminated with trace amounts of carbon monoxide, (a) unfluorinated LaNi_5 , (b) fluorinated LaNi_5 , [57]

Use of a wet ball-milling fluorination technique in an aqueous solution containing fluoride ions has been investigated by Liu *et al.* [97]. The technique produced Ni-enriched surfaces enveloped by a LaF_3 network structure, with the removal of passivating rare earth sesquioxide layers (e.g. La_2O_3), thereby increasing the availability of catalytic surface sites for hydrogen absorption and desorption. Also, it is the LaF_3 surface structure, obtained after fluorination, which selectively and exclusively allows hydrogen to diffuse to the bulk material [57]. The fluorine solution also acted as a reducing agent for the removal of sesquioxide layers from the surface of the alloy. The fluorination process may then occur as follows [69]:



Some of the hydrogen ions (H^+) in the fluoride solution recombine to form hydrogen gas, which is nucleated at the solid-liquid interface between the fluoride solution and the alloy particle surface, whereas some H^+ ions penetrate the core alloy to form a

hydride, with subsequent pulverization of the alloy leading to increases in the activation characteristics and the specific surface area [100].

2.8. METAL LAYER ENCAPSULATION IN THE PROMOTION OF HYDROGEN SORPTION

Significant improvements in the hydrogenation performance of AB₅-type alloys are achievable by surface modification with various types of metal coatings. For enhanced rates of hydrogenation and surface poisoning resistance in hydrogen absorption and desorption the metal catalysts should preferably be deposited on the outer surface of the hydride-forming alloy particles to ensure the best catalytic effect, as incorporation of the catalytic metal within the bulk of the hydride-forming alloy particles significantly reduces contact between the catalytic metal and hydrogen and has no significant enhancing effect on hydrogen absorption and desorption [101]. The sorption performance of metal hydride alloys in contaminated hydrogen streams can be enhanced by surface encapsulation using metallic coatings which exhibit good mechanical stability and high poisoning tolerance without negatively affecting the hydrogenation and kinetic properties. Platinum group metals (PGM's) have been identified as possessing the ability to dissociate hydrogen molecules with no or very little activation energy required [32]. Also, these metals are attractive in the surface modification of metal hydride-forming alloys since thermochemical data suggests that the oxides of these metals can be reduced in H₂ at room temperature, making these metals promising in the enhancement of hydrogen absorption kinetics of metal hydride-forming alloys [102]. It is also known that the surface deposition of Pd, Ni, or Cu layers result in improvements in the activation of the grains of hydride-forming metal alloys [39].

2.9 PLATINUM GROUP METAL ENCAPSULATION IN THE PROMOTION OF HYDROGEN SORPTION

PGM's (Ru, Pt, Pd, Os, Ir, Rh) are generally considered to be the best catalysts for many reactions involving hydrogen and have a strong ability to absorb hydrogen. PGM's have the ability to dissociate hydrogen molecules into hydrogen atoms which can then be transported into the crystal structure of the metal. Importantly, surface coatings of PGM's have the potential to add poisoning resistance to metal hydride-forming alloys in oxidizing environments over extended periods of time, as they themselves are not easily oxidised [103]. PGM surface coatings may enable hydrogen to pass rapidly through the surface of metal hydride-forming alloys to the bulk while still maintaining the hydrogenation activity even after extensive exposure to oxidising environments [56].

Ruthenium-modified metal sorbents were found to absorb and desorb hydrogen at rates appreciably faster than the corresponding unmodified metal sorbents [101]. The Ru coating was also able to prevent deactivation of the metal hydride-forming alloys after prolonged exposures to air [64]. Ru and Pd-Ru encapsulation on metal hydride-forming AB₅-type alloys were extensively researched by Willey, Harris, Pratt, Doyle, and the Johnson Matthey Company [47,64,103].

Rhodium-based materials can be used as hydrogen sorption media as Rh is able to desorb hydrogen at low temperature. However, the hydrogen sorption capacity is exceptionally insignificant at 0.1 wt.% H₂. Rh is capable of absorbing two molecules of hydrogen at room temperature and atmospheric pressure and desorbs hydrogen under the stimulus of a small electrical current [104]. Rh can also be used as a catalyst in the thermal decomposition of ammonium borane to produce hydrogen [105]. Unfortunately, no information is available pertaining to the practical application of Rh as a hydrogenation catalyst on metal hydride-forming alloys.

Palladium is well known for its catalytic properties in the chemical and automotive industries [106]. It is also an exceptionally good catalyst for hydrogenation reactions such as the conversion of alkadienes and alkynes to alkenes [107]; and the hydrodechlorination of 1,2 dichloroethane to ethylene [108]. Importantly, Pd is an exceptionally good catalyst for surface reactions involving hydrogen exchange processes and serves as a type of metal “sponge” as a result of its ferocious affinity towards the absorption of hydrogen [109]. However, from knowledge gathered in the study of hydrogen separation using dense Pd membranes it is known that pure Pd exhibits intolerance towards poisoning by H₂S, after repeated cycling, leading to a noticeable decline in hydrogen absorption and selectivity. Pd is mostly available in “politically-sensitive” supply for H₂ separation / purification / storage with the largest concentrations available in South Africa and Russia. Zaluski *et al.* have also reported on the presence of Pd as a catalyst on Mg₂Ni, LaNi₅ and FeTi systems, which enhanced the absorption rates at low temperatures and maintained less sensitivity to air exposures [60].

Osmium-based complexes have previously been employed as catalysts for the hydrogenation of nitrile-butadiene copolymers [110]. No literature is available regarding the practical application of osmium-based materials as catalysts for hydrogen extraction / purification / storage using metal hydride-forming alloys.

Iridium, and more specifically iridium-based complexes such as IrH₄(C₆H₃(CH₂P(C(CH₃)₃)₂)₂), have previously been employed for catalysis in hydrogenation / dehydrogenation of hydrocarbons [111]. High surface area iridium has also been used to catalyze the thermal decomposition of ammonia and recombination and desorption of hydrogen. The iridium catalyst was prepared by heating atomically flat pieces of iridium in oxygen, then exposing them to hydrogen to remove the oxygen [112]. No literature is available regarding the practical application of iridium-based materials as catalysts for hydrogen extraction / purification / storage using metal hydride-forming alloys.

Catalysts, such as platinum, lower the activation energy for the surface dissociation of molecular hydrogen by providing a modified mechanism. In the mechanism, H₂ adsorbs to Pt surface sites where the energy of interaction between hydrogen and Pt surface atoms contributes to the breaking of the bond between the hydrogen atoms. The H⁺ are then free to react at the Pt surface or leave the surface to participate in reactions elsewhere in the chemical system. However, Harris *et al.* found that the catalytic behaviour of Pt layers deposited onto the surface of AB₅-type alloys was largely affected by temperature, where low temperature led to a large decrease in the activation kinetics of metal hydride-forming alloy encapsulated with Pt [103].

Pd and Ru are the most attractive catalysts in the PGM group for surface reactions involving hydrogen exchange processes. However as previously discussed, Ru and Pd-Ru encapsulation on metal hydride-forming AB₅-type alloys was extensively researched by Willey, Harris, Pratt, Doyle, and the Johnson Matthey Company [47,64,103]. The application of Pd as a catalyst on metal hydride-forming alloys has been extensively researched [37,54,55,60,62,102,113-119]. Pd exhibits higher permeability towards hydrogen at lower temperatures compared to the other PGM's. [109]. Pd catalysis represents a means to potentially enhance hydrogen sorption rates and offer protection towards the surface of metal hydride-forming alloys, and for this reason was investigated as a potential surface modification technology. The application of Pd metal in the sorption of hydrogen was further discussed in Section 2.10.

2.10. PALLADIUM IN THE SORPTION OF HYDROGEN

The employment of Pd in H₂ separation and purification systems is a result of its unique ability to absorb large volumes of H₂ (*ca.* 600-900 times its own volume at room temperature) and its unique hydrogen diffusion properties [38,120]. Also, at increased temperatures the metal has the ability to expel hydrogen gas possessing ultra-high purity. It is impermeable to larger molecules, especially organic molecules, and as a result Pd also exhibits an infinitely high selectivity towards hydrogen.

Hydrogen is highly soluble in Pd metal and diffuses through the lattice by a solution-diffusion mechanism, which is unique to Pd-H systems [37]. Also, Pd is oxidation-resistant, but where oxidation does occur the reactivity of Pd after exposure to oxygen is recovered during exposure to hydrogen because of the easy decomposition of Pd oxides [106].

The hydrogenation behaviour of Pd can be illustrated with reference to its characteristic pressure-composition isotherms (Figure 2.7).

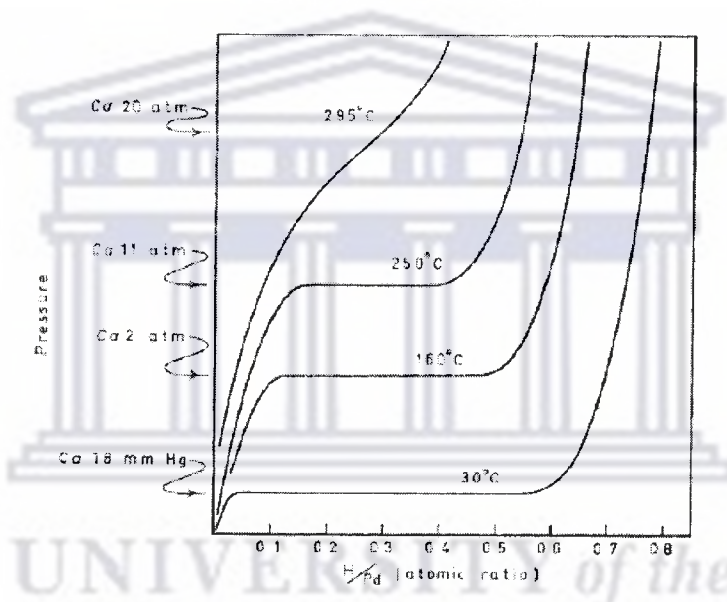


Figure 2.7. Pressure-composition isotherms for pure Pd metal in high-purity hydrogen [37]

The random dispersion of hydrogen atoms in Pd is known as the α -phase, which is a solid solution [106]. The Pd α -phase is observed at near-to-ambient temperatures and pressures and exists over a very small concentration range of the absorbed hydrogen. In this region the hydrogen occupies interstitial sites within the Pd crystal lattice. When the hydrogen atoms start to assemble themselves into an order within the Pd, and this order is long-range in nature, a β -phase Pd binary hydride is formed, as Pd-H. The Pd β -phase, is only observed once higher concentrations of hydrogen are absorbed into the Pd. The absorbed hydrogen occupies tetrahedral and octahedral

sites in the face-centred cubic crystal structure of the Pd. Also, Pd is one of the very few metals in which hydrogen occupies the octahedral sites [121].

As atomic hydrogen is absorbed into the Pd crystal lattice so the lattice parameter (a_0) of the material changes. There exists a 3% linear size difference between the face-centred cubic Pd α -phase solid solution and the body-centred cubic Pd-H binary hydride β -phase [46]. This size difference introduces dislocations and defects upon cycling Pd in H₂ at low temperatures. The phase transition will eventually lead to imperfectly reversible dimensional changes where up to a 10% increase in the unit cell volume has been stated upon inducing H/Pd ratios of 0.6 formula units [52]. Pandey *et al.* have observed the a_0 in pure Pd to increase from 3.883Å before H₂ cycling to a maximum of 4.018Å after H₂ cycling at low temperature [122]. Lewis observed the a_0 to change as follows, relative to the H/Pd molar ratio upon cycling Pd in H₂ under mild temperature and pressure [37]:

Pure Pd (H/Pd = 0.00):	$a_0 = 3.889 - 3.890\text{\AA}$
α -phase Pd-H (H/Pd = 0.015):	$a_0 = 3.893 - 3.895\text{\AA}$
β -phase Pd-H (H/Pd = 0.6):	$a_0 = 4.013 - 4.025\text{\AA}$

Under conditions of low temperature and pressure a large invariant equilibrium pressure plateau, or Pd α - β mixed-phase transitional region, is observed over a large absorbed hydrogen concentration range. The length of this miscibility gap between the α -phase and β -phase of Pd was observed to decrease with increasing temperature. Importantly, the α - β mixed-phase transitional region is associated with the hydrogen embrittlement effect in Pd, which leads to the deterioration of the structural integrity of Pd-based materials and where small defects are formed between Pd grains. Hydrogen embrittlement occurs when dissolved hydrogen gas accumulates at lattice defects, such as the Pd grain boundaries, and promotes brittle behaviour [44]. Hydrogen embrittlement is the major deterrent to the employment of pure Pd media in large-scale hydrogen separation / purification / storage from hydrogen-rich reaction zones [52]. Embrittlement of pure Pd is also observed wherever Pd is subjected to

repeated absorption/desorption and thermal cycles and as a result pure Pd does not exhibit long lifetimes in hydrogen separation / purification / storage processes. At the critical temperature ($T_c = 295 \text{ }^\circ\text{C}$) the α - β phase transition plateau is completely eradicated, as this mixed phase cannot coexist under equilibrium conditions above the T_c , with the plateau being converted into an inflexion point and the Pd absorbent making a completely direct transition from the α -phase to the β -phase [37]. In doing so the hydrogen embrittlement effect can be completely eliminated when cycling Pd in hydrogen absorption [37].

In terms of thick Pd-based continuous layers the diffusion of atomic hydrogen through the metal lattice is the rate-determining step in the permeation of H_2 . For thin Pd-based continuous layers the rate-determining step is the surface adsorption and dissociation of H_2 molecules [43]. Also, generally at temperatures greater than 300°C , the rate-determining step is the diffusion of atomic hydrogen into the Pd structure [35].

2.11. MECHANISM OF HYDROGEN SORPTION THROUGH PALLADIUM-BASED LAYERS

Pd and Pd-based materials generally catalyse the dissociation and recombination of hydrogen molecules. In terms of Pd-based layers deposited onto the surface a metal hydride-forming alloy, high quantities of atomic hydrogen can be produced by the Pd-based layer which then further diffuse into the core material. Hydrogen separation on Pd-based layers occurs via a stepwise solution-diffusion mechanism, illustrated in Figure 2.8 [36,120]:

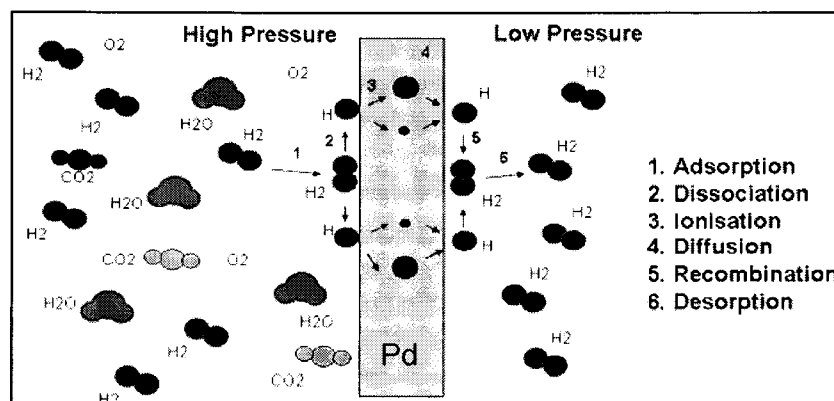


Figure 2.8. Solution-diffusion transport mechanism of H_2 through a Pd-based layer

The solution-diffusion phenomenon exhibited by Pd is constituted by stepwise processes, given as follows [123-125]:

1. H_2 molecules in the exterior gas phase surrounding the Pd layers are transported towards the laminar gas layer flowing over the surface. The molecules then physically sorbed to the Pd surface (physisorption).
2. Dissociation of the H_2 molecules occurs at the Pd catalytic surface sites. The resultant hydrogen atoms are chemisorbed to the metal surface.
3. The H atoms then diffuse through the bulk Pd lattice by occupying interstitial sites with octahedral symmetry and forming Pd hydrides (Pd-H). The H atoms diffuse through the lattice by “interstitial hopping” between octahedral sites via tetrahedral sites. The H atoms are highly soluble in Pd metal and alter the lattice properties of the metal.
4. The H atoms, pressed on by a concentration gradient, emerge on the permeate side of the Pd layer.
5. A recombination process occurs to form H_2 molecules and subsequent desorption of H_2 from the metal surface.

6. H_2 molecules are then transported away from the metal surface into the exhaust gas stream. The Pd metal retains its original lattice properties.

The basic driving force behind this type of diffusion through a Pd layer is a concentration gradient. The hydrogen diffusing to the permeate side of the Pd-based material may be considered to be of the highest purity.

2.12. APPLICATION OF PALLADIUM MIXED-METAL LAYERS IN HYDROGEN SORPTION TECHNOLOGY

Previous works by Willey *et al.* illustrated that Pd surface-modified AB_5 -type alloys were still prone to low levels of surface poisoning after long periods of exposure to air, manifesting in the gradual deterioration of hydrogen sorption capacity with repeated cycling [64]. To address this problem it was suggested that surface modification be conducted using mixed-metal coatings instead of pure Pd coatings.

It is commonly accepted that the best way to improve the sulphur-resistance of noble metal catalysts is to modify their electronic properties, where catalysts containing electron-deficient metal atoms on the surface are more sulphur-resistant. Electron-deficient species can be formed either by the interaction of metal and acid sites on a support material or by bimetallic interaction. It is known that bimetallic catalysts potentially perform better than either of its monometallic components in terms of selectivity, resistance to poisoning, and catalytic activity. The two highly-dispersed active metals are thought to exist as bimetallic clusters and the high sulphur-resistance is attributed to structural and electronic effects rather than the degree of metal dispersion in bimetallic catalysts. The bimetallic interaction may bring about an increase in the amount of electron-deficient metal sites, which may improve the sulphur-resistance by reducing electrophilic sulphur adsorption. The adsorption properties of hydrogen or H_2S on bimetallic metal surfaces are also expected to be different from those on monometallic metal surfaces due to the interaction between the two metal components.

2.12.1. Hydrogen sorption properties of palladium mixed-metal layers

Pd alone is not suitable for hydrogen uptake due to its unfavourable equilibrium pressure, high cost, and susceptibility to sulphurous gases [126]. From an economical perspective, the use of large amounts of Pd to increase the hydrogenation properties of AB₅-type alloys is not encouraged as appreciable quantities of the deposited Pd do not participate in the sorption of hydrogen [64]. Few known attempts have been made to study the influence of encapsulation of Pd-based mixed-metals on the hydrogenation performances of metal hydride-forming alloys. Employment of mixed-metal catalysts instead of single-metal catalysts for a given reaction can enhance activity and/or selectivity [127]. For these reasons the use of Pd mixed-metal coatings to enhance the kinetic rate of reaction was investigated.

Pratt *et al.* observed that AB₅-type alloys modified with mixed coatings of Pd-Ru exhibited much faster hydrogen absorption / desorption rates compared to that modified with pure Pd and Ru coatings [56]. This type of observation merits the modification of AB₅-type alloy surfaces using mixed-metal coatings instead of modification using pure Pd coatings only.

Mixed coatings of interest, gathered from an extensive review of the available literature, which may further enhance the properties of the metal hydride-forming alloys, compared to pure Pd coatings, include Pd-Cu; Pd-Ni; Pd-Ru; Pd-Pt; Pd-Ag; Pd-V; and Pd-Nb.

Copper is known to only take up very small quantities of hydrogen, the volume of which is considerably less than that observed for Pd [126]. Pd-Cu mixed metal layers may potentially possess the high selectivity and poisoning resistance required to be considered as viable candidates for the surface modification of metal hydride-forming alloys for use in separation / purification / storage of hydrogen derived from contaminated hydrogen feeds. Pd-Cu alloyed layers have been observed to reduce the deactivating effects of surface poisoning, particularly that of sulphurous compounds [128]. Bimetallic clusters of Pd-Cu may potentially have the same ability as the

corresponding alloyed Pd-Cu layers. In addition, Pd-Cu layers have been associated with enhanced resistance to thermal degradation and reduced material costs, due to a decrease in the amount of Pd used [54]. Alloys of Pd-Cu have been associated with hydrogen diffusivity superior to that of pure Pd, albeit that the hydrogen solubility decreases somewhat. [126]. Some or all the enhanced properties observed upon mixing Pd and Cu may be attributed to a change in the electronic effects [53]. It is known that hydrogen may still attack the integrity of the copper coating. Although hydrogen attack is largely eliminated by the introduction of oxygen-free copper materials, hydrogen attack nevertheless still occurs wherever oxygen-containing copper and copper alloys are exposed to hydrogen at moderate temperatures [44].

Nickel too is known to only take up very small quantities of hydrogen, the volume of which is considerably less than that observed for Pd [126]. Although the Ni-H system has been less studied than Pd-H, it is clear that Ni also absorbs hydrogen, albeit under different conditions [129]. Mixing Ni with Pd has been known to increase mechanical strength and the catalytic capacity of Pd [55]. Ni-Pd encapsulation layers have also been observed to increase the cycle lifetimes of metal hydride-forming alloys, although it was noted that the deposition was conducted sequentially with Pd as the secondary layer [47,56]. Hydrogen molecules have a strong affinity for nickel and readily dissociate and adsorb onto fresh nickel-rich surfaces. Through the addition of one atomic percent of Ni to Mg, Holtz and Imam achieved a decrease in the temperature for the onset of hydrogenation from 275°C to 175 °C, and a lowering of the dehydrogenation onset temperature from 350 to 275 °C [130]. However, the hydrogen diffusivity generally decreases with increasing nickel content [126]. By encapsulating the AB₅-type alloy particles with Pd and Ni a rich quantity of hydrogen atoms can be produced which can diffuse to the core alloy [32,63]. In addition, metal hydride-forming alloys surface-modified using Ni and Pd can potentially exhibit superior resistance towards chemical attack by surface contaminants.

The works of Willey [64], Harris [103], Pratt [56], Doyle [47] and the Johnson Matthey Company represent the only conclusive literature related to Pd-Ru

deposition on the surface of metal-hydride forming alloys. Willey *et al.* observed that Pd-Ru layers may act to protect AB₅-type materials from poisoning by air after periods of exposure [64]. Changes in the activation kinetics of these surface-modified alloys were credited to an increase in the hydrogen transfer properties. Harris *et al.* used 8.0 wt% sequentially-deposited coatings of Pd-Ru, Ru-Pd, and Pt-Ru on AB₅-type alloys [103]. Unfortunately, Willey *et al.* used only sequential depositions of Pd and Ru without consideration of the potential hydrogenation properties of AB₅-type alloys modified using co-deposited Pd-Ru coatings [64]. In addition, Doyle *et al.* have stated that where Pd and Ru are to be sequentially-deposited onto the surface of a metal hydride-forming alloy, it is advisable to conduct the Pd deposition first [47].

Platinum is known to offer extended cycle life to metal hydride electrodes in electrochemical processes, in alkaline solution, by preventing the oxidation of the electrode material [131]. Harris *et al.* found that platinum layers deposited onto the surface of AB₅-type alloys enhanced the activation kinetics at 25°C [103]. However, the absorption behaviour of Pt layers is largely affected by temperature, where low temperature leads to a large decrease in the activation kinetics of metal hydride-forming alloy encapsulated with Pt.

Silver too is known to only take up very small quantities of hydrogen, the volume of which is considerably less than that observed for Pd [126]. Pd-Ag alloys are typically used in the preparation of hydrogen separation membranes exhibiting high resistance to hydrogen embrittlement. Pd-Ag alloys have lower *4d* orbital density compared to that of pure Pd, and as a result the physical properties (electrical resistance, magnetic susceptibility) as well as the thermodynamic properties (relative chemical potential, relative partial molar enthalpy and entropy) of the Pd-Ag-H system are different from that of the Pd-H system [132]. Ag also acts as an electron donor once introduced into the Pd matrix [133]. Pd-Ag layers are favourable wherever there is a repetition in the charge/discharge of hydrogen in the absorbent material, as a result of the high mechanical stability during the absorption of hydrogen through the structure of the coating [134]. These types of coatings are also known to be highly selective

towards hydrogen. Although hydrogen is practically not soluble in pure silver, the hydrogen solubility and mechanical stability in Pd-Ag is greater than that observed in pure Pd [42,135]. Similar behaviour may potentially be realised using the deposition of bimetallic Pd-Ag mixed metal clusters.

Vanadium has a strong affinity towards hydrogen, is highly soluble towards hydrogen, and forms strong V-H hydrides which restrict movement through the coating, thus decreasing the hydrogen diffusivity. It is also known that V may facilitate the diffusion of hydrogen at room temperature [136]. V is known to possess better hydrogen permeation characteristics compared to Pd. Unfortunately, at the same time V suffers from two vital shortcomings: hydrogen embrittlement and surface complications. V absorbs hydrogen strongly and exothermically, but exhibits large-scale and rapid disintegration during repeated hydrogen sorption cycling [137]. Also, the surface of V is easily oxidized with the resultant oxide acting as a barrier towards hydrogen permeation. Increasing the V content in Pd-V mixed-metal coatings has the effect of decreasing the hydrogen diffusivity, with V substituting Pd in the crystal structure [126]. Previous investigations have been in the catalysis of hydrogen storage in activated carbon nanofibres using vanadium pentoxide [130] and hydrogen spillover catalysis on carbon nanotubes [136].

Similarly to V, niobium has a strong affinity towards hydrogen, is highly soluble towards hydrogen, and forms metastable Nb-H hydrides which restrict movement through the coating, thus decreasing the hydrogen diffusivity. Previous investigations have been in the use of Nb₂O₅ for catalysis of magnesium in hydrogen storage [138]. Unfortunately, Nb-based layers are known to suffer from hydrogen-induced fracturing, large stresses, and strains as a result of large lattice expansions in hydrogen absorption [139]; and are easily pulverised in hydrogen-rich environments [140]. Similarly to V, increasing the Nb content in Pd-Nb mixed metal coatings has the effect of decreasing the hydrogen diffusivity, with Nb substituting Pd in the crystal structure [126].

2.12.2. Conclusions from review of palladium mixed-metal layers in hydrogen sorption technology

Based on a comprehensive review of the available literature, Pd mixed-metal coatings with Ni and Cu were found to be very attractive for investigation based on their high affinity for hydrogen absorption, their prohibition of diffusion passage of oxygen to metal hydride-forming alloy surfaces, and the surface poisoning resistance they may potentially provide to metal hydride-forming alloys [141]. Encapsulation of AB₅-type alloys with sequentially-deposited Ni-Pd was also demonstrated to result in improvements in the cycle lifetime in electrochemical hydrogen sorption [55]. Similar observations may occur in the study of Ni-Pd coatings in gas phase hydrogen sorption. Pd mixed-metal coatings with Ag were considered for investigation based on knowledge of the high permeability offered by Pd-Ag alloys in hydrogen separation [142]. Pd mixed-metals with Pt were considered for investigation based on the ability of the Pd-Pt alloys to separate hydrogen isotopes (i.e. protium, deuterium, and tritium) at room temperature without disintegration of the separating element [143].

Although hydrogen separation studies using Pd-Cu, Pd-Ag, and Pd-Pt layers were conducted using the alloys thereof it is conceivable that some of the advantageous properties encountered in these materials, such as enhanced kinetic properties, can be observed and utilised upon deposition of the bimetallic clusters produced in Pd-Cu, Pd-Ag, and Pd-Pt mixed-metal deposition.

2.13. ENHANCING HYDROGEN SORPTION KINETICS AND POISONING RESISTANCE BY SURFACE DEPOSITION OF PALLADIUM AND PALLADIUM MIXED-METAL COATINGS

Composite materials developed by combining the properties of Pd-based layers and metal hydride-forming alloys may potentially have extraordinary characteristics due to a synergistic effect between the unique properties of the two components [144].

This type of composite material may potentially produce a remarkable change in hydrogenation and kinetic properties compared to that of the parent alloy.

Pd-based encapsulation may potentially give AB₅-type alloys the ability to absorb hydrogen at low temperature without a special activation step, enhanced absorption properties, and enhanced activation rates [115]. In addition, Pd-based catalytic layers have the ability to catalyse the dissociation and recombination of hydrogen, thereby increasing the stability of the absorption capacity of hydride-forming alloys in contaminated hydrogen feeds [54]. Thin metal layers are also known to increase the hydrogen absorption rate due to the removal of passive layers by a H₂-H₂O reaction on the surface at room temperature [102]. Importantly, Pd is not oxidized by H₂O, CO, or CO₂ which may thereby increase the poisoning resistance of support materials towards these specific poisoning species [113]. The resistance of Pd towards these species may lead to the protection of Ni clusters on AB₅-type alloy against oxidation when plated onto the alloy surface. The deposition of Pd and Pd mixed-metal coatings on the surface of AB₅-type alloys will also result in the virtual elimination of incubation periods in hydrogen absorption [49].

Willey *et al.* deposited up to 8.0 wt% of the total weight of the metal hydride alloy in platinum group metals using electroless plating [64]. This represents a rather large quantity of PGM's and should be drastically reduced without the reduction in performance and lifetime of the surface-modified alloy. Similarly, Geng observed significant enhancements in the hydriding/dehydriding ability of AB₅-type alloys after the electroless plating of about 1.0 wt% Pd on the surface [55]. Bratanich *et al.* observed that AB₅-Pd composites containing up to 1.5 wt% Pd demonstrated reversible hydriding/dehydriding behaviour in H₂/CO mixtures containing up to 5.0 vol% CO [54]. Also, Bratanich *et al.* observed that AB₅-Pd composites containing up to 1.0 wt% Pd demonstrated reversible hydriding/dehydriding behaviour in H₂/CO₂ mixtures containing up to 90 vol% CO₂ [113]. It should be noted that Bratanich *et al.* prepared AB₅-Pd composites by cold pressing the AB₅-type alloy with Pd black [113]. In contrast, modification methods producing more homogenous deposition of

Pd on the surface of the AB₅-type alloy were employed in this investigation. Also, acceptable quantities of Pd (~1.0 wt. %) were utilised in the surface modification of the metal hydride-forming alloys.

2.14. METHODS OF METAL SURFACE LAYER DEPOSITION

A number of methods and techniques are available for the modification of AB₅-type alloy surfaces with metal layers. Unfortunately, when the deposition of precious metal surface layers is required for practical use as a catalyst the choice of deposition methods are severely limited [145]. Different deposition methods give layers with different microstructures, particle size, and general morphology. The catalytic surface layers can be deposited by physical or chemical methods, including sputter deposition, mechanochemical deposition, chemical vapour deposition, electrolytic plating, and electroless plating. The deposition methods will further be discussed and analysed in Sections 2.14.1 – 2.14.6.

2.14.1. Sputter deposition

Sputter deposition is a coating technique in which atomized material is removed from a metal target by bombardment with highly-energetic argon atoms (due to a large negative applied voltage) within a vacuum, and subsequently deposited on the surface of a substrate situated at a fixed distance within a vacuum chamber. Generally when a positive ion collides with atoms at the surface of the metal target an energy transfer occurs. When this energy (approximately equal to the heat of sublimation) is significantly greater than the binding energy surface atoms are dislodged in the form of a “metal cloud”. The dislodged atoms travel towards the substrate, under the influence of an applied electric field, where they are coated onto the surface [146]. The sputter process has almost no restrictions in the target materials.

The grain size of Pd layers deposited on a substrate using sputtering is generally 20-50 nm [147]. It was found by McCool *et al.* that Pd-based layers deposited using

sputtering exhibited lower hydrogen permeance than that prepared using electroless plating or chemical vapour deposition [147]. This observation may be associated with the grain size of the deposited Pd layers, where smaller particle sizes lead to generally poorer absorption [148].

Ultimately, the sputtering technique is not practically preferred for application in surface modification of hydride-forming metal alloy powders [101].

2.14.2. Mechanochemical deposition

Shan *et al.* were able to introduce Pd onto the AB₅-type alloy surface by introducing controlled quantities of a Pd black powder to the core material and simply fine grinding using a mortar and pestle [49]. Large enhancements in the hydrogenation rate and activation kinetics were observed as a result. Bratanich *et al.* used a similar method, except with the use of cold-pressing instead of hand grinding, and observed similar enhancements in hydrogenation rate and activation kinetics [54,113].

A popular technique for the mechanical deposition of metal catalysts on the surface of metal hydride-forming alloys is ball-milling. Although ball-milling does not exclusively deposit metal layers on the surface, but also modifies the bulk material, it is still considered a deposition technique as it promotes changes in the hydrogenation properties by the introduction of dopants. Ball-milling of a small amount of Pd or platinum with the metal hydride-forming alloys was shown to greatly improve their hydrogen absorption and desorption performances [49]. However, ball-milling alters the physical state of the starting parent material by the introduction of catalytic anomalies into the bulk structure and for this reason introduces a degree of uncertainty into the observation of surface enhanced catalysis of the hydrogen dissociation process. Also, ball milling can introduce contaminants into the material being ball-milled. The level of contamination may or may not affect the hydrogen sorption properties of the material.

2.14.3. Chemical vapour deposition

Chemical vapour deposition (CVD) is a chemical process in which volatile reactants, diluted in a carrier gas, are decomposed onto a desired heated substrate to produce surface deposits. Unfortunately, the quantities of metals that can be deposited using CVD are limited and usage has primarily been limited to the deposition of Al, Cu, Mo, Ta, Ti, and W. The rate of reaction is quite slow and limited by the geometry of the substrate. Additional major problems include the unavailability of suitable Pd precursors with high volatility and good thermal stability [149]; and difficulty in depositing mixed-metal layers [150]. CVD also suffers from high levels of impurities and complexity [151].

2.14.4. Electrolytic plating

Electrolytic plating is a simple deposition technique with relatively low operational cost. Electrolytic plating requires the substrate material to be attached to an external electrical circuit, while submerged in a solution containing the metal of interest in cationic form, so as to activate the electrochemical process [152]. The nature of the AB₅-type alloys allows for very little of the total content of an ingot to be coated by Pd using electrolytic plating; and the use of powdered materials requires the material to be compressed into electrodes, resulting in similar problems of limited surface contact with the metal precursor solution (only the external surfaces are modified) and impracticality. Electrolytic plating is also affected by other factors such as ohmic drop and poor mass transport limitations. As a result the surface coating of Pd layers will not exhibit homogeneity as a complete electrical connection is necessary. Often the electroplated Pd metal is not fully adherent, tends to be porous, often develops cracks and is generally quite brittle.

2.14.5. Electroless plating

Electroless plating is a wet chemical reduction process in which aqueous metal ions, in alkaline or acidic baths, are autocatalytically reduced at a solid-liquid interface in the absence of an applied external electrical current to activate the process. The process involves an electron transfer across the solid-liquid interface after decomposition of a reducing agent [153]. Most PGM's can be plated onto surfaces using this technique. Deposition rate is normally in the order of $10 \text{ \AA}\cdot\text{s}^{-1}$. Grain sizes of Pd layers deposited on a substrate surface using electroless plating are usually greater ($\geq 100 \text{ nm}$) than that observed after Pd layer deposition using sputter deposition [147]. Importantly, the electroless plating technique is able to plate surface layers on materials with irregular shape (i.e. powders).

2.14.6. Conclusions from review of methods of surface layer deposition

Metal catalyst deposition techniques such as ball milling and electrolytic plating cannot simultaneously control the dispersion of catalyst particles on the surface of a substrate and facilitate the deposition of homogeneous coatings. In contrast, electroless plating offers the ability to control the surface chemistry of the modified system on a molecular or atomic domain, produce homogeneous coatings, and offers the possibility of large scale application [101,106]. It is as a result of uniformity of deposited layers, ability to plate irregular surfaces and shapes, and simplicity of equipment that electroless plating was implemented as the Pd and Pd mixed-metal layer deposition technique for the surface modification of AB₅-type alloys.

2.15. MECHANISM OF ELECTROLESS PLATING

As previously discussed, electroless plating provides metal coating on a substrate by simple immersion in a suitable aqueous solution and the decomposition of a reducing agent. Metal coatings grown through electroless plating have been valued for their macroscopic chemical and/or mechanical properties. These coatings are easy to

prepare, have very low cost, and in many cases are suitable for industrial use. Other advantages of the electroless plating technique include [163]:

- The ability to plate non-conductive surfaces such as ABS plastics (plastics based on acrylonitrile-butadiene-styrene copolymers)
- Plated layers are ductile and can be used on flexible materials such as polymeric membranes
- Deposition of metal layers of uniform thickness, concentration, and low porosity
- Thickness of the deposited layer is easily controllable and can be tailored by modification of the plating variables (i.e. plating time, temperature, metal precursor concentration, reducing agent concentration)
- The ability to plate irregular surfaces and shapes (e.g. powders)

Most transition metals can be plated using electroless plating and a multitude of bath compositions are available, each with their distinct advantages and disadvantages. Generally, each bath contains the following components: metal salt precursor; reducing agent; complexing agent; and bath stabilizer. The metal salt precursor contains the metal cations to be reduced into the metallic form; the reducing agent undergoes oxidation and provides the electrons to be donated to the metal salt precursor which is then reduced to the metal of interest; the complexing agent maintains the metal precursor cation concentration in the bath by forming a complex with the metal precursor cations thereby controlling the availability of the metal cations and preventing depletion from occurring too rapidly; and the bath stabilizer optimizes the pH of the bath thereby increasing the storage life. Other additives may be included to the bath composition to increase the metallic lustre of the deposit and to reduce mechanical stress [129]. All the components of the electroless plating bath are in a metastable state [155].

From an electrochemical perspective, electroless plating can be considered as simultaneous reactions of cathodic metal deposition and anodic oxidation of a

reducing agent based on the mixed-potential theory. According to the mixed-potential theory, both the cathodic deposition of metal and the anodic oxidation of the reducing agent occur at the catalytic surface with a mixed potential due to contributions from both partial reactions where both attempt to establish their own equilibrium [142,156]. However, the baths are formulated in such a way that the standard potentials for the reduction of the metal precursor are favoured, and therefore positive.

Two fundamental processes exist in the electroless plating process, namely surface sensitization and activation; and film growth by decomposition of the reducing agent. These processes are further discussed in Sections 2.15.1 and 2.15.2.

2.15.1. Surface sensitization and activation

Activation of a substrate by the deposition of Pd nuclei is a necessary step as without activation the deposition of metal layers onto a substrate surface would be a slow and tedious operation resulting in very low plating efficiency [157,163]. The Pd nuclei act as plating initiators and have a profound influence on the smoothness, homogeneity, coverage, adhesion, and surface quality of the deposited metal layer [158]. The Pd nuclei also have the ability to lower the activation energy for the reaction to initiate and catalyse the oxidative decomposition of the reducing agent. Activation of a substrate surface prior to electroless plating can be accomplished using a variety of techniques including thermal decomposition of the salts containing the active nuclei, and the use of activating solutions [159]. However, activation is commonly achieved by immersion of the substrate in an aqueous PdCl₂ solution.

Enhancements in adhesion of the Pd nuclei to a substrate can be accomplished by increasing the surface roughness. Sensitization of the substrate surface is commonly used to increase the surface roughness and is achieved using an aqueous SnCl₂ solution. The sensitization/activation process can be conducted stepwise or by mixing the two solutions, although for the purposes of this study the process was conducted

in a mixed mode using a colloidal solution (“exchange process”). Traditionally, the two-step process is more often used, although the one-step process is technologically attractive. The mixed acidic $\text{PdCl}_2\text{-SnCl}_2$ colloidal solution consists of colloidal particles with a core made of Pd and Sn, and surrounded by a Sn-rich layer [158,160]. The Sn-rich layer consists of hydrolysed stannic (Sn^{2+}) and stannous (Sn^+) species as well as chloride ions. The combined particle has a net negative electrical charge as the Pd^{2+} core particle is surrounded by the negatively-charged Sn-related species, and in this way interaction between neighbouring particles and their agglomeration is avoided by electrical repulsion between particles. The result is that good overall dispersion of the Pd-nuclei can be achieved over the surface of the substrate, resulting in better quality metal deposition in the electroless plating step.

A detailed description of the sensitization / activation process is given. Firstly, Sn^{2+} sensitizes and roughens the substrate surface allowing for future anchoring of Pd nuclei. Activation then commences by Pd^{2+} nucleating into Pd nuclei, assisted by the oxidation of Sn^{2+} . The process is illustrated in the following reaction: $\text{Sn}^{2+} + \text{Pd}^{2+} \rightarrow \text{Sn}^{4+} + \text{Pd}^0$

The Sn^{2+} ions attach themselves to the surface oxide or hydroxyl groups during sensitization, followed by the Pd^{2+} ions attaching themselves, by oxidation, onto the surface of the Sn^{2+} ions to form Pd metal. The complete sensitization/activation of metal surfaces can be illustrated as Figure 2.9, where M represents the metal substrate surface.

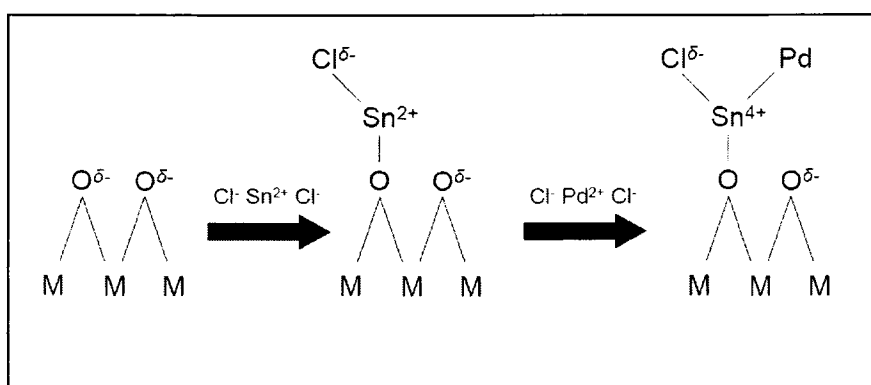
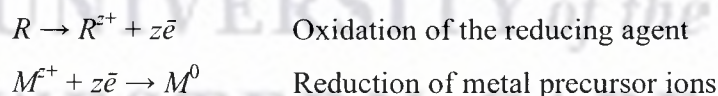


Figure 2.9. General representation of the sensitization / activation process on metal surfaces during electroless plating of metal layers on a metal substrate

The growth of the metal layer proceeds auto-catalytically, where a metal precursor is further reduced onto the Pd nuclei which act to catalyse the reduction reaction. The Sn component should dissolve back into the bulk solution as SnCl₄, but in practice some of the tin is retained on the substrate surface. Excess Sn may result in blocking of Pd surface activation sites, decreasing oxidation efficiency towards the reducing agent, and subsequent inhomogeneity of the deposited metal layer. It is therefore imperative to remove Sn from the surface during the acceleration step so as to expose the catalytic Pd nuclei. Acceleration is commonly achieved using dilute acidic solutions.

2.15.2. Film growth by decomposition of the reducing agent

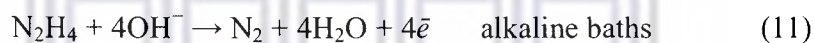
During electroless plating, electrons are generated by the partial oxidation of the reducing agent which then aids the reduction of the metal precursor ions. The general reaction can be given as follows, where *R* represents the reducing agent and *M* represents the metal:



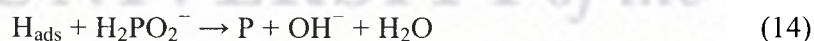
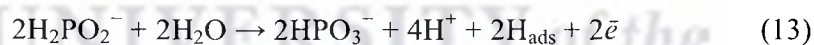
Film growth is driven by the oxidation of the reducing agent, typically sodium borohydride; sodium hypophosphite; hydrazine; formaldehyde; or dimethylamine borane. The electroless plating reaction itself is diffusion-controlled whereas the decomposition of the reducing agent is activation-controlled [156]. The use of sodium borohydride and dimethylamine borane as reducing agents for the deposition of Pd is not advisable due to the deposition of boron into the film, which may adversely affect the catalytic ability of the coating in dissociating hydrogen molecules [158,161]. Formaldehyde is not a good reducing agent due to a small potential difference

between the reduction and oxidation of the molecules. Hydrazine does not leave any impurities in metal films, although the quality of the film is not very good because of the high plating rates and instability of the plating solution. Sodium hypophosphite has been associated with traces of phosphorous in the film composition, although in the case of nickel plating (as Ni-P) the phosphorus has the effect of increasing the overall mechanical strength of the deposited film, compared to pure Ni films. The physical, electrical, and surface properties are altered with increasing phosphorus content, ranging between 1 and 14 % by weight [106]. The same observation may potentially be observed in the electroless plating of Pd-P and Cu-P.

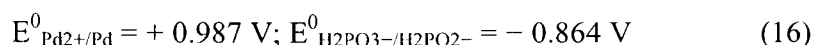
The two favoured bath formulations are based on hydrazine and sodium hypophosphite. Hydrazine is able to reduce metal ions in both acidic and alkaline electroless plating baths, donating electrons as follows [161]:



Sodium hypophosphite reduces metal ions, with the associated deposition of phosphorus within the film, by donating electrons as follows [161]:



The reduction of Pd^{2+} to Pd^0 by NaH_2PO_2 is thermodynamically favoured, considering the redox potentials of the concerned chemical couples [155]:



Bonding between the metal layer and the substrate surface occurs via metal-oxygen bond formation. The metal clusters or islands which form on the substrate surface during electroless plating are known to grow laterally and tightly coalesce to form continuous films to minimize the surface energy.

2.16. CONCLUSIONS OF THE LITERATURE REVIEW

From the classes of hydrogen sorption materials under consideration, metal hydride-forming alloys were identified as having the biggest practical potential for application in hydrogen separation / purification/ storage systems. This is a result of their ability to selectively and reversibly absorb and release pure hydrogen in hydrogenation / dehydrogenation processes.

AB₅-type metal hydride-forming alloys were identified as the one of the most attractive groups of metal hydride-forming alloys for the separation / purification/ storage of hydrogen from contaminated gas feeds due to hydrogen absorption rates nearly an order of magnitude faster than that of other metal hydride-forming alloys; reasonable absorption kinetics; and applicability in over a wide temperature and pressure range (0-200 °C; 1-200 bar).

Generally, the shortcomings of hydrogen sorption using these AB₅-type hydride-forming alloys are surface poisoning and deactivation of catalytic surface sites; low rates of hydrogen absorption due to oxide formation; the presence of incubation periods; and high activation pressures. Surface poisoning of AB₅-type alloys by electrophilic molecules (e.g. CO; H₂S; H₂O; and O₂) presents the most significant shortcoming in the separation / purification / storage of hydrogen from gaseous mixtures containing aggressive components. Surface poisoning is observed as a rapid loss in hydrogen sorption capacity and a large decrease in the overall absorption kinetics. For AB₅-type alloys to be considered suitable media in the separation / purification / storage of hydrogen from aggressive mixed gases (e.g. coal gasification product mixtures) the reaction kinetics should satisfy the sorption kinetic requirements of the gas recovery system and should demonstrate superior poisoning resistance in contaminated hydrogen.

These problems can be addressed using surface modification and nano-engineering as they are non-intrinsic and can be avoided. Encapsulation and fluorination were

identified as the most attractive methods for the surface modification of the AB₅-type alloys as a result of their phenomenal hydrogen selectivity; surface catalysis of the hydrogen dissociation process; large improvement in surface Ni content; large increase in specific surface area, and potential increase in surface poisoning resistance. In addition, no known attempts were made to study the influence of the combination of encapsulation and fluorination on the hydrogenation performances of metal hydride-forming alloys. By combination of the poisoning resistance provided by fluorination, the exceptional hydrogen selectivity of Pd-based encapsulation, and the temperature-pressure stability of metal hydride-forming alloys, sorbent materials demonstrating superior qualities in the separation / purification / storage of hydrogen from gaseous admixtures can be fabricated. From a technological standpoint, the combined approach is significant because the result may be a further improvement of the hydrogenation characteristics of the surface-modified AB₅-type alloy, compared to that modified using encapsulation or fluorination only.

Pd was identified as an exceptionally good catalyst for surface reactions involving hydrogen exchange processes as a result of its ferocious affinity towards the absorption of hydrogen. Pd encapsulation represented a means to potentially enhance hydrogen sorption rates and offer chemical protection towards the surface of metal hydride-forming alloys. For this reason Pd encapsulation was investigated as a potential surface modification technology on AB₅-type hydride-forming alloys.

It is known that pure Pd exhibits intolerance towards poisoning by extremely aggressive sulphurous gas species leading to a noticeable decline in hydrogen absorption and selectivity with repeated cycling. Also, Pd alone is not suitable for hydrogen uptake due to its unfavourable equilibrium pressure, high cost, and non-participation of large amounts of Pd in the sorption of hydrogen. Few known attempts have been made to study the influence of encapsulation of Pd mixed-metal coatings on the hydrogenation performances of metal hydride-forming alloys. Pd mixed-metal coatings with nickel and copper were identified for investigation based on their potentially high affinity for hydrogen absorption; prohibition of diffusion passage of

oxygen; and improvements in cycle lifetime during hydrogen sorption. Pd mixed-metal coatings with silver were identified for investigation based on knowledge of the high permeability offered by these the corresponding alloy materials in hydrogen separation. Pd mixed-metal coatings with platinum were selected for investigation based on the ability of the alloyed coating to separate hydrogen isotopes (i.e. protium, deuterium, and tritium) at room temperature without disintegration of the separating element. Although hydrogen separation studies using Pd-Cu, Pd-Ag, and Pd-Pt layers were conducted using the alloys thereof it is conceivable that some of the advantageous properties encountered in these materials, such as enhanced kinetic properties, can be observed and utilised upon deposition of the bimetallic clusters produced in Pd-Cu, Pd-Ag, and Pd-Pt mixed-metal deposition.

Electroless plating was identified as the method for encapsulation of AB₅-type metal hydride-forming alloys as it offers the ability to control the surface chemistry of the modified system on a molecular or atomic domain and the possibility of large scale application.

2.17. EXPERIMENTAL TASKS

From a materials science standpoint the fabrication of multiphase hydrogen sorbent materials based on AB₅-type metal hydride-forming alloys and Pd surface modification are of greatest importance in terms of efficient hydrogen extraction / purification / storage from contaminated hydrogen and delivery thereof. AB₅-type metal hydride-forming alloys modified by using the discussed approaches can result in the breakthrough hydrogen technologies and can be implemented as key elements in the greater scheme of the envisaged hydrogen economy.

Advanced surface-modified metal hydride-forming materials characterized by rapid H₂ charge / discharge cycle times and stable H₂ capacity in presence of the gas impurities will be developed. Based on the review of the literature, the scientific

approach (Figure 2.10) was formulated in the preparation of advanced metal hydride-forming alloys surface-modified using mixed-metal layers using electroless plating.

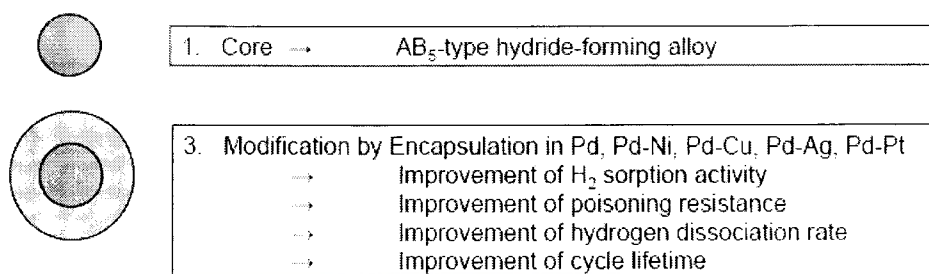


Figure 2.10. Scientific approach used in the preparation of metal hydride-forming alloys surface-modified with Pd and Pd mixed-metal layers deposited by electroless plating

A novel fluorination-encapsulation approach was also formulated and used in the preparation of advanced surface-modified metal hydride-forming alloys (Figure 2.11).

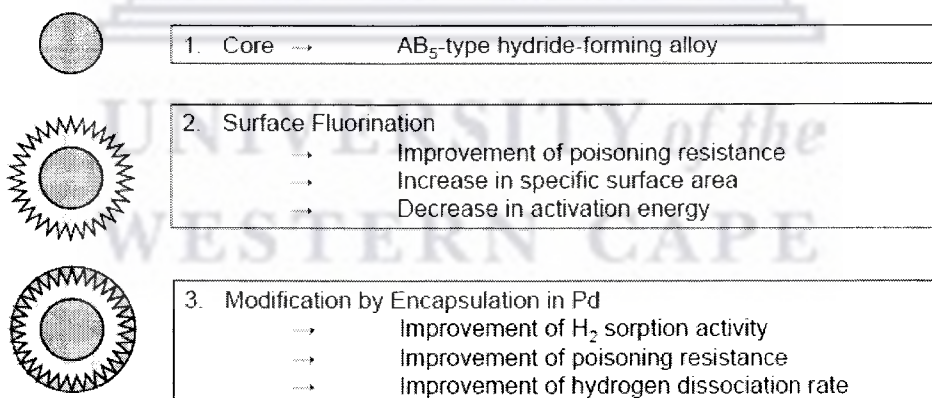


Figure 2.11. Scientific approach used in preparation of metal hydride-forming alloys surface-modified with fluoride and Pd layers deposited by a wet treatment technique and electroless plating

Based on the review of the literature the following experimental tasks were undertaken in this study:

1. Selection of a suitable mischmetal AB₅-type metal hydride-forming alloy based on an investigation of morphological; elemental; and thermodynamic data. A study of the pressure-composition isotherms of the optimal mischmetal AB₅-type metal hydride-forming alloy was conducted.
2. Preparation and structural characterization of Pd(-P) surface-modified mischmetal AB₅-type metal hydride-forming alloys.
3. Preparation and structural characterization of Pd-Ni-P, Pd-Cu-P, Pd-Ag, and Pd-Pt surface-modified mischmetal AB₅-type metal hydride-forming alloys.
4. Preparation and structural characterization of surface-modified mischmetal AB₅-type metal hydride-forming alloys subjected to encapsulation and fluorination of the surface.
5. Analysis of kinetic properties of surface-modified materials without pre-activation, under moderate conditions ($P_{H_2} = 5.0$ bar, $T = 20$ °C, 24 hours), and after ~2 week pre-exposure to air.

The research design and methodologies which address the minimum set of sample characteristics of the surface-modified AB₅-type metal hydride-forming alloys, and the experimental tasks used in their investigation, are described in detail in *Chapter 3*. Analytical tools employed in the characterization study are discussed and reviewed in detail in *Chapter 3*. The principles in their operation, sample preparation, and experimental parameters will also be discussed.

2.18. RESEARCH AREA AND HYPOTHESIS

General objectives of the study include the development of advanced materials based on metal hydride-forming alloys and platinum-group metals, using electroless plating

and fluorination, as key components of hydrogen separation / purification / storage / systems.

The problem statement of the study can be hypothesized as follows:

Development of surface modification techniques, based on electroless plating and fluorination, for the preparation of advanced composite materials, based on rare earth metal hydride-forming alloys and platinum group metals, for the effective sorption of hydrogen from contaminated feed streams. The fabricated materials should exhibit fast kinetics of hydrogenation, excellent hydrogen sorption stability, and superior dynamics of activation in non-inert environments.

In addressing the hypothesis the following sub-objectives will be satisfied:

1. Investigation of the optimal starting AB₅-type metal hydride-forming alloy material for subsequent surface modification.
2. Investigation of the optimal preparation conditions in the encapsulation of AB₅-type metal hydride-forming alloys using the electroless plating of Pd.
3. Study of the influence of secondary metal additions (i.e. Ni, Cu, Ag, Pt) on hydrogenation properties after the electroless plating of Pd mixed-metal layers on AB₅-type metal hydride-forming alloys.
4. Investigation of optimal preparation conditions in the encapsulation of AB₅-type metal hydride-forming alloys using the electroless plating of Pd mixed-metal layers.
5. Investigation of the influence of fluorination on hydrogenation properties of AB₅-type metal hydride-forming alloys.
6. Study of the influence of the combination of fluoride layers and Pd-based encapsulation layers on the hydrogenation properties of AB₅-type metal hydride-forming alloys.

2.19. RESEARCH FRAMEWORK AND DESIGN

Assumptions formulated in this study are given as follows:

1. Formaldehyde, formic acid, hypophosphoric acid, trimethoxyborohydride, sodium borohydride, and dimethylamine borane represent inefficient reducing agents in the electroless plating of Pd, Cu, Ni, Ag, and Pt on the surface of AB₅-type metal hydride-forming alloys.
2. Pd and Pd mixed-metal coatings with copper, nickel, silver, and platinum represent the most effective metal layers for surface encapsulation of AB₅-type metal hydride-forming alloys.
3. Preparation costs of the surface-modified AB₅-type hydride-forming alloys represent a fraction of the cost of that of dense Pd-based separation / purification membranes.
4. Preparation costs of the surface-modified AB₅-type hydride-forming alloys represent a fraction of the cost of that of compressed and liquefied hydrogen storage vessels.
5. Fluorination from agitation in fluoride solutions represents the most efficient method in fluorinating AB₅-type hydride-forming alloys, compared to direct fluorination in fluorine gas, electrochemical fluorination, and fluoride salt sublimation.

Metal hydride-forming alloys will be selectively modified using metal layer encapsulation and fluorination. The properties of the prepared materials will be characterized using a host of analytical techniques. The hydrogenation and kinetics properties of the surface-modified alloys represent the principle characteristics for investigation.

2.20. DELIMITATIONS OF THE STUDY

In the current study the following research areas will not be investigated:

1. Surface modification of AB, A₂B, AB₃, and A₂B₇ hydride-forming alloys or light metal hydrides (e.g. magnesium) due to time constraints and scope of the investigation.
2. Study of the influence of elemental composition of the parent mischmetal AB₅-type hydride-forming alloys on the corresponding surface-modified materials due to constraints of time.
3. Encapsulation using Pd mixed-metal layers other than those including of Ni, Cu, Ag, and Pt as the secondary metal due to time constraints.
4. Investigation of the influence of direct gas phase fluorination or alternative fluorination methods, in the preparation of AB₅-type alloys surface-modified using a combination of fluorination and encapsulation, due to time constraints.
5. Direct application of fabricated materials in hydrogen separation, purification, storage systems due to constraints of time and scope of the investigation.
6. Employment of surface-modified materials in electrochemical applications as it is outside the scope of the investigation. Likewise, electrochemical characterization of the surface-modified materials was not undertaken as it is outside the scope of the investigation.

CHAPTER 3

METHODOLOGY

Chapter 3 is dedicated to the research design of the experimental approaches for the preparation and characterization of the surface-modified AB₅-type hydride-forming alloys of interest. All aspects in the preparation of sample materials, characterization, and treatment of data will be discussed. The chapter is initiated with an introduction to the detailed methodologies for the preparation of the surface-modified AB₅-type hydride-forming alloys followed by a detailed review and validation of characterization techniques used in the study, and the experimental parameters used in their operation.

3.1. SELECTION OF THE AB₅-TYPE HYDRIDE-FORMING ALLOY PARENT MATERIAL

Mischmetal AB₅-type hydride-forming alloy powders were prepared from high-purity metals by a modified arc melting technique under an inert gas atmosphere and reduced pressure, in collaboration with the Guangzhou Research Institute of Non-Ferrous Metals (China). The metals were cast into sheets using a special high-pressure roller system fitted within a furnace. The rolling speed was varied between 5-15 m.s⁻¹. The resulting alloy sheet was annealed at 1295 °C for 2 hours under an inert atmosphere to ensure homogeneity. The sheet was then mechanically pulverized by ball-milling in a sodium hypophosphite solution and sieved. Three different compositions of the mischmetal AB₅-type hydride-forming alloy were prepared and characterized: DL1, DL2, DL4 (material identification as prescribed by the Guangzhou Research Institute of Non-Ferrous Metals). The alloys were stored in non-inert atmospheres to form metal oxide layers on the surface of the powders.

3.2. ENCAPSULATION OF AB₅-TYPE HYDRIDE-FORMING ALLOYS USING ELECTROLESS PLATING

Pd(-P), Ni-P, Cu-P, Ag, and Pt encapsulation layers were deposited onto the surface of the AB₅-type hydride-forming alloys using hypophosphite (NaH₂PO₂) and hydrazine (N₂H₄) based electroless plating baths. NaH₂PO₂ and N₂H₄ were exclusively used as the reducing agents in the electroless plating to facilitate co-deposition using mixed-metal bath formulations. In addition, no available literature was found regarding the use of NaH₂PO₂-based electroless plating baths in the surface modification of metal hydride-forming alloys. The electroless plating of mixed-metal Pd-based coatings on the surface of the alloys were conducted in sequential deposition and co-deposition modes [47].

Prior to the encapsulation of the AB₅-type hydride-forming alloy powders the surface required activation using “one-step” sensitization / activation. 5.0 g AB₅-type hydride-forming alloy powders were firstly rinsed in acetone and deionised water, dried at 80°C, and sensitized / activated in 50 mL of a Pd-Sn colloidal solution for 20 minutes at room temperature. The Pd-Sn colloidal solution was prepared as follows:

Solution A: 0.3 g PdCl₂ was dissolved in 2.15 g HCl solution and 5.0 mL deionised water at 70 °C with stirring (200 rpm).

Solution B: 25 g SnCl₂·2H₂O was dissolved in 14.5 g HCl solution (preheated to 50 °C). The mixture was cooled to room temperature after which 30 mL deionised H₂O was added.

Solution B was added to *Solution A* and *Solution (A+B)* was heated to 90-100 °C for 15-20 minutes.

Solution C: 8.75 g KCl was dissolved in 250 mL deionised H₂O. 80 mL HCl was then added to the KCl solution.

Solution C was then added to *Solution (A+B)* and made up to 500 mL with deionised water

After sensitization / activation and washing with copious amounts of deionised H₂O, filtration, and drying at 80 °C, the Sn layer was removed (acceleration) through suspension of the powders in 100 mL 100 g/L disodium ethylenediaminetetraacetic acid (Na₂EDTA) solution for 10 minutes at 250 rpm. The Na₂EDTA was dissolved by heating at 70°C, with constant agitation, and allowed to cool. The accelerated powders were then rinsed in pure CH₃OH and deionised H₂O and allowed to dry at 80°C. Fresh Pd-Sn colloidal solution was used for the activation of each sample.

Metal layers were deposited onto the surface of the activated AB₅-type alloy by immersion in 50 mL of the freshly-prepared electroless plating baths for measured plating periods and under specific plating conditions (Table 3.1). The experimental parameters are given as Figure 3.1. Plating of Pd-Cu-P; Pd-Ni-P; Pd-Ag; and Pd-Pt mixed metal layers onto the surface of the substrate was conducted using both co-deposition and sequential deposition modes. The electroless plating bath, containing the activated AB₅-type alloy, was subjected to constant agitation (250 rpm) during the reaction period, which was varied between 1 minute and 30 minutes. AB₅-type hydride-forming alloys surface-modified using the sequential deposition of two metallic layers was sensitized, activated, and accelerated prior to the deposition of each layer. 50 mL of the reducing agent (NaH₂PO₂ or N₂H₄) was rapidly added to initiate the reaction. The reducing agent was always added separately as complete Pd baths tended to be unstable during storage. This observation was identical to that observed by Rhoda *et al.* [145] and Keuler *et al.* [162], where the addition of the reducing agent was conducted using a separate solution to avoid decomposition during storage. Finally, the plated powders were washed with copious amounts of deionised water, filtered, and allowed to dry at 80°C.

All plating solutions were allowed to stabilize after immediate preparation, with mechanical agitation, for 24 hours. The buffer solution, used in N_2H_4 -based Pd and Ag electroless plating, was prepared by dissolving NaOH in H_3BO_3 solution.

Table 3.1. Pd(-P), Cu-P, Ni-P, Ag, and Pt electroless plating bath formulations and plating conditions

	Pd (NaH_2PO_2) [163]	Pd (N_2H_4) [164]	Ag (N_2H_4) [164]	Cu (NaH_2PO_2) [165]	Ni (NaH_2PO_2) [166]	Pt (N_2H_4) [163]
$PdCl_2$	2.0 g/L	2.0 g/L	-	-	-	-
$AgNO_3$	-	-	0.2 g/L	-	-	-
$CuSO_4$	-	-	-	10 g/L	-	-
$NiSO_4$	-	-	-	1.6 g/L	12 g/L	-
$NiCl_2$	-	-	-	-	1.5 g/L	-
Na_2EDTA	-	60 g/L	60 g/L	-	15 g/L	-
HCl	4.0 ml/L	-	-	-	-	-
NH_4OH	160 ml/L	200 ml/L	200 ml/L	-	-	-
NH_4Cl	27 g/L	-	-	-	-	-
$Na_3C_6H_5O_7$	-	-	-	25 g/L	1.0 g	-

	Pd (NaH ₂ PO ₂) [163]	Pd (N ₂ H ₄) [164]	Ag (N ₂ H ₄) [164]	Cu (NaH ₂ PO ₂) [165]	Ni (NaH ₂ PO ₂) [166]	Pt (N ₂ H ₄) [163]
H ₃ BO ₃	-	-	-	35 g/L	-	-
NaH ₂ PO ₂	10 g/L	-	-	35 g/L	5.0 g/L	-
N ₂ H ₄	-	30 g/L	30 g/L	-	-	1 g/L
Buffer solution	-	100 mL/L	100 mL/L	-	-	-
Na ₂ Pt(OH) ₆	-	-	-	-	-	17.5 g/L
NaOH	-	-	-	-	-	5.0 g/L
CH ₃ CH ₂ NH ₂	-	-	-	-	-	10 g/L
pH	9.8 ± 2.0	-	-	10	9.0	-
Temperature (°C)	50	60	60	70	50	25

After and prior to all depositions of metallic layers the reaction vessel was thoroughly cleaned from all metallic residues using *aqua regia* solution [167], followed by washing with copious amounts of deionized water.

Plating was conducted in alkaline solution as NaH₂PO₂ and N₂H₄ are better reducing agents in alkaline solution rather than acidic solution. The high pH value reduced losses in the metal precursor and stabilizer Ag content, facilitated high cation exchange and stability of the metal complexes, increased the Pd²⁺ → Pd⁰ turnover rate, and ensured the correct potential difference for the oxidation of the reducing agent [52,158].

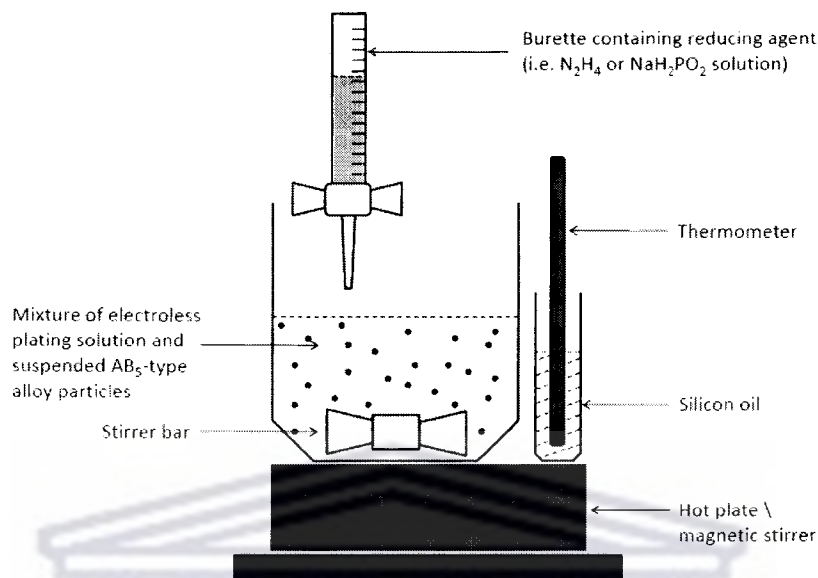


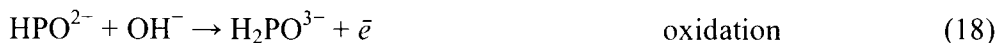
Figure 3.1. Experimental design for the surface-modification of AB₅-type hydride-forming alloy powder by electroless plating of Pd, Pt, Ag, Ni, and Cu layers

NH₄Cl was added to the NaH₂PO₂-based electroless Pd-P plating bath to form highly stable Pd complexes thereby reducing loss of Pd precursor ions in solution and to control the conductivity. Baths containing PdCl₂ and NH₄Cl are also known to produce heavy Pd deposits [167]. NH₄OH was added to provide stability, facilitate oxidation of the reducing agent, and control the buffer capacity of the electroless plating bath [129].

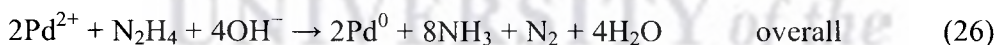
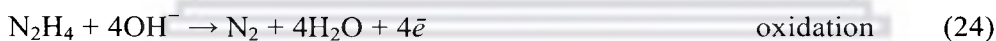
The concentration of the reducing agents were kept at intermediate strengths as low concentrations cannot drive the electroless plating process to completion and high concentrations result in precipitation of the metal of interest, as well as instability and decomposition of the electroless plating bath [168].

Deposition of Pd-P using NaH₂PO₂ as the reducing agent can be illustrated in the reaction mechanism given below [161]. Pd deposited using NaH₂PO₂ as the reducing agent included phosphorus atoms in the Pd layer, thus taking on an amorphous nature

as Pd-P. The thickness of the deposited Pd-P layers may typically be 0.2-1.0 μm , according to Zheng *et al.* [118].

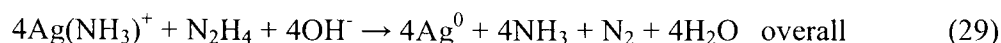


Deposition of Pd using N_2H_4 as the reducing agent can be illustrated as given below [161]. The deposited Pd layers are crystalline in nature as N_2H_4 decomposes into N_2 and H_2 only. Hampel [167] claimed layers as thick as 60 μm when depositing Pd onto metal surfaces using N_2H_4 as the reducing agent.

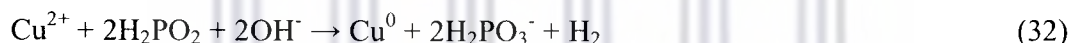
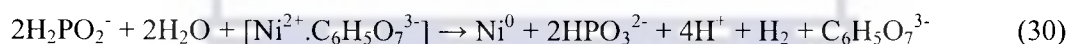


The optimal preparation conditions for the electroless plating of catalytic Pd layers on the surface of the AB_5 -type hydride-forming alloys were otherwise investigated in this study. Although the optimal conditions were known in terms of the quality and coverage of the surface, not much was known with regards to the relationship between preparation conditions in electroless plating and catalysis of hydrogenation processes on the surface of AB_5 -type alloys.

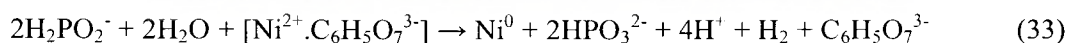
Deposition of Ag using N_2H_4 as the reducing agent can be illustrated using the following reaction mechanism [168]. The Ag layer was assumed to be crystalline in nature as N_2H_4 was used as the reducing agent.



In the case of the Cu electroless deposition bath a Ni salt was added as catalyst as Cu does not have a high catalytic activity towards the oxidation of NaH_2PO_2 [165]. The complete reaction for Cu deposition thus involves: reaction (30) reduction of Ni to the surface of the activated substrate; reaction (31) replacement of Ni metallic particles with Cu. The reaction mechanism is given below [165,169]. The deposited Cu layer will also be amorphous in nature as a result of the inclusion of P into the Cu layer to form Cu-P.



Nickel deposition by NaH_2PO_2 could be represented by the equation given below [169]. Phosphorus atoms were incorporated into the Ni coating composition to form amorphous Ni-P layers. The influence of the phosphorus atoms on the overall hydrogenation performance of the Ni-P layer was unclear, but Ni-P layers are known to demonstrate enhanced mechanical strength compared to pure Ni layers.



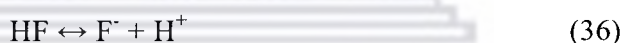
Logical steps for optimization of the encapsulation process, using electroless plating, include: Pd surface loading; Pd total loading; quality of coating; PdCl_2 concentration; deposition time; reducing agent concentration; and type of deposition (co-deposition or sequential deposition).

3.3. SURFACE FLUORINATION OF AB₅-TYPE METAL HYDRIDE-FORMING ALLOYS

Four approaches were available for the fluorination of the AB₅-type hydride-forming alloys: direct fluorination, sublimation of fluoride salts, electrochemical fluorination, and wet treatment in fluoride-containing solutions. Direct fluorination involves the formation of a fluoride shell on the alloy surface using pure or diluted fluorine gas (e.g. 5% F₂ - 95% He) [170]. However, there exists significant safety issues associated with the use of fluorine-containing gas and the process requires special gas-tight reactors and equipment. Fluorination through the sublimation of fluoride salts can be conducted using salts such as xenon difluoride, cobalt fluoride, and silver fluoride. However, the process requires special reactors and equipment; the fluoride salts are extremely costly; and rare earth metals are known to burn vigorously in halogen vapours above 200°C [167]. In electrochemical fluorination hydrofluoric acid is used as the electrolyte solution and electrochemical cycling facilitates the deposition of fluorine on the cathode. Unfortunately, the technique requires that the metal hydride-forming materials of interest be fabricated into an electrode, which does not guarantee sufficient surface coverage on the particles within the interior of the electrode. Fluorination through wet treatment involves mild agitation or ball-milling of the AB₅-type hydride-forming alloy in fluoride-containing solutions. These solutions typically contain hydrofluoric acid and the modified materials require copious amounts of washing after treatment [71,169,171].

Based on the review of the available methods, the fluorination of the AB₅-type metal-hydride forming alloy was conducted using a wet treatment technique as the procedure is simple, inexpensive, the reagents are easy to handle, and the technique does not require specialised equipment or reactors. The technique simply requires that the substrate material is stirred in a fluoride-containing solution under controlled conditions, with repeated washing.

The fluoride solution was prepared by dissolving 0.1M KF, 0.017M HF, and 0.076M NiF₂·4H₂O in ultrapure water. The solution was filtered and refrigerated overnight. 5.0g of the AB₅-type alloy powder was mechanically agitated in 100 mL of the fluoride solution for 24 hours at 70°C. After treatment, the mixture was filtered, rinsed five times with ultrapure water, and dried at 80°C [171]. For the rare earth metal AB₅-type alloys, the resultant fluoride shell was constituted by LaF₃. Wang *et al.* used a similar fluorination method and determined the resultant LaF₃ shell to be between 1-3 μm in thickness [172,173]. The wet treatment technique was accompanied by a dramatic change in the pH of the fluoride solution due to the removal of the surface oxide layer of the AB₅-type alloy (as NiO and Ni(OH)₂), the subsequent decrease in the H⁺ ion concentration, and the formation of OH⁻ ions. The F⁻ ions are supplied by the HF²⁻ ions and HF in equilibrium with the H⁺, F⁻, and HF²⁻ ions in the presence of K⁺ and OH⁻ ions [100,169]. The process can be expressed as follows:



In this solution, the most stable Ni species was NiF₆⁴⁻, which acted to replenish any nickel that had been leached out into the solution [169]. Fluorination of the alloy surface is associated with a large increase in the specific surface area due to alterations in the surface morphology upon chemical treatment [172]. Resultant increases in the reaction rate kinetics were also linked with fluorination treatment of the alloy surface.

3.4. MATERIALS CHARACTERIZATION

The enhancement of the kinetic rate of hydrogenation of AB₅-type alloys by metal layer encapsulation is a rather complex phenomenon and many additional factors should be considered in addition to transport through the alloy. Factors to be

considered include the potential presence of surface oxides on the core alloy surface, porosity, and morphology of the deposited layers [102]. For these reasons, as well as numerous others, a comprehensive characterization of surface-modified alloys was conducted.

3.4.1. Elemental analysis of surface-modified AB₅-type alloys

It was of paramount importance in the study to ascertain the density of metal deposited on the surface of the AB₅-type alloy, as well as the total quantity of metal deposited onto a unit weight of the substrate material. These properties give good indication of the magnitude of dispersion on the surface of the alloy particles, the concentration of the deposited metal used, the density of the metal deposition on the surface, and how the preparation history affects the magnitude of modification on the surface. These important properties can be analysed using energy-dispersive x-ray spectroscopy (EDS) and atomic absorption spectroscopy (AAS).

EDS is a trace analytical technique used in elemental microanalysis of sample materials. Using EDS, the surface chemical composition of materials can be ascertained and quantified (i.e. surface loading). This information gives a good indirect indication of the density of the deposited layer on the surface of the alloy. The technique is extremely versatile in that it can be used in the qualitative determination of unknown sample materials, the quantitative analysis of known elemental components, as well as in mapping the elemental distribution on the surface of the sample material. Also, the speed and ease of the analysis and interpretation of collected data is attractive. Advantages of using EDS in the quantitative analysis of the surface chemical composition of the surface-modified alloys are that trace quantities of the elemental components can be detected, the technique offers analytical precision and accuracy, and the technique is largely non-destructive where electrostatic charging is not too severe [174]. Typical applications of EDS are in the analysis of corrosion, analysis of coating composition, rapid identification of metal

alloys, identification of material phases, and determination of elemental distribution [175].

In this study, EDS was used in the quantitative determination of the surface loading of deposited metals (Pd, Pt, Ag, Cu, Sn, P), metalloid (Si), and oxygen (as oxides) as a function of the preparation history of the sample materials. It was also used in the analysis of the chemical compositions of the AB₅-type alloy starting materials.

The basis of the technique is the measurement of the interaction between high-energy electrons and the sample surface. During the interaction, electrons in the ground state of the sample material are excited by a high-energy electron beam, thus ejecting these low-energy ground state electrons from the sample surface. Electrons from the excited states then shed energy in the hope of filling the vacant ground state, with this lost energy being released in the form of x-rays phonons. X-rays phonons emitted by the sample material are detected and analysed by an energy dispersive spectrometer, including a Si(Li) or Ge solid-state detector, the data is acquired by the x-ray analyser and the relationship between the intensity of the emitted x-rays and their corresponding energies is formed to give an EDS spectrum [174]. The emitted x-rays are of differing energies which are characteristic to the atomic structure of the elements. As a result, the chemical composition of sample materials can be identified. The intensity of the identified x-rays can also be related to the quantity of certain elements in the chemical composition of the sample material. The minimum detection limits vary from about 0.1 weight percent (i.e. 10^{-9} g; 200-500 $\mu\text{g.g}^{-1}$) to a few percent depending on the element and matrix [176]. EDS analyses were conducted in conjunction with scanning electron microscopy (SEM), where the electron beam from the electron microscope was used as the electron source for EDS.

Samples were dispersed on double-sided conductive carbon tape, which in turn was adhered to aluminium sample stubs. Analysis of the surface metal loading was conducted using an EDAX Genesis spectrometer (baseline - 1500 counts-per-second, time - 100 live seconds) coupled to a Hitachi X-650 EM electron microscope

(working distance - 15 mm; accelerating voltage - 25 kV; emission current - 60 μA ; amperage time – 100 μs).

AAS is a spectro-analytical technique capable of qualitative and quantitative analyses of the elemental content of sample materials by employing absorption of mono-energetic radiation by gaseous free atoms [177]. The detection limits of the AAS technique are in the low ppm domain depending on the analyte element of interest.

In this study, AAS was used in the determination of the total elemental content of the deposited metal layer (i.e. Pd, Pt, Ag, Cu, Sn) on the AB_5 -type alloy as a function of unit weight of the surface-modified sample. This property gives a good indication of how the preparation history of the sample materials influences the magnitude of surface modification.

The principle of the technique is based on the Beer-Lamberts law (i.e. $A = \epsilon\ell C$), which relates the absorption of light by a sample material to its chemical properties. The law states a dependence of the absorbance of the sample (A) to the elemental concentration (C), the path length that the characteristic light travels through the sample (ℓ), and the absorption coefficient or molar absorptivity (ϵ) of the sample [178]. In AAS solvated metals are aspirated by a pneumatic nebulizer into either a flame, plasma, or a heated element (e.g. graphite furnace), typically at 3-6 $\text{mL}\cdot\text{min}^{-1}$. The solvent is vaporised, the particles volatilized, and the gaseous molecules are dissociated into a free atom aerosol [177]. A beam of light with a characteristic wavelength is then passed through the aerosol. Atoms corresponding to the atomic composition of the light source (i.e. hollow cathode lamp) are excited and will absorb light of the characteristic wavelength. The amount of light, and the difference in the light intensity before and after passing through the atomized metal, is monitored by a photomultiplier tube. The difference in the light intensity is then related to the absorbance of the sample material. By careful construction of a calibration curve using standard solutions the absorbance of the sample material can be related to the concentration of the metal of interest in the sample solution.

The sample solutions were prepared by acid digestion of 1.0g of the surface-modified materials in 50 mL *aqua regia* solution (1 part HNO₃ per 3 parts HCl) at 50°C for 30 minutes and 300 rpm [167]. The *aqua regia* solution formed the highly reactive NOCl species which completely decomposed all components of the sample materials [179]. The digestion was conducted under reflux conditions by inclusion of a condenser to minimise loss of the analyte metal. The solutions were allowed to cool to room temperature, were gravity-filtered, and made up to 100 mL using ultrapure water.

Dilute sample solutions were relatively stable and no significant spectral interferences were encountered. To minimize sorption losses the sample solutions were strongly acidified ($\text{pH} \leq 2$) using excess *aqua regia*, were refrigerated, were stored only in borosilicate glass, and all glassware was washed with HNO₃ and ultrapure water to remove chlorides and prevent precipitation in solution [177].

As AAS is a relative analytical method quantification requires calibration with reference standard solutions and the construction of calibration graphs [178]. Calibration standard solutions were all freshly prepared in ultrapure water. A minimum of five standards per element were prepared with the range depending on the sensitivity of the instrument towards the analyte. The concentration of the sample solutions were determined by interpolation from the calibration curves. To confirm the accuracy of the collected analytical data the calibration standard solutions were remeasured after every fifth analysis of the sample solutions and once again after the completion of analysis of all the sample solutions. A blank solution (i.e. *aqua regia* and ultrapure water) was measured directly after the calibration standards to rule out contributions from the solvent and in that way ensure the stability of the analytical baseline. Five measurements were collected for each sample solution to ensure precision in the average absorbance reported.

The experimental parameters using the spectrometer (Philips PU9100) and the elemental conditions are given in Table 3.2. The hollow cathode lamp was optimally

realigned prior to each analysis and allowed to stabilize for 30 minutes. All measurements were optimised using deuterium lamp background correction.

Table 3.2. Experiment parameters for the analysis of total deposited metal content using AAS

	Pd	Pt	Ag	Cu	Ni	Sn
Principle absorption line (nm)	247.6	265.9	328.1	324.8	232.0	224.6
Air-C ₂ H ₂ flow rate (L.min ⁻¹)	0.9 – 1.2	0.8 – 1.1	0.9 – 1.2	0.8 – 1.1	0.8 – 1.1	1.1 – 1.5
Standard solutions (ppm)	20 – 100	20 – 100	2 - 10	2 – 10	2 – 10	20 – 100
Lamp Current (mA)	11	11	3	5	11	7
Gain	80	80	80	80	80	80
Bandpass (nm)	0.2	0.5	0.5	0.5	0.2	0.5
Detection limit (ppm)	0.15	1.0	0.02	0.03		0.04

3.4.2. Analysis of surface morphology and crystallinity

Diffraction studies of surface morphology and crystalline structure of the unmodified and surface-modified materials were conducted using x-ray powder diffractometry (XRD) and synchrotron x-ray diffractometry (SR-XRD) analyses.

XRD is a valuable tool in the research and development of advanced materials. XRD is a versatile, non-destructive analytical technique in the study of crystalline and chemical structure of materials, and forms an integral part in a comprehensive characterization study thereof. XRD is capable of the identification of single and multiple phases in unknown materials and the quantification thereof, detection of impurities, determination of the crystallographic structure of materials (i.e. space group determination; indexing; structure refinement; structure identification, orientation of crystallites), texture analysis, structure deformation, residual stress analysis, studies of lattice properties, and crystallite size determination.

The pivotal role XRD plays in the structural characterization of advanced materials cannot be overstated. No comprehensive materials characterization study would be complete without an XRD investigation. Information gained from XRD analysis can be used in conjunction with chemical information to establish a structure-chemical relationship in surface-sensitive reactions.

For the purposes of this study XRD was used in the investigation of crystal/atomic structure and the identification of phases. XRD was also used in the study of the correlation between structural features of the deposited Pd layers on the AB₅-type alloy and its observed chemical properties.

In XRD, solids are bombarded with a collimated x-ray beam which causes crystal planes atoms, serving as diffraction gratings, to diffract x-rays in numerous angles. Each set of crystal planes (*hkl*) with interplanar spacing (*d_{hkl}*) can give rise to diffraction at only one angle. The diffractions are defined from Bragg's Law ($n\lambda = 2d \sin \theta$), where the intensities of diffracted x-rays are measured and plotted against corresponding Bragg angles (2θ) to produce a diffractogram. The intensities of diffraction peaks are proportional to the densities or abundance of the corresponding crystal facets in the sample lattice. Diffractograms are unique for different materials and can therefore qualitatively be used in material identification [180-182].

In the XRD analysis, dry surface-modified alloy samples were mounted in plastic sample holders and the surface was flattened to promote maximum x-rays exposure. Experimental parameters for the XRD analysis are given as follows:

X-ray Diffractometer:	Bruker AXS D8 Advance
Detector:	Sodium Iodide
Monochromator:	Graphite
Generator current (mA):	40
Electron Intensity (keV):	40

X-ray source:	Cu-K; $\alpha_1= 1.540598 \text{ \AA}$, $\alpha_2= 1.544426 \text{ \AA}$, $\alpha_1/\alpha_2= 0.497$
Scan range (2θ °):	5-100
Scan rate (°/min):	0.05

After the collection of the XRD data, Rietveld refinement of the diffractograms using General Structure Analysis System (GSAS) software was performed [183]. Refinement facilitated treatment of complex diffractograms by means of curve-fitting, in which the least-squares analysis minimized the difference between the experimental and calculated diffractograms [184]. The refinement also facilitated the quantification of the relative abundances of multiple phases on the surface-modified materials.

Ex-situ high-resolution XRD studies, using synchrotron radiation (SR-XRD), of the unmodified and surface-modified AB₅-type alloys were performed to ascertain the crystallographic structures of the sample materials.

Ex-situ SR-XRD studies enabled the study of crystallographic structure, structural phases, and quantities of each phase detected. The significance of SR-XRD is its ability to precisely resolve crystallographic features which cannot be observed using ordinary x-ray beams (i.e. CuK_α or MoK_α) as the radiation source. Advantages of the synchrotron radiation source include: high intensity, high penetration, high flux, brilliance, superior collimation, high monochromatism, high polarization, measurement time constants $> 100 \text{ s}^{-1}$ [185]. These qualities of synchrotron radiation are a direct result of the characteristic wavelength being exceptionally small compared to the size of the accelerated particles [186].

Ex-situ SR-XRD studies of the unmodified and surface modified AB₅-type alloys were performed using the BM01B diffractometer ($\lambda = 0.5000 \text{ \AA}$) coupled to the Swiss-Norwegian beam line of the third-generation synchrotron radiation accelerator (6.0 GeV) at the European Synchrotron Radiation Facility, Grenoble, France. The

experimental design for the analysis is given as Figure 3.2. Small amounts of the sample material were introduced into quartz glass capillaries (0.7 mm diameter), which were then sealed to the gas distribution system using carbon ferrules. The capillaries were connected to a goniometer head and oscillated, under vacuum, around their axis to minimize orientation effects [187]. The sample materials were then irradiated using x-rays photons from the synchrotron storage ring. After collection, the SR-XRD data was further refined by profile analysis with the GSAS software [183].

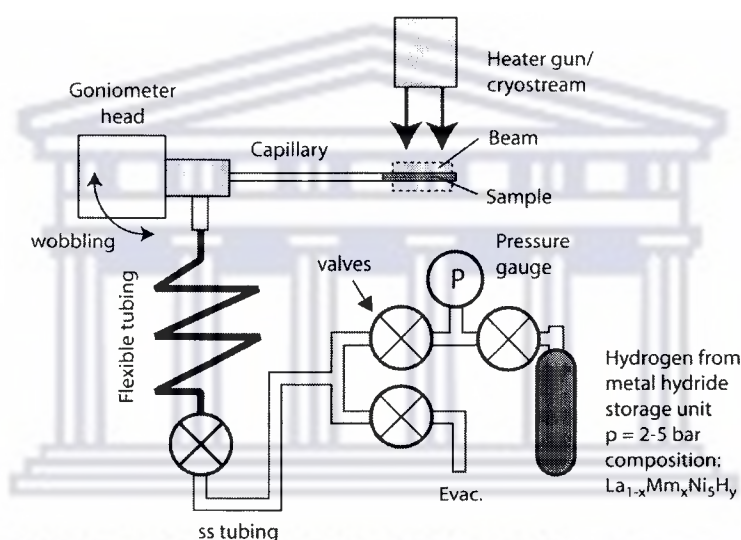


Figure 3.2 . Experimental design for SR-XRD analyses of the surface-modified AB₅-type alloys

3.4.3. Direct study of surface and structure morphology using electron microscopy

Scanning electron microscopy (SEM) is a versatile imaging technique capable of producing three-dimensional profiles of material surfaces. SEM can be used to extract quantitative and qualitative information pertaining to particle size/shape and surface dispersion. In addition, the nanometre-resolution imaging provided by high-resolution field-emission scanning electron microscopy (FESEM) makes possible the

investigation of morphological features which play vital roles in the chemical behaviour of materials [188].

In this study, high-resolution scanning electron microscopy was used in the study of AB₅-type alloy particle size/shape; AB₅-type alloy particle size distribution; Pd particle dispersion on the surface of the AB₅-type alloy particles; Pd particle size/shape; and Pd particle size distribution.

The basic operation in SEM entails the interaction of an accelerated highly mono-energetic electron beam, originating from a cathode filament, with the atoms at a sample surface. The electron beam is focused into a fine probe which is rastered over the sample surface. The scattered electrons are collected by a detector, modulated, and amplified to produce an exact reconstruction of the sample surface and particle profile [189-191].

The surface-modified AB₅-type alloy powders of interest were supported on double-sided conductive carbon tape and mounted onto aluminium sample stubs. Carbon sputtering was required wherever fluorination was performed to make the corresponding materials electron-conductive (Agar Turbo Carbon Coater; 8 seconds; 2.0 kV; 150 mA). Cross-sections of the surface-modified materials were prepared by dispersing alloy particles in a cold-mounting resin (Struers Epofix). Air was removed from the mixture using a vacuum installation (Struers Epovac). The mixture was allowed to cure overnight and was mechanically polished using 1200-grit (3.0 µm) silicon carbide paper and a polishing wheel (Struers Knuth Rotor). The sample was subsequently ion-etched (Ion Tech Ltd.; 4.0 mA; 4.0 kV; 15°; 4.0 bar Ar) and carbon coated (Agar Turbo Carbon Coater; 8 seconds; 2.0 kV; 150 mA). Ion-etching was used to remove mechanically-induced surface roughness, as a result of the polishing process, which may result in image degradation, thereby enhancing topographical contrast [176]. Carbon coating (resistivity - 3500 µΩ.cm⁻¹ at 20°C) enhanced the electrical conductivity of the sample surface which was primarily insulating as a

result of the cold-mounting resin, thereby improving topographical contrast, stabilizing the surface structure, and preventing electrostatic charging.

Four different microscopes were used in the analysis of the morphology of the surface-modified materials. Their description and experimental parameters are given:

FESEM - Zeiss Ultra 55 Limited Edition and Zeiss Supra 55VP; working distance = 3-11 mm; accelerating voltage = 5-10 kV (Norwegian University of Science and Technology, Trondheim, Norway). The in-lens and secondary electron detectors (SE) of the microscope was used to study the particle size, particle shape, particle size distribution; and coating thickness of the Pd and fluoride surface-modified materials;

HRSEM - Hitachi S-4800; working distance = 15 mm, accelerating voltage = 20 kV; emission current = 9800-11400 nA (Institute for Energy Technology, Kjeller, Norway). The scintillator-type backscattered electron detector (YAGBSE) of the microscope was used to study the particle size, particle shape, particle size distribution of the parent AB₅-type alloy materials;

SEM - Hitachi X-650 EM; working distance = 15 mm; accelerating voltage = 25 kV; emission current = 75-80 μA (University of the Western Cape). The electron gun of the microscope was also used as the electron source for EDS elemental studies of the surface-modified materials.

Calculations of surface area of the Pd-based coating, from SEM data, were carried out using the formula:

$$S = \frac{6Ks}{\rho d} \quad (37)$$

These values were repeated and averaged to yield the calculated surface area of the coating. The formula illustrated the dependence of specific surface area on particle size where S (m²/g) is the specific surface area; ρ (g/m³) is the material density; d [m]

is the diameter of a circle having the same area as the particle of interest; and K_s is the shape factor or reciprocal circularity calculated from a circle of equivalent diameter and perimeter (p [m]) as the particle of interest:

$$K_s = \frac{1}{C} = \frac{P}{\pi d} \quad (38)$$

3.4.4. Analysis of surface elemental dispersion on surface-modified AB₅-type alloys

While EDS was able to investigate the relative surface elemental composition of a given sample, particle-induced x-ray emission spectroscopy (*micro*-PIXE) has the ability to map elemental distributions of a multitude of elements over large sample areas.

Micro-PIXE is a trace analytical technique capable of yielding both qualitative and quantitative information non-destructively and without chemical separation. This was achieved through the detection of characteristic x-rays emitted by a sample surface upon bombardment with accelerated protons or α -particles originating from a particle accelerator. Using dynamic analysis, images yielding information pertaining to the chemical composition and elemental distribution on a sample surface could be constructed. An advantageous feature of *micro*-PIXE was the ability to study samples of unknown compositions. The technique had very low detection limits (1.0 ppm observed upon bombardment with 2.0-3.0 MeV protons) and large amounts of sample matrices were not necessary as 2.0-3.0 MeV beams had the ability to sample layers less than 75 μm thick [192-195].

Dynamic analysis in *micro*-PIXE was conducted to qualitatively study the surface elemental distribution of Pd, Pt, Ag, and Cu on the AB₅-type powders; and to determine whether continuous or discontinuous films were attained on the surface of the alloy.

Samples were mounted onto double-sided carbon tape, adhered to aluminium supports, and fixed into a sample holder. Prior to the analysis, the analyte particles were identified using a light microscope (Nikon SMZ1500) fitted with a digital camera (Nikon DXM1200F). The sample particles were selected in the size range 30-60 μm . Samples were then fitted into the sample holder and loaded into the *micro*-PIXE spectrometer (Oxford). Irradiation was provided by a nuclear microprobe (iThemba Laboratory for Accelerator-Based Science), where proton and α -particle beams were supplied by a 6.0 MeV single-ended Van De Graaff particle accelerator [196]. Since information at relatively good beam resolution was required, the proton beam was focused to a size $\sim 3 \times 4 \mu\text{m}^2$. Experimental parameters for the *micro*-PIXE analysis are given as follows:

Sample area (μm^2):	3 x 4
Proton accelerating velocity (MeV):	3.0
Proton probe resolution (mm):	3.0
Absorber:	125 μm Be foil
Detector-target distance (mm):	22
Total charge collected (mC):	1.0
Number of pixels:	128 x 128
X-ray analysis line:	L-shell

Analysis of PIXE spectra was performed and dynamic analysis mapping conducted with the semi-quantitative on-line imaging software package, Geo-PIXE II [197].

3.4.5. Analysis of surface chemical composition using x-ray studies

The surface chemical composition of the metal alloys may play a significant role in the hydrogenation characteristics, especially where the behaviour may be limited by surface processes. Therefore it is necessary to have succinct knowledge of the nature of the surface and the entities which may, or may not, be involved in the

hydrogenation characteristics. For these reasons, the surface chemical composition of unmodified and surface-modified metal AB₅-type hydride-forming alloys were analysed using scanning x-ray photoelectron spectroscopy (SXPS).

In SXPS, the analysis was conducted by irradiating a sample surface, under ultra-high vacuum conditions, with monochromatic x-rays to ionize atoms and liberate photoelectrons. The photoelectrons are collected and the kinetic energies of the photoelectrons analyzed to produce a spectrum of emission intensity versus electron binding energy [198,199]. The x-ray beam samples electrons emitted from the top 2–5 nm of the surface layer, giving information relevant to the sample surface and not of the bulk material. The detection limit of SXPS is approximately 0.1 at. %. The technique can be used in qualitative analysis (i.e. chemical composition, surface chemical state, surface contamination) of the elemental components of the surface since each element produces peaks which have a unique series of characteristic binding energies. Also, analysis of the peak area yields quantitative information pertaining to the corresponding elemental component of the sample surface. In this study, SXPS was used in the analysis of the surface chemical state of the surface-modified AB₅-type alloys.

A small quantity of the sample powder was mounted onto a sample stub, using conductive double-sided adhesive tape, and loaded into the spectrometer. The experimental parameters are given as follows:

Instrument:	Physical Electronics Quantum 2000
X-rays:	Al K _α
Wavelength (nm):	0.83386 nm
Photon Energy (eV):	1486.7
X-ray Power (W):	20
Beam Diameter (μm):	100
Wide Pass Energy (eV):	117,4
Narrow Pass Energy (eV):	29,35

Peak shift (calibration): Carbon

3.4.6 Determination of specific surface area by nitrogen physisorption

In the study the specific surface area of the surface-modified AB₅-type hydride-forming alloys was determined using nitrogen physisorption. By combining specific surface area information with kinetic constants a relationship can be demonstrated between surface microstructure and catalytic activity of the AB₅-type alloy after surface-modification. The technique is particularly useful when the surface morphologies of materials are unknown [200,201].

The specific surface area of the unmodified and surface-modified materials was determined using a porosity and surface area analyser (Micromeritics Tristar). The surface area analyser consisted of a mercury manometer; gas-tight burette, thermostat; liquid N₂-cooled Dewar flask, and a high-vacuum rotary pump. High pressures and cryogenic temperatures were used to increase the adsorption rate onto solid surfaces [202]. In the basic operation, solid samples are placed in an evacuated sample holder at constant temperature. The sample holder is filled with helium to flush contaminating gases from the sample surface and pores. The helium is then purged from the system. Evacuated samples are cooled to -196 °C in a liquid N₂ bath while the sample holder is filled with high-purity N₂ gas. Pressure within the sample holder is monitored over time and then rapidly reduced to reach an equilibrium state where the quantity of gas adsorbed onto the surface is equivalent to the quantity of gas removed from the gas phase. By plotting the quantity of N₂ adsorbed versus the equilibrium pressure an adsorption isotherm is obtained, which together with the Brunauer-Emmett-Teller (BET) equation can be used to determine the specific surface area of the materials of interest. This adsorption isotherm can be defined as the plot of the dependence of the fractional coverage of surface-adsorbed molecules on pressure, at constant temperature [203]. The BET equation can be given as follows:

$$\frac{1}{W[(P_0/P) - 1]} = \frac{1}{W_m C} + \frac{(C-1)}{W_m C} \frac{P}{P_0} \quad (39)$$

where W is the weight of N_2 adsorbed at a given relative pressure (P/P_0), W_m is the weight of gas producing monolayer coverage, and C is a constant related to the heat of adsorption.

Approximately 5.0g of the sample material was dried for 3 hours in a vacuum oven at 80°C. The sample material was then transferred to a quartz sample tube and dried overnight at 200°C under constant nitrogen flow (50 mL/min) using a drying apparatus (Micromeritics Flowprep 060 Degasser). Calibration with a silica-alumina standard was conducted prior to analysis. The density of all sample materials was given as 7.9 g/cm³ as determined from the x-ray diffraction analysis. A 15-point BET surface area analysis in nitrogen (pressure range = 0.01 - 0.9 P/P_0) was used as the analysis method. An isothermal jacket and filler rod were used.

Determination of the surface area of the Pd-based coating (S) on the alloy substrate (S_0) was calculated from the BET results, and was estimated as follows:

$$S^* = \frac{S - S_0}{X_{Pd}} \cdot 100 \quad (40)$$

where X_{Pd} [wt. %] is the total loading of Pd on the surface-modified material, determined from AAS analysis.

3.4.7. Construction of pressure-composition isotherms of the parent AB_5 -type hydride-forming alloy

The construction of pressure-composition (PCT) isotherms was vital in determining the applicability of metal hydride-forming materials in hydrogen separation /

purification / storage systems. The isotherms gave a clear understanding of the hydrogenation / dehydrogenation properties and phase changes occurring in the hydrogen sorption material, hydride stability, and equilibrium relationships between the hydrogen pressure and hydrogen concentration. These isotherms are very sensitive to variations in composition and homogeneity of metal-hydride forming materials and were therefore an excellent method in assessing the quality of fabricated materials [204]. The PCT relationship describes the dependence of the hydrogen equilibrium pressure on the quantity of hydrogen absorbed into the metal hydride-forming alloy at constant temperature [205].

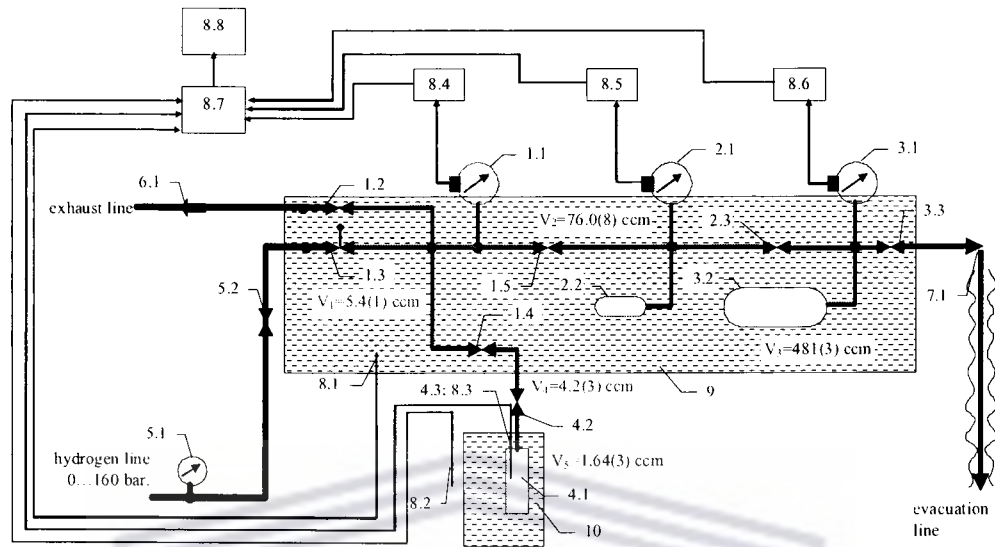
The construction of PCT isotherms for the unmodified AB₅-type hydride-forming alloy facilitated the determination of the hydrogen sorption capacity, thermodynamic properties such as entropy (ΔS) and enthalpy (ΔH), and the absorption behaviour of the starting material [184]. ΔH gives a good indication of thermal stability of metal hydride-forming alloys of interest and is directly related to the hydrogen dissociation process [206]. It was determined from Van't Hoff plots of $[(\log P) \text{ vs. } T^{-1}]$ and was ultimately used in screening the starting materials.

The construction of PCT isotherms was conducted using a Sieverts-type volumetric installation (South African Institute for Advanced Material Chemistry, SAIAMC). The installation conducted precise volumetric measurements of quantities of hydrogen absorbed or desorbed by hydrogen sorption materials. The procedure consists of determining the quantity of hydrogen absorbed or desorbed by the material at systematically varied equilibrium pressures at a fixed temperature, and after thermal activation in vacuum. The installation consists of gas distribution, control, and measurement systems. The pressure within the system was monitored using 2.5, 16, and 160 bar absolute pressure transducers. The estimated accuracy in the determination of the H sorption capacity was estimated as $\sim 1.1 \text{ cm}^3 \cdot \text{bar}$ at STP (or $\sim 0.04 \text{ H/AB}_5$ formula units). A schematic diagram of the installation at SAIAMC is given as Figure 3.3. All parts were machined from 316L stainless steel (Swagelok) to prevent carbon segregation and hydrogen embrittlement, and maintain a high heat

transfer coefficient making measurements up to 500°C and 160 bar H₂ possible. Sealing in the autoclave reactor, prior to each analysis, was achieved using stainless steel gaskets and 0.5 µm-rated filter gaskets (Swagelok). The volume of the system was regularly calibrated to ensure accuracy in collected data.

1.6 g of the AB₅-type alloy powder was loaded into the reactor housing and activated by heating to 200 °C in a muffle furnace in vacuum better than 1.0×10^{-5} mbar for 90 minutes, followed by hydrogenation (99.999% H₂) at room temperature (final pressure 12 bar, calculated H sorption capacity corresponded to H/AB₅ = 5.70). After the first cycle subsequent hydrogenation occurred rapidly: more than 90% of the maximum H capacity was reached within 1 minute. The hydrogen sorption performances of the alloy were reproducible within the second hydrogenation cycle. As a result, the measurements of the PCT characteristics of the starting material were initiated from the third cycle and included the reactivation of the sample (T = 200 °C, vacuum better than 10^{-5} mbar, duration 5–10 hours) followed by subsequent measurements of absorption and desorption isotherms through the specified temperatures (30, 90, 150 °C) using standard volumetric procedures. All the calculations of the quantity of hydrogen gas absorbed or desorbed were performed taking into account its compression factor, and the post-treatment of the recorded data was similar to that described by McLennan *et al.* [207].

Hydrogen absorption / desorption isobars were also constructed, in which the parent AB₅-type alloy was heated at a slow rate (T = 0-200 °C), after equilibration at a fixed hydrogen pressure (P = 0.1-10 bar H₂), while monitoring the absorbed / desorbed hydrogen concentration. The isobars illustrated the temperature dependence of the material of interest.



- | | |
|---|--|
| 1. High-pressure collector: | 5. H ₂ supply line: |
| 1.1. Pressure sensor 160 bar FS | 5.1. Manometer 160 bar FS |
| 1.2. Exhaust valve | 5.2. H ₂ supply valve |
| 1.3. H ₂ input valve | 6. Exhaust line: |
| 1.4. Reactor valve | 6.1. Check valve |
| 1.5. Medium-pressure connection valve | 7. Evacuation line |
| 2. Medium-pressure collector: | 7.1. Vacuum valve |
| 2.1. Pressure sensor 16 bar FS | 8. Data acquisition system |
| 2.2. Buffer cylinder 75 cm ³ | 8.1. Thermistor measuring bath temperature |
| 2.3. Low-pressure connection valve | 8.2. Thermistor measuring room temperature |
| 3. Low-pressure collector: | 8.3. Thermocouple measuring sample temperature |
| 3.1. Pressure sensor 2.5 bar FS | 8.4. 160 bar pressure indicator / transmitter |
| 3.2. Buffer cylinder 500 cm ³ | 8.5. 16 bar pressure indicator / transmitter |
| 3.3. Evacuation valve | 8.6. 2.5 bar pressure indicator / transmitter |
| 4. Reactor assembly | 8.7. 34970A data acquisition / switch unit |
| 4.1. Reactor body | 8.8. PC |
| 4.2. Gas connection line with locking valve | 9. Bath (filled with ethylene glycol) |
| 4.3. Thermocouple | 10. Thermostat / furnace |

Figure 3.3. Schematic diagram of the Sieverts-type volumetric installation at SAIAMC

3.4.8. Analysis of dynamics in hydrogen absorption using surface-modified AB₅-type hydride-forming alloys

The kinetics of the surface-modified materials is dependent both on the bulk and surface properties of the materials, which were both fundamental factors in determining whether sample materials are of practical interest in hydrogen separation / purification / storage applications. A study of the sorption kinetics of the modified

materials would give valuable insight into the surface reactivity, reaction mechanism, poisoning resistance, and catalytic activity towards hydrogen on the surface-modified materials [208]. With that, the influence of surface modification on the hydrogen sorption performances of AB₅-type hydride-forming alloys was studied by a comparison of the dynamics of activation in hydrogen absorption under mild temperature and pressure, after ~2 week pre-exposure to air, and without pre-activation by simultaneous heating and evacuation. A similar method was used by Willey *et al.* after 150 min exposure to air at room temperature [64]. Since all the experiments were carried out under the same conditions, their results can be considered as a semi-quantitative estimation of the influence of the surface modification on the tolerance of the materials to their surface poisoning by innocuous, retarding, reactive, and poisoning impurities present in air. Species typically present in air, and their standard concentrations include: N₂ (78.08 %), O₂ (20.95 %), Ar (0.93 %), H₂O (0.4 %), CO₂ (0.04 %), Ne (2 x 10⁻³ %), He (5 x 10⁻⁴ %), CH₄ (2 x 10⁻⁴ %), Kr (1 x 10⁻⁴ %), H₂ (6 x 10⁻⁵ %), NO (5 x 10⁻⁵ %), Xe (9 x 10⁻⁶ %), O₃ (7 x 10⁻⁶ %), NO₂ (2 x 10⁻⁶ %), I₂ (1 x 10⁻⁶ %), CO (< 1 x 10⁻⁶ %), and NH₄ (< 1 x 10⁻⁶ %) [209].

The kinetic curves were constructed by relating the quantity of hydrogen lost from a reference pressure in a known volume to the quantity of hydrogen gas absorbed by a sample material. By ensuring that the gas distribution system is leak-free all changes in the hydrogen pressure of the volumetric system could be attributed to absorption by the sample material. The number of moles present in the system from the onset of the reaction, under experimental conditions, was determined accurately using the ideal gas relationship ($n = PV/RT$) and corrected for deviation from this relationship using a compressibility factor (Z) to yield $n = PV/ZRT$.

The analysis was conducted using volumetric installations at SAIAMC (Figure 3.3) and the Institute for Energy Technology (IFE) (Figures 3.4). The installation at IFE was fitted with differential and absolute pressure transducers allowing for measurement of incremental changes in the starting pressure of the buffer cylinders.

$$(H/AB_5) = (H/AB_5)_{\max} \cdot \left\{ 1 - \exp \left[- \left(\frac{t}{t_0} \right)^n \right] \right\} \quad (41)$$

where (H/AB_5) was the actual hydrogen concentration in the alloy; $(H/AB_5)_{\max}$ was the maximum hydrogen concentration in the alloy (equal to 5.0 formula units, determined in the corresponding PCT studies); t is time; t_0 is the characteristic time of the hydrogenation (reciprocal rate constant); and the index n is the morphological parameter and is related to the reaction mechanism or the dimensionality of growth.

Førde *et al.* found that the values for n were generally below 1.0 wherever thermal ballast (e.g. Cu powder) was not used, which is the case in this investigation [212]. Using the reciprocal of the best value fitted for t_0 , the rate constant (k) was calculated, which was representative of the activation kinetics at the alloy surface, and therefore indirectly related to the resistance of the surface to degradation after prolonged exposure to non-inert environments (i.e. poisoning resistance).

3.5. LIMITATIONS IN THE CHARACTERIZATION OF SURFACE-MODIFIED AB₅-TYPE HYDRIDE-FORMING ALLOYS

Fundamental and fairly novel analytical techniques, used in this study, are not without limitations or restrictions in their resolution or applications. Electron microscopy may allow for the imaging of nanophase Pd-based catalysts on the surface of the AB₅-type hydride-forming alloys, but suffers from the time taken in statistical sampling of data, preparation artefacts, and the destructive nature of the technique.

In terms of XRD particle sizing, the use of the Scherer equation may lead to inconsistencies in particle sizing data. This is due to the Scherer equation being developed for spherical particles, whereas many metal nanoparticles are irregular in shape.

The contribution of Ni-P particles in the deposited layers were difficult to separate from the analytical signal for the AB₅-type alloy as the surface matrix was predominantly constituted of Ni. As a result the deposited layer was difficult to detect using elemental analysis techniques such as PIXE, EDS, and AAS.

A loss of data at the onset of hydrogenation was observed as a result of the time resolution of the data acquisition system and the large instantaneous change in volume open exposing the sample in the reactor to hydrogen. As a result, the molar fraction (H/AB₅) did not start at absolute zero.

3.6. CONCLUSIONS OF THE METHODOLOGY

AB₅-type hydride-forming alloys were surface-modified, in this investigation, for the purposes of increasing the absorption kinetics and poisoning tolerance for application in hydrogen separation / purification / storage systems. Layers of Pd, mixed metals, and fluorine were used to modify the surface of the alloy. The surfaces were modified using the electroless deposition of Pd, Pt, Ag, Cu, and Ni.

Logical steps for optimization of the encapsulation process, using electroless plating, included: Pd loading; quality of coating; Pd concentration; deposition time; reducing agent; type of deposition (co-deposition or sequential deposition).

The preparation methods were comprehensively discussed and scrutinized; the selection of characterization techniques was justified in terms of a review of the properties of interest and analytical considerations; the fundamental principles of the selected characterization techniques were discussed and their operational parameters were given; and methods in the post-analysis treatment of data were discussed. Characterization techniques used in this investigation included SR-XRD, SEM, EDS, AAS, PIXE, SXPS, N₂ physisorption, PCT studies, and kinetic analysis in hydrogenation.

CHAPTER 4

RESULTS AND DISCUSSION

4.1. SELECTION OF THE PARENT AB₅-TYPE METAL HYDRIDE-FORMING ALLOY

The first step undertaken in developing the advanced composite materials for application in hydrogen separation / purification / storage systems was to find the most suitable alloy amongst the numerous currently available, through a comprehensive literature review, which would operate over the required pressure and temperature range. It followed that the prime criterion aiding selection was the initial resistance to surface poisoning. Based on this criterion it was decided that rare earth metal AB₅-type alloys were the most suitable for surface-modification and application in hydrogen separation / purification / storage systems.

Three different available compositions of the mischmetal AB₅-type hydride-forming alloy, categorized as DL1; DL2; DL4 by the Guangzhou Institute for Non-Ferrous Metals, were analysed in terms of surface morphology, elemental composition, and thermodynamic properties in determination of the best parent alloy for surface modification in this investigation.

4.1.1. Morphology and crystallinity of the mischmetal AB₅-type alloys

The surface morphologies of the available mischmetal AB₅-type alloy powders were analysed by SEM analysis, using both SE and YAGBSE detectors.

Images of the AB₅-type (DL1) alloy are given as Figure 4.1 (a)-(b). The alloy powder consisted of particles varying in size (~10-100 μm), which generally exhibited irregular shape and relatively smooth surfaces, which were free of porous structure.

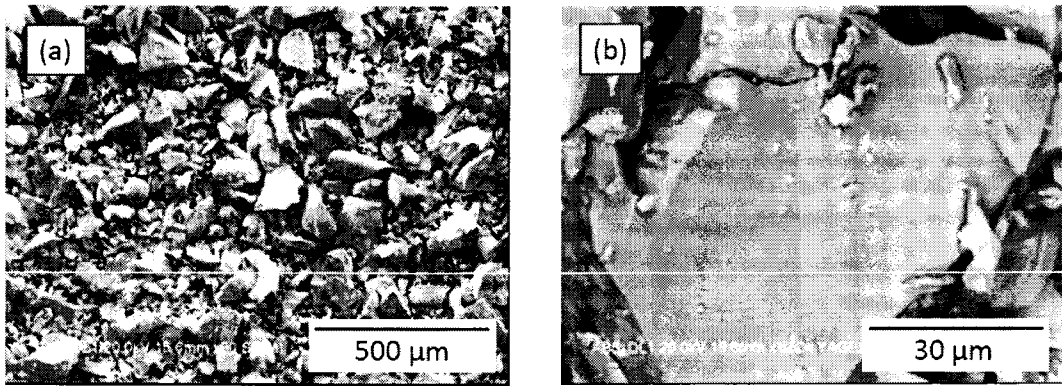


Figure 4.1. SEM images of AB₅ (DL1) alloy, (a) 90x mag. (SE); (b) 1500x mag. (YAGBSE)

Images of the AB₅-type (DL2) hydride-forming alloy are presented as Figure 4.2 (a) and (b). The morphology of the alloy powder was similar to that of the AB₅ (DL1) powder (Figure 4.1), however the material possessed a smaller particle size (~10-50 μm) compared to that of the AB₅-type (DL1) alloy. The surfaces of the alloy were relatively smooth and free of porous structure.

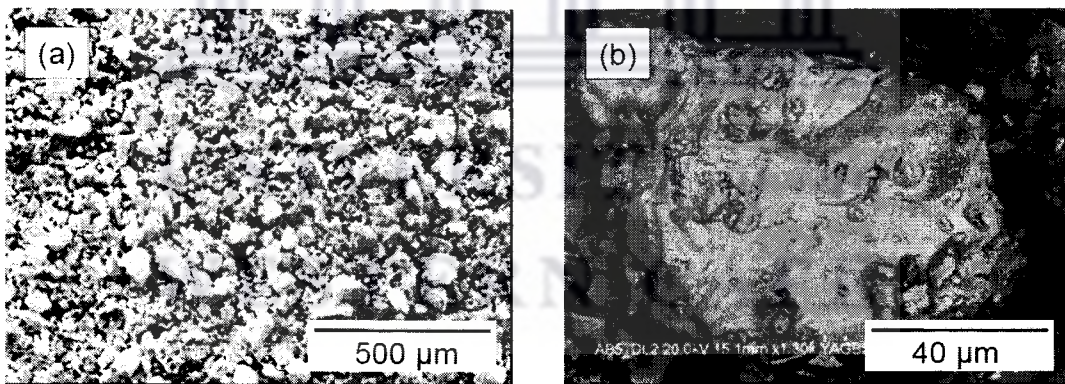


Figure 4.2. SEM images of AB₅ (DL2) alloy, (a) 100x mag. (SE); (b) 1300x mag. (YAGBSE)

Images of AB₅-type (DL4) alloy are given in Figure 4.3 (a) and (b). Generally, the particle size was slightly larger compared to that of the other two AB₅-type alloys. The surfaces of the alloy were relatively smooth and free of porous structure.

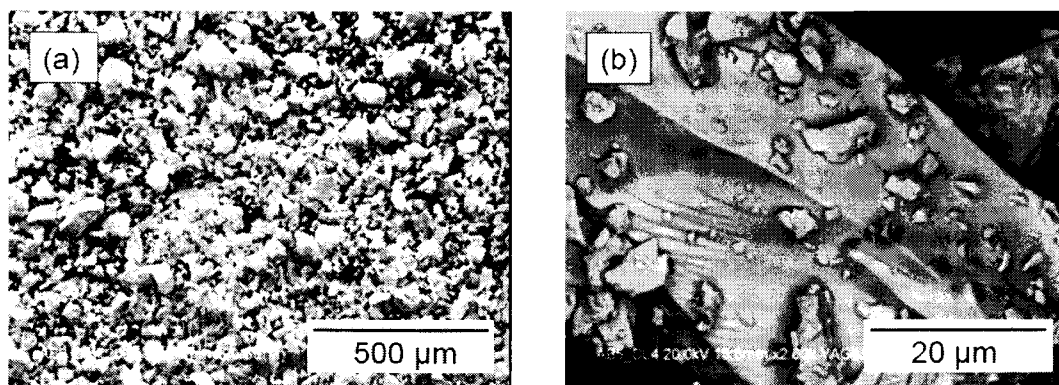


Figure 4.3. SEM images of the AB₅ (DL4) alloy, (a) 90x mag. (SE); (b) 2000x mag. (YAGBSE)

The particle size distribution of the AB₅-type (DL4) alloy powder was determined, using Carl Zeiss Axiovision[®] software, as ~10–90 μm representing about 90% of the particles (Figure 4.4). It was observed that the majority of the AB₅ (DL4) alloy particles have particle size ~10–30 μm. The estimated specific surface area (0.05 m²/g), taking into account particle shape distribution and the introduction of a particle shape correction factor (K_S) corresponded well to the measured N₂ physisorption results (0.045 m²/g). The K_S (Figures 4.5) was introduced to indicate how much the specific surface area exceeded the area of a sphere having the diameter d .

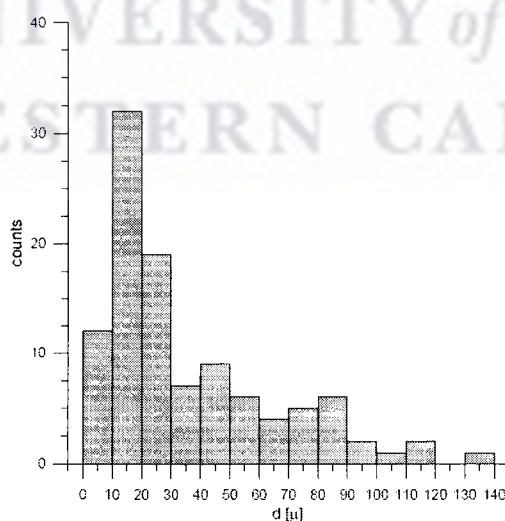


Figure 4.4. Particle size distribution histogram determined from SEM data for AB₅-type (DL4) alloy

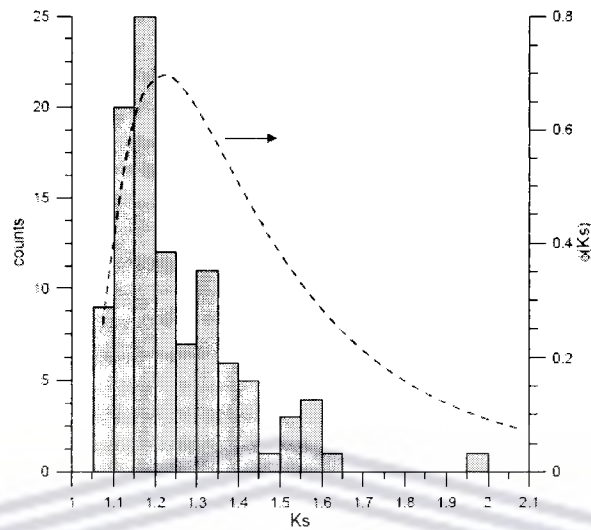


Figure 4.5. Shape factor distribution histogram for AB₅-type (DL4) alloy determined from SEM data

It was observed from Figure 4.5 that most of the particles have shapes which differ from being ideally spherical as the majority of particles have a shape correction factor greater than $K_S = 1.0$, which corresponds to a perfect sphere.

4.1.2. Comparison of chemical composition of mischmetal AB₅-type alloys

In parallel to the SEM studies, EDS analyses were conducted to determine the elemental compositions of the mischmetal AB₅-type hydride-forming alloy powders.

The EDS analysis of the AB₅ (DL1) alloy (Table 4.1) illustrated that the composition of the material corresponded to the formula A_{1.16}B_{4.84} (A = La, Ce, Nd, Pr; and B = Ni, Co, Al, Mn), which was relatively close to the AB₅-type alloy stoichiometric composition.

EDS data of the AB₅ (DL4) alloy (Table 4.3) showed that the composition of the sample corresponded to the formula A_{1.22}B_{4.78}, meaning it was slightly enriched in the rare-earth “A” component compared to the AB₅ (DL1) and AB₅ (DL2) alloys. The AB₅ (DL4) alloy also had the highest cerium and lowest lanthanum concentrations, as well as similar Mn and Co contents compared to the AB₅ (DL2) alloy.

Table 4.3. Quantitative elemental composition data for the AB₅-type (DL4) alloy

Elemental Line	Net Counts	Weight %	Atom %
Al <i>K</i>	821	3.80	10.10
Mn <i>K</i>	1786	7.18	9.37
Co <i>K</i>	1613	8.41	10.23
Ni <i>L</i>	3102	40.94	50.01
La <i>L</i>	4343	13.42	6.93
Ce <i>L</i>	5064	19.70	10.08
Pr <i>L</i>	439	1.52	0.77
Nd <i>L</i>	1364	5.03	2.50
Total	-	100.00	100.00

Based on the EDS results and knowledge of the benefits of the specific additions to the mischmetal alloy, AB₅ (DL1) was assumed to potentially have the strongest affinity towards hydrogen; AB₅ (DL2) was assumed to potentially have improved cyclic stability, hydrogen sorption capacity retention, and activation; and AB₅ (DL4) was assumed to potentially have improved cyclic stability, improved activation, the ability to minimize volume expansion upon hydrogenation, and lowest equilibrium pressure [39,213].

Comparison of the fractions of the “A” components of the AB₅-type metal hydride-forming alloys (Table 4.4) indicated that AB₅ (DL4) was a typical mischmetal alloy, meeting all the criteria thereof. AB₅ (DL1) and AB₅ (DL2) did not meet all the criteria of typical mischmetal hydride-forming alloys [213,214]. Based on its higher

cerium content observed in the analysis of the “A” component, the AB₅-type (DL4) alloy was determined to be a potentially better starting material for hydrogen separation / purification / storage applications. The high Ce content of the AB₅ (DL4) alloy should facilitate the lowest thermal stability (ΔH) among the studied alloys, and therefore greater ease in expelling absorbed hydrogen from the material due to a lower metal-hydrogen binding energy.

Table 4.4. Fractions of the “A” components of the studied AB₅-type alloys

Sample	Fraction of “A” component, %			
	La	Ce	Pr	Nd
DL1	54.47	31.16	5.32	9.04
DL2	46.59	36.36	6.04	11.00
DL4	34.17	49.70	3.80	12.33
Typical mischmetal AB ₅ -type alloy content	25 – 30	40 – 50	4 – 15	4 – 15

The chemical state of alloy surface is largely influenced by the nature of the “B” component. The AB₅ (DL1) alloy contained less Ni (substituted by Co and Mn), and it is known that Ni segregates to the surface to yield clusters that are catalytically-active towards hydrogen dissociation / recombination processes. On the other hand, Co has a higher affinity than Ni towards oxygen and this alloy is therefore more easily surface-oxidized. This observation made the AB₅ (DL1) alloy unfavourable for use as the substrate material in this investigation. AB₅ (DL2) and AB₅ (DL4) alloys had almost identical compositions in terms of the “B” component. Table 4.5 illustrated the distribution of fractions of the “B” components for the studied alloys. All three alloys were observed to be hypo-stoichiometric (i.e. B/A < 5).

Table 4.5. Fractions of the “B” components of the studied AB₅-type alloys

Sample	Fraction of “B” component, %				B / A
	Al	Mn	Co	Ni	
DL1	9.54	8.52	18.84	63.11	4.17
DL2	10.47	12.35	12.07	65.12	4.17
DL4	12.67	11.76	12.83	62.74	3.93

4.1.3. Thermodynamic analysis of the AB₅-type hydride-forming alloys

Changes in the thermodynamic properties of the studied AB₅-type alloys could be estimated from known thermodynamic data for other AB₅-based hydride-forming alloys, where Ni is substituted with Al, Mn and Co, and La with Ce [214,215]. Since similar data for hydride formation entropies (ΔS) are unavailable, a typical value of $\Delta S = -110 \text{ J}/(\text{mole H}_2 \text{ K})$ was assumed as a fixed value.

The enthalpies for the formation of hydrides (ΔH) from similar metal hydride-forming alloys facilitated the investigation of the influence of the i -th factor (i.e. the fraction of a substituting metal relative to the total amount of A or B components), on the stoichiometry (X_i) of the studied AB₅-type alloys and the heat of formation of the corresponding hydride (Y). This influence was determined from equations (1) and (2). Assuming the independence of all the factors, the total influence was roughly estimated using equation (2).

$$Y = A_i X + B_i \quad (1)$$

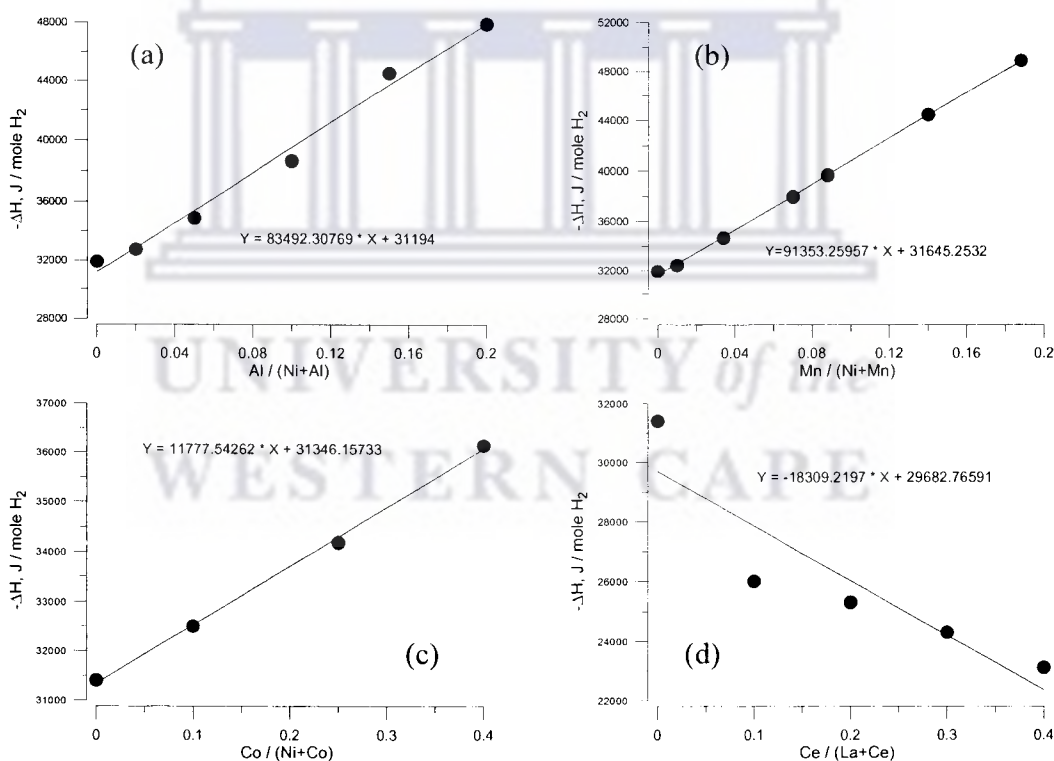
$$Y = \sum_{i=1}^n A_i X_i + \bar{B}; \quad (42)$$

$$\bar{B} = \frac{\sum_{i=1}^n B_i}{n}$$

Confirmation of the model presented in equation (2) was carried out using literature data for similar AB₅-type alloy compositions [216]. It was determined that the model

facilitated the qualitative prediction of changes in the stabilities and thermodynamic properties of AB_5H_x hydrides upon changes in their Ce content.

The corresponding reference data for the formation enthalpies of the metal hydrides (ΔH) are presented in Figure 4.6 (a–e) [214,215]. It was clear that the increase in the content of Al, Mn, and Co had the effect of increasing the ΔH and energy necessary for hydrogen expulsion (Figures 4.6 (a–c)), whereas increasing the Ce content (Figure 4.6 (d)) decreased the ΔH . The non-stoichiometric $LaNi_{5-x}$ alloy (Figure 4.6 (e)) took into account the mixture of all additives and illustrated the importance of the composition of the “A” component in determining the final ΔH value, and the influence of the Ce content in determining the stability of the hydride.



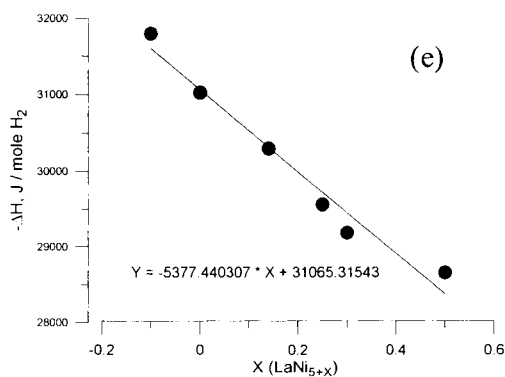


Figure 4.6. Determination of hydride formation enthalpies for reference AB₅-type alloys: (a) La(Ni,Al)₅; (b) La(Ni,Mn)₅; (c) La(Ni,Co)₅; (d) (La,Ce)Ni₅; (e) non-stoichiometric LaNi_{5+x}

The enthalpy of hydride formation (ΔH) was determined from the following equation:

$$\ln P = -\frac{\Delta S}{R} + \frac{\Delta H}{RT} \quad (43)$$

where, ΔS = entropy of formation, ΔH = enthalpy of formation, R = ideal gas constant (8.314472 J.K⁻¹.mol⁻¹).

Estimated thermodynamic properties for the AB₅-type alloys are presented in Table 4.6. The hypo-stoichiometry of the alloys was not taken into account and the fractions of the components were related to the AB₅-type alloy composition.

Table 4.6. Calculated values of thermodynamic properties of the studied AB₅-type alloys

Starting alloy	Fractions of the components for AB ₅ composition (X _i)				Calculated thermodynamic properties, assuming $\Delta S = -110 \text{ J}/(\text{mole H}_2\cdot\text{K})$		
	Ce / A	Co / B	Mn / B	Al / B	$-\Delta H$ (kJ/mole H ₂)	P _D (bar), T = 30 °C	P _D (bar), T=150 °C
DL1	0.31	0.16	0.07	0.08	40.25	0.06	5.99
DL2	0.36	0.10	0.10	0.09	42.19	0.03	3.45
DL4	0.50	0.10	0.09	0.10	39.83	0.08	6.75

It was observed that all the alloys had calculated equilibrium plateau pressures (P_D) which were significantly lower than atmospheric pressure at 30°C. This may be a result of the high degree of Co, Mn and Al substitution of Ni, which may significantly increase the stabilities of the hydrides. The thermodynamic property of greatest importance would be the enthalpy of hydride formation (ΔH), which gives an indication of the thermal stability of the alloy material; quantifies how much heat energy is necessary to form the corresponding AB₅H_x hydride; quantifies how much heat energy is necessary to expel absorbed hydrogen; and is related to the hydrogen dissociation process [204]. All three alloys exhibited ΔH values which made them suitable for battery applications ($-\Delta H = 25\text{-}50 \text{ kJ}/\text{mole H}_2$) [205]. All three materials also had an enthalpy slightly lower than that observed for pure LaNi₅ ($-\Delta H = 30 \pm 0.04 \text{ kJ}\cdot\text{mol}^{-1} \text{ H}_2$), illustrating the influence of the mischmetal additions and substitutions on the thermodynamic properties of the material [204]. Importantly, all three alloys had equilibrium pressures less than 0.1 bar at room temperature. The AB₅ (DL4) alloy also demonstrated the highest equilibrium pressure at high temperature.

Based on the calculated thermodynamic properties and enthalpies given in Table 4.6, it was observed that the AB₅ (DL4) alloy required the least amount of exothermic energy to initiate the expulsion of absorbed hydrogen. Importantly, in the context of this study, the AB₅-type (DL4) hydride-forming alloy was identified as the most suitable available parent material for hydrogen sorption applications.

The thermodynamic studies of the AB₅ (DL4) alloy were further complimented by the construction of PCT isotherms.

4.1.4. Construction of pressure-composition isotherms for the parent AB₅-type alloy

The PCT isotherms for the AB₅ (DL4) alloy were analysed at three different temperatures (i.e. 30, 90, 150 °C) and are presented in Figure. 4.7. The experimental data were fitted using the model of phase equilibria in metal–hydrogen systems and compared to the calculated isotherms [217,218]. The PCT model assumed hydrogen occupies the metal matrix as a Van der Waals lattice gas, where parameters of the H–H interaction have a random nature caused by inhomogeneities in the AB₅ (DL4) hydride-forming alloy.

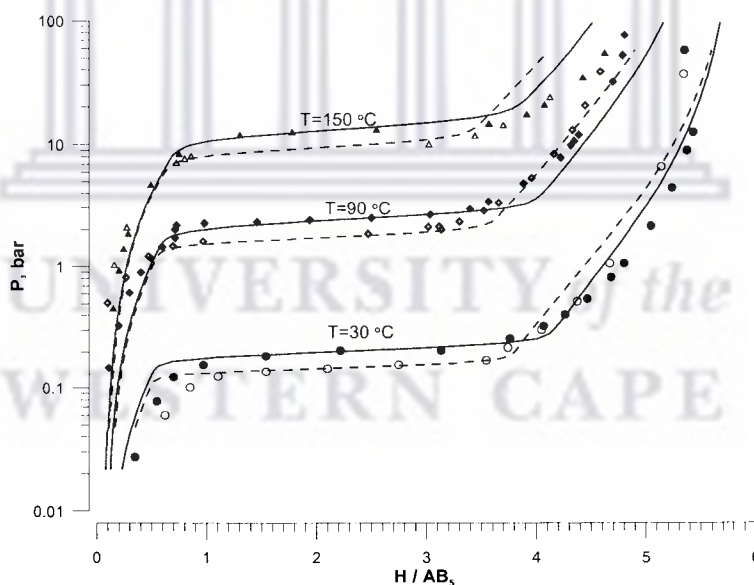


Figure 4.7. Hydrogen absorption / desorption isotherms for the AB₅ (DL4) alloy; experimental data (points) and calculated data (curves); filled symbols / solid lines correspond to absorption; opened symbols / dashed lines correspond to desorption

The hystereses observed in the plateau region of all three isotherms may have been a result of small differences in the free energy between hydrogenation and dehydrogenation, lattice expansions upon hydrogenation, or the formation of non-stoichiometric hydrogen vacancies in the lattice upon dehydrogenation [32]. Slight sloping of the equilibrium plateau regions in the isotherms was also observed and may have been a result of inhomogeneity in the AB₅-type alloy [32,204]. Maximum hydrogen absorption capacity of the AB₅ (DL4) alloy was determined as 1.27 wt. %.

Expectedly, the length of the plateau region was observed to decrease with increasing temperature. This observation agreed well with that observed by Ivey and Northwood [32].

The calculated fitting parameters of the PCT isotherms are listed in Table 4.7. The best fit was obtained when three equilibrium plateau segments were introduced. The lower segment took into account the asymptotic behaviour of $\ln(P)$ at small H concentrations corresponding to non-zero H content in the material, $C = C_{\min}$. This phenomenon was a result of H trapping by the alloy. It was taken into account by introducing an imaginary “zero” low-pressure equilibrium plateau segment with a very low critical temperature $T_C \sim 0$. The next segment represented the main equilibrium plateau properties of the alloy. Finally, the thermodynamic behaviour of the AB₅-H system at high H concentrations was described by the significant sloping of the upper segment of the equilibrium plateau.

Table 4.7. PCT fitting parameters for the AB₅-type (DL4) hydride-forming alloy

Parameter		Value (main segment / upper segment), where applicable	
		Absorption	Desorption
Segment	'Zero' pseudo-segment	0.026	0.031
	Main / upper segments	0.656 / 0.318	0.605 / 0.364
Ultimate H concentration, H/AB ₅		6.565	6.565
Critical temperature, K		581.5 / 484.1	566.4 / 509.4
Entropy contribution into concentration-independent term of $P(C,T)$ function, J / (mole H ₂ ·K)		-98.70 / -104.48	-96.25 / -112.22
Standard deviation of the entropy term, J / (mole H ₂ ·K)		2.49 / 22.06	2.28 / 21.60
Enthalpy contribution into concentration-independent term of $P(C,T)$ function, J / mole H ₂		-8840 / -11668	-9675 / -12346
Standard deviation of the enthalpy term, kJ / mole H ₂		454 / 1502	588 / 1000
Correlation coefficient between the entropy and enthalpy terms		1.00 / 0.50	0.94 / 0.50
Mean fitting deviation, H/AB ₅		0.035	0.038

The apparent PCT properties of the AB₅ (DL4) alloy calculated from the results of fitting of the experimental PCT data are presented in Table 4.8. They are also represented in Figure 4.8 as a set of isobars calculated in the range $P = 0.1$ -10 bar and $T = 0$ -200 °C. The hydrogen isobars indicated that the absorption of hydrogen by the AB₅-type alloy was very temperature dependent with little or no hydrogen absorption above the critical temperature at the onset of the equilibrium pressure plateau.

Table 4.8. Summary of the calculated PCT properties for the AB₅-type (DL4) hydride-forming alloy

Parameter	Absorption			
	<i>T</i> = 30 °C	<i>T</i> = 100 °C	<i>T</i> = 150 °C	<i>T</i> = 200 °C
Plateau midpoint (<i>C</i> ₀), H/AB ₅	2.316	2.263	2.205	2.126
ΔS^0 , J/moleH ₂ /K (<i>C</i> = <i>C</i> ₀)	-104.13	-101.69	-100.03	-98.46
ΔH^0 , kJ/moleH ₂ (<i>C</i> = <i>C</i> ₀)	-35.560	-34.181	-33.232	-32.322
$d(\ln P)/d(H/AB_5)$	0.082	0.115	0.140	0.172
<i>P</i> (<i>C</i> = <i>C</i> ₀), bar	0.2051	3.366	13.28	37.56
<i>C</i> (<i>P</i> =50 bar), H/AB ₅	5.602	4.862	4.253	3.414
<i>C</i> (<i>P</i> =1 bar), H/AB ₅	4.601	0.431	0.272	0.202
	Desorption			
	<i>T</i> = 30 °C	<i>T</i> = 100 °C	<i>T</i> = 150 °C	<i>T</i> = 200 °C
Plateau midpoint (<i>C</i> ₀), H/AB ₅	2.139	2.053	1.985	1.911
ΔS^0 , J/moleH ₂ /K (<i>C</i> = <i>C</i> ₀)	-101.40	-98.91	-97.23	-95.63
ΔH^0 , kJ/moleH ₂ (<i>C</i> = <i>C</i> ₀)	-35.547	-34.175	-33.233	-32.335
$d(\ln P)/d(H/AB_5)$	0.071	0.095	0.119	0.152
<i>P</i> (<i>C</i> = <i>C</i> ₀), bar	0.1484	2.414	9.469	26.65
<i>C</i> (<i>P</i> =50 bar), H/AB ₅	5.575	4.711	4.050	3.417
<i>C</i> (<i>P</i> =1 bar), H/AB ₅	4.431	0.447	0.280	0.211
Hysteresis energy losses, $RT \ln\left(\frac{P_A}{P_D}\right)$, J/moleH ₂ (<i>C</i> = <i>C</i> ₀)	815	1031	1189	1349

The influence of the mischmetal addition can be observed thermodynamically in that the ΔH was less negative in the case of the parent LaNi₅ material (-30 ± 0.04 kJ.mol⁻¹ H₂ at 30°C) [204]. Importantly, the maximum hydrogen-to-metal ratio (H/AB₅) under mild conditions (*T* = 30 °C) was equal to H/AB₅ = 5.6 and 5.0, at *P*_{H₂} = 50 and 5.0 bar, respectively.

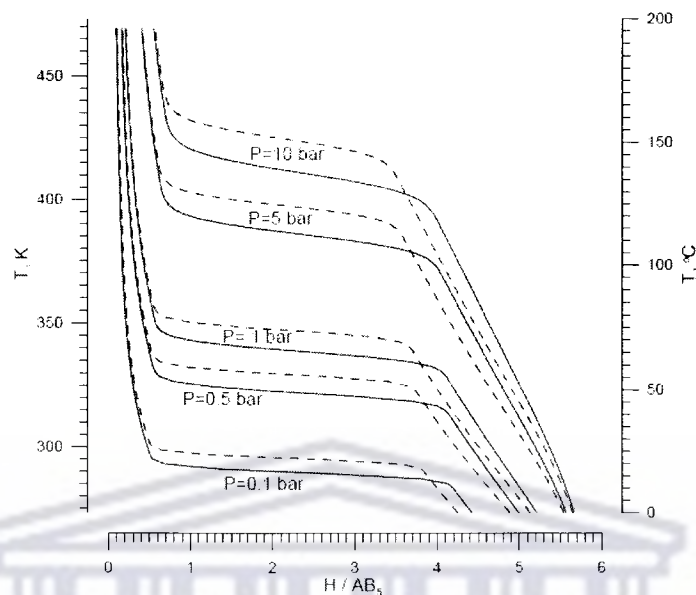


Figure 4.8. Calculated isobars for hydrogen absorption (solid) and desorption (dashed) with the AB_5 (DL4) hydride-forming alloy

The AB_5 -type (DL4) alloy was concluded to exhibit typical AB_5 -type alloy behaviour. Maximum volume of H_2 absorbed by the alloy was determined as $149 \text{ cm}^3/\text{g}$. The number of hydrogen atoms absorbed per unit volume was therefore determined to be about $5.5 \times 10^{22} \text{ H atoms/cm}^3$. The maximum molar ratio of the fully-hydrated alloy was 5.5 formula units, thereby giving a stoichiometry of $AB_5H_{5.5}$. The fast activation kinetics of the alloy was also observed where the equilibrium pressure plateau was reached rapidly, and the rate thereof increased with an increase in the sorption / desorption temperature.

Importantly, as the H absorption capacity ($T=30 \text{ }^\circ\text{C}$) for the starting AB_5 (DL4) alloy was equal to $H/AB_5 = 5.6$ and 5.0 , at $P_{H_2} = 50$ and 5.0 bar, respectively, all subsequent kinetic investigations of hydrogen absorption by the non-activated surface-modified samples were conducted at 20°C with $P_{H_2} \sim 5.0$ bar.

4.1.5. Crystallinity of the AB₅-type alloy parent material

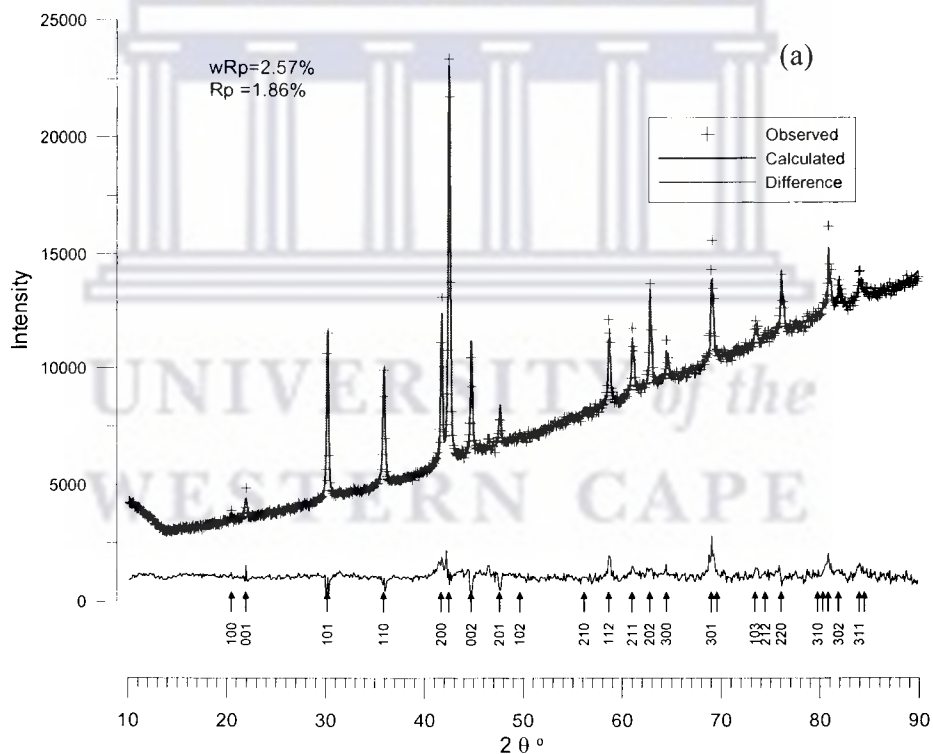
The diffractograms of the hydrogenated / non-hydrogenated parent AB₅-type alloy were presented in Figures 4.9 (a-b). The sample was hydrogenated under the conditions given in Section 4.2. The collected diffractograms were further analysed using the Powder Cell 2.4 and GSAS software. Details of the analysis are given in Table 4.9. The sloping background signal observed in the diffractograms may be due to X-ray absorption by the sample materials.

X-ray diffraction studies of the non-hydrogenated AB₅-type alloy (Figure 4.9 (a)) have shown that the material contains a major CaCu₅-type intermetallic phase with the periods of hexagonal unit cell: $a = 5.0019 \text{ \AA}$, $c = 4.0511 \text{ \AA}$. The calculated occupancies of the components to yield the best fitting of the XRD data corresponded to the sample formula $\text{La}_{0.40}\text{Ce}_{0.48}(\text{Nd,Pr})_{0.16}\text{Ni}_{3.34}\text{Co}_{0.64}\text{Al}_{0.63}\text{Mn}_{0.58}$, which was similar to the EDS results. The lattice parameters were in good correspondence with literature data ($a = 4.95 - 5.05 \text{ \AA}$, $c = 4.02 - 4.05 \text{ \AA}$) for a similar alloy $\text{La}_{0.8(1-x)}\text{Ce}_{0.8x}(\text{Pr,Nd})_{0.2}\text{B}_5$, ($x = 0 - 1$) where B₅ is $\text{Ni}_{3.55}\text{Co}_{0.75}\text{Mn}_{0.4}\text{Al}_{0.3}$ [38].

XRD studies of the hydrogenated sample (Figure 4.9 (b)) showed the presence of two main phases: the major phase of β -hydride AB₅H_x characterized by the same symmetry as the starting AB₅-type intermetallide and expanded unit cell ($\Delta a/a_0 = 5.27\%$, $\Delta c/c_0 = 2.82\%$, $\Delta V/V_0 = 12.6\%$); and the minor α -solid solution of hydrogen in the AB₅-type ($\Delta a/a_0 = 1.04\%$, $\Delta c/c_0 = 0.82\%$, $\Delta V/V_0 = 2.66\%$). The two phases shared the same space group type and symmetry ($P6/mmm$) as the parent material and hence the symmetry elements were arranged similarly within the unit cells of the two samples. A lattice expansion of 12.6% was observed for the β -hydride AB₅H_x phase. The lattice expansion was not severely large and was almost two times less than that typically observed in LaNi₅. Most probably, it is the result of the addition of Co to the mischmetal composition [64]. Less significant increases in the lattice constants and unit cell volume were observed in the solid solution AB₅H₋₀ phase. Large decrepitation of the brittle starting alloy size was also observed after hydrogenation,

similar to that observed by Willey *et al.* [64]. Another significant observation was the decrease in the measured particle size with the formation of the two phases indicative of the pulverization of the alloy particles upon hydrogenation. Very good fitting of the observed and calculated diffractograms were observed.

The sloping of the background was a result of fluorescence radiation from the sample. X-ray fluorescence is particularly strong for the samples containing elements immediately preceding the element of the anode of the x-ray tube. For the Cu anode, such elements causing fluorescence are Fe, Co and Mn. Co and Mn are components of the parent AB₅-type alloy, which explains the sloping.



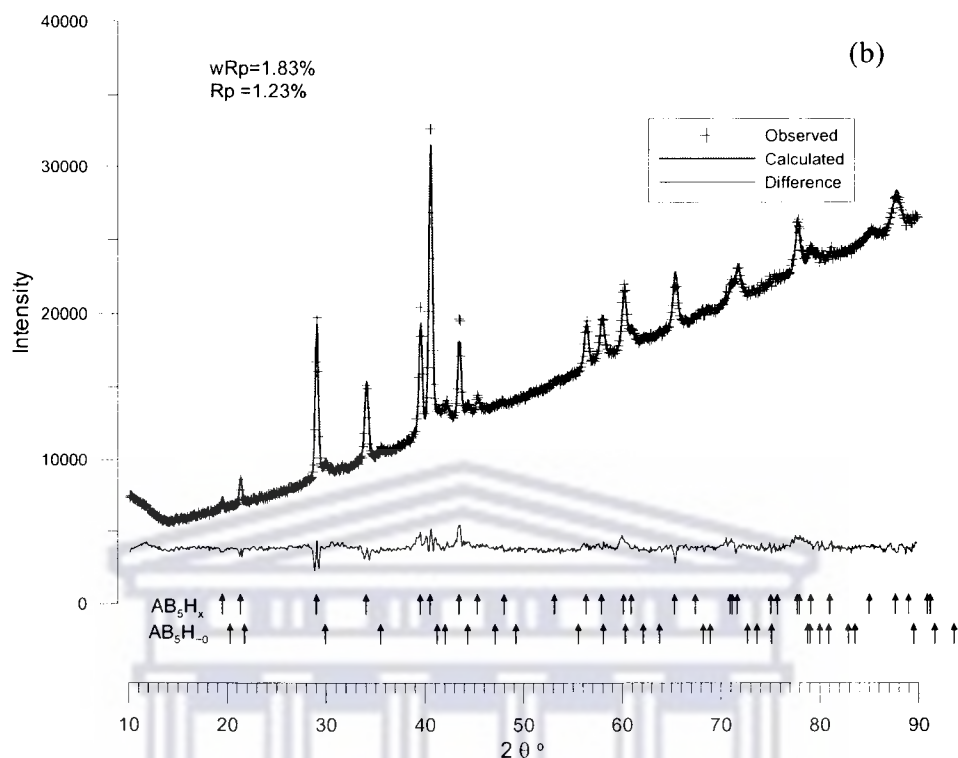


Figure 4.9 (a-b). Fitted XRD diffractograms of the parent AB_5 (DL4) alloy, (a) before hydrogenation and (b) after hydrogenation

Table 4.9. Results of fitting of diffractograms of the AB_5 -type alloy before and after hydrogenation

Profile parameter		Before hydrogenation (AB_5)	After hydrogenation (AB_5H_x)	AB_5H_{-0}
Abundance (%)		100	88.01	11.99
Space group type		$P6/mmm$	$P6/mmm$	$P6/mmm$
Lattice constants (Å)	a	5.0019	5.2636	5.0411
	c	4.0511	4.1648	4.1160
Unit cell volume (Å ³)		V	87.776	98.822
Lattice expansion (%)		$(\Delta V/V_0)$	-	12.6
Density (g.cm ⁻³)		ρ	7.961	7.071
Particle size (µm)			43.3	29.75
Strain			9.33×10^{-4}	8.96×10^{-4}

4.1.6. Summary

Three different AB₅-type alloys, with different compositions (DL1, DL2, DL4), were analysed in terms of their morphology; elemental composition; and thermodynamic properties for selection of the ideal starting material for surface modification.

It was found that the particles generally exhibited a particle size distribution of about 10-100 µm and a specific surface area of about 0.05 m²/g.

All three alloys were determined to be lanthanum-enriched and satisfactory for application as the negative electrode of batteries. All three alloys were determined to be typical mischmetal alloys.

Based on its high cerium content, low thermal stability, and lowest energy requirements for hydrogen desorption, the AB₅ (DL4) alloy corresponding to the formula La_{0.4}Ce_{0.48}(Nd,Pr)_{0.16}Ni_{3.34}Co_{0.64}Al_{0.63}Mn_{0.58} was selected as the most suitable parent material for application in hydrogen separation / purification / storage systems.

4.2. AB₅-TYPE ALLOYS SURFACE-MODIFIED USING THE ELECTROLESS PLATING OF PALLADIUM: MORPHOLOGY AND HYDROGEN SORPTION STUDIES

After the selection of the best available starting material for surface modification the electroless plating of Pd coatings on the surface of the alloy was undertaken.

The influence of surface morphology on the hydrogenation rate was investigated in terms of the following preparation variables: type of reducing agent; reducing agent concentration; Pd precursor concentration; substrate-to-solution concentration; reaction temperature; plating solution pH.

4.2.1 Palladium surface-modified AB₅-type alloys: retrospectives in synthetic approaches

Surface catalysis plays a vital role in improving the hydrogen sorption kinetics in metal hydrides, enabling rapid rates of hydrogen absorption at the surface [31]. In turn, the rate of absorption is dependent on the rate of hydrogen dissociation and the rate of hydrogen transport from the surface into the bulk material. Surface poisoning directly affects the rate of hydrogen dissociation with the result that the rate of hydrogen absorption is affected. Therefore, by enhancing the surface catalysis towards hydrogen dissociation on AB₅-type alloys it is possible to enhance the surface poisoning resistance and increase the hydrogenation rate at low temperature.

The hydrogen absorption mechanism exhibited by the Pd surface-modified AB₅-type alloys is constituted by stepwise processes. Firstly, H₂ molecules in the gas phase surrounding the Pd surface-modified alloy form a gas layer flowing laminally over the deposited Pd-based surface layer, driven by a pressure or concentration gradient. Dissociation of the H₂ molecules occurs at the surface of the Pd catalyst layer and the resultant hydrogen atoms are chemisorbed to the Pd catalyst surface. The dissociatively adsorbed hydrogen atoms are in a lower energy state than that in the gas phase surrounding the material, so that desorption of hydrogen atoms is very unlikely. The H atoms are highly soluble in the Pd catalyst and diffuse through the lattice by occupying the lowest energy face-centred cubic interstitial sites and forming Pd hydrides. The H atoms, pressed by a driving force, diffuse through the Pd catalyst layer by a solution-diffusion mechanism. H atoms arrive at the interface between the Pd layer and the surface of the alloy. The H atoms are then integrated into the metal matrix of the AB₅-type alloy by diffusing through the lattice by “interstitial hopping”, between octahedral sites via tetrahedral sites, and chemical bonding to form a hydride.

Alternatively, where the Pd layer is not continuous or where there is a dispersion of Pd catalyst particles on the surface of the AB₅-type alloy hydrogen spillover may

occur in combination with solution-diffusion of hydrogen through the Pd layer. In hydrogen spillover the hydrogen molecules are dissociated at the surface of the Pd catalyst particles to form hydrogen atoms which then "spillover" onto the surface of the metal hydride-forming alloy. Some of the dissociated hydrogen atoms remain attached to the Pd catalyst whilst others diffuse to the metal hydride-forming alloy, where they migrate to nearby catalytic sites or into the interstitial sites. The hydrogen spillover effect was identified as a means of enhancing the catalytic activity towards the hydrogen dissociation process [125]. Enhancements in the catalytic activity with hydrogen spillover are due to increases in the active surface area of the Pd catalyst on the alloy surface. The phenomenon is dependent on the catalyst loading, catalyst dispersion, active surface area of the catalyst, as well as the interfacial contact area between the catalyst and the surface of the support material [219]. Hydrogen spillover may also eliminate the negative effect of poisoning of the metal surfaces.

4.2.2. Influence of the reducing agent on the morphology and kinetic properties of surface-modified AB₅-type alloys

The influence of the type of reducing agent (i.e. N₂H₄ and NaH₂PO₂) on the morphological and kinetic properties of the AB₅-type alloy, surface-modified with Pd, was investigated by studying the crystallinity, Pd particle size / shape, Pd surface dispersion, specific surface area, and hydrogenation kinetics.

The first step in the surface modification of the alloy, by electroless plating, was the deposition of Pd nuclei by sensitization and activation in a Pd-Sn colloidal solution. Subsequent to this step phase changes on the alloy were characterised through XRD analysis. The corresponding diffractogram is given as Figure 4.10. No additional peaks or changes in peak position were observed with sensitization / activation. After sensitization and activation the Pd surface loading was determined as 0.43 wt%, Pd total loading was determined as 0.02 wt%, and specific surface area was determined as 0.08 m²/g, representing a marginal increase compared to the parent alloy.

The influence of the deposition time on the crystal structure of the Pd surface-modified alloy was investigated using alloys modified in hypophosphite-based baths as model materials (Figure 4.11). Similarly, additional phases or changes in existing phases were not observed. The Pd content on the surface-modified powders may have been very small (> 1.0 wt. %). This observation was identical to that observed by Zaluski *et al.* [60]. Similar observations were made for the AB₅-type alloys surface-modified using N₂H₄-based Pd plating baths.

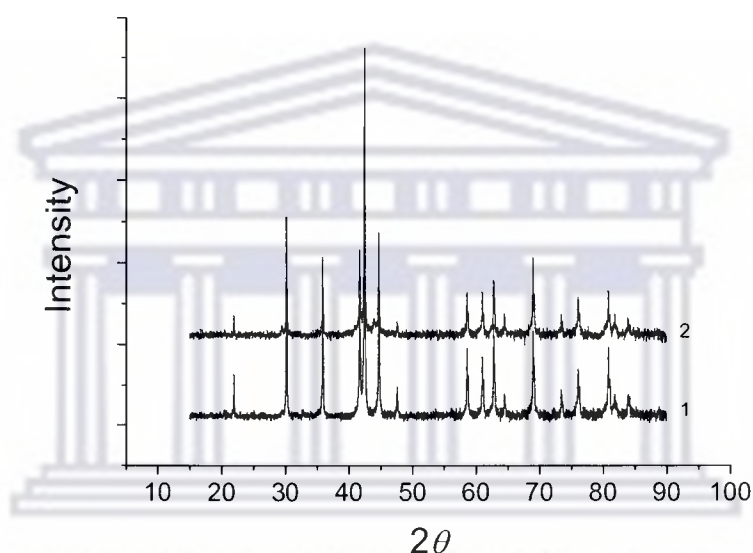


Figure 4.10. Diffractograms of the unmodified and sensitized-activated AB₅ (DL4) alloys, (1) unmodified AB₅-type alloy; (2) Pd-Sn sensitized / activated AB₅-type alloy

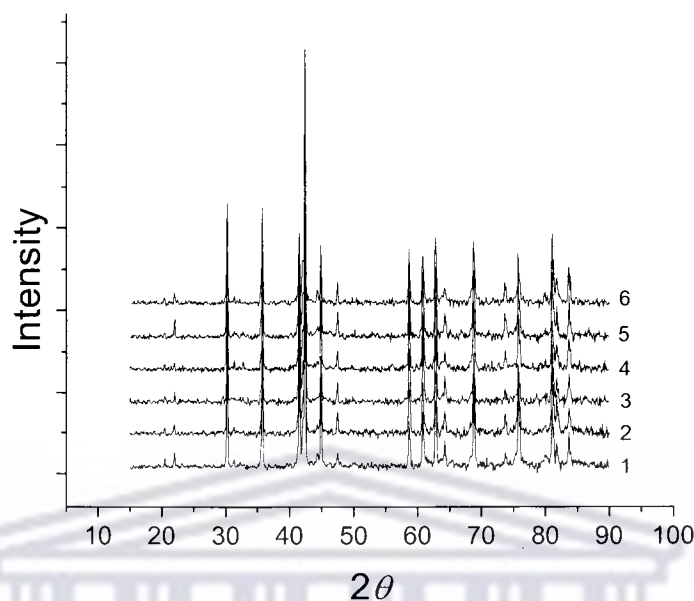


Figure 4.11. Influence of deposition time on crystallinity of Pd-modified AB₅-type alloys (NaH₂PO₂, 50°C), (1) unmodified; (2) 1 minute; (3) 5 minutes; (4) 10 minutes; (5) 20 minutes; (6) 30 minutes

To attain higher resolution in the study of the crystallinity of the surface-modified alloys SR-XRD analysis was conducted. The diffractograms collected by SR-XRD for the unmodified alloy and alloys modified in N₂H₄- and NaH₂PO₂-based electroless plating baths are presented as Figures 4.12 (a)-(c). The collected data was further analysed using the GSAS software and the results tabulated (Table 4.10).

The presence of the major CaCu₅-type intermetallic phase (95 wt. %) was again confirmed and the presence of a minor AB₅-type alloy phase (4.7 wt. %) characterized by the same structure and increased periods of the hexagonal unit cell was also detected. Most probably, the presence of the second AB₅-type alloy was a direct result of inhomogeneity in the B-component (Ni, Mn, Co, Al) of the parent AB₅-type alloy. Similarly, Willey *et al.* detected the presence of 10 wt. % of a second phase, ascribed as A₂B₇ [64]. Another possibility could be the presence of the α -phase solid solution of the AB₅-type alloy, which has good stability, where hydrogen may still be present as an artefact after preparation of the powdered alloy by ball-milling

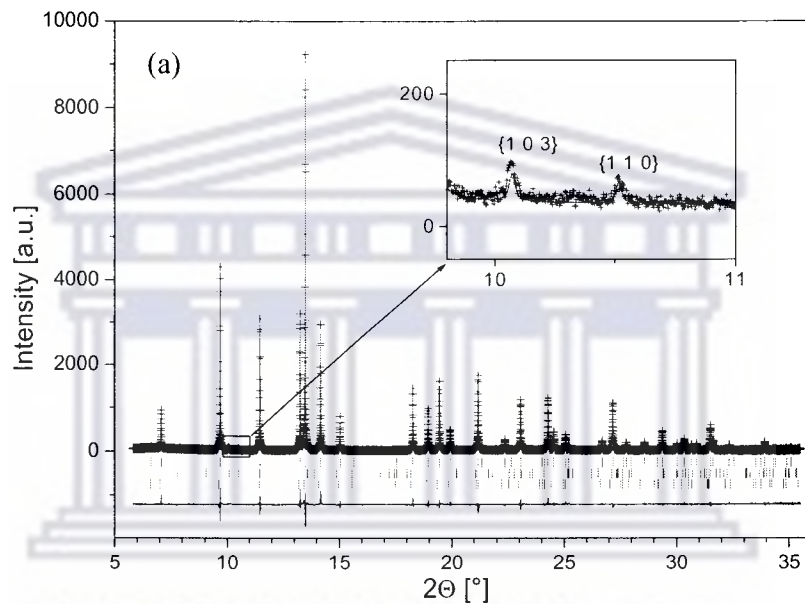
in NaH_2PO_2 . Trace quantities (0.7 wt. %) of a mixed rare-earth – nickel oxide (RE_2NiO_4) perovskite-type complex oxide phase, (having K_2NiF_4 -type structure [220]) were detected and most probably originated from the surface oxidation of the material.

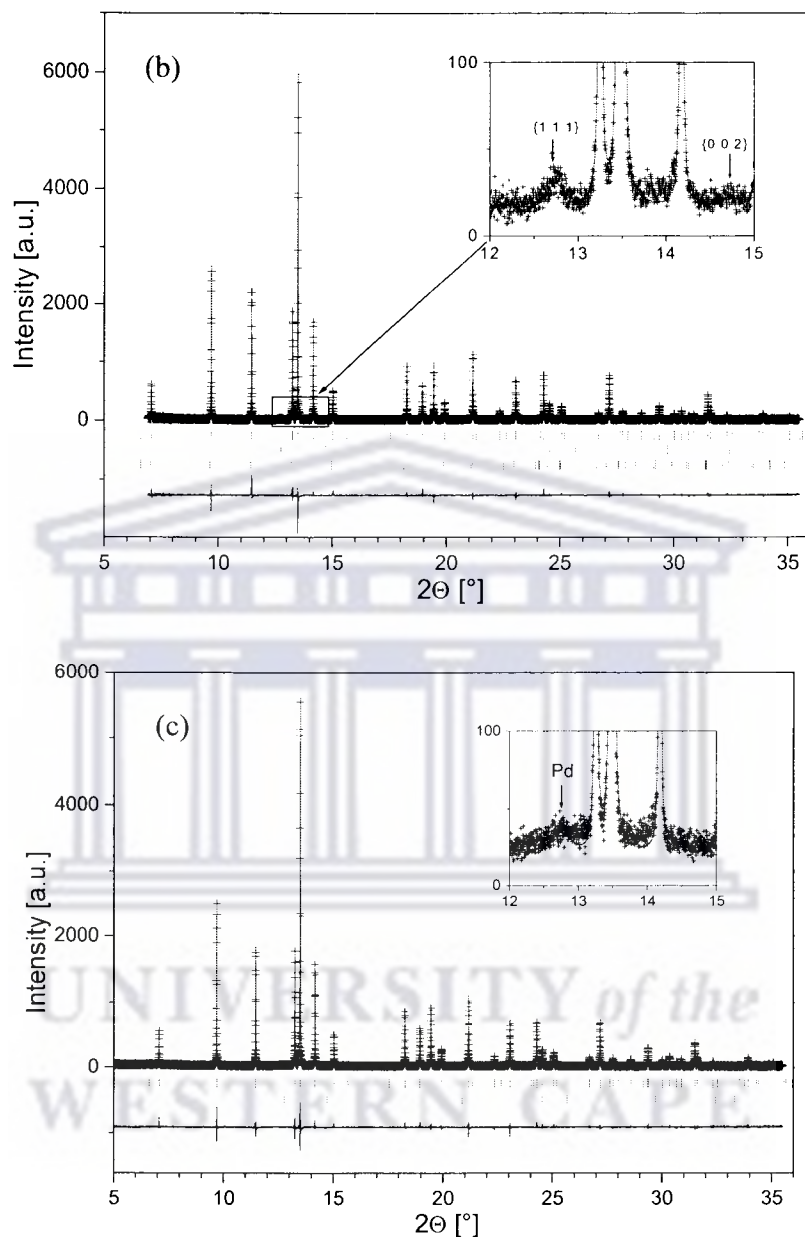
The SR-XRD diffractogram of the AB_5 -type alloy surface-modified by Pd coatings derived from N_2H_4 -based electroless plating baths showed that the material contained more-or-less unchanged lattice constants in terms of the major AB_5 phase (Figure 4.12 (b)). A crystalline Pd phase (the corresponding (111) and (002) peaks are shown in the inset) was detected (~ 1.5 wt. %) and the crystallographic peaks were indexed accordingly. Fairly small crystallites were detected on the surface of the AB_5 -type alloy after surface-modification in the N_2H_4 -based Pd plating bath. The Pd crystallite size calculated from the fitted LX profile parameter using different procedures was found to be between $7.9 (\pm 0.07)$ and $12 (\pm 1)$ nm for (111) and (002) crystallites, respectively. When the crystallites become smaller than 100-150 nm, a broadening of the diffraction peaks takes place, which develops more and more as the crystallites reduce in size. The extent of the broadening is related to the half-width of the peaks by simple analytical expression. Our analysis of the experimental SR-XRD pattern showed presence of a broad yet distinct Bragg reflection from Pd. The refinements yielded the Pd crystallite size of $7.9(7)$ nm, indicating its nanocrystallinity. Thus, it was concluded that the Pd was nanocrystalline in nature.

Importantly, it was observed that the RE_2NiO_4 phase observed in the parent alloy was completely removed after surface modification. The removal of this oxide phase at the onset of Pd electroless plating may have facilitated the adhesion of the Pd particles onto the surface of the alloy.

The AB_5 -type alloy surface-modified in the NaH_2PO_2 -based Pd plating bath exhibited a very broad diffused peak at $2\theta \sim 12.8^\circ$, which was attributed to amorphous Pd. In order to find a fraction of amorphous Pd on the surface of modified material, its SR-

XRD peak was modelled as coming from the “pseudo-crystalline” phase with a large size broadening coefficient corresponding to a grain size of ~ 1.0 nm. This extremely small size is on the edge between the nanocrystalline and amorphous materials. It is known that phosphorous is impregnated into the Pd layer and promotes the formation of amorphous coatings when using NaH_2PO_2 as the reducing agent during electroless plating.





Figures 4.12. Fitted SR-XRD diffractograms of the unmodified and surface-modified AB₅-type alloys: (a) unmodified alloy; (b) alloy modified in N₂H₄-based Pd plating bath; (c) alloy modified in NaH₂PO₂-based Pd plating bath

Table 4.10. Results of fitting of SR-XRD diffractograms of the Pd surface-modified AB₅-type alloy

Sample	Unmodified AB ₅	AB ₅ Pd (N ₂ H ₄)	AB ₅ Pd (NaH ₂ PO ₂)
Identified phases, abundance, and space group types	AB ₅ #1 (94.6 wt%, <i>P6/mmm</i>), RE ₂ NiO ₄ (0.7 wt%, <i>I4/mmm</i>), AB ₅ #2 (4.7 wt%, <i>P6/mmm</i>)	AB ₅ #1 (98.2 wt%, <i>P6/mmm</i>) Pd (1.5 wt%, <i>Fm-3m</i>) AB ₅ #2 (0.3 wt%, <i>P6/mmm</i>)	AB ₅ : (99 wt%, <i>P6/mmm</i>) Amorphous Pd: 1.0 wt%
Lattice constants (Å)	AB ₅ #1: $a = 5.003$; $c = 4.051$	AB ₅ #1: $a = 5.003$; $c = 4.051$	AB ₅ : $a = 5.003$; $c = 4.051$
	RE ₂ NiO ₄ : $a = 3.857$; $c = 12.66$	Pd: $a = 3.90$	
	AB ₅ #2: $a = 5.023$; $c = 4.079$	AB ₅ #2: $a = 5.018$; $c = 4.085$	
Pd crystallite size (nm)	-	10	-

Direct determination of the Pd particle size distribution was conducted using high-resolution FESEM (Figure 4.15 (a)-(b)). The experimental parameters for the analyses were given in Section 3.4.3. The micrographs collected for the AB₅-type alloys surface-modified using N₂H₄- and NaH₂PO₂-based electroless plating baths are given as Figures 4.13 and 4.14, respectively.

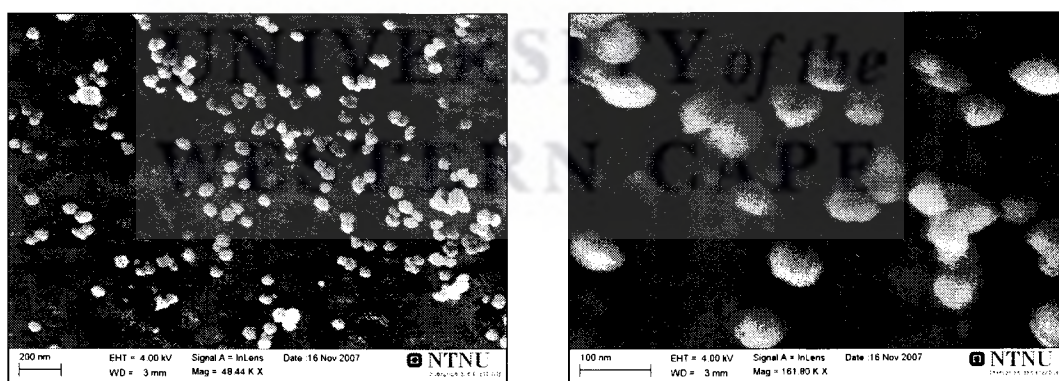


Figure 4.13. SEM micrographs of Pd-modified AB₅-type alloy (N₂H₄, 60°C, 30 min)

Crystalline Pd layers on the AB₅-type alloy surface, derived from N₂H₄-based electroless plating baths, were found to be discontinuous. A regular (close to

spherical) Pd particle shape was observed on the surface of the AB₅-type alloy. A fairly good surface dispersion of the crystalline Pd particles was observed upon deposition. Agglomeration of the Pd particles was not observed on the alloy surface. In comparison, Pratt *et al.* observed large agglomeration of the deposited Pd coating on certain faces of the AB₅-type alloy particles [56]. Willey *et al.* also observed discontinuous layers of plate-like Pd particles on the surface of modified AB₅-type alloys [64]. The specific surface area was determined as 0.23 m²/g indicating a large increase in coverage of the alloy with Pd deposition; the Pd total loading was determined as 0.4 wt% with a Pd surface loading of 1.3 wt. %. Discrepancies in the determined Pd total loadings were observed in the results obtained in the SR-XRD and AAS analyses. The loading determined in the SR-XRD analysis (~ 1.5 wt. %) may have been overestimated.

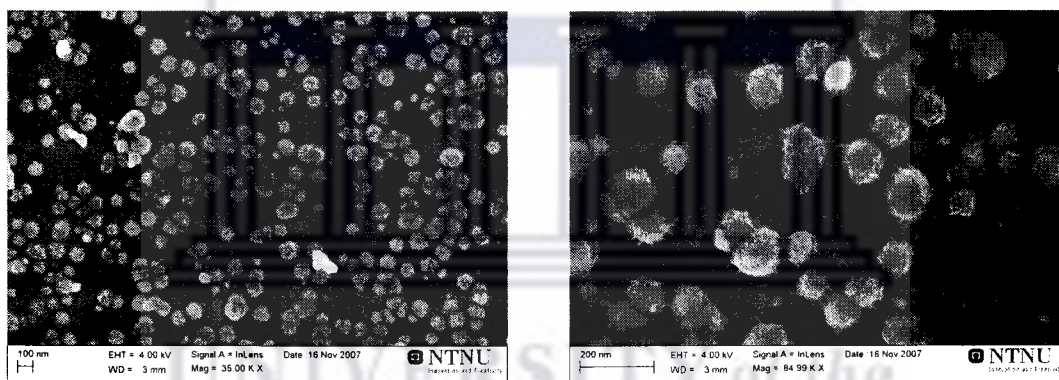


Figure 4.14. SEM images of Pd-modified AB₅-type alloys (NaH₂PO₂, 50°C, 30 min)

Pd-P coatings, derived from NaH₂PO₂-based electroless plating baths, on AB₅-type alloys, were also found to be discontinuous. A denser dispersion of the Pd-P particles on the surface of the alloy was observed upon deposition from NaH₂PO₂-based electroless plating baths, even better than that of the sample surface-modified in N₂H₄-based electroless plating baths. The Pd-P particles, after deposition from NaH₂PO₂-based electroless plating baths, exhibited a coarse granular appearance that may be credited to the amorphous nature of the Pd-P deposits. It was evident that the amorphous Pd-P particles were noticeably larger than their crystalline counterparts.

Agglomeration of the Pd-P particles was not observed on the alloy surface. The specific surface area was determined using N₂ physisorption as 0.16 m²/g indicating a large increase in surface area of the alloy with Pd deposition; the Pd total loading was determined as 0.64 wt% with a Pd surface loading of 2.5 wt.%.

In both cases the deposited Pd particles were somewhat spherical in appearance. In comparison, Willey *et al.* observed discontinuous coatings, on an AB₅-type alloy, housing smooth plate-like Pd particles with an average particle diameter of about 150 nm [64]. The Pd particles prepared in this study were generally smaller (Figure 4.15). In addition, there were similarities to the observations made by Harris *et al.*, where the Pd(-P) coatings exhibited a tendency to preferentially deposit on certain facets of the AB₅-type alloy particles [103]. The observation of discontinuous Pd coatings on the surface of the AB₅-type alloy was shared with Willey *et al.*, Harris *et al.*, Pratt *et al.*, and Doyle *et al.* [47,56,64,103]. Also, Doyle *et al.* stated that 80 – 100 % of the surface-modified AB₅-type alloy particles may house discontinuous metal coatings after PGM deposition [47].

It was observed that the crystalline Pd (N₂H₄) particles exhibited a uniform particle size distribution of 30-60 nm, compared to the larger and wider size distribution exhibited by the amorphous Pd-P (NaH₂PO₂) particles ~ 80-110 nm (Figure 4.15). Both size distributions are extremely well-defined and relatively narrow. It is known that stronger reducing agents, in this case N₂H₄, favour the formation of smaller Pd particles [221]. The larger Pd particle sizes after plating in NaH₂PO₂-based baths were credited to the influence of the P atoms impregnated into the Pd layer. Discrepancies in the determined Pd total loadings were observed in the results obtained in the SR-XRD and AAS analyses. The loading determined in the SR-XRD analysis (~ 1.0 wt.% estimated) may have been overestimated.

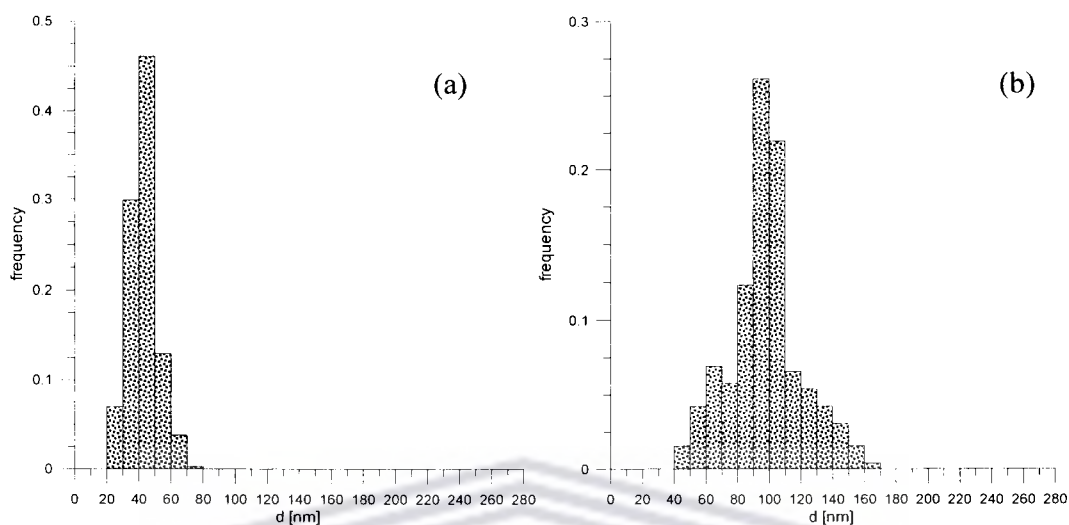


Figure 4.15. Pd(-P) particle size distribution histograms on AB₅-type alloy, (a) Pd (N₂H₄, 30 min, 60°C); (b) Pd-P (NaH₂PO₂, 30 min, 50°C)

Dynamic analysis in *micro*-PIXE was conducted to qualitatively study the surface elemental distribution of Pd on the AB₅-type alloy powders, and to determine whether continuous or discontinuous layers were attained on the surface of the alloy. The spectrum was recorded and is presented as Figure 4.16. The dynamic analysis maps are given as Figures 4.17 and 4.18.

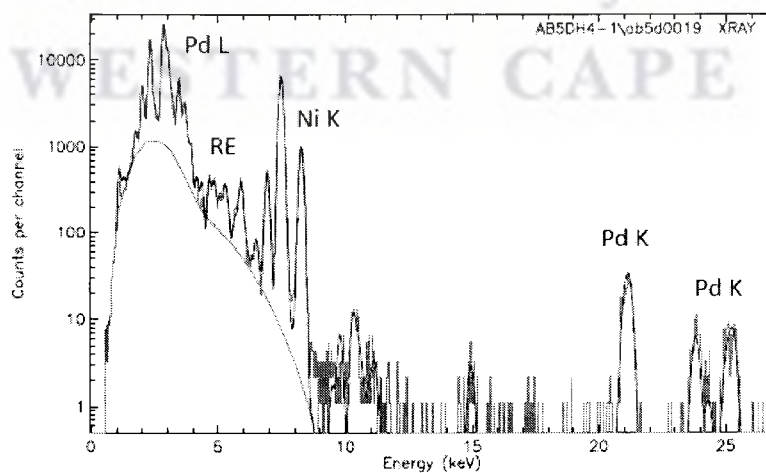


Figure 4.16. Typical *micro*-PIXE spectrum obtained on Pd-modified AB₅-type alloy (proton beam energy = 3.0 MeV, total collected charge = 50 nC; proton beam lateral resolution = $3 \times 4 \mu\text{m}^2$)

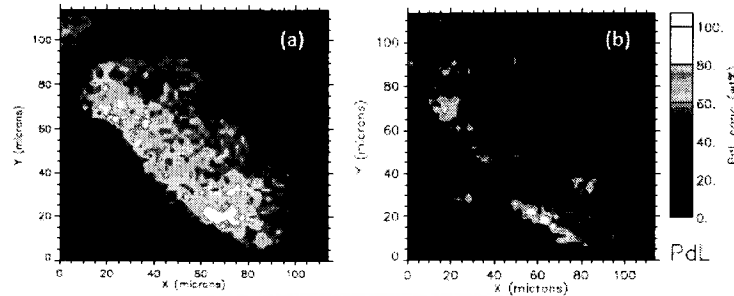


Figure 4.17. Dynamic analysis map of the Pd surface-modified AB₅-type alloy (N₂H₄, 60°C, 30 min), (a) total background; (b) Pd L

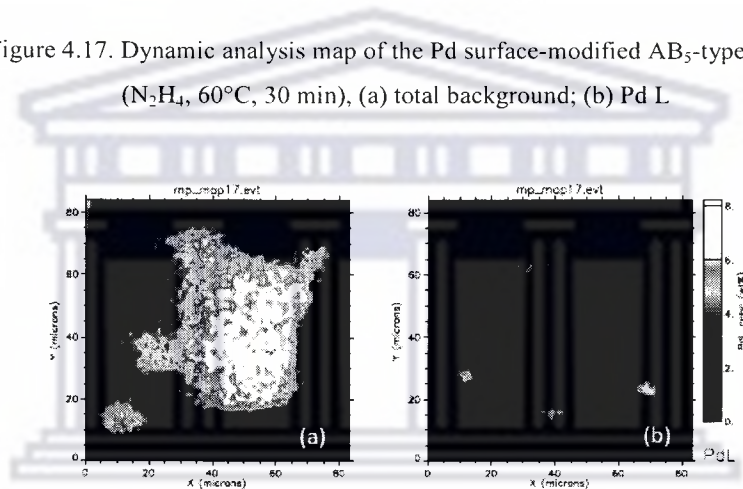


Figure 4.18. Dynamic analysis map of the Pd surface-modified AB₅-type alloy (NaH₂PO₂, 50°C, 30 min), (a) total background; (b) Pd L

It was confirmed that a discontinuous Pd layer was deposited on the surface of the AB₅-type alloy after treatment in a N₂H₄-based Pd electroless plating bath. In comparison, a similar type of discontinuous Pd-P coating was observed on the surface of the AB₅-type alloy after treatment in a NaH₂PO₂-based Pd electroless plating bath. It was thus concluded that the current plating conditions did not facilitate the deposition of continuous Pd layers. There was great interest in the attributes of AB₅-type alloys surface-modified using continuous Pd layers, and this required further investigation, using an approach given in Section 4.3.

Studies of the hydrogenation performances and kinetics of the unmodified alloy substrate and the surface-modified samples were conducted using a volumetric Sievert-type installation, after ~ 2 week pre-exposure of the sample materials to air and without pre-activation. The analysis was conducted under mild conditions ($P_{\text{H}_2} = 5.0$ bar, $T = 20$ °C, $t = 24$ hours). The results of the study of hydrogenation performance and kinetics are given as Figure 4.19.

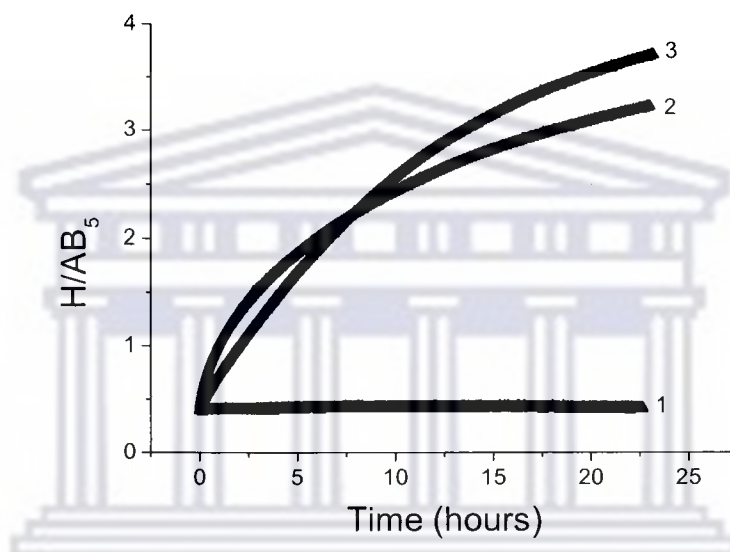


Figure 4.19. Dynamics of hydrogen absorption ($T = 20$ °C, $P_{\text{H}_2} = 5.0$ bar, $t = 24$ hours) by the AB₅-type alloy surface-modified in Pd plating baths, (1) unmodified (2) NaH₂PO₂ 30 min; (3) N₂H₄ 30 min

The parent alloy was observed to absorb hydrogen very slowly ($k = 9.8 \times 10^{-6} \text{ h}^{-1}$) as a result of the passive RE₂NiO₄ phase on the surface, as detected via the SR-XRD analysis, behaving as a diffusion barrier inhibiting the transport of hydrogen atoms through the surface and into the bulk material. Similarly Pratt *et al.* observed the slow kinetics of absorption and desorption of freshly prepared AB₅-type alloys, with the alloy only reaching a hydrogen-to-metal ratio of $\text{H}/\text{AB}_5 = 0.75$ after 20 hour exposure to hydrogen. After exposure to air for moderate periods the kinetics of hydrogen absorption were infinitely slow [56]. In comparison, the hydrogenation rates of the surface-modified materials were significantly enhanced compared to the unmodified

material and was initially not found to depend on the nature of the reducing agent, NaH_2PO_2 ($k = 3.8 \times 10^{-3} \text{ h}^{-1}$) and N_2H_4 ($k = 3.7 \times 10^{-3} \text{ h}^{-1}$). The enhanced kinetics was a result of the removal of the RE_2NiO_4 layer with surface-modification. It was clear that the deposition of amorphous and crystalline Pd layers, prepared from NaH_2PO_2 - and N_2H_4 -based plating baths, on the surface of the AB_5 -type alloy similarly promoted the hydrogenation rate and exhibited similar catalytic activities towards the dissociation of H_2 and subsequent absorption of H atoms into the substrate alloy.

The influence of the substrate-to-solution concentration on the surface morphology and hydrogenation kinetics was investigated in terms of “high-loading” (1:100) and “low-loading” (1:20). The surface morphology was investigated using FESEM. It was observed that increases in substrate-to-solution concentration resulted in a greater density of Pd-P particles on the surface of the alloy (Figure 4.20), compared to that prepared with a smaller substrate-to-solution concentration (Figure 4.14). By increasing the substrate-to-solution concentration the surface loading was increased from 2.5 wt.% to 17 wt.%; the total loading was increased from 0.64 wt% to 0.94 wt% Pd; and the specific surface area was increased from $0.16 \text{ m}^2/\text{g}$ to $0.19 \text{ m}^2/\text{g}$

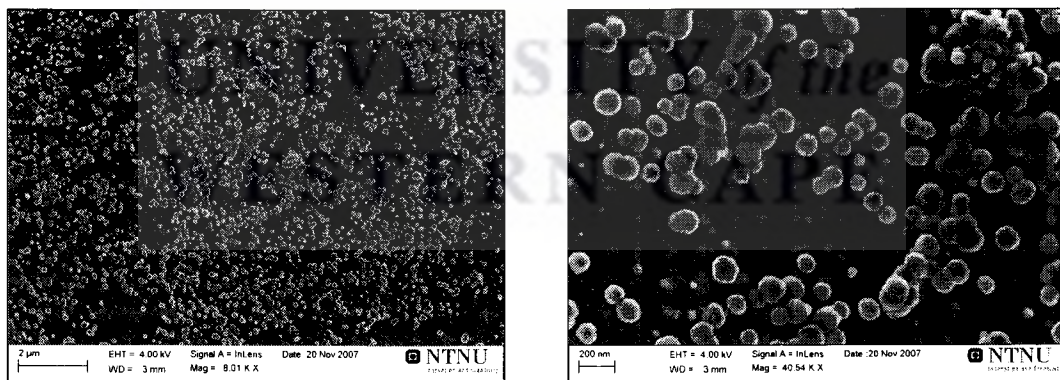


Figure 4.20. FESEM images of AB_5 -type alloy surface-modified using Pd-P high-loading ($\text{AB}_5\text{:Pd} - 1\text{:}100$, NaH_2PO_2 , 50°C , 30 min),

With regards to the kinetic properties, after ~ 2 week pre-exposure to air and without pre-activation, an increase in the substrate-to-solution concentration facilitated an

enhancement in the rate constant from $k = 3.8 \times 10^{-3} \text{ h}^{-1}$ to $k = 1.9 \times 10^{-1} \text{ h}^{-1}$ under mild conditions ($P_{\text{H}_2} = 5.0 \text{ bar}$, $T = 20 \text{ }^\circ\text{C}$, $t = 24 \text{ hours}$) (Figure 4.21). This observation demonstrated that the kinetic properties of the surface-modified materials are highly dependent on the availability of the metal ion precursor (i.e. Pd^{2+}) with respects to the quantity of the alloy substrate.

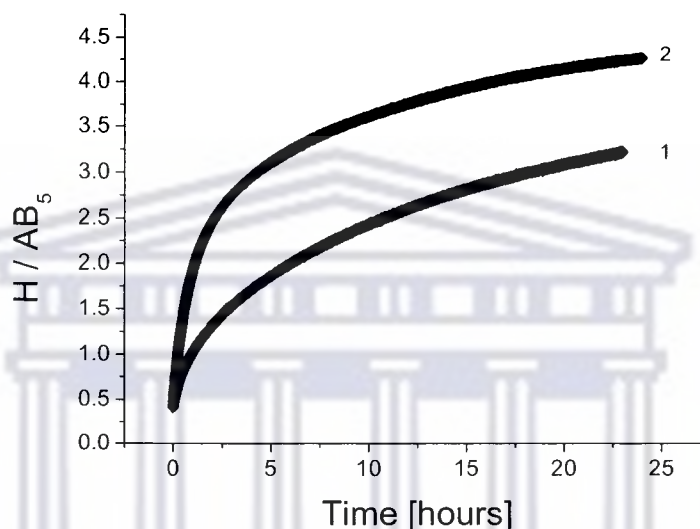


Figure 4.21. Dynamics of hydrogen absorption ($T = 20 \text{ }^\circ\text{C}$, $P_{\text{H}_2} = 5.0 \text{ bar}$, $t = 24 \text{ hours}$) by the AB_5 -type alloy surface-modified in Pd plating baths, (1) NaH_2PO_2 (1:20); (2) NaH_2PO_2 high-load (1:100)

A similar study was conducted after increasing the substrate-to-solution concentration in both the alloys surface-modified with Pd layers derived from N_2H_4 and NaH_2PO_2 plating baths. A summary of the morphological features of the sample materials is given as Table 4.11. It was observed that after increasing the substrate-to-solution concentration the samples surface-modified in N_2H_4 -based baths maintained a smaller particle size distribution and average particles size compared to that surface-modified in NaH_2PO_2 -based baths. The smaller Pd particles of the alloy modified in the N_2H_4 -based bath further confirm the larger measured specific surface area compared to that of the alloy modified in the NaH_2PO_2 -based bath. Based on the measured specific surface area and the particle sizes measured in the FESEM analyses it was possible to

estimate the surface area of the Pd coating. It was observed that the alloy modified in the N_2H_4 -based bath exhibited a larger measured specific surface area of the Pd coating compared to that of the alloy modified in the NaH_2PO_2 -based bath.

Also, with respects to the elemental composition it was observed that an increase in the substrate-to-solution concentration facilitated an increase in surface loading of N_2H_4 -based materials from 1.3 wt.% to 10.4 wt.%, and an increase in total loading from 0.4 wt.% to 0.54 wt.%. Similarly, increases in substrate-to-solution concentration facilitated an increase in surface loading of the NaH_2PO_2 -based material from 2.5 wt.% to 17 wt.%, and an increase in Pd total loading from 0.64 wt.% to 0.94 wt.%. The sample prepared by “high-loading” in a N_2H_4 -based bath was found to possess a specific surface area of $0.23 \text{ m}^2/\text{g}$.

Table 4.11. Morphological summary of Pd surface-modified AB_5 -type metal hydride-forming alloys

Sample	Size and shape factor of Pd particles in the coating (SEM; ranges for 90% of the particles measured)		Surface area [m^2/g]		
	d [nm]	K_s	BET data	Calculated (coating)	
				BET	SEM
Pd (N_2H_4) high load	30–60	1.05–1.2	0.23(2)	33.6	10.9
Pd (NaH_2PO_2) high load	60–130	1.05–1.17	0.19(3)	15.1	6.1

With respect to the hydrogenation characteristics of the materials surface-modified using a larger substrate-to-solution concentration, it was found that the kinetics strongly depended on the nature of the reducing agent, N_2H_4 ($k = 5.9 \times 10^{-2} \text{ h}^{-1}$), and NaH_2PO_2 ($k = 1.9 \times 10^{-1} \text{ h}^{-1}$). It was clear that the deposition of amorphous Pd-P layers, prepared from NaH_2PO_2 -based plating baths, on the surface of the AB_5 -type alloy further promoted the hydrogenation rate as a result of the increased quantities of

Pd deposited on the substrate alloy surface, compared to that of the crystalline Pd deposits prepared from N_2H_4 -based plating baths (Figure 4.22).

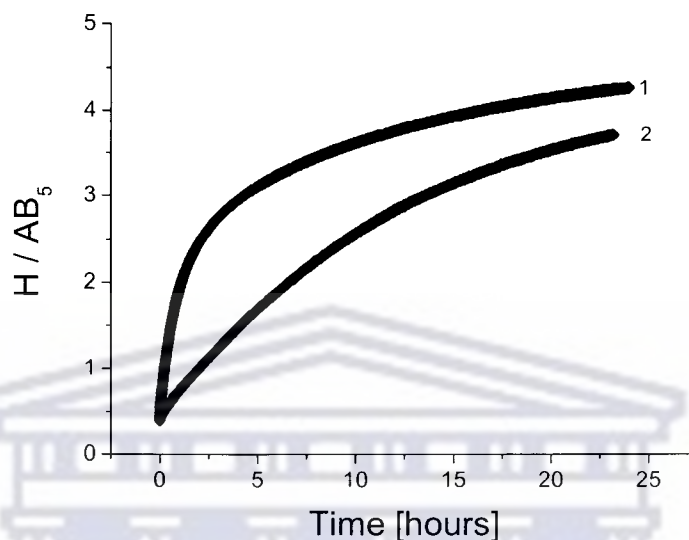


Figure 4.22. Dynamics of hydrogen absorption ($T = 20\text{ }^{\circ}\text{C}$, $P_{H_2} = 5.0\text{ bar}$, $t = 24\text{ hours}$) by the AB_5 alloy surface-modified in Pd plating baths, (1) NaH_2PO_2 high-load 30 min; (2) N_2H_4 high-load 30 min

4.2.3. Influence of preparation variables of palladium electroless plating baths on elemental composition, surface morphology, and kinetic properties of surface-modified AB_5 -type alloys

Although the influence of preparation conditions on the plating rate and quality of Pd coatings on smooth substrates (e.g. silicon, ceramics) are well known, not much is known regarding the influence of preparation conditions on the surface morphology and hydrogenation performance of surface-modified hydride-forming alloys. The preparation variables are known to directly determine the Pd plating in electroless plating. The plating rate employed is of the utmost importance when depositing metal layers by electroless plating, where faster rates tend to lead to a rough product with defects. The increased plating rate may be a result of the use of high temperatures or

high reducing agent concentration. For this reason an investigation was conducted into the influence of deposition time, temperature, Pd precursor concentration, reducing agent concentration, and plating solution pH on the surface morphology, elemental composition, and hydrogenation performance of surface-modified hydride-forming alloys. Unless stated, all Pd deposition was conducted in NaH_2PO_2 -based baths as model Pd plating baths.

The Pd-P deposition time may play a large role in influencing the thickness and density of the surface coating and therefore may potentially have a direct influence on the effectiveness of hydrogen dissociation on the alloy surface. The influence of the Pd-P deposition time on surface density, particle size, surface loading, total loading, and hydrogenation kinetics was investigated in the standard NaH_2PO_2 -based Pd-P plating bath (2.0 g/L PdCl_2 , 10 g/L NaH_2PO_2 , 50 °C).

The influence of the deposition time on the Pd-P surface density and particle size on AB_5 -type alloys was investigated using FESEM. The results of the investigation are given as Figures 4.23 and 4.24.



UNIVERSITY of the
WESTERN CAPE

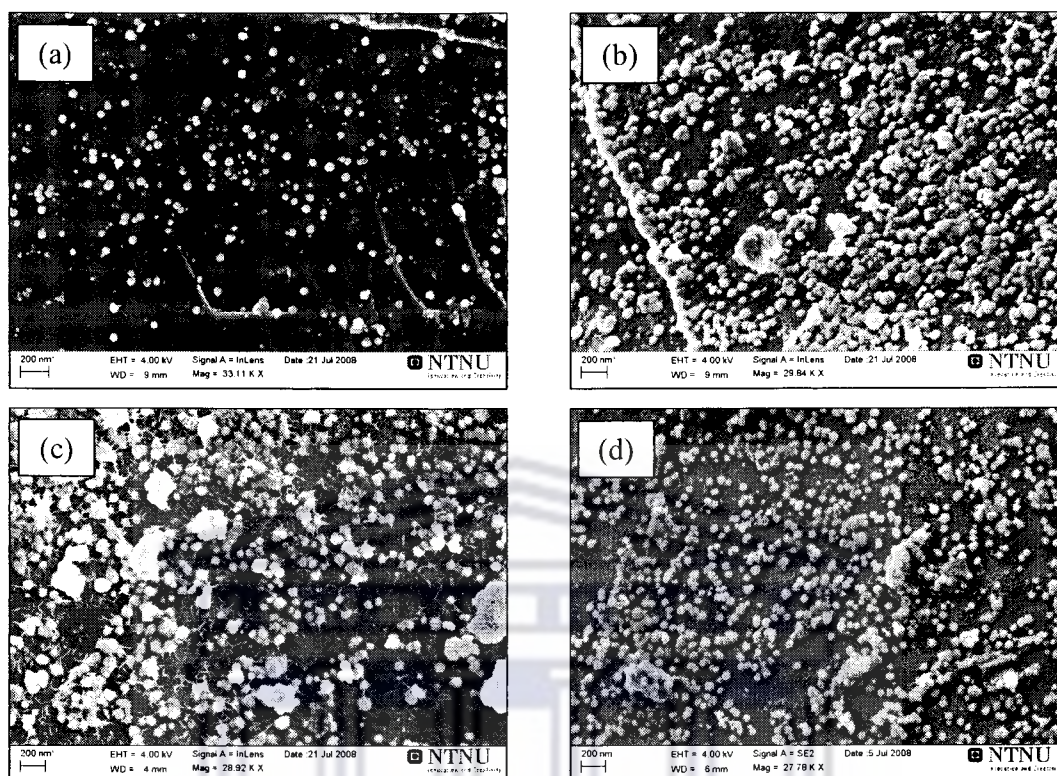


Figure 4.23. Influence of deposition time on Pd-P surface morphology and dispersion (NaH_2PO_2 , 50°C): (a) 1 minute; (b) 5 minutes; (c) 10 minutes; (d) 30 minutes

It was observed that the deposition time had a profound influence on the surface dispersion and density of the Pd-P on the AB_5 -type alloy surface. Generally, the surface dispersion, surface density, and level of surface agglomeration of the Pd layer increased with an increase in the deposition time. It was deduced that an increase in deposition time influences the approach of the Pd-P surface layer from surface particles towards a continuous surface layer.

Particle size of the surface catalysts plays an important role in hydrogen sorption/release. Different deposition methods also give rise to surface layers with different microstructures and particle size. The particle / grain size of Pd layers may play a pivotal role in the diffusivity of hydrogen through the deposited Pd layers into the bulk of the alloy substrate. This is because hydrogen diffusivities through Pd

differ greatly as a result of the differing particle size, which largely determines hydrogen diffusivity [134]. To illustrate, Yeung *et al.* found that hydrogen permeation through electroless plated pure Pd layers increases with increasing grain size [148]. Also, since the grain size of the deposited layers are nano-sized the hydrogen uptake characteristics are distinctly different from that observed in bulk Pd layers, and the nano-sized Pd particles may potentially absorb large quantities of gas by virtue of their high surface area.

An increase in deposition time produced initial rapid growth in the Pd-P particle size followed by a rapid decrease in the critical size of the Pd-P particles (Figure 4.24). An expected change in the pH of the Pd-P plating solution was observed as more of the hydroxides were consumed after the decomposition of the NaH_2PO_2 reducing agent.

Shafeev *et al.* have stated that when the plating time is kept shorter than 10 minutes the deposited metal takes on a smooth lustrous appearance, whereas longer plating times lead to the appearance of dark, aggregated, rough deposits due to instabilities of the autocatalytic metal growth [159].

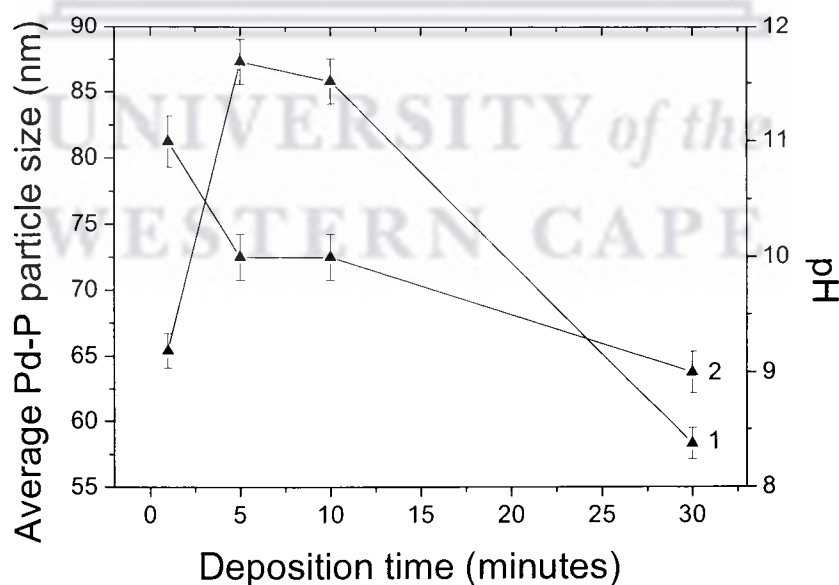


Figure 4.24. Influence of deposition time on Pd-P particle size and pH of plating bath:
(1) average Pd-P particle size vs. deposition time; (2) pH vs. deposition time

An EDS study was initiated to determine the influence of deposition time on the Pd-P surface loading on the AB₅-type alloy. The results of the study are presented as Figures 4.25 and 4.26. It was observed that an increase in deposition time generally facilitated an almost linear increase in the Pd surface loading. The increase in the Pd surface concentration was easily detectable as an amplitude increase in the Pd peak at about 3.0 keV in the corresponding EDS spectra (Figure 4.25). At the same time, an almost linear increase in the P concentration in the Pd-P surface layer was observed with an increase in the deposition time. Generally, an increase in the surface Pd content facilitated a parallel increase in the surface P content (Figure 4.26).

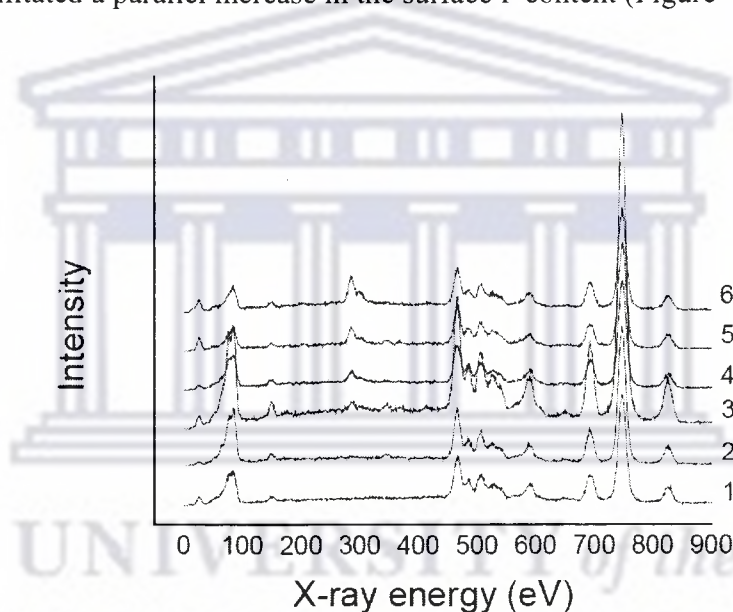


Figure 4.25. Comparative EDS spectra illustrating the influence of deposition time on Pd-P surface loading on the AB₅-type alloys (NaH₂PO₂, 50°C): (1) unmodified; (2) 1 minute; (3) 5 minutes; (4) 10 minutes; (5) 20 minutes; (6) 30 minutes

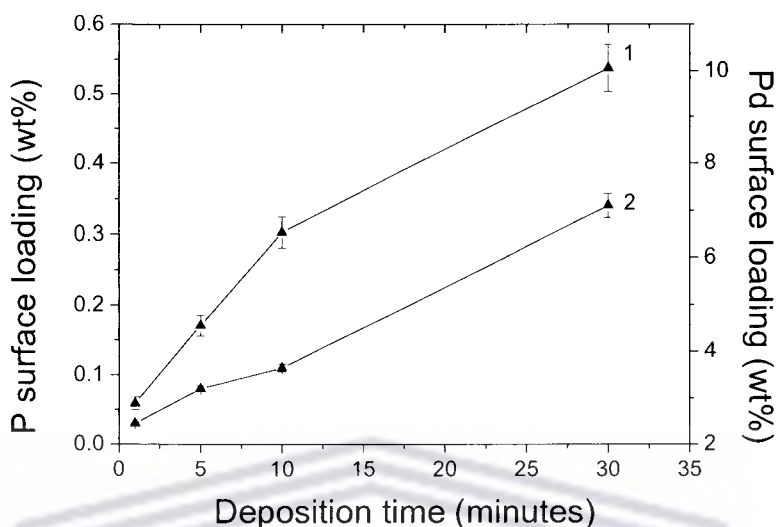


Figure 4.26. Influence of deposition time on Pd and P surface concentration of Pd-P layers deposited on the AB₅-type alloy surface: (1) Pd surface loading vs. deposition time; (2) P surface loading vs. deposition time

Doyle *et al.* [47] advised that the surface-modified metal hydride-forming alloy should not support more than 10 wt% of the total weight in PGM, to avoid significant losses in hydrogenation performances. Preferably the surface of the alloy should support trace amounts (i.e. $\ll 2.0$ wt.%) of the PGM. It was also expressed that the concentration of PGM deposited on the AB₅-type alloy surface should range between trace amounts (≤ 0.1 wt.%) to 2.0 wt.%.

In terms of total Pd loading in the Pd-P coating deposited on the surface of the AB₅-type alloy an almost linear increase in the Pd concentration was observed with an increase in the deposition time (Figure 4.27). Parallel increases in Pd surface and total loadings are therefore observed with an increase in deposition time. In comparison Doyle *et al.* reported Pd total loadings between 0.1 – 2.0 wt.% (w/w) [47].

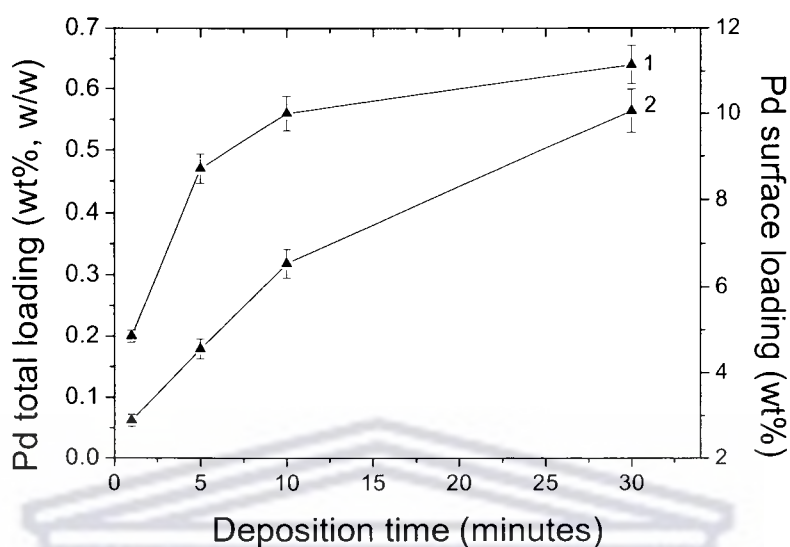


Figure. 4.27. Influence of deposition time on Pd total concentration of Pd-P layers deposited on the AB₃-type alloy: (1) Pd total loading vs. deposition time; (2) Pd surface loading vs. deposition time

A hydrogenation study of the surface-modified samples were studied after ~ 2 week pre-exposure to air, without pre-activation, and under mild conditions ($P_{H_2} = 5.0$ bar, $T = 20$ °C, $t = 24$ hours) to investigate the influence of the Pd-P deposition time on the kinetic properties (Figure 4.28).

It was observed that increases in Pd-P deposition time had the adverse effect of decreasing the kinetics of hydrogenation. Generally, after 10 minutes of deposition a significant loss in kinetics was observed, and after about 30 minutes of deposition stability in the rate constant was attained. By reference to the surface morphologies observed in the SEM analysis, three domains were observed: 1-10 minutes, 10-30 minutes, and 30-60 minutes. In the first domain, Pd growing particles were observed in which the mechanism of hydrogen dissociation was predominantly hydrogen spillover. Within this domain the formation of highly-active Pd “black” on the surface of the core alloy occurred. The Pd “black” corresponded to the deposition of the first Pd layer on the surface and is more catalytically-active than metallic Pd. In

the second domain, the initial stages of Pd island growth were observed in which the mechanism of hydrogen dissociation was a combination of hydrogen spillover and solution-diffusion through the Pd layer. Subsequent plating resulted in the formation of metallic Pd-P layers with lower catalytic activity. In the third domain, the initial stages of Pd film growth were observed in which the mechanism of hydrogen dissociation was predominantly solution-diffusion through the Pd layer.

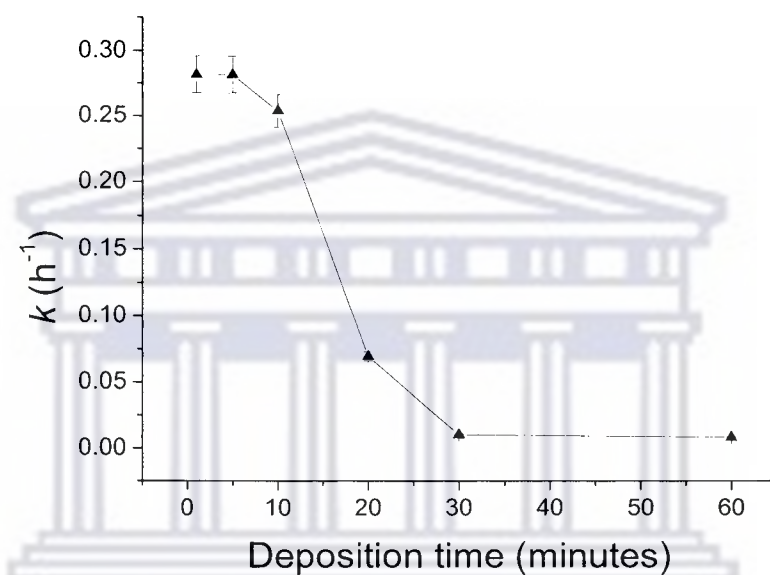


Figure 4.28. Influence of Pd-P deposition time on dynamics of hydrogenation ($T = 20\text{ }^{\circ}\text{C}$, $P_{\text{H}_2} = 5.0$ bar, $t = 24$ hours) by the AB_5 -type alloy surface-modified in NaH_2PO_2 -based plating baths

It should be noted that although samples prepared by the 1-10 minute Pd-P deposition exhibited the highest kinetics of hydrogenation, as a result of the formation of highly-active “Pd black” particles, 30 minute Pd-P deposition was employed as the standard deposition time based on the observation of greater pH stability in the electroless plating bath after longer deposition times (Figure 4.24).

The aforementioned hydrogen spillover phenomenon occurs in catalyzed hydrogen exchange reactions and involves the dissociative adsorption of hydrogen molecules on the surface of metal catalysts to form hydrogen atoms which then “spillover” onto

the support material (i.e. metal hydride-forming alloy). Some of the dissociated hydrogen atoms remain attached to the metal catalyst, whilst others diffuse to the support material, where they migrate to nearby catalytic sites or into the interstitial sites of the support material (Figure 4.29). This process not only modifies the chemical nature of the support but also induces subsequent hydrogen physisorption.

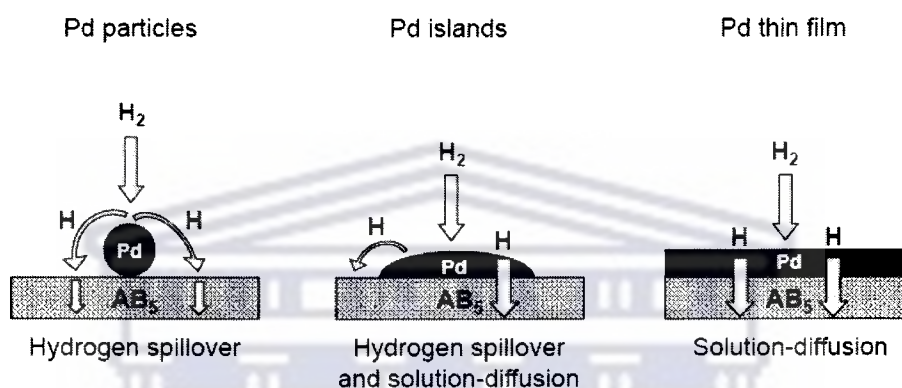


Figure 4.29. Proposed mechanisms of hydrogen dissociation on surface-modified AB₅-type alloys

The hydrogen spillover effect was identified as a means of enhancing the catalytic activity towards the hydrogen dissociation process [125]. Enhancements in the catalytic activity with hydrogen spillover are due to increases in the effective active surface area support material. The phenomenon is dependent on the catalyst loading, catalyst dispersion, active surface area of the catalyst, as well as the interfacial contact area between the catalyst and the surface of the support material [219]. Hydrogen spillover may also eliminate the negative effect of poisoning of the metal surfaces.

Reaction temperature plays a significant role in the plating rate in electroless plating. It was assumed that the lower plating temperatures are known to lead to a slower plating rate and the formation of smaller metal particles, whereas higher plating temperatures are known to result in a faster plating rate and the formation of larger metal particles. Increases in temperature result in increases in the potential difference

$E_{\text{Pd}^{2+}/\text{Pd}^0}$ according to the Nernst equation. However, it is well known that large potential differences result in the decomposition of the plating bath. It is therefore imperative to optimise the temperature to conditions which are sufficient enough to ensure fast plating rates, but also low enough to maintain the bath stability by optimization of the potential difference [158]. For these reasons, it became imperative to investigate the influence of the plating temperature on the morphology, elemental composition, and hydrogenation properties of the surface-modified AB₅-type alloy materials.

High-resolution SEM and parallel EDS studies were conducted to ascertain the influence of the plating temperature on the Pd-P particle size and the Pd surface loading of the surface-modified materials. The results are presented as Figure 4.30. It was confirmed that an increase in the plating temperature resulted in an increase in the Pd-P particle size, with particles growing as large as 117 nm at 90°C. At the same time, the measured Pd surface loading was found to be greatest at ~50°C, which was subsequently followed by a significant decrease in the surface loading. A similar maximum value in the Pd total loading was observed in Figure 4.31. It would seem that the deposition of Pd-P particles on the surface of the alloy was optimised at mild temperatures.

UNIVERSITY of the
WESTERN CAPE

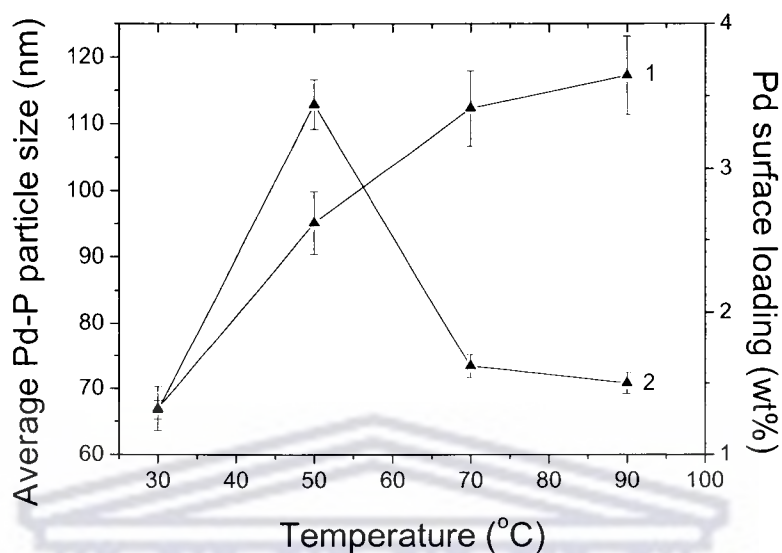


Figure 4.30. Influence of plating temperature on Pd-P particle size and Pd surface loading, (1) Pd-P particle size vs. temperature; (2) Pd surface loading vs. temperature

As was previously mentioned, the temperature used in the plating process had a significant influence on the Pd total loading, in which it was observed that the Pd total loading had a maximum value at $\sim 50^{\circ}\text{C}$ (Figure 4.31). In terms of the kinetics of hydrogenation, lower rates were observed at low plating temperatures. Subsequently, a maximum value was observed under mild conditions $\sim 50^{\circ}\text{C}$, after which the rate constant (k) attained an equilibrium. For these reasons all Pd-P layers deposited in this study were conducted under mild temperatures (i.e. $50\text{-}70^{\circ}\text{C}$).

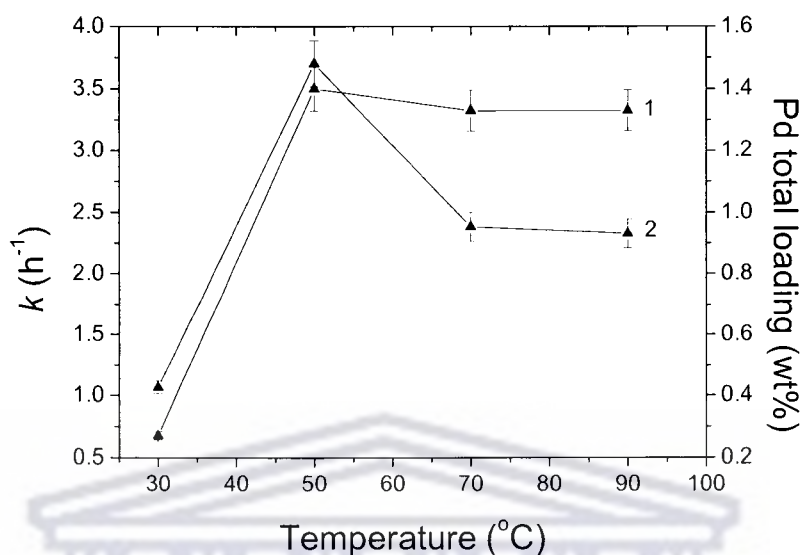


Figure 4.31. Influence of temperature on Pd total loading and kinetics of hydrogenation, (1) Pd total loading vs. temperature; (2) k vs. temperature

High-resolution SEM and parallel EDS studies were conducted to ascertain the influence of the PdCl_2 salt concentration in the NaH_2PO_2 -based plating bath on the Pd-P particle size and the Pd surface loading of the surface-modified materials. The results are presented as Figure 4.32. It was confirmed that an increase in the PdCl_2 concentration resulted in a decrease in the Pd-P particle size, with particles growing as large as 142 nm at 0.1 g/L PdCl_2 and as small as 83 nm at 2.0 g/L PdCl_2 . At the same time, the measured Pd surface loading showed a sharp increase as the PdCl_2 concentration was increased, eventually reaching an equilibrium at ~ 0.5 g/L. A maximum Pd surface loading of ~ 6.0 wt.% was observed.

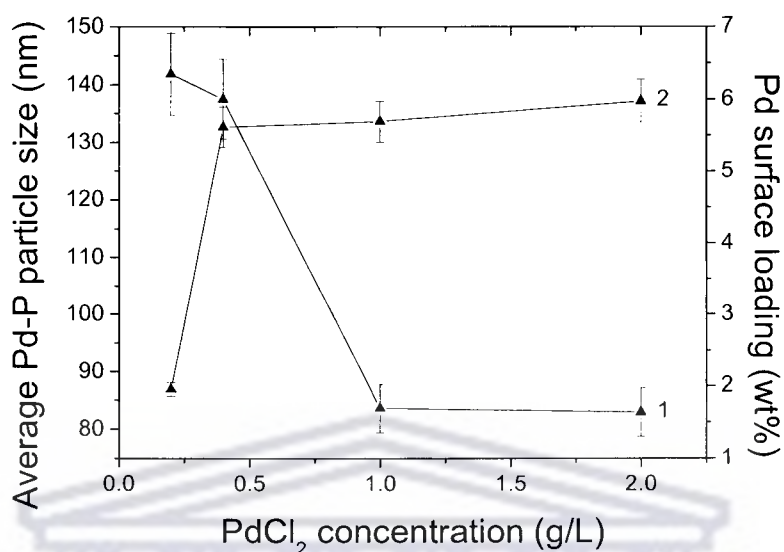


Figure 4.32. Influence of PdCl₂ concentration of Pd-P bath on Pd-P particle size and Pd surface loading, (1) Pd-P particle size vs. PdCl₂ concentration; (2) Pd surface loading vs. PdCl₂ concentration

In terms of the influence of the PdCl₂ concentration on the Pd total loading and kinetics, the total loading and kinetics were both observed to increase with an increase in the PdCl₂ concentration (Figure 4.33). The result illustrated that to achieve high Pd content on the surface of the AB₅-type alloy and parallel fast rates of hydrogen absorption higher concentrations of the metal salt precursor are necessary. In comparison, Shan *et al.* also observed increases in the hydrogenation/dehydrogenation properties of the AB₅-type alloy material with an increase in the Pd salt concentration [49].

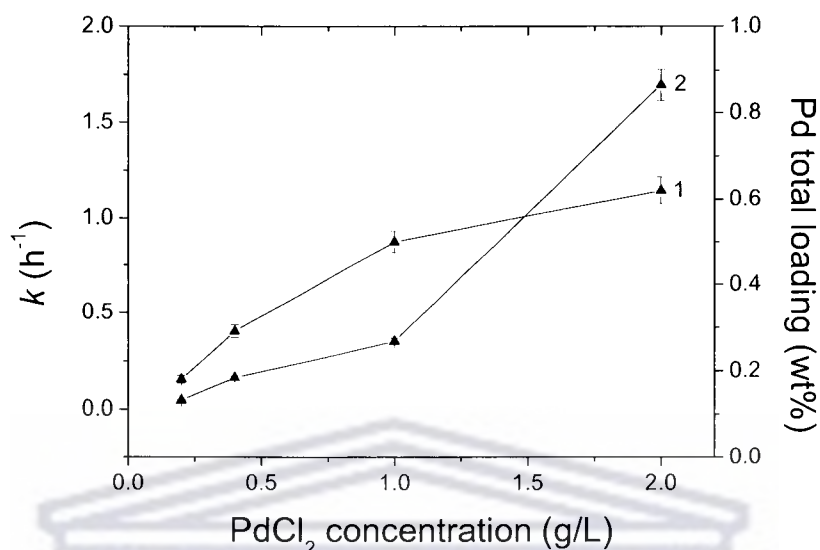


Figure 4.33. Influence of PdCl₂ concentration of Pd bath on Pd total loading and kinetics of hydrogenation: (1) Pd total loading vs. PdCl₂ concentration; (2) k vs. PdCl₂ concentration

The pH of the plating solution may have a large influence on the outcome of the morphological and kinetic properties. In the investigation, the pH of the Pd-P bath was adjusted accordingly over a full range using quantities of HCl and NH₄OH solutions. The influence of the bath pH on the Pd-P particle size and the Pd surface loading can be observed in Figure 4.34. Generally, the Pd-P particle size was observed to decrease with an increase in the bath pH before reaching an equilibrium at about pH 9-12. The particle size is therefore highly dependent on the pH of the plating bath. At the same time, a maximum in the Pd surface loading was observed at about pH 10, with the best loadings in the range pH 5-9.

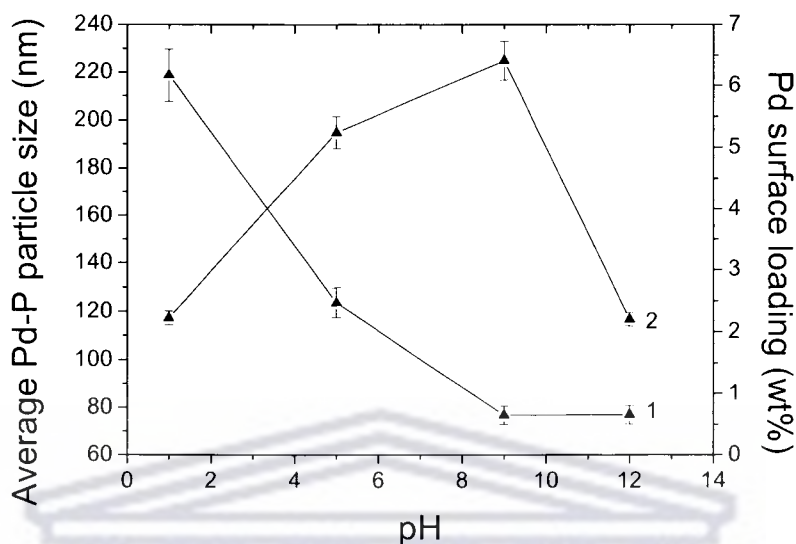


Figure 4.34. Influence of Pd-P bath pH on Pd-P particle size and Pd surface loading,
(1) Pd-P particle size vs. pH; (2) Pd surface loading vs. pH

With regards to the influence of the bath pH on the Pd total loading it was observed that the Pd total loading increased with an increase in the bath pH (Figure 4.35). With regards to the influence of the bath pH on the kinetics of hydrogenation it was observed that the rate constant increased with an increase in the bath pH, eventually attaining a maximum at about pH 9. It was deduced that the bath is most stable in this pH region with the NaH_2PO_2 readily decomposing to liberate hydrogen which will optimally reduce the Pd^{2+} cations in solution to form Pd^0 .

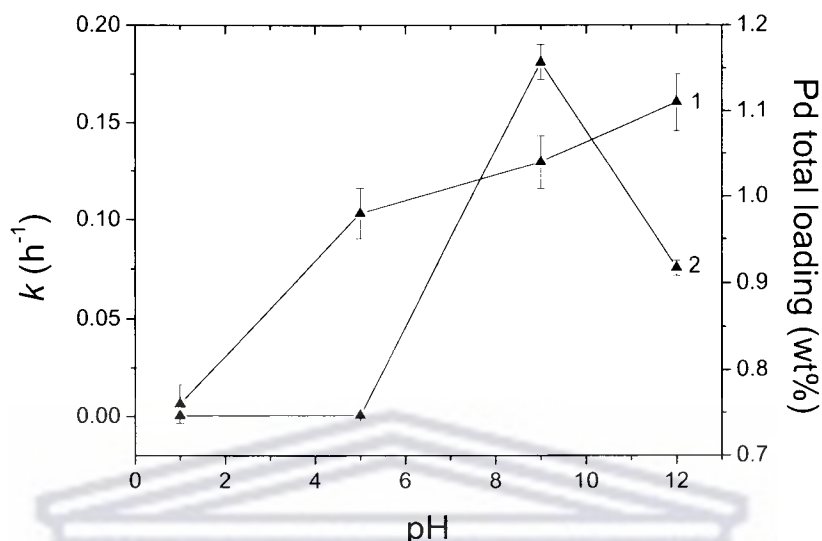


Figure 4.35. Influence of bath pH on Pd loading and kinetics, (1) Pd total loading vs. pH; (2) k vs. pH

An important factor of the electroless plating process, in the surface modification of the AB_5 -type alloy surface, is the concentration of the reducing agent. The concentration is known to have a direct influence on the plating rate and efficiency. High-resolution SEM and parallel EDS studies were conducted to ascertain the influence of the NaH_2PO_2 concentration on the Pd-P particle size and the Pd surface loading of the surface-modified materials. The results are presented as Figure 4.36. It was observed that the increase in the reducing agent concentration facilitated an increase in the Pd-P particle size. This observation may be a result of the increased rate of reaction and availability of electrons for reduction after decomposition, spurring the ($\text{Pd}^{2+} + 2\bar{e} \rightarrow \text{Pd}^0$) conversion process to completion. Higher reducing agent concentrations may have had the effect of increasing the plating efficiency and conversion rate, facilitating an increased growth rate in the Pd-P particles. With respects to the Pd surface loading it was observed that higher loadings were attained at concentrations ranging between 5-10 g/L NaH_2PO_2 . This concentration range may have been best to optimise the ($\text{Pd}^{2+} + 2\bar{e} \rightarrow \text{Pd}^0$) conversion rate and drive the reaction towards completion.

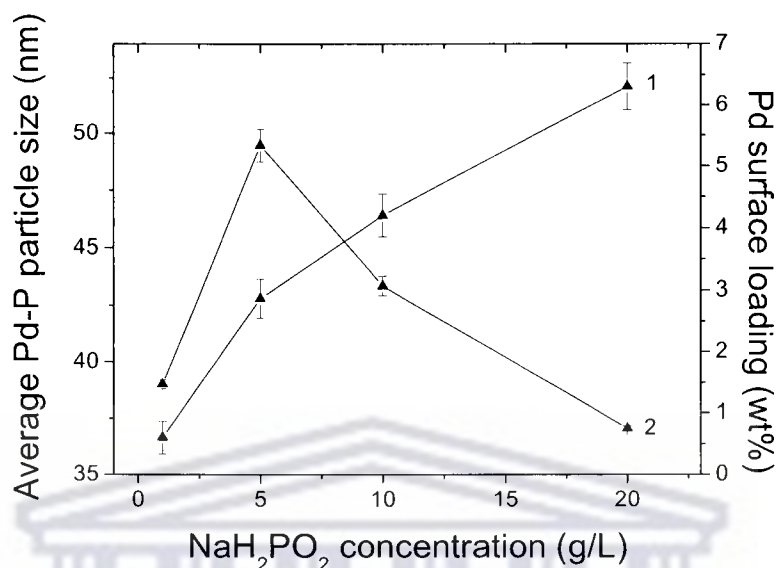


Figure 4.36. Influence of NaH₂PO₂ concentration on Pd-P particle size and Pd surface loading: (1) Pd-P particle size vs. NaH₂PO₂ concentration; (2) Pd surface loading vs. NaH₂PO₂ concentration

In terms of the influence of the reducing agent concentration on the total Pd loading it was observed that the loading increased slightly with an increase in the NaH₂PO₂ concentration. Discrepancies may exist in this observation as the Pd surface loading was observed to generally be lowered at concentrations greater than 10 g/L. The discrepancy may have arisen as a result of inhomogeneity in the quality of the discontinuous Pd-P coating of the sample of interest. It is also accepted that wherever a discontinuous coating of PGM's is applied there will be particles which possess no coating at all or possess continuous coatings on the surface. It is also accepted that between 5 and 100% of the particles will possess a discontinuous coating after surface modification [47]. Pratt *et al.* also observed that Pd particles were more concentrated and agglomerated on certain faces of alloy substrate particles [56]. In this respect the discrepancy may be a result of unavoidable error in the sampling, where the inhomogeneity of the sampled particles had generated uncertainty in the dataset.

With respect to the influence of the reducing agent concentration on the kinetic properties of the surface-modified AB₅-type alloys a maximum rate constant was observed at more dilute concentrations (Figure 4.37), which may have been a result of the smaller Pd-P particle size observed in Figure 4.36. The significant reduction in the rate constant may be associated with the increase in the Pd-P particle size with larger particles exhibiting lowered catalytic activity towards the hydrogen dissociation process.

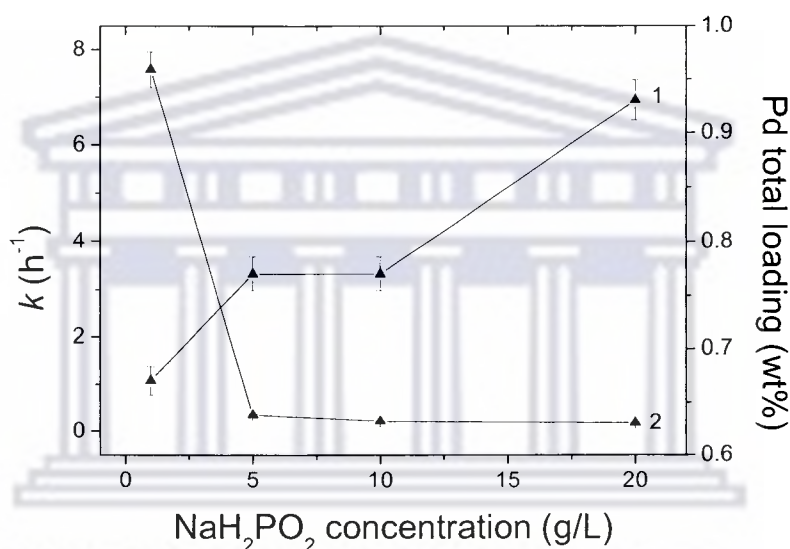


Figure 4.37. Influence of NaH₂PO₂ concentration on Pd total loading and kinetics of hydrogenation, (1) Pd total loading vs. NaH₂PO₂ concentration; (2) k vs. NaH₂PO₂ concentration

4.2.4. Summary

A mixed RE₂NiO₄ phase was detected on the surface of the unmodified AB₅-type alloy and led to the assumption of a surface oxide layer. This layer was deduced to be responsible for surface passivation of the AB₅-type alloy starting material and the subsequent poor kinetics of hydrogenation observed under mild conditions. It was observed that this oxide layer was removed after surface treatment in the Pd plating

baths, facilitating enhanced rates of hydrogen sorption. Also, deposition of Pd coatings facilitated a significant increase in the specific surface area of the alloys.

NaH₂PO₂-based Pd coatings (80-110 nm) were determined to be amorphous in nature as a result of the impregnation of P atoms in the Pd layer. In comparison, N₂H₄-based coatings (30-60 nm) were crystalline in nature. Both coatings exhibited very narrow and well-defined particle size distributions, were spherical in nature, with the amorphous NaH₂PO₂-based Pd particles generally being larger than their crystalline counterparts. Also, the hydrogenation kinetics of both alloys were comparable, although the NaH₂PO₂-based coatings prepared after increasing the substrate-to-solution concentration facilitated significantly better kinetics of hydrogenation compared to that prepared from N₂H₄-based coating after increasing the substrate-to-solution concentration. For these reasons, amorphous Pd layers were preferred for the surface modification of AB₅-type alloys for application in hydrogen separation / purification / storage units.

Significant influences of preparation factors (i.e. PdCl₂ concentration; reducing agent concentration; temperature; pH; deposition time) on the morphology and kinetics of hydrogenation were observed. These preparation factors would therefore be optimised in all subsequent sample preparation.

Importantly, both the crystalline and amorphous coatings on the surface of the AB₅-type alloy were discontinuous in nature. It was thus concluded that the current plating conditions did not facilitate the deposition of continuous Pd layers. However, great interest still existed in the potential attributes of AB₅-type alloys surface-modified using continuous Pd layers, and this required further investigation. It was deduced that the nature of the physical bonding between the AB₅-type alloy surface and the Pd layer may have limited the density and quality of the coating, hence the observation of discontinuous coatings as the physical bonding was not strong enough to prevent dislodging of Pd nuclei. Subsequently, an approach was adopted to utilise chemical

bonding to strongly adhere Pd nuclei to the surface of the AB₅-type alloy, and in doing so to facilitate the deposition of continuous Pd layers on the alloy surface.

4.3. SURFACE FUNCTIONALIZATION IN PALLADIUM ELECTROLESS PLATING ON AB₅-TYPE ALLOYS USING AMINOSILANES

As was previously discussed, Pd coatings deposited on the surface of the AB₅-type alloys using electroless plating were discontinuous in nature. Great interest existed in the potential attributes of AB₅-type alloys surface-modified using continuous Pd layers, and this required further investigation. A pre-treatment technique was previously developed by Williams *et al.* to facilitate the electroless plating of continuous Pd-P layers onto ZrO₂-TiO₂ composite membranes in the preparation of multi-functional porous membranes for hydrogen separation [221]. Using a similar method of surface functionalization, developed by Williams *et al.*, continuous layers of the Pd catalyst can be deposited on the AB₅-type hydride forming alloy for the purpose of further enhancing the kinetics of hydrogenation, enhancing the quality of the coating, and increasing the plating efficiency in the electroless plating of Pd layers [222,223]. In addition, decomposition of the precious metal plating baths can be prevented. The attractiveness of the functionalization method, in the electroless plating of metal layers, was thus demonstrated.

4.3.1. *Chemical conjunction between metal layers and substrate surfaces using aminosilanes*

It is accepted that conventional electroless plating is hampered by a number of difficulties because of the structural incompatibility between the substrate and platinum group metal (PGM) layer [224], leading to low deposition efficiency and subsequent PGM losses. The effectiveness of the electroless plating technique in plating metal layers onto a substrate is measured by the ability to effectively activate the substrate surface, which in turn is determined largely by the cohesion between the

Pd nuclei and the substrate [225]. Previous attempts at increasing the effectiveness of the activation have been aimed towards enhancement of the mechanical cohesion between the Pd nuclei and the substrate surface. Unfortunately, this increase in the physical adhesion proves unfavourable as it typically involves etching or roughening of the surface in aggressive reagents to produce abrasive surfaces. As a result, the surface chemistry of the material may be indirectly altered, which would be detrimental to the sorption performance as the hydrogen dissociation process is a surface-sensitive process [226]. However, the enhancement of the chemical adhesion between the Pd nuclei and the substrate surface does not affect the surface chemistry negatively and provides strong chemical interaction between the deposited layer and the substrate instead of a weaker physical bond. In using chemical conjunction between the deposited layer and the substrate surface strong adhesive forces are created between the two components. Also, by increasing the adhesion between the Pd nuclei and the substrate surface through a chemical conjunction, maximum utilization of the precious metal ions in solution is guaranteed and stability of the bath is ensured by preventing the dislodging of Pd nuclei from the substrate surface.

As was previously observed in the SR-XRD study of the parent alloy, the presence of a RE_2NiO_4 oxide phase, assumed to be in the form of a thin layer, on the rare earth metal hydride-forming alloy was confirmed after storage in non-inert environments (Figure 4.12 (a)). This RE_2NiO_4 layer is catalytically inactive towards the surface-sensitive hydrogen dissociation reaction and is known to decrease adhesion towards deposited metal layers. It may therefore be practical to remove this layer prior to electroless plating and subsequent hydrogenation. Another approach would be to modify this oxide layer prior to electroless plating so as to promote increased adhesion towards Pd nuclei [116]. The end result would be enhanced facile penetration of the hydrogen atoms into the core material.

Functionalization of the surface represents a “soft” pre-treatment method which does not damage the alloy surface. Surface functionalization allows for the optimization of the electroless plating technique by grafting chemically accessible functional groups

at the periphery of the metal hydride-forming alloy. This ensures maximum usage of PGM precursor ions in solution and increases the quality of surface activation by Pd nuclei. Surface functionalization may aid the surface immobilization of the Pd nuclei and the subsequent electroless plating of metal layers onto the hydr(oxide)-rich metal hydride-forming alloy surface. Ramifications of surface functionalization range from altering the surface wetting by increasing the hydrophilicity of the surface; enhancing adhesion properties; increasing the dispersion of metal particles on the surface of the metal alloy substrate; increasing the catalytic properties; ensuring maximum turnover of Pd ions into Pd metal; and ordering the interfacial region [144]. Surface functionalization also addresses two major shortcomings of electroless plating: low deposition rates and bath decomposition due to plating of Pd nuclei suspended in solution. By promoting the immobilization of Pd nuclei onto the surface of the substrate and by increasing the adhesion of the substrate surface towards the Pd nuclei, both of these shortcomings can be addressed and circumvented.

The challenge in functionalization chemistry, with respect to the AB₅-type alloys, is developing a method to introduce functionalities onto the surface of the core alloy leading to sufficient control of the encapsulated metal layer, and which does not adversely affect the hydrogen absorption properties of the core alloy. Researchers such as Dressick *et al.* have used functionalizing agents such as polyacrylic acid prior to sensitization / activation, where the immobilization of Pd nuclei onto the polyacrylic acid assembled layer was due to an ion exchange process [160]. Unfortunately, the polyacrylic acid assembled layer still required surface roughening of the substrate for the adhesion of the assembled layer itself. Also, the immobilization capacity of this type of assembled layer towards the Pd nuclei was very low and the activation process required very large concentrations of Pd-Sn colloidal solution. A similar approach was used by Brandow *et al.* in which assembled layers of 4-chloromethylphenylsiloxane were deposited onto silicon wafers for the purposes of immobilizing Pd nuclei prior to the electroless plating of nickel [227].

The ability of ligand-bearing water-soluble aminofunctional silanes to improve adhesion on inorganic materials is well documented [228,229]. They are typically used as a pre-treatment technique for the modification of adsorbents in chromatographic studies. Aminofunctional silanes form very strong covalent linkages to the surfaces of inorganic materials due to the catalytic ability of the amine functionality on polycondensation. Amine-terminated γ -aminopropyltriethoxysilane (γ -APTES) $\text{H}_2\text{N}(\text{CH}_2)_3\text{Si}(\text{OC}_2\text{H}_5)_3$ was identified as a possible coupling agent for the functionalization of AB_5 -type alloy surfaces due to its commercial availability, simple functionalization mechanism, high water solubility, high branching capacity, high flexibility, ability to polymerize, ability to improve control of the interfacial chemistry during electroless plating, and high affinity for surface oxides or hydroxides.

Functionalization using γ -APTES can occur in both aqueous and non-aqueous solution. Technologically, it is preferable to conduct γ -APTES functionalization in aqueous solution, where hydrolysis of the γ -APTES molecules results in the formation of the silanol derivative γ -aminopropyltrihydroxysilane $\text{H}_2\text{N}(\text{CH}_2)_3\text{Si}(\text{OH})_3$, with the ejection of three ethanol molecules in solution. Also, γ -APTES functionalization in aqueous solution leads to a more-preferred network structure being grafted to the surface of substrates, which might potentially have better adhesive properties. The γ -APTES molecules align themselves perpendicular to the substrate surface where they form a network structure of ladder-like polysiloxane chains which may influence the mechanical performance of the substrate [230]. In contrast, γ -APTES functionalization in non-aqueous solution leads to the formation of brush-like structures on the substrate surface (Figure 4.38).

γ -APTES molecules are typically bifunctional allowing for chemical bonding at both ends of the molecule. Bonding occurs by the reaction of oxide or hydroxyl groups on the substrate surface (primarily in the form of RE-OH) with the silanol group of the γ -APTES molecule, with the ejection of water molecules. In this way an assembled

layer of γ -APTES can be grafted to the AB₅-type alloy surface [226]. One layer of the aminosilanes may potentially range between 5.0 and 25 Å in thickness [160].

The surface functionalization by γ -APTES provides a platform onto which the electron-accepting Pd nuclei (as Pd²⁺ ions), from the activation solution, can be anchored. This is achieved through terminal amine groups (-NH₂) on the γ -APTES molecule which further bond covalently to the Pd nuclei. The terminal amine group, on the γ -APTES molecule, is hydrolysable and has the ability to react with inorganic materials due to its electron-donating nature, and as a result possesses great ligand capability to metal ions due to lone pair electrons on the nitrogen atom [231]. It is known that Pd has an affinity towards nitrogen atoms, such as that of the terminal amine group on the γ -APTES molecule [155]. The ability of a surface ligand to covalently bind Pd nuclei from a solution requires that the ligand be available to the solution species and that the Pd nuclei should possess at least one sufficiently labile coordination site [160]. The Pd nuclei (as Pd²⁺) possess unoccupied lower energy *p*- and *s*-orbitals (i.e. 4d⁸5s⁰5p⁰) which have high affinities towards the lone electrons on the aforementioned nitrogen atoms on the terminal aminofunctional group of the γ -APTES molecule [232]. Upon immobilization of Pd nuclei on the γ -APTES assembled layer, a chemical bond is formed between the nitrogen atoms and the Pd nuclei [226]. The Pd nuclei later graduate into Pd⁰ catalysts at the onset of the reduction reaction.

4.3.2. Methodological approach in surface functionalization of AB₅-type hydride-forming alloys using γ -aminopropyltriethoxysilane

AB₅-type hydride-forming alloys were pre-functionalized using aqueous and non-aqueous (dry toluene) γ -APTES solutions. Although no restrictions on the concentration of the γ -APTES solution existed, concentrations between 0.001 to 10 vol.% were ideal. [168]. Three γ -APTES solutions were prepared: 0.5; 1.0; and 5.0 vol. %. γ -APTES solutions were pH-neutralized with 10 vol.% HCl, which prevented dissolution of the alloy surface during the pre-functionalization step. Imori [168]

strongly advised that the pre-functionalization step be conducted at 60-100°C for between 3-60 minutes to achieve complete monolayer coverage of γ -APTES molecules on the substrate surface. For this reason, pre-functionalization in this study was conducted by heating the powders, suspended in γ -APTES solution, at 90 °C for 1 hour with mechanical agitation (300 rpm) [222]. Subsequently, the standard method of sensitization and activation was conducted on pre-functionalized powders. Schematic diagrams for the functionalization-sensitization-activation process in aqueous and non-aqueous solution are given as Figures 4.38 and 4.39 [221,223]. Brief descriptions of the methodology involved in the process are given below:

1. *Functionalization*: reaction of oxide or hydroxyl groups on the alloy surface with a hydroxyl of the γ -APTES silanol derivative, resulting in chemical bonding with the substrate and creating an assembled γ -APTES layer
2. *Sensitization*: substitution of H in free hydroxyls of γ -APTES molecules with Sn^{2+} ions, facilitating anchoring of Pd nuclei onto the substrate (step 3).
3. *Activation*: Pd^{2+} ions are reduced by the sensitized Sn^{2+} ions to yield Pd^0 . As a result, Pd nuclei chemically bound to the substrate via the γ -APTES derivative are formed. In addition, Pd^{2+} ions form complexes by their bonding to the nitrogen atom from the terminal amine group of the γ -APTES derivative. These bound Pd^{2+} ions later instantaneously graduate into Pd^0 upon the introduction of the reducing agent and the onset of metal plating.
4. *Acceleration*: use of dilute Na_2EDTA solution to remove Sn^{2+} from the support leads to formation of Sn^{4+} (step 3), which leaches back into solution.

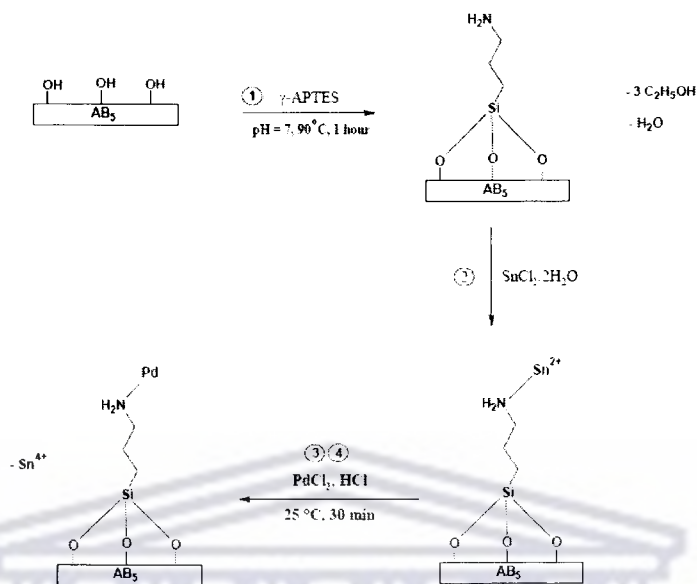


Figure 4.38. Schematic representation of functionalization, sensitization, activation, and acceleration on the surface of the AB₃-type hydride-forming alloy using non-aqueous γ -APTES solution

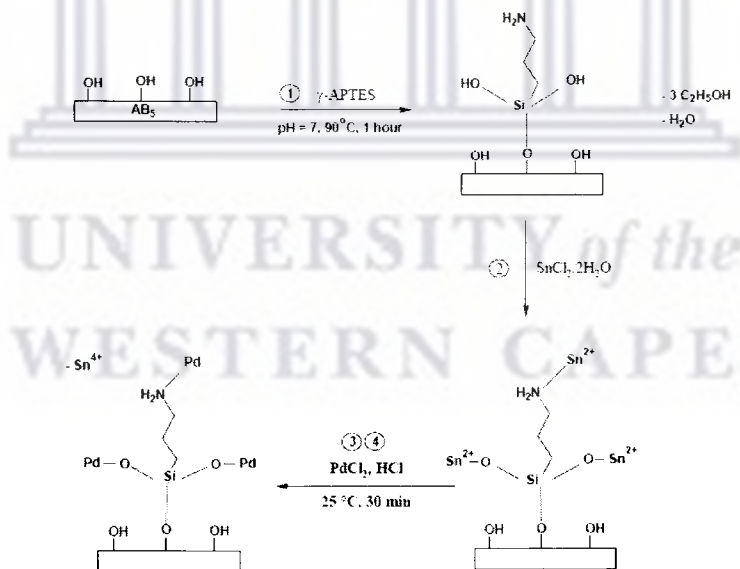


Figure 4.39. Schematic representation of functionalization, sensitization, activation, and acceleration on the surface of the AB₃-type hydride-forming alloy using aqueous γ -APTES solution

The final step of the surface modification procedure was in the deposition of the Pd-P layer, through immersion of the functionalized and activated powders in the standard NaH_2PO_2 -based electroless plating bath, given in Table 3.1 [163].

Confirmation of the successful γ -APTES functionalization of the AB_5 -type alloy surface was conducted using EDS analysis, with 3.8 wt.% Si being detected on the surface after functionalization. Also, using the functionalization step the total quantity of Pd nuclei adhered to the surface was increase from ~ 0.02 wt% Pd to ~ 0.08 wt% Pd, as determined using AAS.

4.3.3. Structural and kinetic characterization of surface-modified AB_5 -type alloys functionalized using γ -aminopropyltriethoxysilane

The surface morphologies of the surface-modified AB_5 -type materials, pre-functionalized in aqueous and non-aqueous 1.0 vol. % γ -APTES solution, were analysed using FESEM. In Figures 4.40 and 4.41 the change in the surface morphology of the AB_5 particles, with pre-treatment in aqueous and non-aqueous 1.0 vol. % γ -APTES solution and immersion in the standard Pd electroless plating bath, can be clearly observed. High loading (1:100) was used in preparing the sample materials. A rich coating of Pd-P particles was clearly observed with pre-functionalization in aqueous γ -APTES compared to the Pd surface particles observed on AB_5 modified without pre-functionalization (Figure 4.27). Similarities in the Pd-P particle size were observed between the sample pre-treated in aqueous γ -APTES solution (157 nm); and that prepared without pre-treatment (117 nm). Application of the surface pre-functionalization with 1.0 vol. % aqueous γ -APTES solution resulted in the formation of high-density surface coatings. In addition, the pH-neutral aqueous γ -APTES was not detrimental to the structural integrity of the alloy surface. The surface Pd content after high loading and functionalization in aqueous 1.0 vol. % γ -APTES solution was determined as 51 wt% Pd, the specific surface area was $0.3 \text{ m}^2/\text{g}$ and the Pd total content was 1.2 wt% Pd. In comparison, the material prepared after high-loading, and without functionalization, exhibited surface Pd content of 17 wt%

Pd, specific surface area of $0.2 \text{ m}^2/\text{g}$ and the Pd total content was 0.9 wt% Pd. This further illustrated the ability of the pre-functionalization step in enhancing the quality of the Pd-P coating on the surface of the AB₅-type alloy.

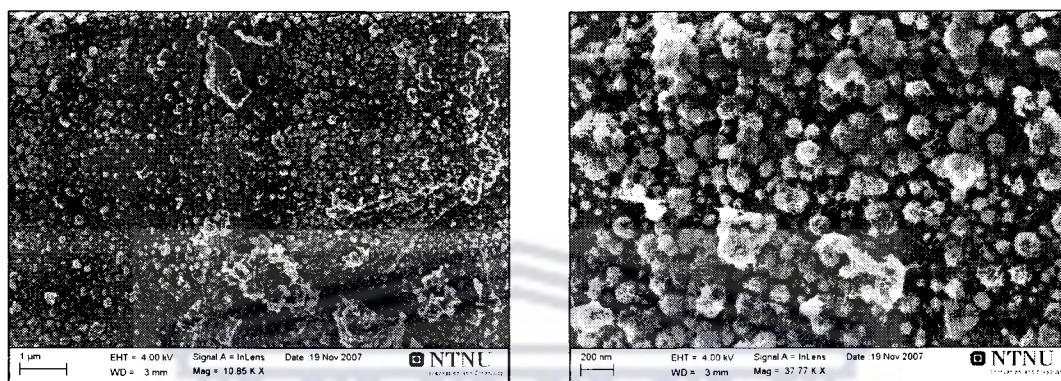


Figure 4.40. SEM images of “high-load” Pd-modified AB₅-type alloy (NaH_2PO_2 , 1:100, 50°C , 30 min) after preliminary surface functionalization in aqueous 1.0 vol.% γ -APTES solution

A comparative table illustrating the surface properties of the Pd-P coating obtained after functionalization in 1.0 vol. % aqueous γ -APTES solution and subsequent plating in the standard NaH_2PO_2 -based bath is given as Table 4.12. It was observed from Table 4.12. that functionalization prior to Pd-P deposition significantly increased the quality, and surface coverage of the coating.

Table 4.12. Structural properties of Pd-P coatings on non-functionalized and functionalized AB₅ alloys

Sample	Pd content (wt%)		Surface area (m^2/g)		
	Surface	Total	BET data	Calculated (coating)	
				BET	SEM
AB ₅ substrate	-	-	0.045(6)	-	-
Pd-AB ₅ (NaH_2PO_2) 30 min high-load	17.00	0.94	0.19(3)	15.1	6.1
γ -APTES Pd-AB ₅ (NaH_2PO_2) 30 min high-load	51.00	1.16	0.29(4)	21.4	8.6

In comparison, the quality of the Pd-P coating after pre-functionalization in 1.0 vol.% non-aqueous γ -APTES was comparable to the Pd surface particles observed on AB₅-type alloys surface-modified without pre-functionalization (Figure 4.20). However, significant amounts of Pd-P agglomeration was observed after pre-functionalization in non-aqueous γ -APTES, which was not clearly observed in the sample modified without pre-functionalization. Similarities in the Pd-P particle size were observed between the sample pre-treated in non-aqueous γ -APTES and “high-loading” (168 nm); the sample pre-treated in aqueous γ -APTES and “high-loading” (157 nm). Interestingly, the “dendrite” structures previously observed between Pd-P particles where 1.0 vol. % γ -APTES pre-treatment was utilized, were not featured on the surface after functionalization in non-aqueous γ -APTES solution. The dendrites were obviously specific to the networked arrangement provided by aqueous γ -APTES solution, and not the brush-like arrangement provided by non-aqueous γ -APTES solution. The surface Pd content after high loading and functionalization in non-aqueous 1.0 vol. % γ -APTES solution was determined as 9.7 wt.% Pd, and Pd total content was 1.2 wt.% Pd. It appeared that functionalization in non-aqueous γ -APTES solution did not facilitate significant increases in Pd-P content on the alloy surface.

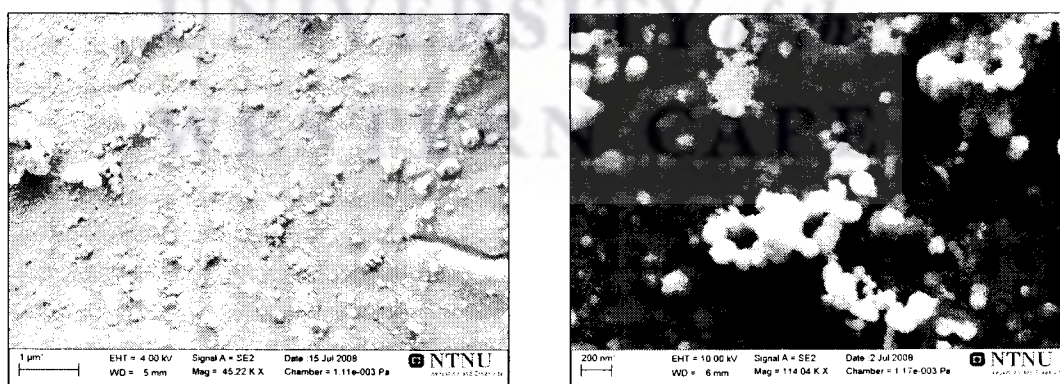


Figure 4.41. SEM images of “high-load” Pd-modified AB₅-type alloy (NaH_2PO_2 , 1:100, 50°C, 30 min) after preliminary surface functionalization in non-aqueous (toluene) 1.0 vol.% γ -APTES solution

Studies of the hydrogenation performances and kinetics of the functionalized samples were conducted after ~ 2 week pre-exposure of the sample materials to air and without pre-activation. The analysis was conducted under mild conditions ($P_{H_2} = 5.0$ bar, $T = 20$ °C, $t = 24$ hours). The results of the study of hydrogenation performance and kinetics are given as Figure 4.42. It was observed that samples functionalized in γ -APTES solution exhibited superior kinetics of hydrogenation, compared to the non-functionalized ($k = 1.9 \times 10^{-1} \text{ h}^{-1}$) and unmodified alloys ($k = 9.8 \times 10^{-6} \text{ h}^{-1}$), to attain the maximum capacity ($H/AB_5 \text{ max} = 5.0$ formula units) in less than 1 hour. In addition, it was observed that the sample material pre-treated in aqueous 1.0 vol. % γ -APTES exhibited slightly better kinetics of hydrogenation ($k = 1.3 \text{ h}^{-1}$) compared to that pre-treated in non-aqueous 1.0 vol.% γ -APTES ($k = 1.1 \text{ h}^{-1}$). For this reason all subsequent functionalization was conducted in aqueous solutions of γ -APTES.

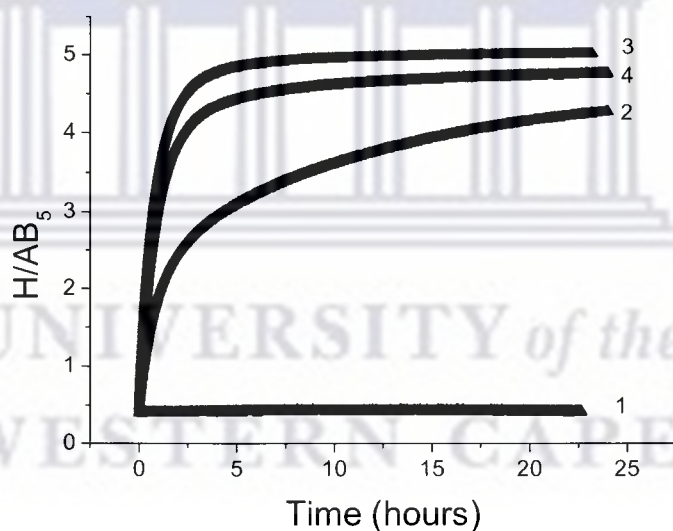
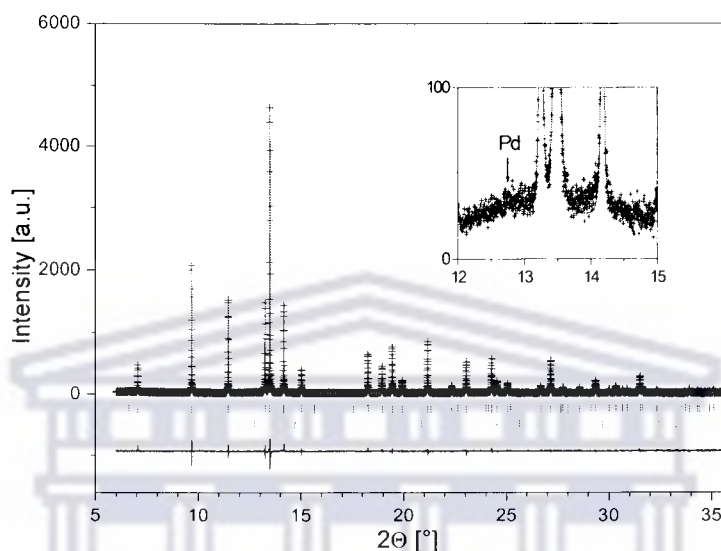


Figure 4.42. Influence of functionalization on the kinetics of hydrogenation of surface-modified AB_5 -type alloys (NaH_2PO_2 , $50^\circ C$, 30 min), (1) unmodified; (2) Pd high-load; (3) aqueous γ -APTES, Pd high-load; (4) non-aqueous γ -APTES, Pd high-load

A crystallographic study of the AB_5 -type alloy coated in a NaH_2PO_2 -based Pd-P electroless plating bath, after surface pre-functionalization aqueous 1.0 vol.% γ -APTES, was undertaken. Figure 4.43 showed incremental changes in the major AB_5

phase: 99 wt.%; $a = 5.00266(3) \text{ \AA}$, $c = 4.05099(3) \text{ \AA}$; CaCu_5 -type structure; space group – $P6/mmm$. Quantities of amorphous Pd were detected on the surface of the AB_5 alloy, with complete removal of the RE_2NiO_4 phase after surface modification.



Figures 4.43. Fitted SR-XRD diffractogram of the AB_5 -type alloy functionalized in 1.0 vol. % aqueous γ -APTES (pH = 7, 90°C , 1 hour) and surface-modified in the standard NaH_2PO_2 -based Pd plating bath

The surface chemical state of the Pd-modified (NaH_2PO_2 , 30 min) and γ -APTES functionalized Pd-modified AB_5 -type alloys (NaH_2PO_2 , 30 min) were analysed using SXPS. Spectra of the chemical analysis are presented as Figures 4.44 and 4.45, and results are tabulated in Table 4.13.

Importantly, the binding energies for the Pd deposited on the surface of the alloy, with and without pre-functionalization, confirmed that for both samples the Pd layers are in the zero-valent state (i.e. Pd^0) [233].

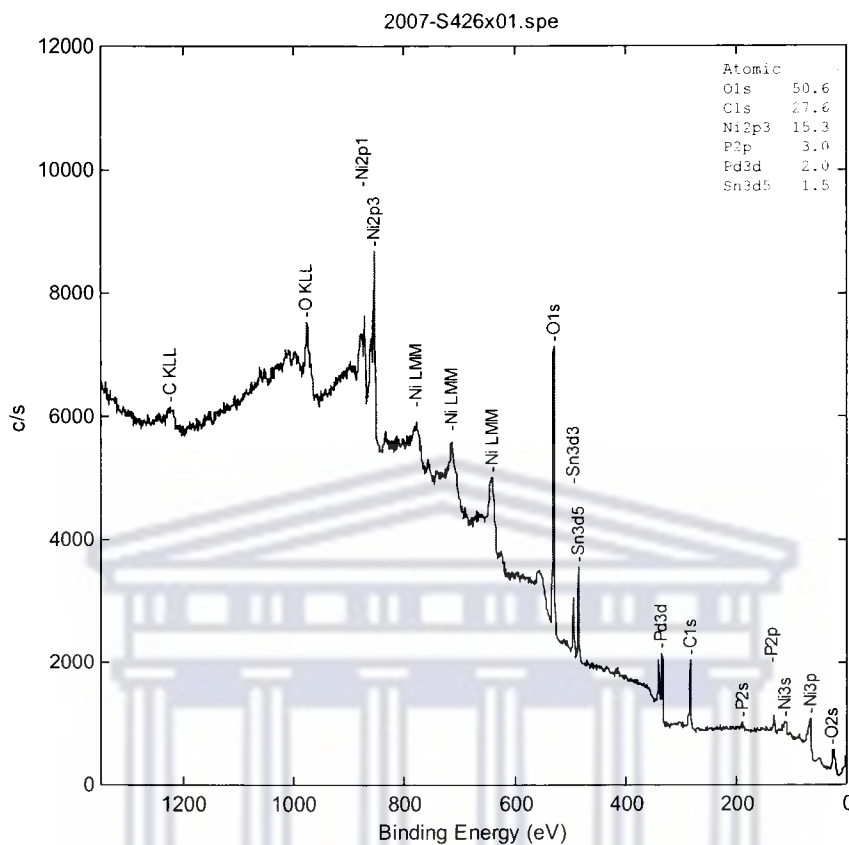


Figure 4.44. SXPS spectrum of AB₃ Pd (NaH₂PO₂, 50°C, 30 minutes)

The spectra mostly confirmed the level of surface contamination on the air-exposed samples. Metal hydride-forming alloys are known to hold significant quantities of carbonaceous species on the surface as a result of atmospheric contamination by CO, CO₂, and hydrocarbons [233]. High quantities of oxygen were also observed (Table 4.13), and it was assumed that this may be due to the presence of an oxide layer on the surface of the alloy. This oxide layer was assumed to be about 10 nm thick, in accordance with works by Ise *et al.* [83]. In addition, the encapsulation of the alloys using carbon- and oxygen-containing chemicals (CH₃OH, Na₂EDTA, γ -APTES) may have added to the carbon and oxygen surface burden of the alloy. Similarly, Harris *et al.* [103] observed large surface quantities of oxygen (27-40 at.%) and carbon (43-63 at.%) after PGM encapsulation. The influence of the carbon layers on the

hydrogenation / dehydrogenation properties are unknown. Schlapbach *et al.* [234] and Briggs *et al.* [199] proposed that the thickness of this layer could vary between 0.5 – 10 nm. However, SXPS analysis samples up to 5.0 nm of the surface. This may explain the strangely high carbon content detected. Briggs stated that the carbon layer does not have to be of significant thickness before it negatively affects the quantitative analysis of sample materials [233]. The adventitious carbon may also be the result of the C peak to shift of the spectra. Generally, the C_{1s} peak at 285 eV is due to carbon atoms binding to themselves or onto hydrogen. In addition, the high level of oxygen detected in the O_{1s} peak (533 eV) may result in shifts of all peaks to slightly higher binding energies [199].

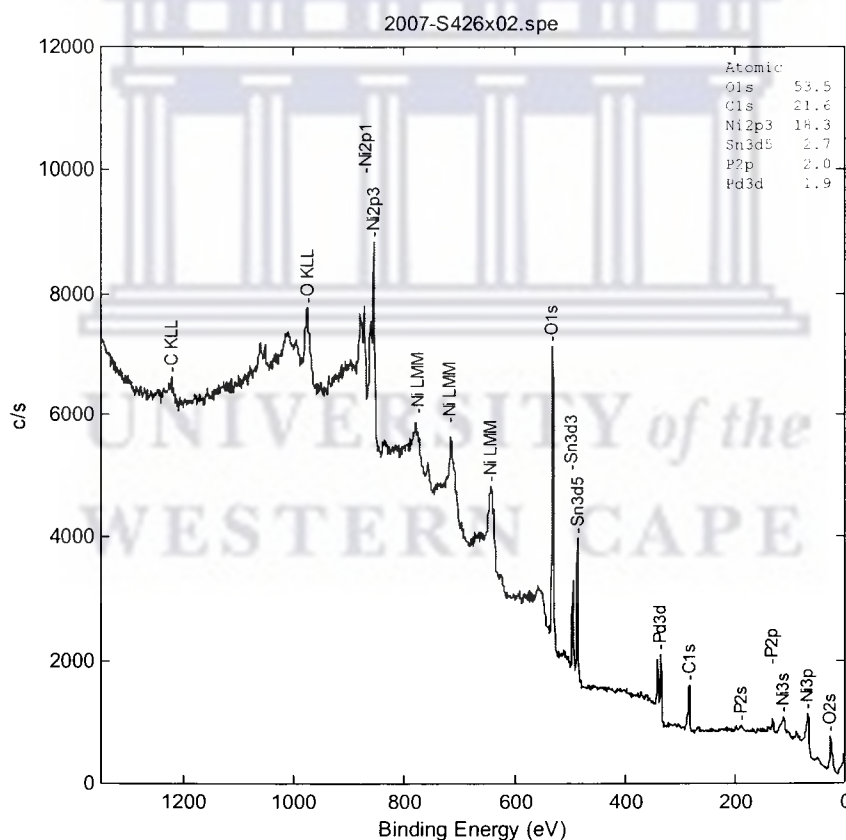


Figure 4.45. SXPS spectrum of AB₃ γ -APTES Pd (1.0 vol.%, NaH₂PO₂, 50°C, 30 minutes)

Pd concentrations (~ 2.0 at.% or 2.1 wt.%) were detected, with and without functionalization, at the surface of the AB₅-type alloy. In comparison, 1.0 – 1.2 wt.% Pd was detected at the alloy surface using AAS, representing an acceptable agreement between the two analytical methods. Similarly, P (2-3 at.% or 0.6-0.9 wt.%) and Sn (1.5-2.7 at.% or 1.8-3.2 wt.%) were detected at the surface of the modified alloys.

Table 4.13. Summarized results of the SXPS chemical analysis of the Pd-modified (NaH₂PO₂, 30 min) and γ -APTES functionalized Pd-modified AB₅-type alloys (NaH₂PO₂, 30 min)

Element	Sample		Probable bond(s)	
	AB ₅ Pd (NaH ₂ PO ₂ , 30 min)	AB ₅ 1.0 vol.% γ -APTES Pd (NaH ₂ PO ₂ , 30 min)		
C	Atomic concentration (%)	27.6	21.6	Adventitious carbon; C-(C,H,O)
	Binding energy (eV)	284.9	284.8	
Ni	Atomic concentration (%)	15.3	18.3	NiO; Ni ₂ O ₃
	Binding energy (eV)	856	855.5	
O	Atomic concentration (%)	50.6	53.5	O-(C,H); metal oxides
	Binding energy (eV)	531.3	531	
P	Atomic concentration (%)	3.0	2.0	Phosphate
	Binding energy (eV)	133.3	132.8	
Pd	Atomic concentration (%)	2.0	1.9	Pd; PdO
	Binding energy (eV)	335.4	335.2	
Sn	Atomic concentration (%)	1.5	2.7	SnO; SnO ₂
	Binding energy (eV)	486.8	486.6	

An investigation into the influence of the concentration of the γ -APTES solution on the surface Pd loading, total Pd loading, specific surface area, and kinetics of hydrogenation after electroless plating was conducted. pH-neutralized aqueous γ -APTES solutions with concentrations of 0.5, 1.0, and 5.0 vol.% were prepared, the surface pre-functionalization performed, and the surface subsequently encapsulated in the standard NaH₂PO₂-based Pd-P plating bath (Table 3.1). A study of the morphology of the surface Pd-P surface coating after functionalization in aqueous γ -APTES solutions was undertaken. Results are presented as Figure 4.46-4.48.

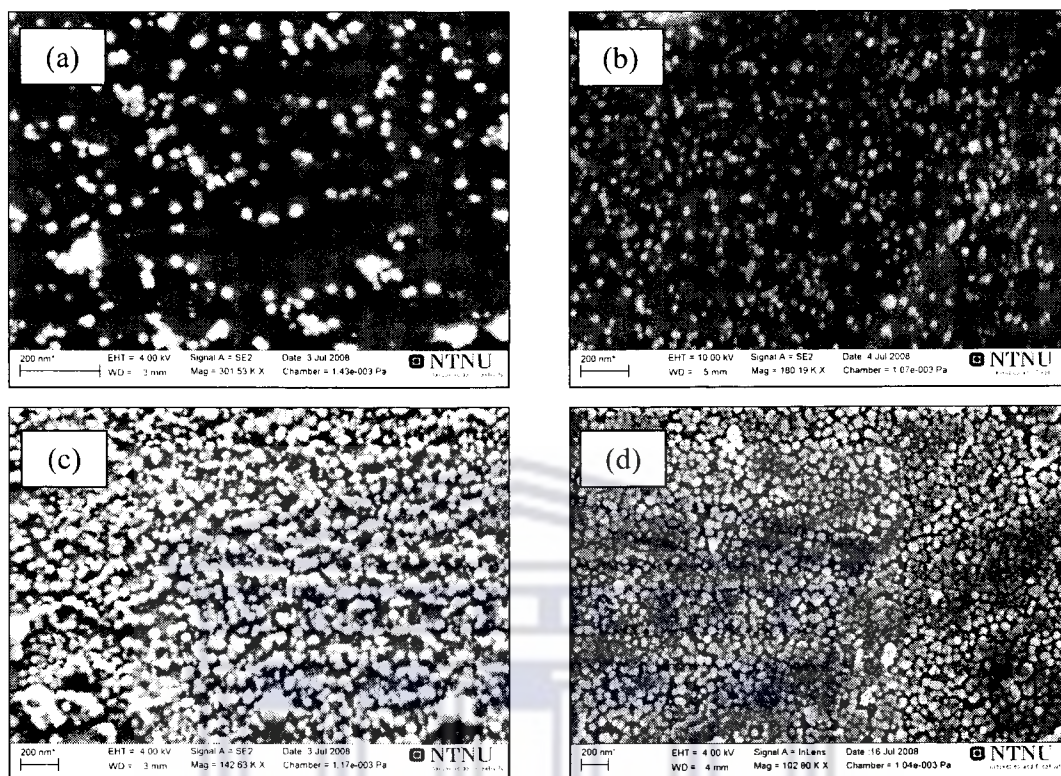


Figure 4.46. SEM images of AB₅-type alloys surface functionalized in 0.5 vol.% γ -APTES solution and Pd-P deposition (NaH₂PO₂, 50 °C), (a) 1 minute; (b) 5 minutes; (c) 10 minutes; (d) 30 minutes

After functionalization in 0.5 vol.% aqueous γ -APTES solution and subsequent Pd-P deposition, the density of the coating was observed to increase with an increase in the deposition time. The quality of the Pd-P coating was observed to be significantly better than that of the samples prepared without the γ -APTES pre-treatment step. Small areas of coalescence of the Pd-P particles were observed on the surface of the alloy after 30 minutes of deposition. In addition, small areas of Pd-P particle agglomeration were observed on the surface of the alloy at the onset of the deposition process. However, the Pd-P layer was discontinuous in nature with voids as large as \sim 150 nm observed in the surface layer.

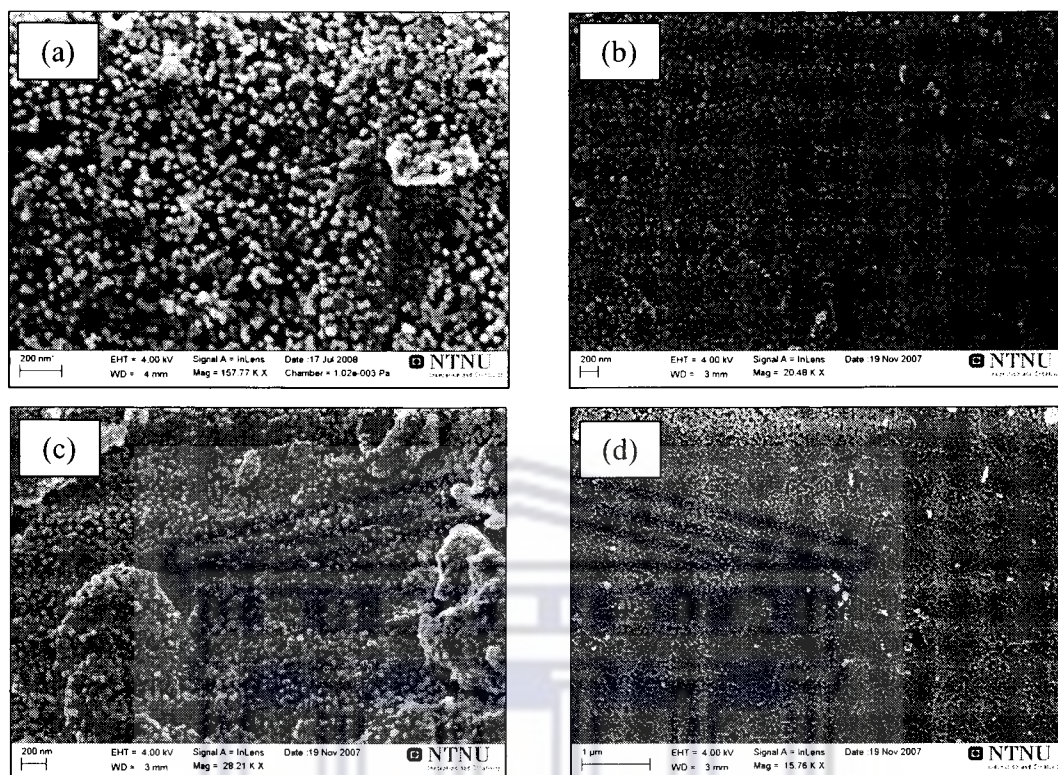


Figure 4.47. SEM images of AB₅-type alloys surface functionalized in 1.0 vol.% γ -APTES solution and Pd-P deposition (NaH_2PO_2 , 50 °C), (a) 1 minute; (b) 5 minutes; (c) 10 minutes; (d) 30 minutes

After functionalization in 1.0 vol.% aqueous γ -APTES solution and subsequent Pd-P deposition, the density of the coating was observed to increase with deposition time (Figure 4.47). The quality of the Pd-P coating was observed to be significantly better than that of the samples prepared without the γ -APTES pre-treatment step, and samples prepared after pre-treatment in 0.5 vol.% and 5.0 vol.% γ -APTES solution. Large areas of coalescence of the Pd-P particles were observed on the surface of the alloy after 30 minutes of deposition. In addition, large areas of Pd-P particle agglomeration were observed on the surface of the alloy at the onset of the deposition process. The best Pd-P surface coverage was realised after surface pre-treatment in 1.0 vol.% aqueous γ -APTES solution. The Pd-P layer was continuous in nature with holes smaller than ~ 150 nm observed in the surface layer.

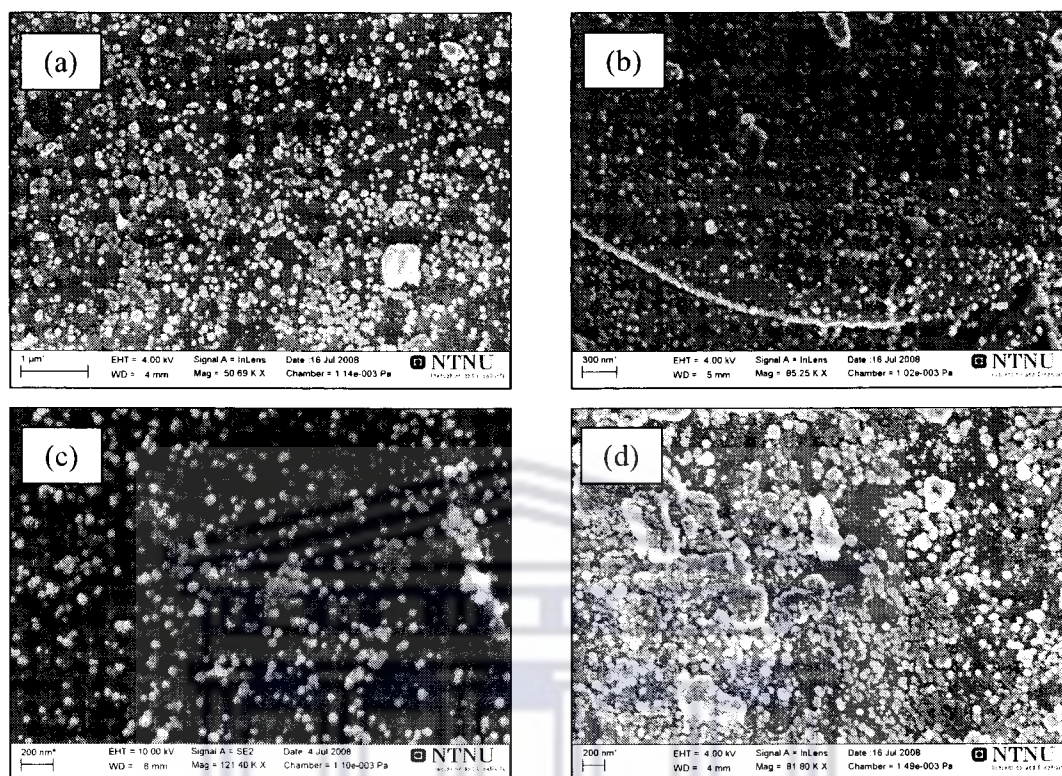


Figure 4.48. SEM images of AB₅-type alloys surface functionalized in 5.0 vol. % γ -APTES solution and Pd-P deposition (NaH_2PO_2 , 50 °C), (a) 1 minute; (b) 5 minutes; (c) 10 minutes; (d) 30 minutes

After functionalization in 5.0 vol.% aqueous γ -APTES solution and subsequent Pd-P deposition, the density of the coating was observed to increase with deposition time. The quality of the Pd-P coating was observed to be significantly better than that of the samples prepared without the γ -APTES pre-treatment step. Large areas of coalescence of the Pd-P particles were observed after 30 minutes of deposition. However, the Pd-P layer was mostly discontinuous in nature with voids larger than 200 nm observed in the surface layer.

Particle nucleation, particle growth, and formation of continuous Pd-P layers using the functionalization approach in electroless plating can be diagrammatically represented as Figure 4.49. In the nucleation step, Pd nuclei of critical size are formed on the substrate surface, assisted by γ -APTES molecules. The nuclei grow three-

dimensionally to supercritical dimensions and coalesce to form Pd islands. The Pd islands merge after the collapse of their boundaries to form a discontinuous layer with holes that later fill to form a continuous layer.

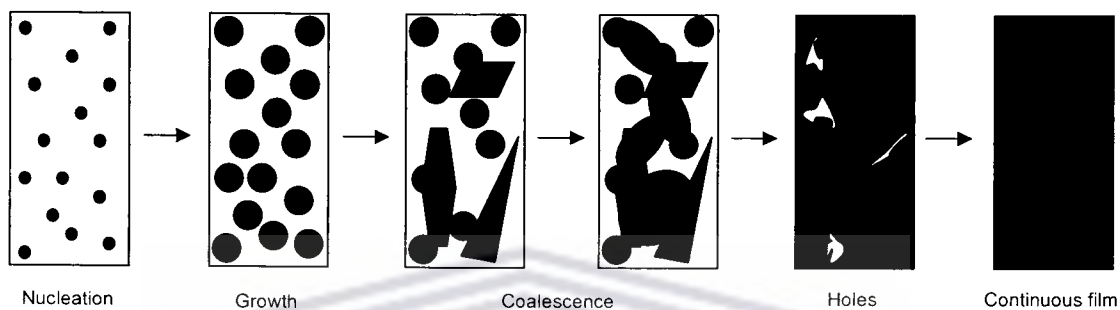


Figure 4.49. General representation of the stages of metal particle growth to form a continuous layer on a substrate surface using electroless plating

Ion beam analysis by *micro*-PIXE had previously confirmed that the AB₅-type alloy surface-modified without functionalization did not facilitate the surface deposition of continuous layers of Pd, and that the Pd particles were scattered (Figure 4.18). In contrast, dynamic analysis confirmed that the AB₅-type alloys surface-modified after functionalization in γ -APTES, supported continuous layers of Pd-P (Figure 4.50).

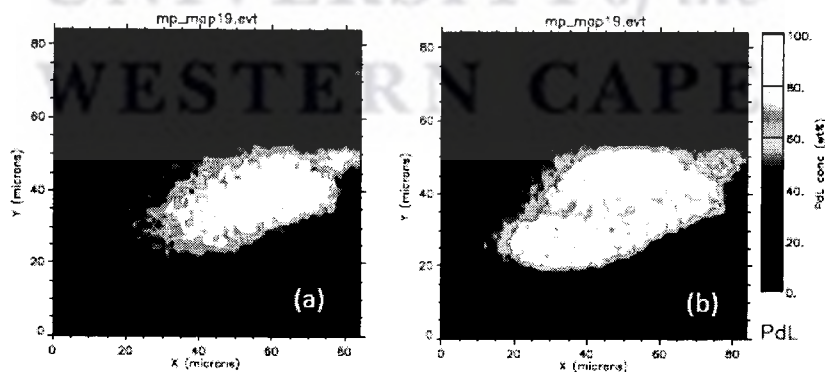


Figure 4.50. Dynamic analysis of Pd-P surface-modified AB₅-type alloy (NaH₂PO₂, 30 min) after pre-treatment in 1.0 vol.% γ -APTES solution, (a) total background; (b) Pd L

Based on the observations made in the *micro*-PIXE study, a cross-section of an AB₅-type alloy particle pre-treated with 1.0 vol. % γ -APTES and coated with Pd-P (NaH₂PO₂, 30 minutes, 50 °C) was prepared to ascertain the thickness of the continuous layer. Details of the preparation of the cross-section are given in Section 3.4.3. The observed layer thickness corresponded to the deposition of ~10 layers of Pd-P particles (average thickness = 550 nm) (Figure 4.51). This thickness was comparable to that of Pd layers deposited by Zheng *et al.* ~0.2-1.0 μ m [118]. The Pd-P surface layers were deduced to be three-dimensional as they possess appreciable thickness in the direction perpendicular to the surface of the AB₅-type alloy particle. It is also well-known in classical film growth theory that after coalescence of particles much of the subsequent growth occurs perpendicular to the plane of the substrate surface, hence the layer thickness grew appreciably thick as the reaction was allowed to progress [120]. In addition, the Pd-P layer may have been subjected to a degree of smearing from the polishing process. Although measures were taken to minimize the smearing, it is unavoidable and may have exaggerated the thickness of the Pd-P layer.

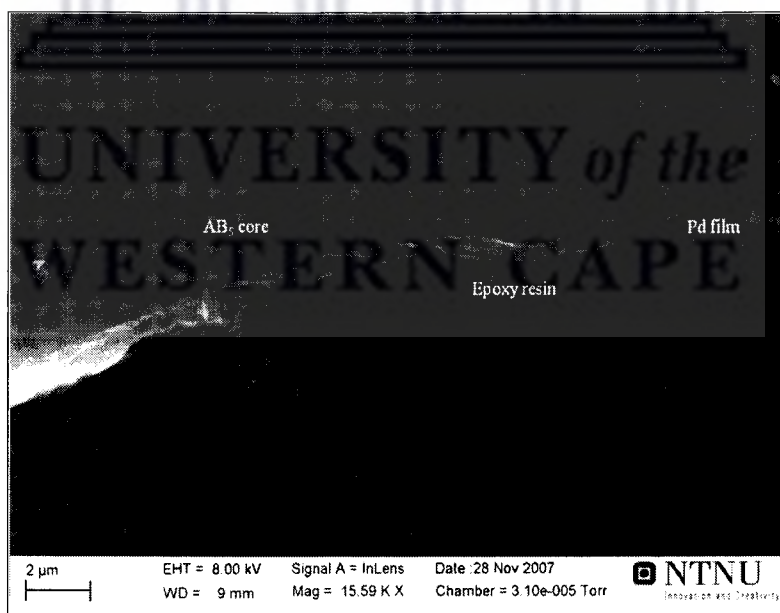


Figure 4.51. Cross-section of AB₅-type alloy surface-modified with Pd-P (NaH₂PO₂, 30 min, 50°C) after pre-treatment in γ -APTES solution (1.0 vol.%, 50°C, pH = 7, 60 min)

Based on the microscopy analysis, a study of the influence of γ -APTES surface functionalization on the Pd-P particle size was conducted. The results were presented in Figure 4.52. Generally, it was observed that the surface functionalization promoted the deposition of Pd-P particles significantly smaller in size, compared to that deposited without the surface functionalization step. The smaller Pd-P particles may account for the better quality and greater density of the surface coatings upon surface functionalization. It was observed that lower concentrations of the γ -APTES solution promoted the deposition of smaller Pd-P particles, with 1.0 vol. % γ -APTES promoting the deposition of the smallest particles. Higher concentrations of γ -APTES promoted the deposition of larger particles which were more agglomerated in nature. It was deduced that an increase in deposition time influences the approach of the Pd-P surface layer from surface particles towards a continuous surface layer, and with that a change in the critical size of the Pd-P particles. In addition, the increase in deposition time produced initial rapid growth in the Pd-P particle size (1-5 minutes) followed by a decrease in the critical size of the Pd-P particles (5-30 minutes). It is assumed that after ~5 minutes the Pd-P particles began to form surface islands after initialization of coalescence.

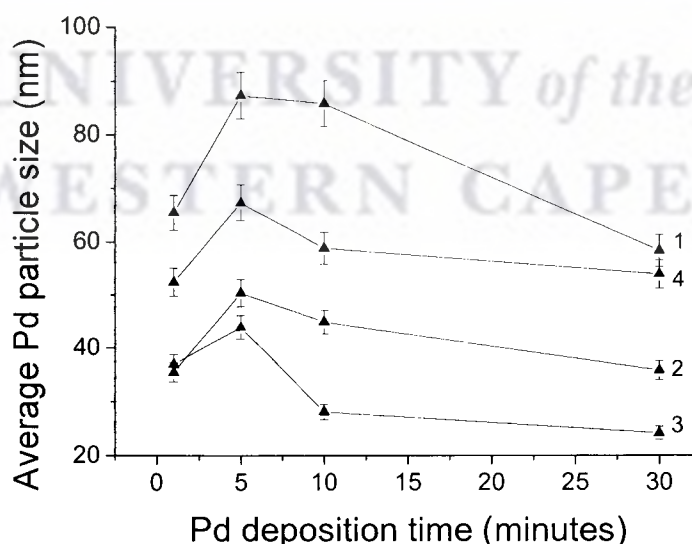


Figure 4.52. Influence of γ -APTES concentration on Pd-P particle size: (1) non-functionalized; (2) 0.5 vol. % γ -APTES; (3) 1.0 vol. % γ -APTES; (4) 5.0 vol. % γ -APTES

The Pd-P particle size distribution of the surface-modified alloy, after γ -APTES pre-treatment (30 minutes, 50°C, high-load), was investigated using the Carl Zeiss Axiovision[®] software. It was observed that the functionalized samples exhibited a fairly wide particle size distribution (~40-170 nm) after increasing the substrate-to-solution concentration, compared to that prepared without the functionalization step (~80-110) (Figure 4.53).

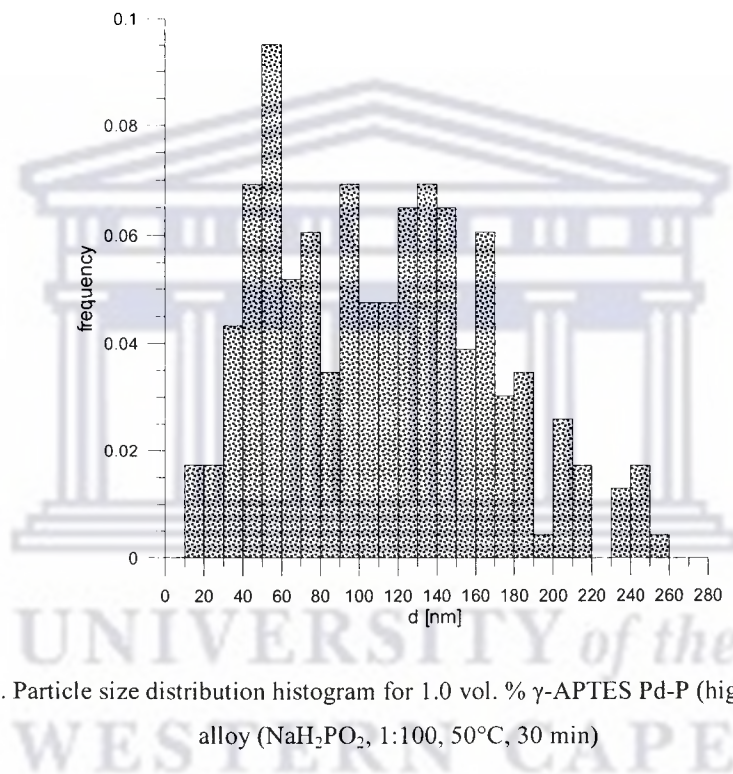


Figure 4.53. Particle size distribution histogram for 1.0 vol. % γ -APTES Pd-P (high-load) AB₅-type alloy (NaH₂PO₂, 1:100, 50°C, 30 min)

An investigation into the Pd surface and total loadings was undertaken to analyse the quantity of Pd-P deposited on the surface of the AB₅-type alloy, and the quality of the coating, after functionalization in γ -APTES solution. The results were presented in Figures 4.54 and 4.55.

It was observed that Pd-P deposition without the use of γ -APTES pre-treatment did not facilitate deposition of large amounts of Pd on the surface of the AB₅-type alloy. It can be explained by the poor adhesion of Pd nuclei to the surface RE₂NiO₄ “skin”

taking place due to the physical conjunction. On the other hand, the pre-functionalization with γ -APTES solutions facilitated the deposition of higher Pd loadings on the surface of the AB₅-type alloy, with the Pd surface loading increasing with an increase in the concentration of γ -APTES solution. The lower Pd surface loadings observed with functionalization in more dilute γ -APTES solution (i.e. 0.5 vol. %) may have been a result of an associated limited coverage by the γ -APTES molecules on the surface of the alloy. In so doing, the Pd nuclei became immobilized on the limited available surface sites modified with γ -APTES molecules, resulting in the lower coverage by the deposited Pd-P layer. On the other hand, the use of higher γ -APTES concentrations (≥ 1.0 vol. %) resulted in the deposition of a fairly homogeneous layer on the surface of the AB₅-type alloy. Pd nuclei, from the activation solution, were immobilized on the maximum quantity of surface sites, which have highest coverage by γ -APTES molecules, resulting in the deposited Pd-P layer having a greater surface coverage. The end result was that more Pd could be deposited on the surface of the AB₅-type alloy with functionalization.

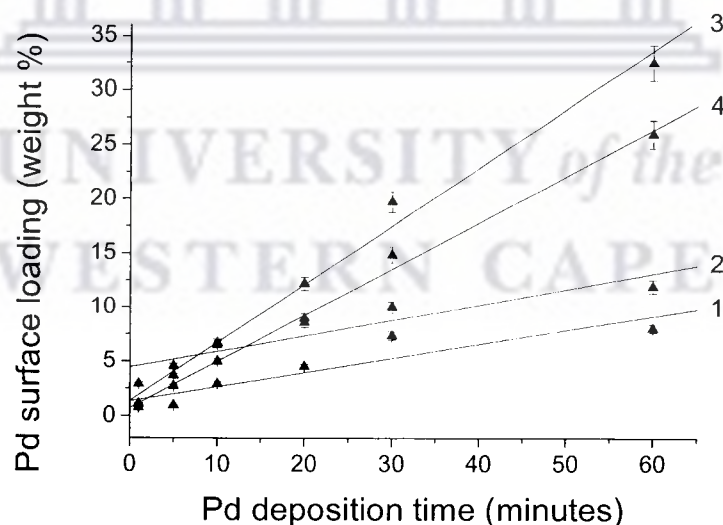


Figure 4.54. Influence of aqueous γ -APTES concentration on Pd surface loading on AB₅-type alloys
(1) unfunctionalized; (2) 0.5 vol. % γ -APTES; (3) 1.0 vol. % γ -APTES; (4) 5.0 vol. % γ -APTES

It was observed that Pd-P deposition, after the γ -APTES pre-treatment, facilitated deposition of larger amounts of Pd on the AB₅-type alloy, compared to that prepared without the pre-treatment step. Similarly, the poorer Pd total loadings observed without the pre-treatment step may be a result of inefficient adhesion of Pd nuclei to the surface RE₂NiO₄ “skin”. It was generally observed that the Pd total loading increased with an increase in the concentration of γ -APTES solution, with the optimal loading observed after pre-treatment in 1.0 vol. % γ -APTES solution. At this concentration the Pd nuclei may have been immobilized on ~1.0 monolayer coverage of γ -APTES molecules, and as a result the deposited Pd layer had greater density and coverage.

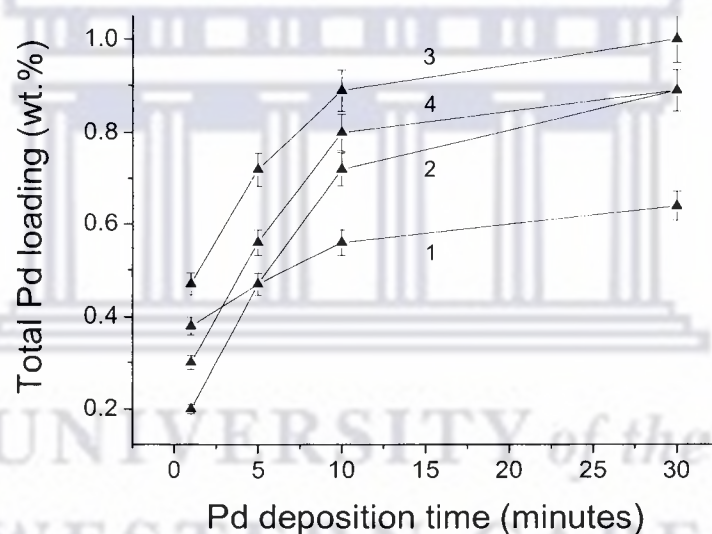


Figure 4.55. Influence of γ -APTES concentration on Pd total loading: (1) unfunctionalized; (2) 0.5 vol. % γ -APTES; (3) 1.0 vol. % γ -APTES; (4) 5.0 vol. % γ -APTES

With an increase in the quantity of Pd-P deposited at the surface of the AB₅-type alloy, as a result of the functionalization in the γ -APTES solution, so the surface area of coverage is expected to exhibit changes. For this reason an analysis of the specific surface area was undertaken to analyse any trends in the surface morphology with functionalization. The results were presented in Figure 4.56. It was observed that the

unfunctionalized alloy exhibited a significantly larger specific surface area than the functionalized samples. This may be a result of the inability to form a continuous Pd-P layer over the studied deposition time (1-30 minutes), as previously observed in Figure 4.20, and the presence of isolated Pd-P particles and clusters. In contrast, the functionalized alloys were observed to form continuous Pd-P surface layers, and as a result exhibited significantly lower specific surface areas. During the initial stages of Pd-P growth on the surface functionalized alloy, the specific surface area was observed to increase as particles began nucleating on the surface of the alloy. Subsequently, the critical Pd-P particle size was attained and the particles began to coalesce, with the observation of a parallel decrease in the specific surface area with the coating approaching a continuous layer. The result clearly illustrates the possibilities of attaining continuous Pd layers with functionalization and the inability of the standard method of electroless plating in depositing continuous layers. It was also noted that the specific surface area of the unfunctionalized samples exhibited more discrepancies in the measured values than that exhibited by the functionalized samples. This indirectly demonstrated the greater control of the surface chemistry of the Pd-P layer with functionalization.

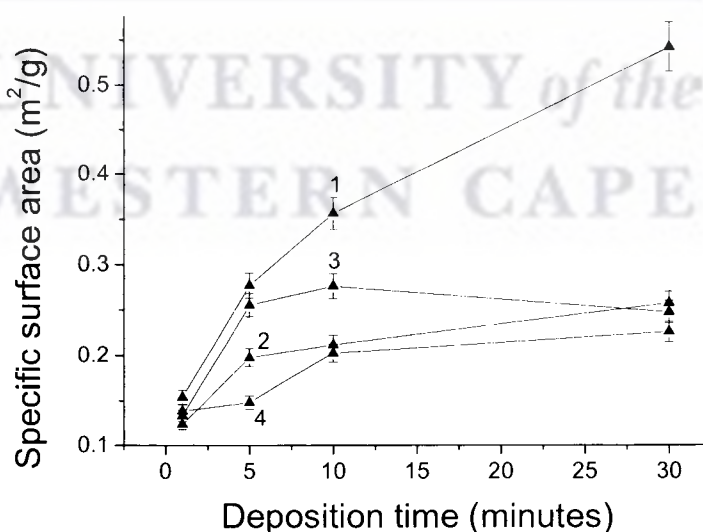


Figure 4.56. Influence of functionalization on specific surface area of Pd-P surface-modified AB₃-type alloy, (1) unfunctionalized; (2) 0.5 vol. % γ -APTES; (3) 1.0 vol. % γ -APTES; (4) 5.0 vol. % γ -APTES

A comparative study of the kinetics of hydrogenation of the γ -APTES functionalized AB₅-type alloys was conducted after ~ 2 week pre-exposure of the sample materials to air, without pre-activation. The alloys were further surface-modified using the standard Pd electroless plating bath (Table 3.1). The analysis was conducted under mild conditions ($P_{\text{H}_2} = 5.0$ bar, $T = 20$ °C, $t = 24$ hours). The results were presented in Figure 4.57.

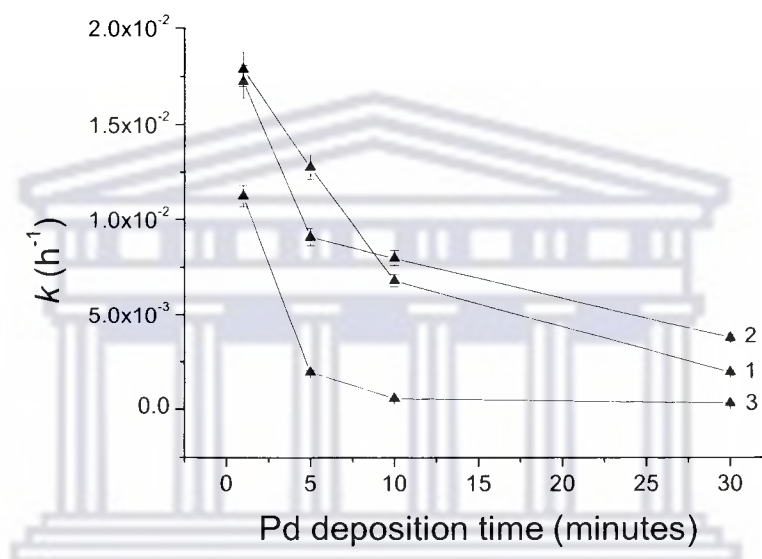


Figure 4.57. Influence of γ -APTES concentration on kinetics of hydrogenation of Pd-P surface-modified AB₅-type alloy, (1) 0.5 vol. % γ -APTES; (2) 1.0 vol. % γ -APTES; (3) 5.0 vol. % γ -APTES

In Figure 4.57 a comparison of the kinetics of hydrogenation of the samples functionalized using three concentrations of aqueous γ -APTES solution was made. It was observed that higher concentrations of the aqueous γ -APTES solution (i.e. 5.0 vol. %) facilitated lower kinetics of hydrogenation. In comparison, dilute concentrations of the aqueous γ -APTES solution facilitated slightly better kinetics of hydrogenation. This behaviour may be a result of the larger Pd-P particle size associated with the use of concentrated aqueous γ -APTES solutions (Figure 4.52). Likewise, the smaller Pd-P particle size associated with functionalization in dilute aqueous γ -APTES solution facilitated better kinetics of hydrogenation (Figure 4.57).

However, as the growth of the Pd-P particles was allowed to progress with deposition time, so the kinetics of hydrogenation of the functionalized materials began to sharply deteriorate. This behaviour was largely due to the large increases in Pd-P surface density and Pd-P particle coalescence with an increase in the deposition time, as observed in Figures 4.46 – 4.48. It was previously deduced that an increase in deposition time influenced the rate at which the Pd-P surface layer progressed from surface particles towards a continuous surface layer (Figure 4.49). The rate of this process was fast as the growth of the continuous surface layer was catalysed by the γ -APTES. In addition, the presence of a continuous layer on the functionalized materials was confirmed by the study of the specific surface area (Figure 4.56), where stability in the specific surface area was observed after about 10 minutes of Pd-P electroless plating on γ -APTES functionalized AB₅-type alloy. It was assumed that the hydrogen selectivity of the alloy surface was infinite, after functionalization, as a result of the presence of a hydrogen-selective continuous Pd-P layer.

It was also observed that the Pd-P deposition time had a profound influence on the hydrogenation properties of the surface-modified materials, where k generally decreased with an increase in the deposition time. This may be a result of the diminishing contribution to the overall hydrogen dissociation by the hydrogen spillover mechanism with an increase in the Pd-P surface density and the beginning of the continuous layer formation. In such a case, solution-diffusion through the Pd layer would become the favoured mechanism for hydrogen dissociation.

A study of n associated with the characteristic time of absorption (t_0) was undertaken to ascertain the mechanism of hydrogenation of the surface-modified alloys with and without pre-treatment in γ -APTES solution. The results were presented in Figure 4.58.

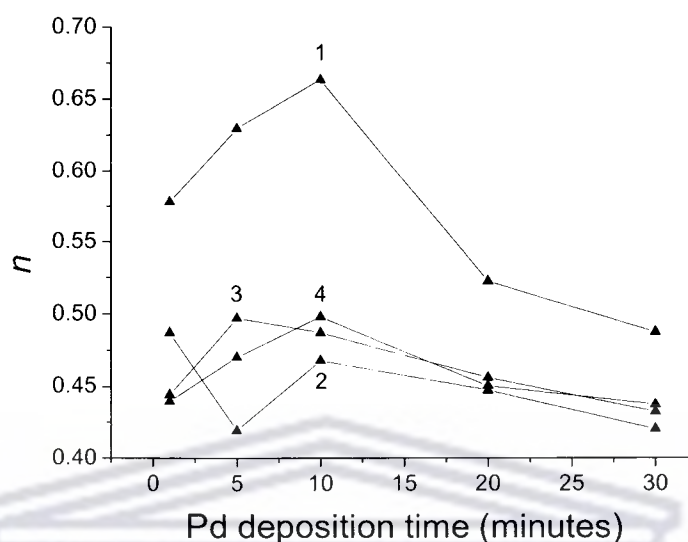


Figure 4.58. Influence of γ -APTES concentration on n of Pd-P surface-modified AB₃-type alloy: (1) non-functionalized; (2) 0.5 vol. % γ -APTES; (3) 1.0 vol. % γ -APTES; (4) 5.0 vol. % γ -APTES

It was observed that the functionalized alloys exhibited morphological dimensionalities of growth that were different to that exhibited by the unfunctionalized alloy, and that n was independent of concentration of the aqueous γ -APTES solution. Changes in the n with functionalization in γ -APTES solution may be a result of changes in the hydrogen dissociation mechanism, from mostly hydrogen spillover to mostly solution-diffusion, with a change in the morphology from Pd-P clusters to Pd-P continuous layers. The n -value was also strongly dependent on surface transport, which was rate-limited by the surface chemical state.

Based on the observation that the RE₂NiO₄ “skin” detected on the surface of the surface-modified alloy facilitated the adhesion of the γ -APTES molecules, an attempt was made to completely pre-oxidize the surface of the alloy prior to functionalization to promote the adhesion of the maximum quantity of γ -APTES molecules onto the surface, and in that way promote the deposition of a continuous Pd-P layer. FESEM

analysis was conducted to ascertain the influence of H_2O_2 pre-oxidation on Pd-P morphology and Pd-P surface density (Figure 4.59).

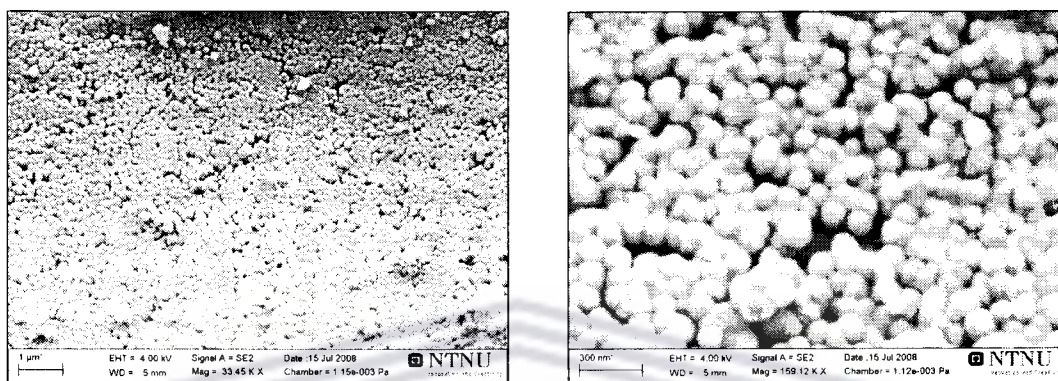


Figure 4.59. Images of AB_5 -type alloys pre-oxidised in H_2O_2 prior to functionalization in γ -APTES solution (pH = 7, 60 minutes, 90°C), and subsequent Pd-P deposition (high-load, 30 minutes, 50°C)

A large initial increase in the specific surface area of the alloy ($0.37 \text{ m}^2/\text{g}$) was observed with pre-oxidation of the alloy surface with H_2O_2 solution and functionalization in 1.0 vol.% γ -APTES solution. Subsequently, a further increase in the specific surface area of the pre-treated sample ($0.38 \text{ m}^2/\text{g}$) was observed with sensitization / activation in the Pd-Sn colloidal solution. The result indicates that H_2O_2 pre-oxidation had facilitated deposition of a complete monolayer of γ -APTES molecules on the alloy surface, which also facilitated the deposition of a complete layer of the Pd-Sn colloidal particles on the surface of the alloy.

It was observed that pre-oxidation of the alloy surface, and subsequent functionalization, facilitated the deposition of an increased surface density of Pd-P particles on the surface of the alloy (Figure 4.59). These surface Pd-P particles were tightly-packed to form a continuous layer. Pd total loading of 1.35 wt.% further illustrated the enhancement in the quantity of Pd that was deposited using pre-oxidation prior to functionalization. A large measured specific surface area ($1.0 \text{ m}^2/\text{g}$) was further indicative of the enhanced Pd-P surface coverage on the AB_5 -type alloy.

The average Pd-P particle size was 137 nm, making it comparable to that observed without the pre-oxidation step (157 nm).

A hydrogenation study of the functionalized samples with and without pre-oxidation in H_2O_2 was conducted after ~ 2 week pre-exposure to air, without pre-activation, and under mild conditions ($P_{\text{H}_2} = 5.0$ bar, $T = 20$ °C, $t = 24$ hours) to investigate the influence of the pre-oxidation step on the kinetic properties (Figure 4.60). It was observed that the samples prepared with the pre-oxidation step exhibited slightly better kinetics of hydrogenation ($k = 2.0$ h⁻¹) compared to that prepared without the pre-oxidation step ($k = 1.3$ h⁻¹).

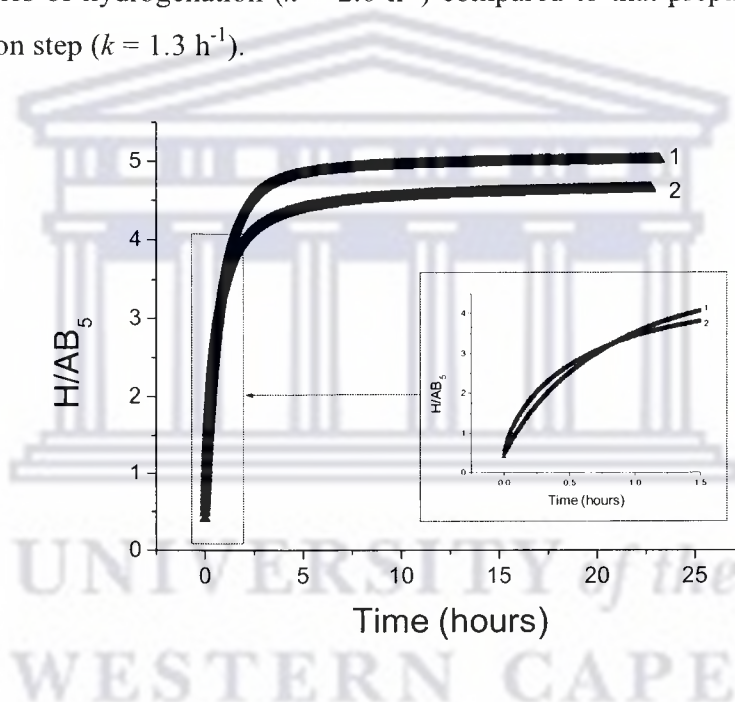


Figure 4.60. Influence of surface pre-oxidation on kinetics of hydrogenation of functionalized Pd-P surface-modified AB₅-type alloy (NaH_2PO_2 , high-loading): (1) no pre-oxidation; (2) H_2O_2 pre-oxidised

4.3.4. Morphology and kinetics of surface-modified AB₅-type alloys after pre-complexation of palladium nuclei with γ -aminopropyltriethoxysilane

An important feature in the standard electroless plating procedure was the sensitization of the AB₅-type alloy surface using SnCl_2 in a colloidal solution. The Sn^{2+} ions in solution had the function of increasing the surface roughness (i.e.

etching, pitting) of the alloy thereby facilitating an enhancement of the physical adhesion between the alloy surface and the Pd nuclei, which was necessary for surface activation. Excess Sn may result in blocking of Pd surface activation sites, decreasing oxidation efficiency towards the reducing agent, and subsequent inhomogeneity of the deposited metal layer [163]. The Sn component should have dissolved back into the bulk solution as SnCl_4 after acceleration, but it was observed through EDS and AAS elemental analyses, that some of the Sn was retained on the alloy surface after Pd-P deposition. It was therefore imperative to exclude Sn from the electroless plating process, and in that way, promote deposition of catalytic Pd nuclei. It was therefore necessary to develop a chemical method of surface activation that would exclude Sn as a sensitizer and promote the deposition of Pd nuclei.

Based on the ability of γ -APTES to increase the surface adhesion towards Pd nuclei in electroless plating, an approach was taken to complex the Pd nuclei within the structure of γ -APTES molecules. In doing so, the quality of surface activation may be increased, the quality of the Pd-P coatings may be enhanced, and the kinetics of hydrogenation may potentially be improved. The Pd nuclei pre-complexation approach was deemed important in the development of electroless plating technology in the encapsulation of metal hydride-forming alloys, and presents the possibility of enhancing the kinetics of hydrogenation.

In the procedure, 0.3g of the PdCl_2 salt was dissolved in dilute HCl at 50°C. The mixture was then diluted into 100 mL aqueous 1.0 vol. % γ -APTES solution, pH-neutralized, and 5.0g of the sample material further suspended in the solution for 1 hour at 90°C. No precipitation of the Pd was observed. The suspension was filtered, the alloy washed with copious amounts of deionised water and methanol, and allowed to dry for 2 hours at 80°C. Importantly, the PdCl_2 concentration in the activation solution was identical to that used in the standard Pd-Sn colloidal solution. The activated alloy was then plated in the standard Pd-P electroless plating bath (NaH_2PO_2 , 50°C, 30 minutes). Finally, the alloy was washed twice with deionised

water and allowed to dry overnight at 80°C. A generalized schematic representation of the experimental approach is given as Figure 4.61.

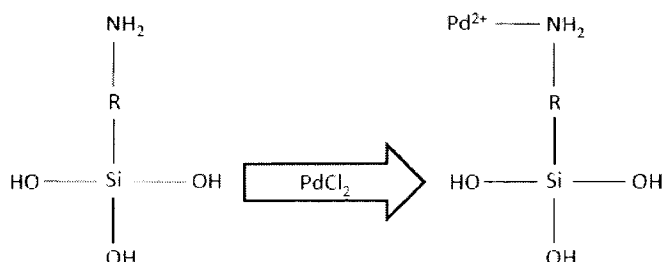


Figure 4.61. General representation of Pd nuclei pre-complexation technique in Pd electroless plating

A morphological study of the alloys prepared after activation with complexed Pd nuclei, and subsequent electroless plating (NaH_2PO_2 , 50°C, 30 minutes) was undertaken using FESEM. The experimental results were presented in Figure 4.62.

It was observed that the activation using complexed Pd nuclei and the subsequent deposition of Pd-P in the standard electroless plating bath facilitated the deposition of a continuous layer on the surface of the alloy. In addition, the Pd-P particles were highly coalesced to form areas of uniform coating and high densities of Pd-P, compared to the scattered Pd-P clusters observed using the standard sensitization / activation approach. The Pd total loading of the sample material after preliminary complexation of Pd nuclei and subsequent Pd-P deposition was 0.8 wt.%, illustrating that the method facilitated the deposition of large quantities of Pd-P on the AB_5 -type alloy. This quantity of Pd significantly exceeded that of the corresponding alloy prepared without the Pd nuclei complexation ~ 0.6 wt.%.

activation nuclei using aqueous solutions of aminosilanes, prior to the electroless plating improved the subsequent process of the electroless plating on hydrogen sorption alloys to yield more dense and uniform coatings, and in such a way, resulted in better hydrogen sorption performances of the surface-modified alloys.

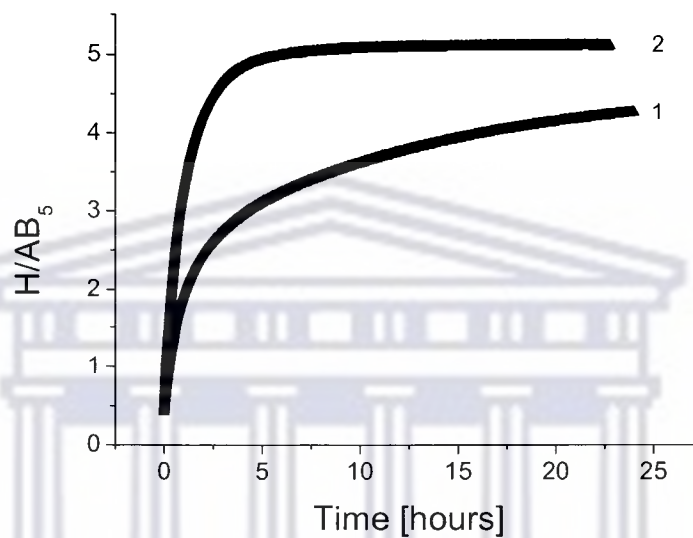


Figure 4.63. Dynamics of H absorption ($P_{H_2} = 5.0$ bar, $T = 20$ °C) by non-activated Pd-modified AB₅-type alloys, (1) after preliminary sensitization-activation in a Pd-Sn colloidal solution and subsequent Pd-P deposition; (2) after preliminary complexation of Pd nuclei and subsequent Pd-P deposition

The influence of the PdCl₂ concentration on the total and surface loadings of the alloys surface-modified after activation with the complexed Pd nuclei was illustrated in Figure 4.64. It was observed that both the Pd surface and total loadings increased linearly with an increase in the PdCl₂ concentration.

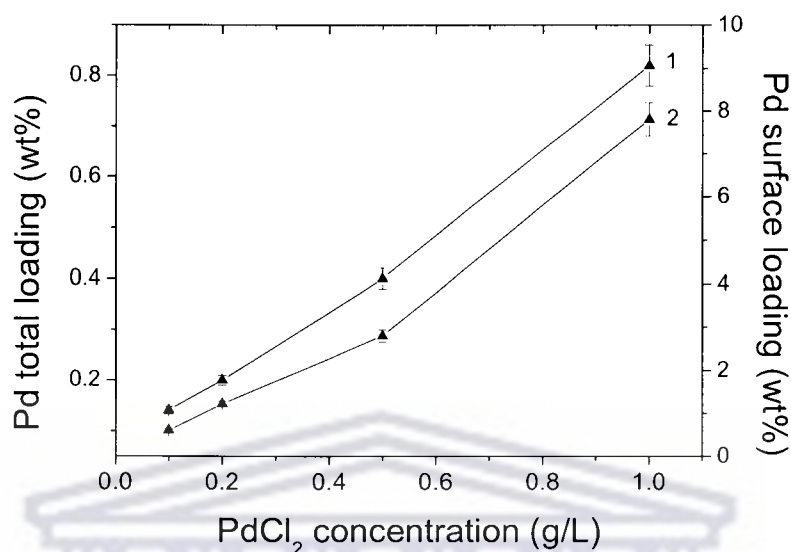


Figure 4.64. Influence of PdCl₂ concentration on Pd total loading and Pd surface loading of AB₅-type alloy surface-modified with Pd-P (30 min, NaH₂PO₂) after Pd nuclei complexation, (1) Pd total loading vs. PdCl₂ concentration; (2) Pd surface loading vs. PdCl₂ concentration

Measurements of the influence of the PdCl₂ concentration on the kinetics of hydrogenation by the AB₅-type alloys surface-modified after Pd nuclei complexation were undertaken after ~ 2 week exposure of the samples to air, and without application of an activation procedure (Figure 4.65). Under the experimental conditions ($P_{\text{H}_2} = 5.0$ bar, $T = 20$ °C, $t = 24$ hours) it was clearly observed that an increase in the PdCl₂ concentration facilitated a parallel increase in the kinetics of hydrogenation of AB₅-type alloys surface-modified using Pd encapsulation after pre-complexation of the Pd nuclei in electroless plating.

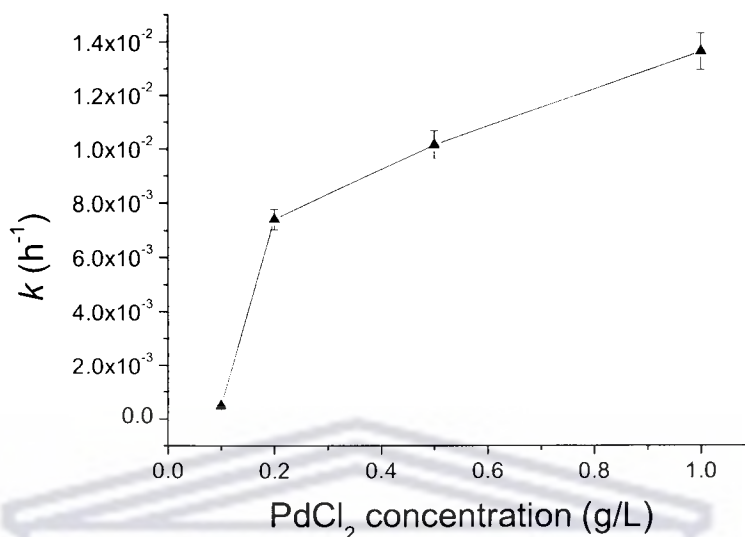


Figure 4.65. Influence of PdCl₂ concentration on kinetics of hydrogenation of AB₅-type alloys surface-modified with Pd-P layers (30 min, NaH₂PO₂) after pre-complexation of Pd nuclei

A serious drawback in the generation of continuous Pd-P layers on the surface of the alloys was the deposition of large quantities of Pd, which may not participate in the catalysis of the hydrogen dissociation process. It was therefore of vital importance, in terms of practical application in hydrogen separation / purification / storage systems, that the quantity of PGM's used in surface-modification of the alloy be reduced without significantly decreasing the rate of hydrogenation. An approach was developed to use the ability of aminosilanes to increase the surface affinity towards solvated PGM cations in dilute PGM precursor solutions. In doing so, significantly lowered concentrations of precious metals can be immobilized and used to form surface catalyst layers to promote the sorption of hydrogen on AB₅-type alloys.

4.3.5. Immobilization of palladium(II) and platinum(IV) ions from dilute solution onto γ -aminopropyltriethoxysilane functionalized AB₅-type alloys

The immobilization of small quantities of metal cations onto solid surfaces taking pre-concentration or separation into account was of particular interest [232]. Metal cations exist in hydrated form or as complexes associated with anions with little or no tendency for transformation. By neutralizing the associated charge it was possible to extract these metal cations from solution [232]. Based on the ability of the γ -APTES molecule to immobilize charged species onto the surface, an approach was adopted in which γ -APTES functionalization would be used to extract minute quantities of PGM cations from dilute solutions and fix them to the surface as a hydrogen dissociation catalyst. By grafting terminal nitrogen-containing groups to the surface of the alloy, the material may become more specific towards PGM cations as they have a large affinity towards nitrogen atoms and their electron lone pairs [155].

Covalent metal-ligand bonding served as an effective mechanism to immobilize PGM cations onto the surface of metal hydride-forming alloys and offered the opportunity to adsorb notable quantities of PGM's from dilute precursor solutions. The end result would potentially be a marked enhancement in the hydrogen absorption characteristics of the material without the use of large quantities of PGM's and the time-consuming electroless plating process. Also, large reductions in preparation costs could be achieved as the technique did not require sensitization / activation of the alloy surface; nor the use of large quantities of precursor solutions; nor the use of additional chemical components (e.g. complexing agent, stabilizer), thereby illustrating the simplicity in the method.

Similarly, Charbonnier *et al.* performed the chemisorption of the Pd²⁺ ions onto plasma functionalized surfaces of polymer membranes (e.g. polyimide; polycarbonate; polypropylene; polytetrafluoroethylene; polyphenylene sulphide; polybutylene terephthalate) by dipping the substrates for 1 min in a dilute aqueous PdCl₂ solution (0.1 g/L) [155]. A similar method was used by Zhou *et al.* to deposit

Pd on MCM-41 in the preparation of catalysts for the Heck reaction [235]. In this work, MCM-41 was functionalized using non-aqueous solutions of γ -APTES and Pd further deposited by suspension of the functionalized material in a dilute solution of PdCl₂. Pd loadings of 1.7 wt.% were achieved.

In the current method, 5.0 g AB₅-type alloy was functionalized in 1.0 vol.% γ -APTES (pH = 7) for 1 hour at 90 °C (250 rpm). The solution was filtered, washed with copious amounts of ultrapure water, and dried at 80°C. The functionalized alloy was then magnetically stirred for 24 hours (250 rpm) at 25°C in 100 mL solution (0.1 – 2.0 g/L) of PdCl₂ dissolved in HCl at 50°C. 100 mL NaH₂PO₂ (10g/L) or 100 mL N₂H₄ (30 g/L) was added. Ultrapure H₂ was also used as a reducing agent (2.0 L/min). The reaction was allowed to progress for 2 hours at 50°C. The alloys were then filtered, washed, and dried overnight at 80°C. An identical approach was also used to conduct the chromatographic adsorption of Pt⁴⁺ cations to the surface of the alloy, using a water-soluble PtCl₄ salt. In this case, the PtCl₄ concentrations (0.02 – 0.2 g/L) used were kept equimolar to that used in the PdCl₂ solutions. The scientific approach used in the preparation of the sample materials is illustrated in Figure 4.66.

UNIVERSITY of the
WESTERN CAPE

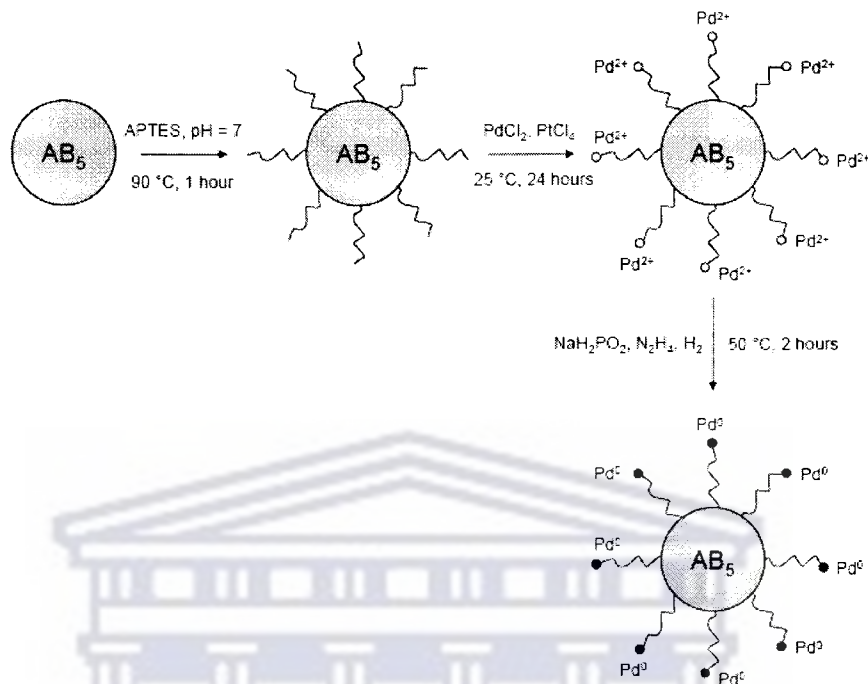


Figure 4.66. Scientific approach for the chromatographic adsorption of Pd and Pt cations, from dilute solutions to the surface of AB_5 -type alloys

In Figure 4.67 SEM images of unmodified and surface-modified AB_5 -type alloys are given. It was seen that the sample which was subjected to surface pre-treatment and further modified using dilute 0.5 g/L $PdCl_2$ solution showed evidence of Pd deposition on the surface, which took on a marbled appearance. Pd was present as a discolouration on the surface of the alloy, and exhibited fairly good surface coverage.

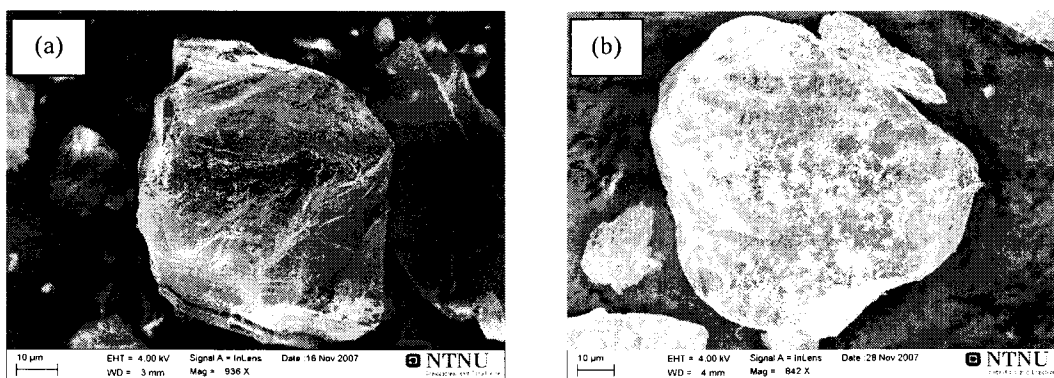


Figure 4.67. SEM images of (a) unmodified AB₅ alloy; and (b) after deposition of assembled layers of γ -APTES and Pd deposition from dilute 0.5 g/L PdCl₂ solution (NaH₂PO₂)

Elemental analysis of PdCl₂ solutions and filtrates after Pd deposition suggested that almost all of the Pd²⁺ precursor cations in the starting solution had been adhered to the alloy surface and reduced to form Pd⁰ (Table 4.14). Similar observations were made for the samples treated using N₂H₄ and H₂ as the reducing agents.

Table 4.14. Elemental analysis of PdCl₂ solution before and after Pd²⁺ immobilization (NaH₂PO₂) on AB₅-type alloys

PdCl ₂ concentration (g/L)	Absorbance			
	PdCl ₂ solution (abs. units)	Pd concentration (ppm)	Filtrate (abs. units)	Pd concentration (ppm)
0.1	0.022	74	0.002	< 20
0.2	0.046	154	0.004	< 20
0.5	0.096	332	0.005	< 20
1.0	0.157	560	0.005	< 20

A corresponding study of the influence of the concentration of the dilute PdCl₂ solution on the Pd surface loading was undertaken to ascertain the quantity of Pd present at the surface after adsorption of Pd²⁺ cations to the alloy surface. A comparison of results was made between samples prepared using NaH₂PO₂ and N₂H₄ as the reducing agent. The results were presented in Figure 4.68.

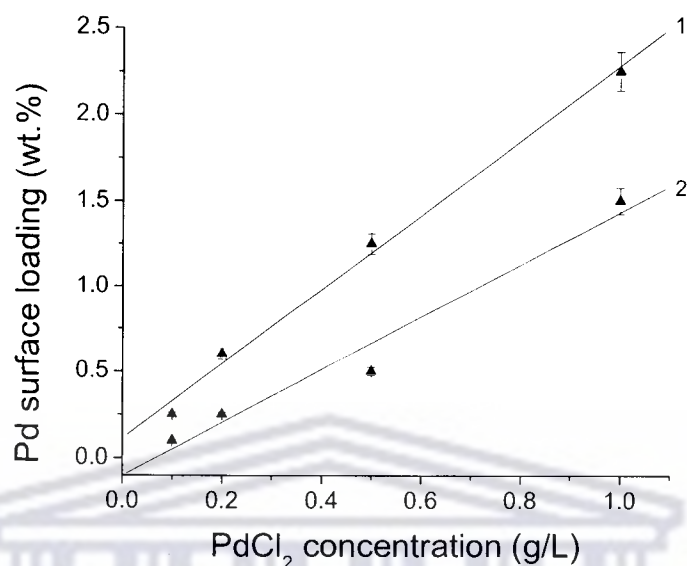


Figure 4.68. Influence of reducing agent on Pd surface loading of AB₅-type alloy after Pd²⁺ immobilization using γ -APTES solution, (1) NaH₂PO₂; (2) N₂H₄

A linear increase in the Pd surface loading with an increasing PdCl₂ concentration was observed, where NaH₂PO₂ and N₂H₄ were used as reducing agents. Similar observations were made where H₂ was used as the reducing agent.

Measurements of the influence of the type of reducing agent on the kinetics of hydrogenation by AB₅-type alloys surface-modified from dilute PdCl₂ solutions, as a function of PdCl₂ concentration, were undertaken after ~ 2 week exposure of the samples to air, and without thermal activation. Three sets of samples were analysed, each set being reduced by either NaH₂PO₂, N₂H₄, or H₂. Under the experimental conditions ($P_{\text{H}_2} = 5.0$ bar, $T = 20$ °C, $t = 24$ hours) the rate constant was generally observed to increase slightly with an increase in the PdCl₂ concentration. The kinetics of hydrogenation of the NaH₂PO₂-reduced samples was generally better than that reduced using N₂H₄ and H₂. Samples reduced using N₂H₄ and H₂ exhibited fairly similar rates of hydrogenation. Overall, fairly high rates of hydrogenation were achievable using fairly dilute solutions of PdCl₂.

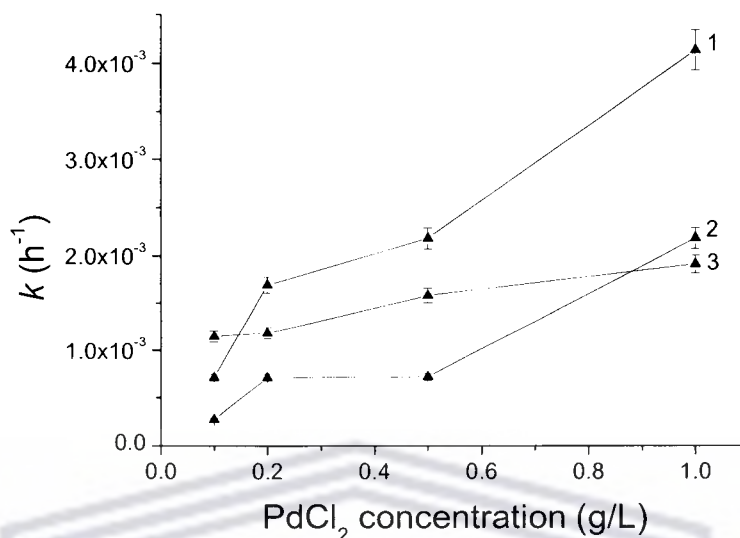


Figure 4.69. Influence of reducing agent on kinetics of hydrogenation of AB₅-type alloys after Pd²⁺ immobilization using γ -APTES solution, (1) NaH₂PO₂; (2) N₂H₄; (3) UHP H₂

A similar approach was adopted to immobilize Pt⁴⁺ cations on the surface of the AB₅-type alloy. PtCl₄ was used in the Pt precursor solution instead of more commercially available reagents, such as H₂PtCl₆, due to its high solubility in water. N₂H₄ was used exclusively as the reducing agent. Measurements of the influence of the PtCl₄ concentration on the Pt surface loading and kinetics of hydrogenation by the AB₅-type alloys surface-modified from dilute PtCl₄ solutions were undertaken after ~ 2 week exposure of the samples to air, and without thermal activation (Figure 4.70). The Pt surface loading was observed to increase with an increase in the PtCl₄ concentration. Under the experimental conditions ($P_{H_2} = 5.0$ bar, $T = 20$ °C, $t = 24$ hours) the rate constant was generally observed to remain steady, up to 0.1 g/L PtCl₄, with an increase in the PtCl₄ concentration. PtCl₄ solution concentrations greater than 0.1 g/L were observed to facilitate a rapid increase in the kinetics of hydrogenation on the surface-modified AB₅-type alloy surface.

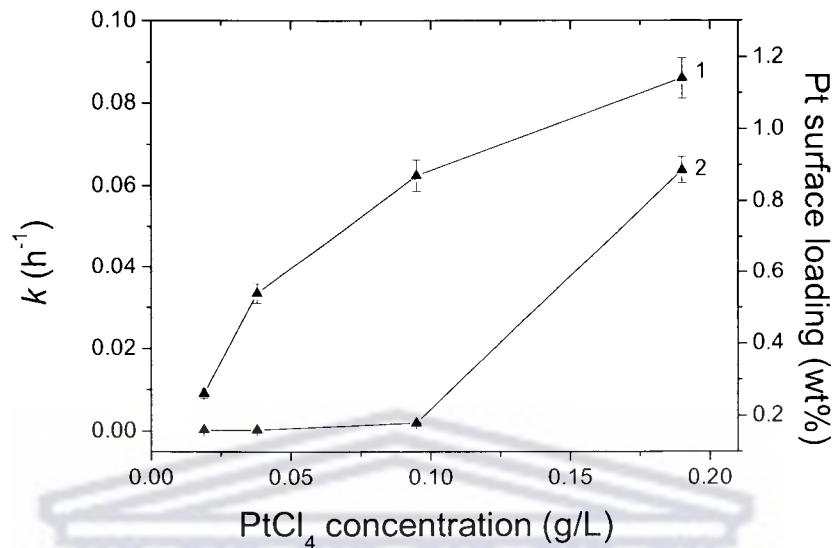


Figure 4.70. Dynamics of hydrogen sorption ($P_{\text{H}_2} = 5.0$ bar, $T = 20$ °C, $t = 24$ hours) by non-activated surface-modified AB₅-type alloys, after Pt⁴⁺ immobilization using γ -APTES solution (N₂H₄), (1) Pt surface loading vs. PtCl₄ concentration; (2) k vs. PtCl₄ concentration

4.3.6. Summary

An aminosilane surface functionalization approach was adopted in the deposition of high-quality continuous Pd-P layers on the surface of AB₅-type alloys. The functionalization method facilitated large increases in Pd-P density, total loading, and surface loading on the alloy compared to that prepared without the functionalization step. Rapid coalescence of Pd-P particles were observed after γ -APTES pre-treatment, constituting the initial formation of continuous surface layers. The Pd-P layer thickness corresponded to the deposition of ~10 layers of Pd-P particles (average thickness 550 nm) after functionalization.

Generally, surface functionalization promoted deposition of Pd-P particles significantly smaller in size, compared to that deposited without the surface functionalization step. The smaller Pd-P particles accounted for the better quality and greater density of the surface coatings upon surface functionalization. It was also

observed that the functionalized sample exhibited a fairly wide particle size distribution compared to that prepared without the functionalization step. In addition, it was observed that the functionalized alloys exhibited significantly lower specific surface areas than the unfunctionalized samples, which indirectly illustrated the attainment of continuous Pd-P layers with functionalization.

It was observed that progression of Pd-P particle growth led to sharp deterioration in the kinetics of hydrogenation of the functionalized materials. This observation may be indirectly indicative of a change in hydrogenation mechanism. Also, when the quantity of Pd-P deposited on the surface of the alloy was significantly increased through “high-loading”, the functionalized alloys significantly outperformed the non-functionalized alloys in terms of the kinetics of hydrogenation. It was deduced that functionalization increased the rate at which the Pd-P surface layer progressed from surface particles towards a continuous surface layers. Also, it was clearly observed that the functionalized alloys exhibited morphological dimensionalities of growth, and therefore hydrogenation mechanisms, which were completely different to that exhibited by the unfunctionalized alloy.

Based on the observation that the surface oxide layer detected on the surface of the alloy facilitated adhesion of γ -APTES molecules, an attempt was made to pre-oxidize the surface of the alloy prior to functionalization and promote the adhesion of the maximum quantity of γ -APTES molecules onto the surface, and in that way promote the deposition of a continuous Pd-P layer. It was observed that the pre-oxidation of the alloy surface, and subsequent functionalization, facilitated the deposition of large quantities of Pd-P particles on the surface of the alloy, resulting in slightly better kinetics of hydrogenation compared to that prepared without the pre-oxidation step.

Pre-complexation of Pd nuclei using aqueous solutions of γ -APTES, prior to electroless plating, improved the process of Pd-P deposition on the alloy surface to yield more dense and uniform coatings, and in such a way, resulted in better hydrogen sorption performances by the surface-modified alloys.

Based on the ability of γ -APTES molecules to immobilize metal cations on the surface, an approach was adopted in which γ -APTES functionalization was used to extract small quantities of PGM cations from dilute solutions and fix them to the surface as hydrogen dissociation catalysts. The kinetics of hydrogenation was generally observed to increase slightly with an increase in PdCl_2 concentration. Also, the kinetics of hydrogenation of NaH_2PO_2 -reduced samples was generally better than that prepared using N_2H_4 and H_2 . Similar observations were made after immobilization of Pt^{4+} cations obtained from dilute PtCl_4 solutions.

4.4. AB_5 -TYPE ALLOYS SURFACE-MODIFIED USING THE ELECTROLESS PLATING OF PALLADIUM MIXED-METAL LAYERS

As previously established, Pd surface-modified AB_5 -type alloys are still prone to losses in hydrogen sorption stability after long periods of exposure to air (and particularly to CO and H_2S), manifesting in the gradual deterioration of hydrogen sorption capacity with repeated cycling [64]. Selective mixing of Pd layers with secondary metals can circumvent the deterioration in the hydrogen sorption properties of the alloys. From a comprehensive review of the available literature in Chapter 2, Pd mixed-metal coatings with Ni, Cu, Ag, and Pt were identified to be attractive for investigation based on their potential properties when deposited onto the surface of AB_5 -type alloys. These properties included improvements to the cycle lifetime in hydrogen, high permeability, poisoning resistance, increased hydrogen transport, and enhanced catalytic properties in hydrogen exchange processes [55,141,142].

In addition, no works could be found into the use of co-deposition of mixed-metal layers to coat the surface of metal hydride-forming alloys, although sequential deposition was attempted [47,55,56,64,103]. Doyle *et al.* have, however, mentioned the possibility of co-deposition of two PGM metals to form a discontinuous layer on the surface of metal hydride-forming alloys [47]. An approach was adopted in which Pd mixed metal coatings (-Ni, -Cu, -Ag, -Pt) were deposited onto the surface of AB_5 -

type alloys to further enhance the kinetics of hydrogenation and promote hydrogen sorption stability on the material.

Surface modification was conducted using the electroless plating of Pd, Ni, Cu, Ag, and Pt by mixed-bath (co-deposition), or sequential deposition, using N_2H_4 or NaH_2PO_2 as the reducing agents. The bath formulations were selected based on the nature of the reducing agent and the pH of the electroless plating bath, where all baths were alkaline in nature.

4.4.1. Characterization of morphological and kinetic properties of AB₅-type alloys surface-modified using palladium mixed-metal coatings

AB₅-type alloy samples were surface-modified using the electroless plating of Pd, Ni, Cu, Ag, and Pt either by single-metal, mixed-bath (co-deposition), or sequential deposition, using N_2H_4 or NaH_2PO_2 as the reducing agent. Samples were subsequently stored in non-inert conditions.

XRD studies were conducted to ascertain changes to the crystallographic structure of the materials surface-modified using Pd mixed metal coatings. This task proved difficult due to overwhelming interferences from the core alloy and difficulty in separating the analytical signals from the deposited surface layer and the alloy substrate. However, increased trace amounts of Ni (as compared to that detected in the unmodified alloy) on the alloys modified by Pd-Ni-P (both sequentially and by co-deposition) were observed. Similarly, trace amounts of Cu, Ag, and Pt were detected on the alloys modified by Pd-Cu-P, Pd-Cu-Ni-P, Pd-Ag, and Pd-Pt. All Pd-Cu and Pd-Ni coatings were expected to be amorphous in nature due to the inclusion of phosphorus, from NaH_2PO_2 , in the Pd layer. Pd-Ag and Pd-Pt coatings were expected to be crystalline in nature as they were deposited from N_2H_4 -based electroless plating baths.

An attempt was made to study the surface morphology of the Pd-Ni-P, Pd-Cu-P, Pd-Ag, and Pd-Pt surface-modified materials using FESEM. The results were presented in Figures 4.71 – 4.80.

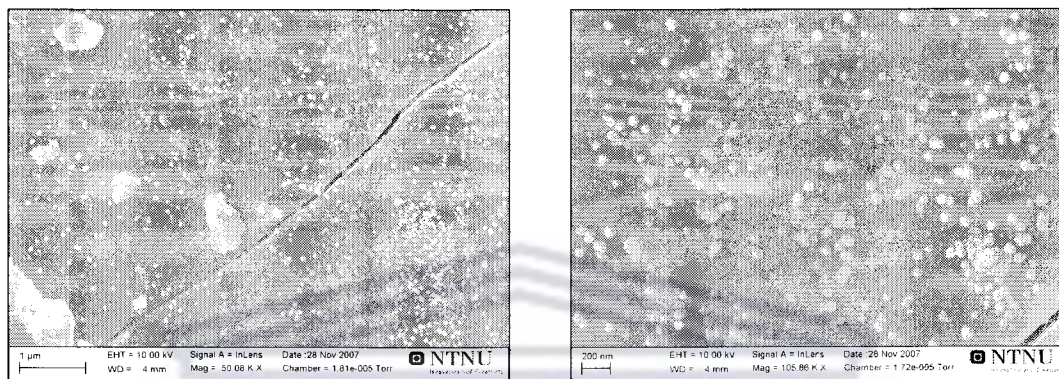


Figure 4.71. FESEM images of AB₅-type alloys surface-modified using Pd-Ni-P sequential-deposition (NaH₂PO₂, 30 min, 50°C)

Good dispersion of Pd-P particles were observed on the surface of the AB₅-type alloy after surface modification by sequential deposition of Pd-Ni-P. It was assumed that Ni-P particles were difficult to resolve from the Ni-rich matrix of the substrate. The Pd-Ni-P sequentially deposited coatings, derived from NaH₂PO₂-based electroless plating baths, were also found to be discontinuous in nature, similar to observations made by Willey *et al.* concerning Pd-Ru coatings on AB₅-type alloys [64]. The Pd-Ni-P coating exhibited a similar dense dispersion of particles on the alloy surface to that of the sample surface-modified by Pd-P layers. Surface particles possessed fairly spherical shape, while very little agglomeration of the Pd-P particles was observed on the alloy surface. An average particle size of 92 nm was determined.

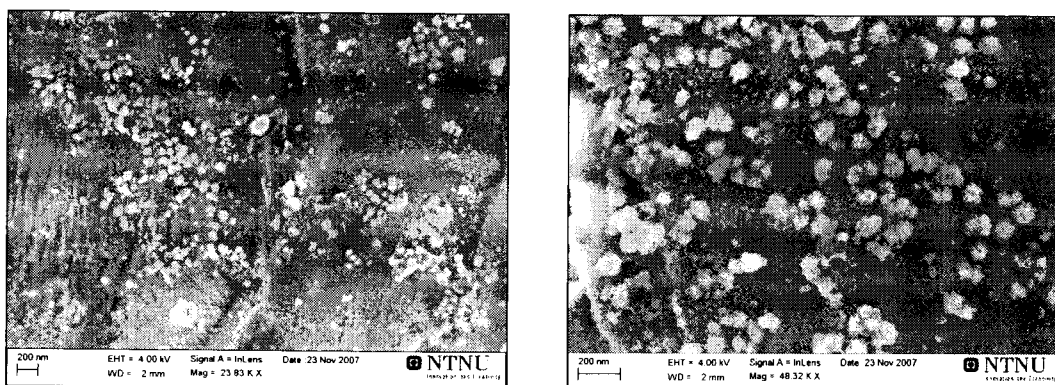


Figure 4.72. FESEM images of AB₅-type alloys surface-modified using Pd-Ni-P co-deposition (NaH₂PO₂, 30 min, 50°C)

Good dispersion of particles was observed on the AB₅-type alloy surface after co-deposition of Pd-Ni-P. The Pd-Ni-P co-deposited coatings were also found to be discontinuous in nature. The surface particles were observed to possess a very rough shape, compared to that of the sample surface-modified by Pd-Ni-P sequential deposition, while very little agglomeration was observed on the alloy surface. An average particle size of 105 nm was determined.

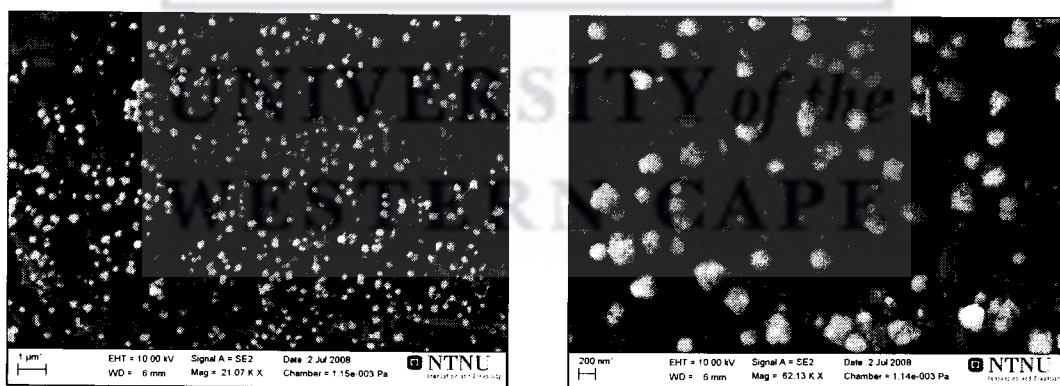


Figure 4.73. FESEM images of AB₅-type alloy surface-modified using Pd-Cu-P sequential-deposition (NaH₂PO₂, 30 min, 60°C)

Good dispersion of Pd-P and Cu-P particles were observed on the surface of the AB₅-type alloy after sequential deposition of Pd-Cu-P. The Pd-Cu-P sequentially-

deposited coatings, derived from NaH_2PO_2 -based electroless plating baths, were also found to be discontinuous in nature. The Pd-Ni-P coating exhibited a similar dense dispersion of particles on the surface of the alloy to that of the sample surface-modified by Pd-P layers. The surface particles were observed to possess fairly rough shape, while very little particle agglomeration was visible. An average particle size of 291 nm was determined. It may have been the case where most of the particles observed were Cu-P particles which were probably larger than the Pd-P particles, and explained the reddish-brown discolouration of the AB_5 -type alloy surface.

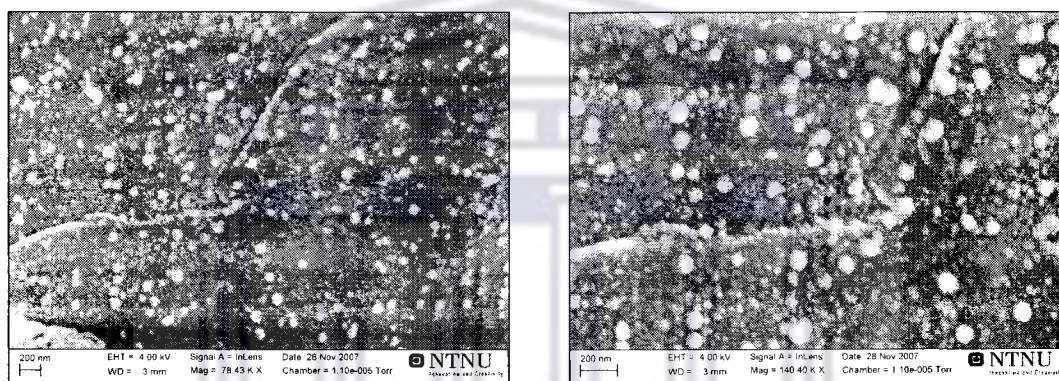


Figure 4.74. FESEM images of AB_5 -type alloy surface-modified using Pd-Cu-P co-deposition (NaH_2PO_2 , 30 min, 60°C)

Good dispersion of Pd-Cu-P particles was observed on the surface of the AB_5 -type alloy after surface modification by co-deposition of Pd-Cu-P. The Pd-Cu-P co-deposited coatings, derived from NaH_2PO_2 -based electroless plating baths, were also found to be discontinuous in nature. The Pd-Ni-P coating was observed to exhibit a similar dense dispersion of particles on the surface of the alloy to that of the sample surface-modified by Pd-P layers. The surface particles were observed to possess a rough spherical shape, while no significant agglomeration of the particles was observed on the alloy surface. An average particle size of 109 nm was determined.

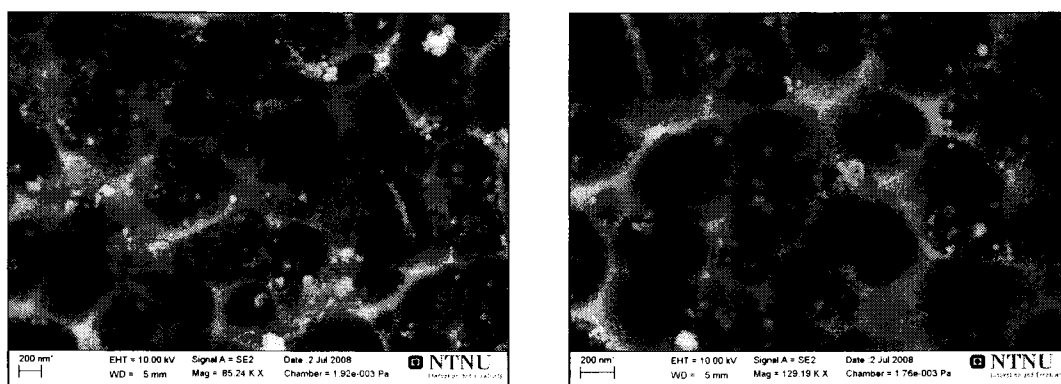


Figure 4.75. FESEM images of AB₃-type alloy surface-modified using Ag-Pd sequential-deposition (N₂H₄, 30 min, 60°C)

Fair dispersion of Ag and Pd particles were observed on the surface of AB₅-type alloys after sequential deposition of Ag-Pd. The Ag-Pd sequentially-deposited coatings, derived from N₂H₄-based electroless plating baths, were also found to be discontinuous in nature. The surface particles were observed to be fairly rough in appearance, while very little agglomeration of the particles were observed on the alloy surface. The appearance of the Ag-Pd particles agrees well with that observed by Chen *et al.*, who demonstrated that Pd and Ag particles deposited by electroless plating were nodular and faceted-crystalline in structure [142]. A wide range of particle sizes were visible, with an average particle size of 69 nm being determined. Surface etching was also observed after Ag-Pd sequential deposition and may be result of the abrasive action of the NaOH in the buffer solution [77,78].

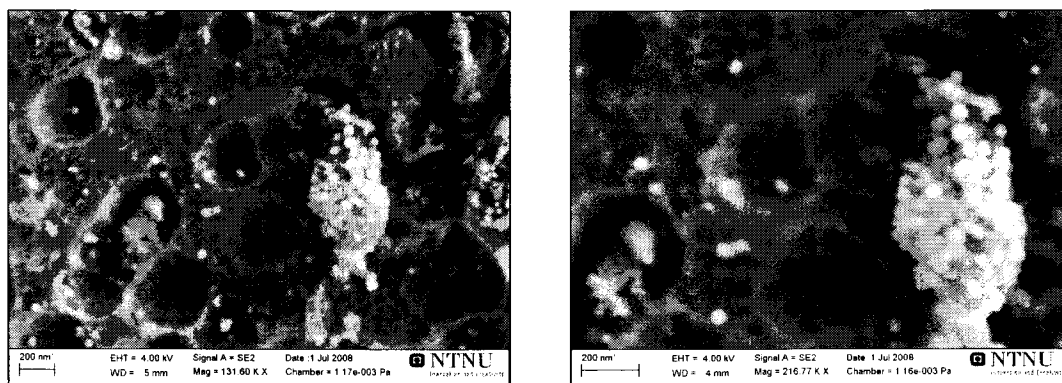


Figure 4.76. FESEM images of AB₅-type alloy surface-modified using Pd-Ag sequential-deposition (N₂H₄, 30 min, 60°C)

Fair dispersion of Pd and Ag particles was observed on the AB₅-type alloy surface after surface modification by sequential deposition of Pd-Ag. The Pd-Ag sequentially deposited coatings, derived from N₂H₄-based electroless plating baths, on AB₅ alloys were also found to be discontinuous in nature. The surface particles were observed to be mostly spherical in appearance, while significant areas of particle agglomeration were observed on the alloy surface. Generally, an average particle size of 54 nm was determined. Surface etching was also observed after Pd-Ag sequential deposition and may be result of the abrasive action of the NaOH in the buffer solution [77,78].

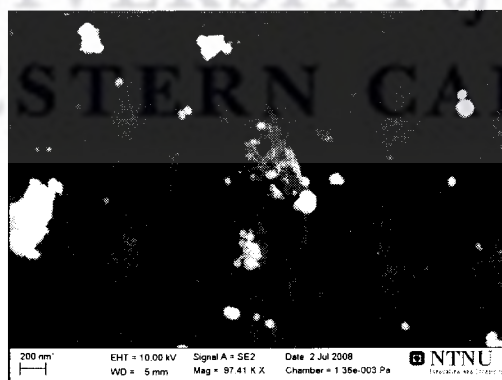


Figure 4.77. FESEM images of AB₅-type alloy surface-modified using Pd-Ag co-deposition (N₂H₄, 30 min, 60°C)

Pd-Ag co-deposited coatings, derived from N_2H_4 -based electroless plating baths, were also found to be discontinuous in nature. The surface particles were observed to be mostly spherical in appearance, while significant areas of particle agglomeration were observed on the alloy surface. Generally, an average particle size of 75 nm was determined. Surface etching was also observed after Pd-Ag co-deposition and may be a result of the abrasive action of the NaOH in the buffer solution [77,78].

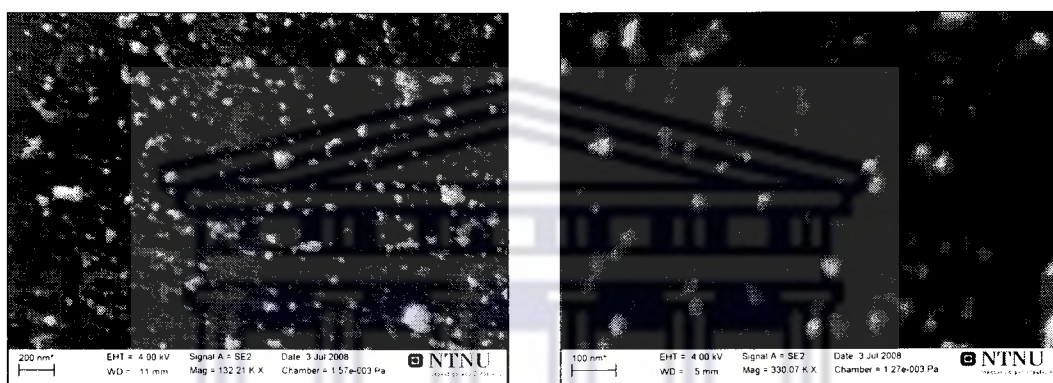


Figure 4.78. FESEM images of AB_5 -type alloy surface-modified using Pt-Pd sequential-deposition (N_2H_4 , 30 min, $60^\circ C$)

Good dispersion of Pt and Pd particles were observed on the surface of the AB_5 -type alloy after sequential deposition of Pt-Pd. The Pt-Pd sequentially-deposited coatings, derived from N_2H_4 -based electroless plating baths, were also found to be discontinuous in nature. The surface particles were nodular in appearance, while very little agglomeration of the particles was observed on the alloy surface. A wide range of particle sizes were visible, with an average particle size of 83 nm being determined. Surface etching was also observed after Pt-Pd sequential deposition and may be result of the abrasive action of the NaOH in the buffer solution [77,78].

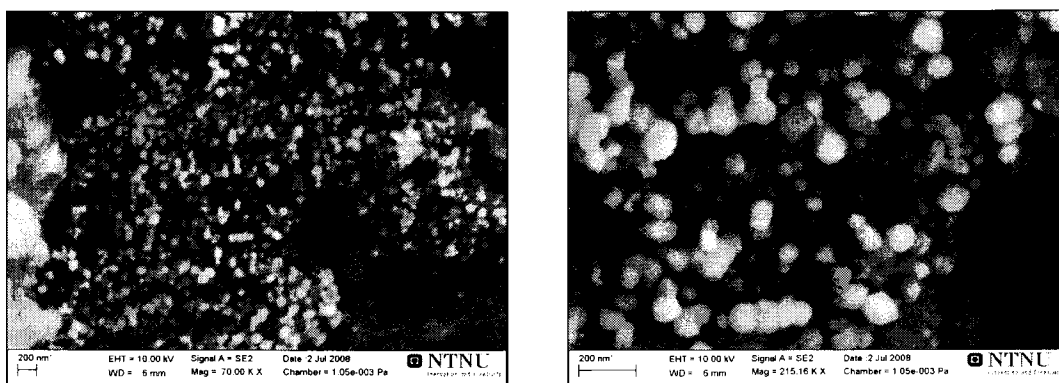


Figure 4.79. FESEM images of AB₅-alloy surface-modified using Pd-Pt sequential-deposition (N₂H₄, 30 min, 60°C)

Good dispersion of Pd and Pt particles were observed on the surface of the AB₅-type alloy after surface modification by sequential deposition of Pd-Pt. The Pd-Pt sequentially-deposited coatings, derived from N₂H₄-based electroless plating baths, were also found to be discontinuous in nature. The surface particles were observed to be spherical in appearance, while mild agglomeration of the particles were observed on the alloy surface. A wide range of particle sizes were visible, with an average particle size of 95 nm being determined.

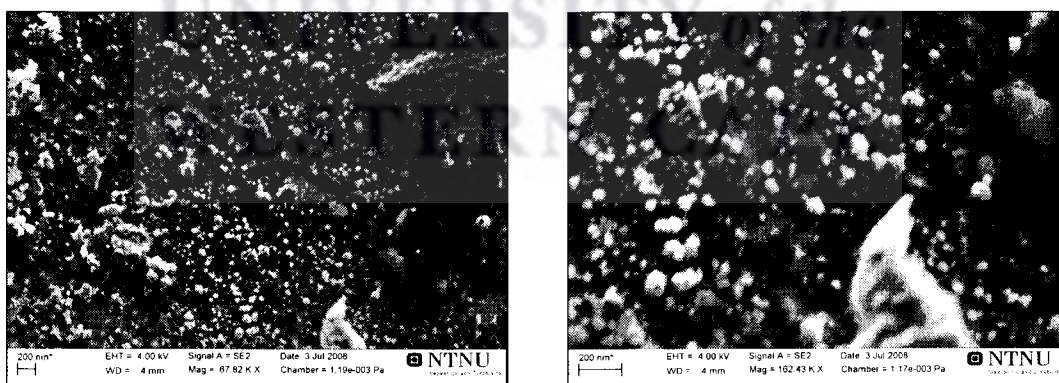


Figure 4.80. FESEM images of AB₅-type alloy surface-modified using Pd-Pt co-deposition (N₂H₄, 30 min, 60°C)

Good dispersion of Pd and Pt particles were observed on the surface of the AB₅-type alloy after co-deposition of Pd-Pt. The Pd-Pt co-deposited coatings, derived from N₂H₄-based electroless plating baths, were also found to be discontinuous in nature. The surface particles were observed to be nodular in appearance, while mild agglomeration of the particles were observed on the alloy surface. A wide range of particle sizes were visible, with an average particle size of 73 nm being determined. Surface etching was also observed after Pd-Pt co-deposition and may be result of the abrasive action of the NaOH in the buffer solution [77,78].

Dynamic analysis in *micro*-PIXE was conducted to qualitatively study surface elemental distribution of Pd, Cu, Ag, and Pt on alloys surface-modified using mixed-metal coatings (Figures 4.81 – 4.86). Deposited Ni could not be separated from the background matrix, which was mostly constituted of Ni surface clusters. Discontinuous layers were observed for all the sample alloys. Isolated clusters of Pd, Cu, Pt, and Ag were observed, illustrating the inability to produce continuous layers on the surface of the alloy.

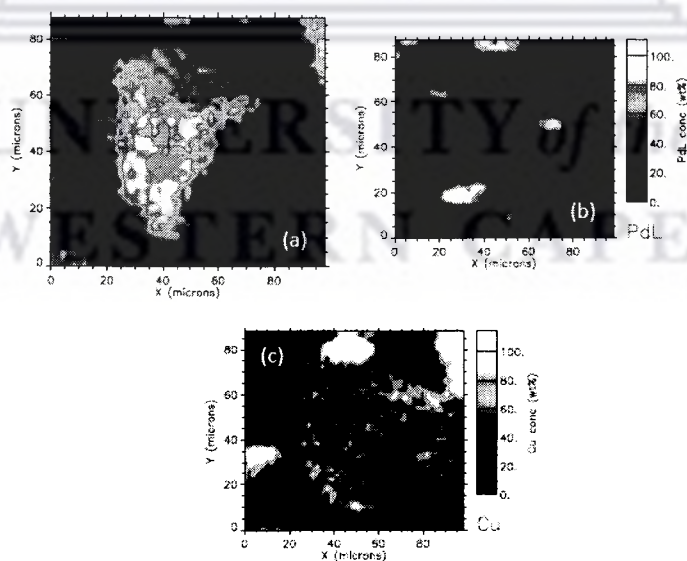


Figure 4.81. Dynamic analysis map of AB₅-type alloy surface-modified using sequential deposition of Pd-Cu-P, (a) total background; (b) Pd L; (c) Cu K

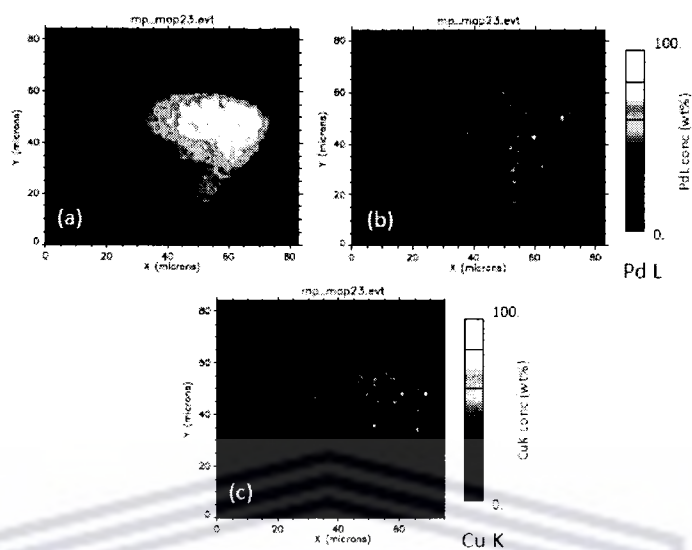


Figure 4.82. Dynamic analysis map of AB₅-type alloy surface-modified by co-deposition of Pd-Cu-P,
(a) total background; (b) Pd L; (c) Cu K

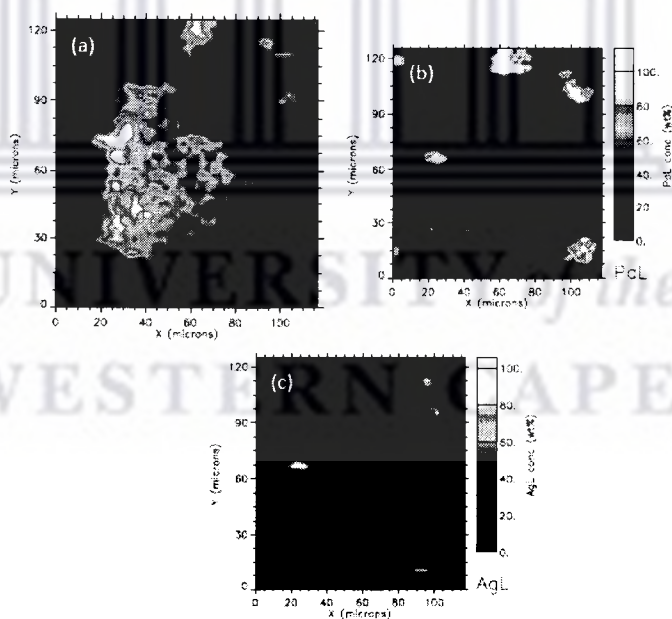


Figure 4.83. Dynamic analysis map of AB₅-type alloy surface-modified using co-deposition of Pd-Ag,
(a) total background; (b) Pd L; (c) Ag L

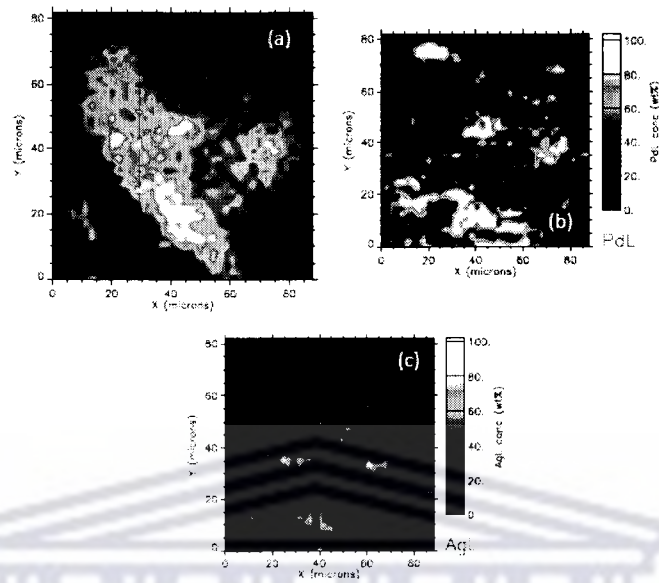


Figure 4.84. Dynamic analysis map of AB₅-type alloy surface-modified using sequential-deposition of Pd-Ag, (a) total background; (b) Pd L; (c) Ag L

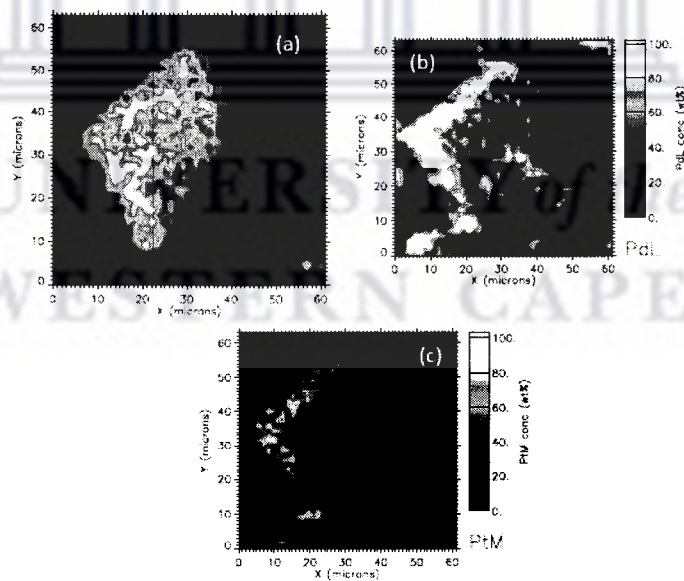


Figure 4.85. Dynamic analysis map of AB₅-type alloy surface-modified using co-deposition of Pd-Pt, (a) total background; (b) Pd L; (c) Pt M

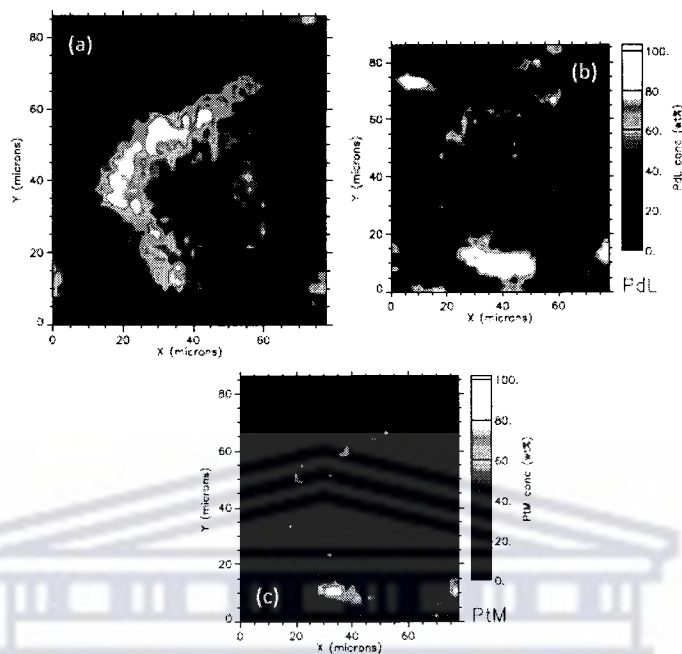


Figure 4.86. Dynamic analysis map of AB_5 -type alloy surface-modified using sequential-deposition of Pd-Pt, (a) total background; (b) Pd L; (c) Pt M

Elemental analysis of the surface and total loadings of Pd, Cu, Ag, and Pt was conducted to analyse the quantity of metal deposited on the AB_5 -type alloy. The deposited Ni-P could not be separated from the background matrix, which was mostly constituted of the Ni surface clusters of the parent alloy. The results were tabulated in Tables 4.15 – 4.17.

Moderately small quantities of Pd were observed on the surface-modified AB_5 -type alloys after treatment by Pd-Ni and Pd-Cu co-deposition and sequential deposition, compared to that observed after the deposition of Pd-P coatings (Table 4.15). In contrast large surface loadings of Cu were observed in sequential and co-deposition of Pd-Cu-P coatings.

Table 4.15. Elemental analysis of Pd and Cu total and surface loading on AB₅-type alloy after sequential- and co-deposition in Pd mixed-metal electroless plating baths

Sample	Total Pd (wt%)	Surface Pd (wt%)	Total Cu (wt%)	Surface Cu (wt%)
Unmodified AB ₅	0.0	0.0	0.0	0.0
AB ₅ Pd-Ni seq-dep (NaH ₂ PO ₂) 30 min	0.38	1.32	-	-
AB ₅ Pd-Ni co-dep (NaH ₂ PO ₂) 30 min	0.24	1.27	-	-
AB ₅ Pd-Cu seq-dep (NaH ₂ PO ₂) 30 min	0.49	1.17	0.05	6.19
AB ₅ Pd-Cu co-dep (NaH ₂ PO ₂) 30 min	0.34	1.93	0.04	5.69
AB ₅ Pd-Ni-Cu co-dep (NaH ₂ PO ₂) 30 min	0.03	1.01	< 0.02	2.09

Table 4.16. Elemental analysis of Pd and Ag total and surface loading on AB₅-type alloy after sequential- and co-deposition in Pd mixed-metal electroless plating baths

Sample	Total Pd (wt%)	Surface Pd (wt%)	Total Ag (wt%)	Surface Ag (wt%)
AB ₅ Pd-Ag seq-dep (N ₂ H ₄) 30 min	0.20	1.14	0.039	2.16
AB ₅ Ag-Pd seq-dep (N ₂ H ₄) 30 min	0.48	2.39	0.035	0.41
AB ₅ Pd-Ag co-dep (N ₂ H ₄) 30 min	0.64	2.76	0.01	0.53

Moderately small quantities of Pd were observed on the surface-modified AB₅-type alloys after Pd-Ag co-deposition and sequential deposition, compared to that observed after the deposition of Pd (N₂H₄) coatings (Table 4.16). In contrast, very small quantities of Ag were observed in both total and surface loadings on the surface-modified AB₅-type alloys after treatment by Pd-Ag co-deposition and sequential deposition.

Table 4.17. Elemental analysis of Pd and Pt total and surface loading on AB₅-type alloy after sequential- and co-deposition in Pd mixed-metal electroless plating baths

Sample	Total Pd (wt%)	Surface Pd (wt%)	Total Pt (wt%)	Surface Pt (wt%)
AB ₅ Pd-Pt seq-dep (N ₂ H ₄) 30 min	0.25	2.0	0.68	5.5
AB ₅ Pt-Pd seq-dep (N ₂ H ₄) 30 min	0.7	2.2	0.34	1.7
AB ₅ Pd-Pt co-dep (N ₂ H ₄) 30 min	0.43	1.6	0.7	3.1

Again, moderate quantities of Pd were observed on the surface-modified AB₅-type alloys after treatment by Pd-Pt co-deposition and sequential deposition, compared to that observed after the deposition of Pd (N₂H₄) coatings (Table 4.17). Also, moderate quantities of Pt were observed in both total and surface loadings on the surface-modified alloys after treatment by Pd-Pt co-deposition and sequential deposition.

Measurements of the influence of the Pd-Ni and Pd-Cu mixed-metal coatings on the kinetics of hydrogenation by the surface-modified AB₅-type alloys were undertaken after ~ 2 week exposure of the samples to air, and without application of thermal activation. The results with respects to the dynamics of hydrogenation were presented in Figure 4.87.

UNIVERSITY of the
WESTERN CAPE

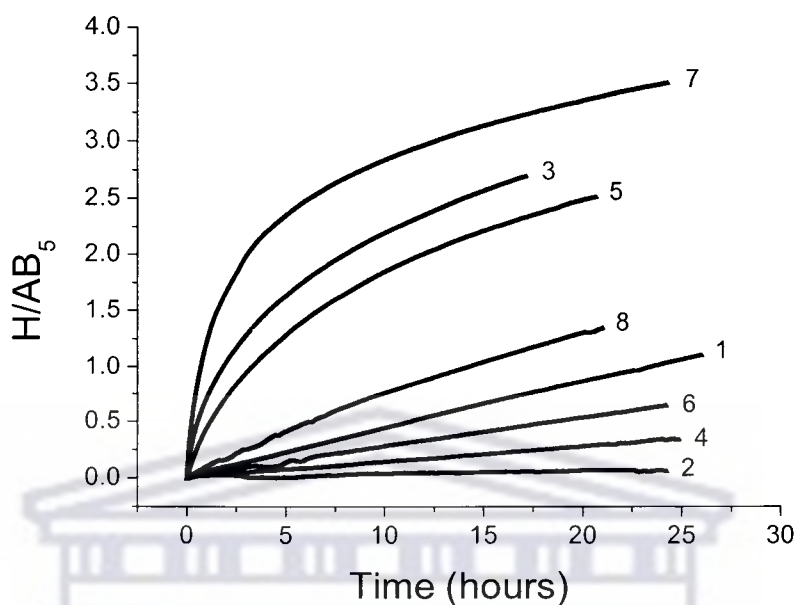


Figure 4.87. Dynamics of hydrogen absorption ($T = 20^{\circ}\text{C}$, $P_{\text{H}_2} = 5.0$ bar, $t = 24$ hours) by the unmodified and surface-modified samples (NaH_2PO_2 , 30 min, $50\text{--}60^{\circ}\text{C}$), (1) unmodified; (2) Pd-Sn sensitized / activated; (3) Pd-P; (4) Pd-Cu-P sequential deposition; (5) Pd-Cu-P co-deposition; (6) Pd-Ni-P sequential deposition; (7) Pd-Ni-P co-deposition; (8) Pd-Ni-Cu-P co-deposition (all measurements conducted on the IFE volumetric installation)

As expected, the unmodified alloy absorbed hydrogen very slowly under the experimental conditions; the amount of hydrogen absorbed within 24 hours was less than $\text{H}/\text{AB}_5 = 1.0$ formula units, or 20% of the maximum H sorption capacity of the activated alloy ($\text{H}/\text{AB}_{5\text{ max}} = 5.0$ formula units.). The poor absorption performance of the parent alloy was a direct result of the oxide layer on the surface retarding the surface-sensitive hydrogen dissociation process. Surface modification, by deposition of Pd-P, or co-deposition of Pd-Ni-P, Pd-Cu-P, and to a lesser extent, Pd-Ni-Cu-P, onto the surface of the alloy resulted in significant improvements to the hydrogen sorption kinetics. In contrast, samples modified by sequential deposition of Pd-Ni-P and Pd-Cu-P exhibited worse kinetics of hydrogenation than that observed with the unmodified alloy. This may be a result of the poor hydrogen sorption capacity of the

secondary metal (i.e. Ni and Cu) acting as a diffusion barrier. Identical observations were made by Doyle *et al.* in which a Ni layer densely covered over the surface of a Pd layer served as a barrier towards the dissociation of hydrogen [47]. In addition, the sequential deposition of Ni and Cu coatings as secondary metals may have resulted in nucleation of these layers on the catalytically-active adsorption sites of the Pd layer, thereby reducing the catalytic activity. Geng [55] also observed similar behaviour when sequentially coating AB₅-type alloys with Pd-Ni. The alloy sensitized / activated in the Pd-Sn colloidal solution practically did not absorb hydrogen under the experimental conditions.

Results of fitting the experimental data (fitting parameters t_0 and n) are presented in Table 4.18. The sequence corresponded to the increase in the rate constant (k).

Table 4.18. Results of fitting of the experimental data by the Avrami-Erofeev equation

Group	Sample	t_0 (hours)	k (h ⁻¹)	n
1	Pd-Sn sensitized /activated	$2.3(2) \cdot 10^3$	4.3×10^{-4}	0.95(2)
2	Pd-Cu-P (sequential deposition)	342(1)	2.9×10^{-3}	1.013(1)
	Pd-Ni-P (sequential deposition)	189.5(7)	5.3×10^{-3}	0.974(2)
	Unmodified	103.0(1)	9.7×10^{-3}	1.0173(6)
	Pd-Ni-Cu-P (co-deposited)	73.82(9)	1.4×10^{-2}	0.9160(6)
3	Pd-Cu-P (co-deposition)	34.59(7)	2.9×10^{-2}	0.645(1)
	Pd-P	26.75(4)	3.7×10^{-2}	0.5612(5)
	Pd-Ni-P (co-deposition)	15.18(4)	6.6×10^{-2}	0.450(1)

It should be noted that the kinetics of hydrogenation in Table 4.18 were measured on the volumetric installation at IFE. Differences in the calculated t_0 , k , and n values between installations were a result of poor installation-to-installation reproducibility, where the measured system pressure was dependent on the volume of the reaction vessel and buffer cylinders and the weight of the sample, which both differed between the installations.

Analysing the data (Table 4.18), three groups of materials could be separated based on their kinetics of hydrogenation under the experimental conditions.

The first group included the alloy sensitized / activated in the Pd-Sn colloidal solution which did not absorb significant quantities of hydrogen in a reasonable time ($k = 4.3 \times 10^{-4} \text{ h}^{-1}$). The amount of hydrogen absorbed within 24 hours corresponded to $\text{H}/\text{AB}_5 = 0.05$ formula units, or 1.0 % of the maximum H capacity of the alloy.

The second group included the unmodified alloy, the alloys modified by sequential deposition of Pd-Ni-P and Pd-Cu-P, as well as the alloy modified by co-deposition of Pd-Ni-Cu-P. These materials were characterised by slow hydrogen absorption, attaining the H storage capacity corresponding to $\text{H}/\text{AB}_5 = 0.35 - 1.35$ ($k = 2.9 \times 10^{-3} - 1.4 \times 10^{-2} \text{ h}^{-1}$) in 24 hours. The fitted n values for the alloys belonging to this group were close to one. The inadequacies in sequential deposition of Pd mixed-metal coatings in producing materials with enhanced activation kinetics were also observed in an electrochemical characterization of Pd-Ni modified alloys [55]. The sequential deposition of Pd followed by Ni resulted in the surface being densely covered by Ni, which made the activation of the material extremely difficult, with the activation time being noticeably longer than that of the unmodified core alloy.

Finally, the third group included the sample modified by Pd-P, co-deposited Pd-Ni-P and Pd-Cu-P. These materials were characterised by significantly faster dynamics of hydrogenation and absorbed more than half of the maximum capacity $\text{H}/\text{AB}_5 = 2.5 - 3.5$ ($k = 2.9 \times 10^{-2} - 6.6 \times 10^{-2} \text{ h}^{-1}$) within 24 hours. These materials exhibited characteristic times of hydrogenation (t_0) 3-7 times faster than that observed for the unmodified alloy. The fitted n values were close to 0.5, indicative of a hydrogenation mechanism which differed from the materials in the second group ($n \sim 1$).

The strongest influence of surface modification on H sorption properties was observed for the AB_5 -type alloy surface-modified by co-deposition of Pd-Ni. It has to be noted that after hydrogenation and unloading this sample from the reactor,

followed by exposure to air, the expulsion of moisture accompanied by self-heating of the material was observed. Such an effect was not observed for the other samples and indicated that this specific material exhibited the highest activity towards hydrogen transfer processes between the bulk material and the surface. It can be concluded that the Pd-Ni-enriched surfaces improved the activation kinetics of the AB₅-type alloy with a significant contribution to the enhancement being due to the synergistic effect observed between Pd and Ni atoms, upon co-deposition. The amorphous Ni of the surface layer may have created an “interfacial bridge” between the crystalline Ni of the alloy substrate and the amorphous Pd of the surface layer, facilitating enhanced transport of H atoms into the alloy.

AB₅-type alloys surface-modified using Pd-Ni layers were compared in terms of kinetics of hydrogenation. A comparison was made between AB₅-type alloys surface-modified by Pd-Ni-P sequential-deposition; Ni-Pd-P sequential deposition; and Pd-Ni-P co-deposition. The results were presented in Figure 4.88.

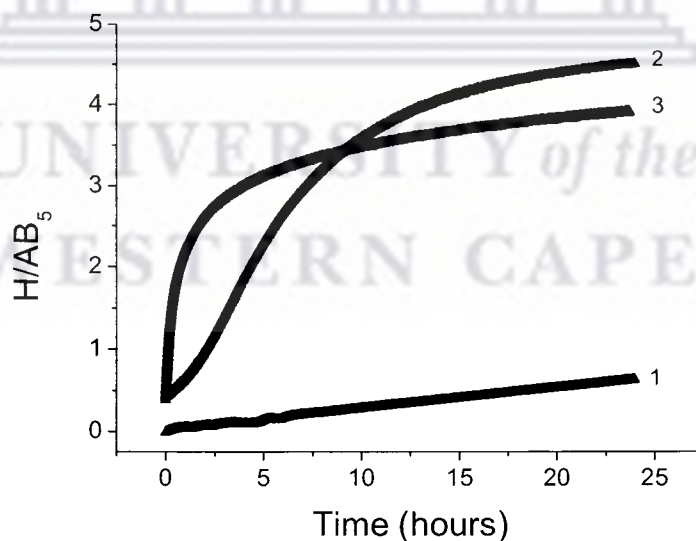


Figure 4.88. Dynamics of hydrogen absorption ($T = 20^{\circ}\text{C}$, $P_{\text{H}_2} = 5.0$ bar, $t = 24$ hours) by the surface-modified samples (NaH_2PO_2 , 30 min, 50°C), (1) Pd-Ni-P sequential-deposition; (2) Ni-Pd-P sequential deposition; (3) Pd-Ni-P co-deposition

It was observed that AB₅-type alloys surface-modified using Pd-Ni-P co-deposition ($k = 6.6 \times 10^{-2} \text{ h}^{-1}$) exhibited kinetics of hydrogenation noticeably better than that of the alloys surface-modified using Pd-Ni-P sequential-deposition ($k = 5.3 \times 10^{-3} \text{ h}^{-1}$) and Ni-Pd-P sequential-deposition ($k = 1.3 \times 10^{-2} \text{ h}^{-1}$). In addition, the AB₅-type alloy surface-modified using Ni-Pd-P sequential-deposition exhibited kinetics of hydrogenation significantly better than that of the alloy surface-modified using Pd-Ni-P sequential-deposition. This result illustrated the action of the Ni layer to behave as a diffusion barrier towards hydrogen sorption to the alloy, and inhibition of surface catalysis of the hydrogen dissociation process.

An attempt was made to study the long-term sorption stability of the surface-modified alloys. Measurements of the kinetics of hydrogenation by the sample materials were undertaken after ~3 month and ~11 month exposures of the samples to air, and without application thermal activation. The results with respects to the kinetics of hydrogenation were presented in Figure 4.89. Rates constants were determined using the Avrami-Erofeev equation, and results tabulated in Table 4.19.

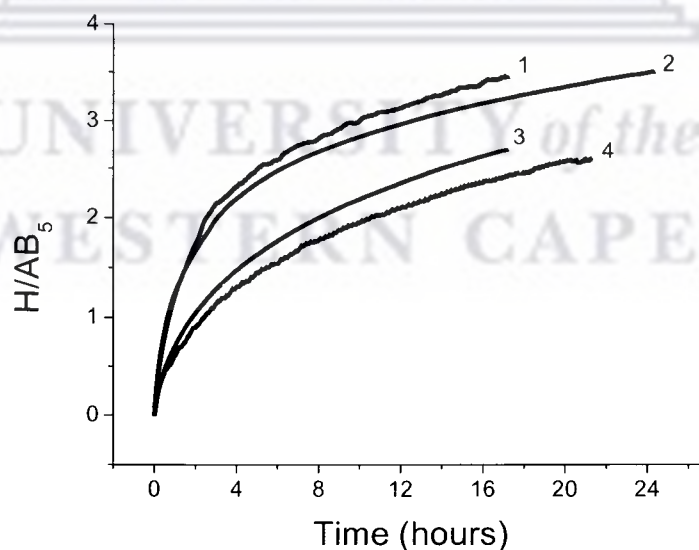


Figure 4.89. Dynamic activation curves for non-activated surface-modified AB₅-type alloys - Pd-Ni co-deposition (NaH₂PO₂, 30 min, 50°C): (1) 3 month exposure; (2) 11 month exposure, Pd (NaH₂PO₂, 30 min, 50°C): (3) 3 month exposure; (4) 11 month exposure

Table 4.19. Results of fitting of the experimental data by the Avrami-Erofeev equation

Sample	k (h^{-1})	
	3 month exposure to air	11 month exposure to air
Pd (NaH_2PO_2 , 30 min, 50°C)	7.2×10^{-2}	4.6×10^{-2}
Pd-Ni co-deposition (NaH_2PO_2 , 30 min, 50°C)	2.0×10^{-1}	1.9×10^{-1}

Rate constants for both the samples did not change very much, illustrating the long-term sorption stability of the materials, compared to the unmodified alloy. In addition, the stability of the sample prepared by co-deposition of Pd-Ni-P showed hardly any deterioration compared to that prepared by deposition of Pd-P, whose stability deteriorated slightly. This illustrated that the addition of Ni to the Pd-based surface layer may have enhanced the sorption stability of the material even further, thus confirming the hypothesis of enhanced sorption stabilities offered by the mixed-metal surface layers on AB_5 -type alloys. In comparison, Willey *et al.* and Pratt *et al.* found no appreciable change in the hydrogen absorption performance of Pd-Ru coated AB_5 -type alloy with short- to medium-term (i.e. 2.5 hours; 42 days) exposure to air [56,64]. In response, in this study no significant changes were found in Pd-Ni-P (co-deposition) coated and Pd-P coated AB_5 -type alloys after 11 months.

Based on the observation of the significant properties of the Pd-Ni-P co-deposited coatings in ensuring the long-term stability of the alloy, further investigation into the benefits of the Pd-Ni-P co-deposited coating was undertaken. An investigation into the influence of the Ni concentration, in the Pd-Ni-P mixed-metal bath, and deposition time on the Pd surface loading, Pd total loading, and kinetic properties of the surface-modified alloys was conducted (Figures 4.90 – 4.92).

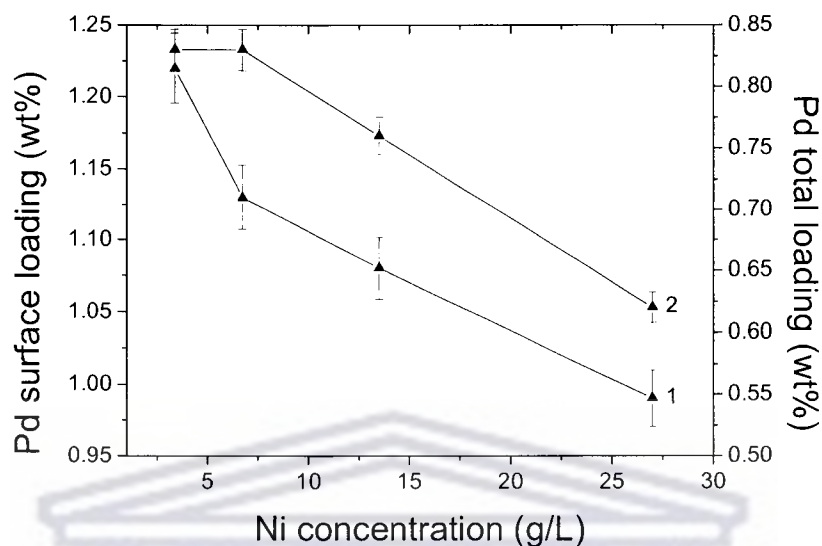


Figure 4.90. Influence of Ni concentration in Pd-Ni-P co-deposition baths on Pd surface loading and total loading: (1) Pd surface loading vs. Ni concentration; (2) Pd total loading vs. Ni concentration

From Figure 4.90, it was expectedly observed that the Pd surface and total loadings decreased, almost linearly, with an increase in the Ni concentration from ~ 3.0 g/L – 28 g/L. The result clearly indicates the competitive nature between the Ni and Pd precursor ions in the mixed-metal bath for surface sites on the AB₅-type alloy.

A study of the influence of the Ni concentration on the kinetic properties of alloys surface-modified using Pd-Ni co-deposition was conducted. Measurements of the kinetics of hydrogenation were undertaken after ~ 2 week exposure of the samples to air, and without application of thermal activation. The results with respects to the kinetics of hydrogenation were presented in Figure 4.91.

It was observed from Figure 4.91 that moderate Ni concentrations of ~ 1.0 – 8.0 g/L NiCl₂ had a profound influence on the kinetics of hydrogenation. Higher concentrations had the effect of decreasing the Pd surface and total loadings (Figure 4.90), with the result that the kinetics of hydrogenation was significantly and adversely affected. A threshold Ni concentration, and a balance of concentration

between the Pd and Ni precursor ions in the mixed-metal bath, was observed in the aforementioned concentration range.

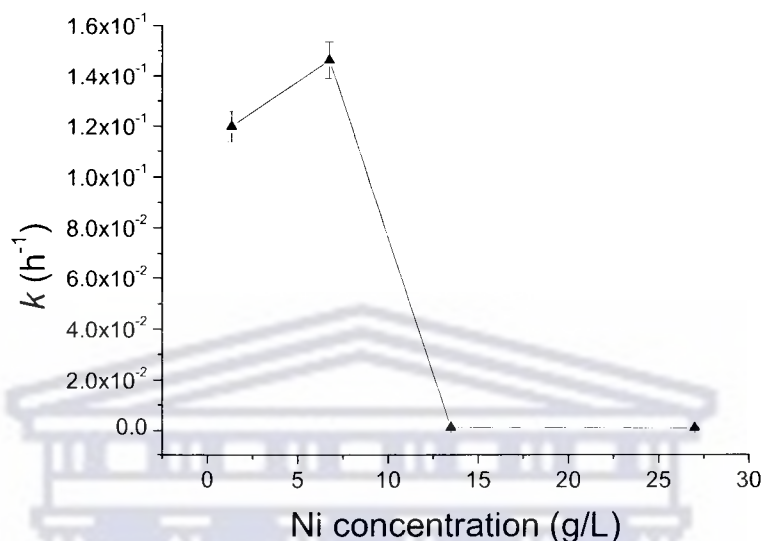


Figure 4.91. Influence of Ni concentration on AB_5 -type alloys surface-modified in Pd-Ni (NaH_2PO_2 , 30 min, 50°C) co-deposition baths on kinetics of hydrogenation

An investigation into the influence of deposition time on the Pd surface loading and kinetics of hydrogenation of alloys surface-modified using Pd-Ni co-deposition was conducted. The results were presented in Figures 4.92 and 4.93. A gradual increase in the Pd surface loading was observed with an increase in the Pd-Ni deposition time in the timescale 1-120 minutes. A maximum Pd surface loading was observed at ~ 2.6 wt.%.

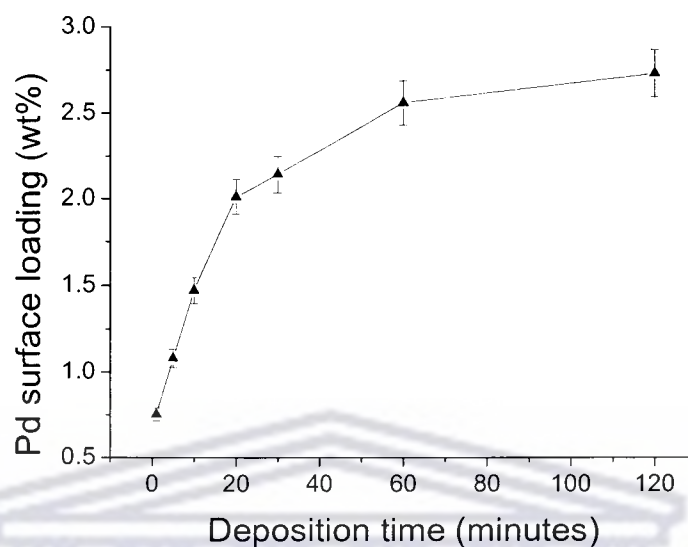


Figure 4.92. Influence of Pd-Ni deposition time on AB₅-type alloy surface-modified using Pd-Ni (NaH₂PO₂) co-deposition on Pd surface loading

Measurements of the influence of the addition of the Ni addition on the kinetics of hydrogenation ($P_{\text{H}_2} = 5.0$ bar, $T = 20$ °C, $t = 24$ hours) were undertaken after ~2 week exposure of the samples to air, and without application of an activation procedure. The results with respects to the kinetics of hydrogenation were presented in Figure 4.93. A comparison of kinetic behaviour was made with the AB₅-type alloy surface-modified with Pd-P. From Figure 4.93 it was observed that alloys surface-modified using Pd-Ni-P co-deposition had an initial kinetics of hydrogenation which was superior to that observed for the alloy surface modified using Pd-P. Generally, an increase in the deposition time resulted in a decrease in the kinetics of hydrogenation, for both coatings. Eventually, an equilibrium rate of $k \approx 1.0 \times 10^{-2} \text{ h}^{-1}$ after ~ 20 minutes of deposition was attained for the AB₅-type alloy surface-modified using the co-deposition of Pd-Ni-P and the alloy surface-modified using the deposition of Pd-P.

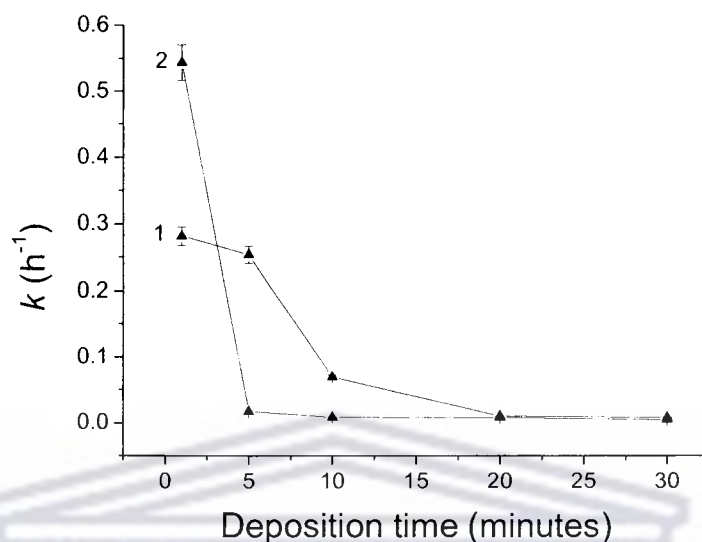


Figure 4.93. Influence of Ni secondary metal addition on kinetics of hydrogenation of Pd surface-modified AB₅-type alloys, (1) Pd-P (NaH₂PO₂, 50°C); (2) Pd-Ni-P co-deposition (NaH₂PO₂, 50°C)

A similar study into the influence of Cu concentration on the Pd total loading and kinetic properties of alloys surface-modified using Pd-Cu co-deposition was undertaken. Measurements of the kinetics of hydrogenation were undertaken after ~2 week exposure of the samples to air, and without application of an activation procedure. The results were presented in Figure 4.94.

It was observed that an increase in the CuSO₄ concentration in the Pd-Cu-P mixed-metal bath facilitated a decrease in the Pd total loading on the AB₅-type alloy resulting in a parallel, and expected, decrease in the kinetics of hydrogenation. The decreased Pd total loading is a result of increased competition for surface sites between the Pd and Cu atoms. The observation of a decrease in the kinetics of hydrogenation with an increase in the CuSO₄ concentration in the Pd-Cu-P mixed metal bath is also a result of the inability of Cu-P to behave as an effective hydrogen dissociation catalyst, and with increasing substitution of the Pd-P catalyst with Cu-P so the catalytic activity of the surface coating decreases. This led to a deterioration in

the ability to cleave the H-H bond and a limitation on the flux of H atoms available for transport into the bulk of the core alloy.

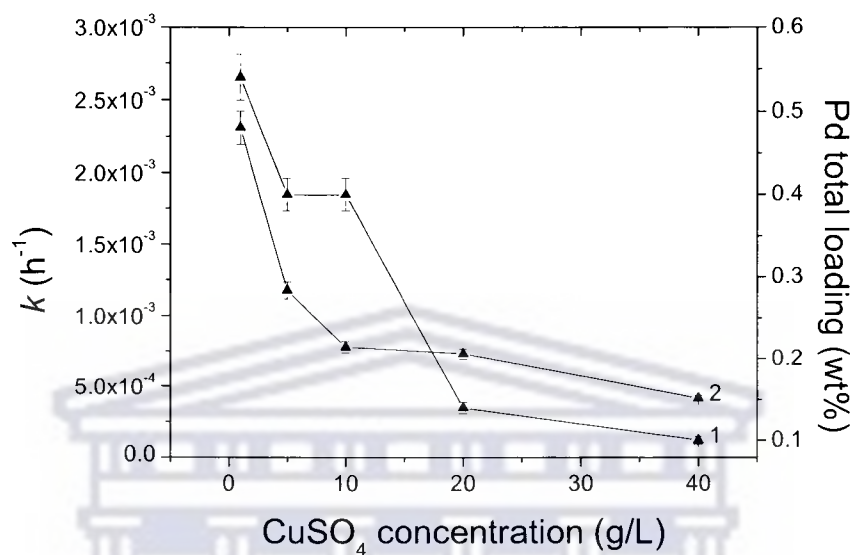


Figure 4.94. Influence of CuSO₄ concentration on Pd total loading and kinetics of hydrogenation of the AB₅-type alloy surface-modified by the co-deposition of Pd-Cu-P (NaH₂PO₂, 30 min, 60°C); (1) Pd total loading vs. CuSO₄ concentration; (2) k vs. CuSO₄ concentration

An analysis of the properties of AB₅-type alloys surface-modified using Pd-Ag (N₂H₄) coatings on AB₅-type alloys was undertaken. An investigation of the type of deposition (i.e. sequential or mixed bath) and influence of the AgNO₃ concentration, in the Pd-Ag mixed-metal bath, on the Ag surface loading; Pd surface loading; Pd total loading, and kinetic properties was conducted. Measurements of the influence of the type of Pd-Ag deposition on the kinetics of hydrogenation were undertaken after ~2 week exposure of the samples to air, and without application of an activation procedure. The results with respects to the kinetics of hydrogenation were compared and are presented as Figure 4.95.

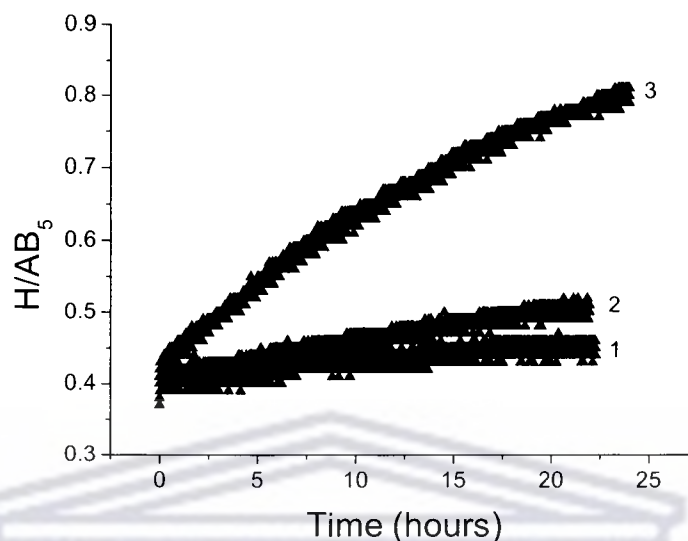


Figure 4.95. Comparison of the influence of Pd-Ag (N_2H_4) mixed-metal layers on the dynamics of activation on surface-modified AB_5 -type alloy, (1) Pd-Ag sequential-deposition; (2) Ag-Pd sequential-deposition; (3) Pd-Ag co-deposition

It was observed that sequential-deposition of Pd-Ag, irrespective of the order of deposition, did not facilitate high rates of hydrogenation on the surface-modified AB_5 -type alloy: Pd-Ag sequential-deposition ($k = 1.3 \times 10^{-3} \text{ h}^{-1}$); Ag-Pd sequential-deposition ($k = 1.4 \times 10^{-3} \text{ h}^{-1}$). In contrast, alloys surface-modified by Pd-Ag co-deposition exhibited slightly better rates of hydrogenation ($k = 3.2 \times 10^{-3} \text{ h}^{-1}$), which were comparable to that exhibited by alloys surface-modified by N_2H_4 -derived crystalline Pd ($k = 3.7 \times 10^{-3} \text{ h}^{-1}$). The co-deposition of Ag into the Pd layer therefore did not significantly or negatively affect the rate of hydrogenation in the surface-modified AB_5 -type alloys.

Subsequent investigation into the influence of the AgNO_3 concentration, in the Pd-Ag mixed-metal bath, on the Ag and Pd surface loading was undertaken. The results were presented in Figure 4.96.

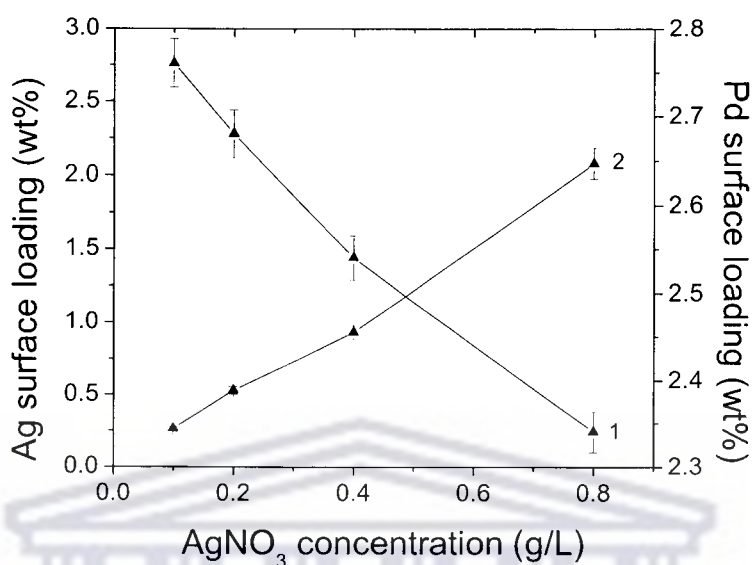


Figure 4.96. Influence of AgNO_3 concentration in the Pd-Ag co-deposition bath (N_2H_4) on Pd and Ag surface loading on AB_5 -type alloy: (1) Pd total loading vs. AgNO_3 concentration; (2) Ag total loading vs. AgNO_3 concentration

As expected it was observed that an increase in the AgNO_3 concentration in the Pd-Ag mixed-metal bath facilitated an increase in the Ag surface loading, and parallel decrease in the Pd surface loading on the AB_5 -type alloy.

Measurements of the influence of the AgNO_3 concentration in the Pd-Ag mixed-metal bath on the kinetics of hydrogenation of AB_5 -type alloys was undertaken after ~2 week exposure of the samples to air, and without application of an activation procedure. The results with respects to the kinetics of hydrogenation were presented as Figure 4.97. A comparison of the kinetics of hydrogenation with the Pd total loading was also made to illustrate the influence of the AgNO_3 concentration on the kinetic properties.

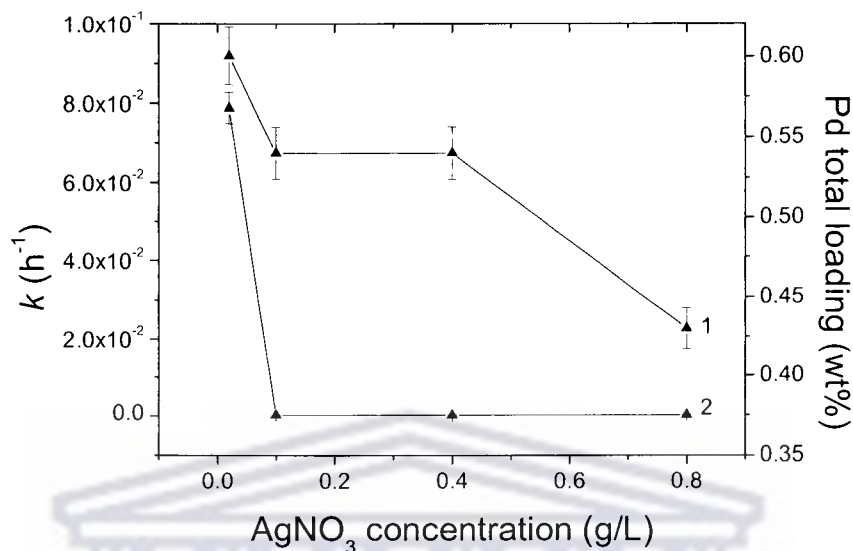


Figure 4.97. Influence of AgNO₃ concentration on Pd total loading and kinetics of hydrogenation of the AB₅-type alloy surface-modified by the co-deposition of Pd-Ag (N₂H₄, 30 min, 60°C); (1) Pd total loading vs. AgNO₃ concentration; (2) k vs. AgNO₃ concentration

It was observed that an increase in the AgNO₃ concentration in the Pd-Ag mixed-metal bath facilitated a decrease in the Pd total loading on the AB₅-type alloy, resulting in a parallel decrease in the kinetics of hydrogenation. The decreased Pd total loading is a result of increased competition for surface sites between the Pd and Ag atoms. The observation of a decrease in the kinetics of hydrogenation with an increase in the AgNO₃ concentration in the Pd-Ag mixed metal bath is a result of the inability of Ag to behave as an effective hydrogen dissociation catalyst. This led to deterioration in the ability to cleave the H-H bond and a limitation on the flux of H atoms available for transport into the bulk of the core alloy.

A comparative study of the influence of high-loading (1:100) on the kinetic behaviour and rate of hydrogenation of AB₅-type alloys surface-modified using mixed-metal layers was conducted. The results were presented in Figure 4.99.

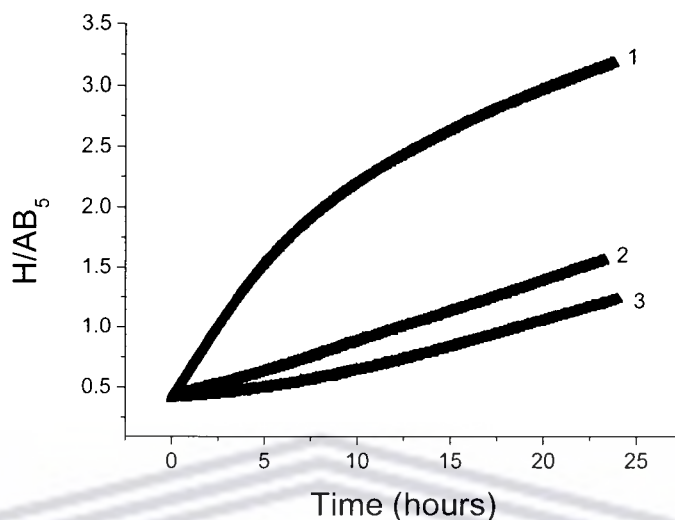


Figure 4.99. Comparison of activation dynamics of non-activated AB₅-type alloys surface-modified using mixed-metal layers ($P_{\text{H}_2} = 5.0$ bar, $T = 20^\circ\text{C}$, $t = 24$ hours): (1) Pd-Ni (NaH_2PO_2) co-deposition high-load 30 min; (2) Pd-Ag (N_2H_4) co-deposition high-load 30 min; (3) Pd-Cu (NaH_2PO_2) co-deposition high-load 30 min

It was observed that the alloy surface-modified by the co-deposition of Pd-Ni (NaH_2PO_2 , high-load) exhibited superior kinetics of hydrogenation ($k = 2.9 \times 10^{-2} \text{ h}^{-1}$) compared to that surface-modified by co-deposition of Pd-Ag (N_2H_4 , high-load) ($k = 1.7 \times 10^{-4} \text{ h}^{-1}$) and co-deposition of Pd-Cu (NaH_2PO_2 , high-load) ($k = 1.3 \times 10^{-4} \text{ h}^{-1}$). The superior kinetics of the Pd-Ni surface-modified, compared to the other mixed-metal layers investigated, may be a result of a synergistic effect between Pd and Ni atoms, upon co-deposition. The Ni atoms in the surface layer may have created an “interfacial bridge” between the Ni clusters of the core material and Pd atoms in the surface layer, facilitating enhanced transport of H atoms into the core material.

An analysis of the properties of the AB₅-type alloys surface-modified using Pd-Pt (N_2H_4) coatings was undertaken. An investigation of the influence of the type of deposition (i.e. sequential or mixed bath) on the kinetic properties of the surface-modified alloy was conducted. Measurements of the influence of the type of Pd-Pt co-deposition on the kinetics of hydrogenation were undertaken after ~2 week

exposure of the samples to air, and without application of an activation procedure. The results with respects to the kinetics of hydrogenation were compared and are presented as Figure 4.98.

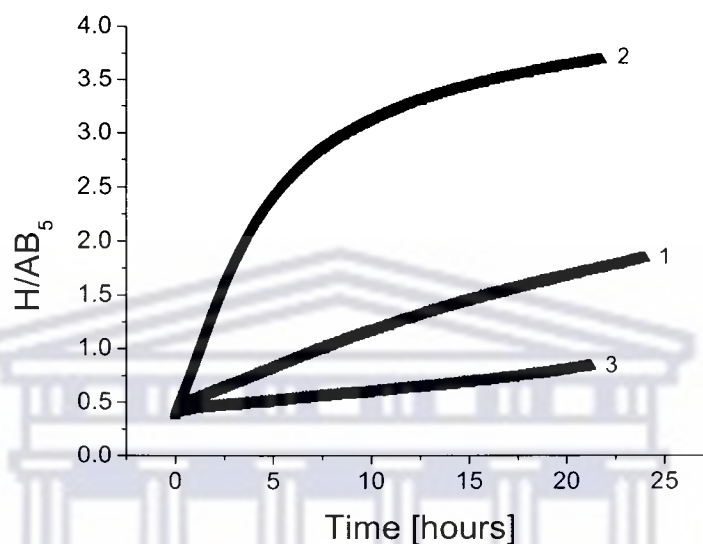


Figure 4.98. Comparison of the influence of Pd-Ag (N_2H_4) mixed-metal layers on the dynamics of activation on surface-modified AB_5 -type alloy, (1) Pd-Pt sequential-deposition; (2) Pt-Pd sequential-deposition; (3) Pd-Pt co-deposition

It was observed that Pd-Pt co-deposition did not facilitate high rates of hydrogenation on the surface-modified AB_5 -type alloy ($k = 1.1 \times 10^{-3} \text{ h}^{-1}$). This observation may have been a result of the preference of the reducing agent (i.e. hydrazine) to decompose and preferentially reduce more Pt ions than Pd ions in the mixed metal bath solution, based on the standard potentials: ($\text{Pd}^{2+} + 2\bar{e} \rightarrow \text{Pd}^0$, $E^0 = +0.915 \text{ V}$) versus ($\text{Pt}^{2+} + 2\bar{e} \rightarrow \text{Pt}^0$, $E^0 = +1.188 \text{ V}$). From the standard potentials it can be estimated that the electrons liberated from the decomposition of N_2H_4 will preferentially reduce more Pt than Pd onto the surface of the AB_5 -type alloy. In addition, the alloy had twice the quantity of Pt on the surface than Pd (Table 4.17), with Pt not being as catalytically-active towards the hydrogen dissociation reaction as Pd. Alloys surface-modified by Pd-Pt sequential deposition ($k = 2.4 \times 10^{-3} \text{ h}^{-1}$)

exhibited slightly higher rates of hydrogenation compared to that modified by Pd-Pt co-deposition, and were comparable to that exhibited by alloys surface-modified by N_2H_4 -derived crystalline Pd coatings ($k = 3.7 \times 10^{-3} \text{ h}^{-1}$). In contrast, alloys modified by Pt-Pd sequential-deposition exhibited rates of hydrogenation ($k = 1.9 \times 10^{-1} \text{ h}^{-1}$) which were significantly better compared to that exhibited by alloys surface-modified by N_2H_4 -derived crystalline Pd. In this case, it was likely that the deposition of Pt prior to Pd may have had the effect of enhancing the transport rate of hydrogen atoms into the core alloy, due to the high activity of Pt towards hydrogen exchange reactions, after hydrogen dissociation on the Pd catalyst at the exterior.

4.4.2. Summary

An approach was adopted in which Pd mixed-metal coatings (-Ni, -Cu, -Ag, -Pt) were deposited on the surface of AB_5 -type alloys to further enhance the kinetics of hydrogenation and promote the hydrogen sorption stability of the alloy.

Isolated clusters of Pd, Ni, Cu, Pt, and Ag were observed on the surface of the AB_5 -type alloy, illustrating the formation of discontinuous Pd mixed-metal layers.

Surface modification by co-deposition of Pd-Ni-P, Pd-Cu-P, and Pd-Ni-Cu-P onto the surface of the alloy resulted in significant improvements to the hydrogen sorption dynamics. The strongest influence of surface modification on H sorption properties was observed for the AB_5 -type alloy modified by co-deposition of Pd-Ni, which exhibited the highest activity towards hydrogen transfer processes between the alloy and the surface layer, as a result of a synergistic effect between Pd and Ni atoms, upon co-deposition. The amorphous Ni of the surface layer created an “interfacial bridge” between the Ni surface clusters of the core material and the amorphous Pd of the surface layer, facilitating enhanced transport of H atoms into the core material. In contrast, samples modified by sequential deposition of Pd-Ni-P and Pd-Cu-P exhibited dynamics of hydrogenation which were worse than that observed for the unmodified alloy. This was a result of the secondary metal acting as a diffusion

barrier, thereby hampering the hydrogen dissociation process and negatively affecting the kinetics of hydrogenation.

Attempts were made to study the long-term hydrogen sorption stability of the surface-modified alloys. The kinetic properties of the sample prepared by co-deposition of Pd-Ni-P did not change after air exposure for an 11 month period, illustrating the long-term sorption stability of the material, compared to the unmodified alloy. It was also observed that higher Ni concentrations on the alloy surface-modified by the co-deposition of Pd-Ni adversely affected the kinetics of hydrogenation.

It was observed that an increase in the CuSO_4 concentration in the Pd-Cu-P mixed-metal bath facilitated a decrease in the Pd total loading on the AB_5 -type alloy, resulting in a parallel decrease in the kinetics of hydrogenation. This observation was a result of the inability of Cu-P to behave as an effective hydrogen dissociation catalyst. Cu addition was also found to negatively affect the catalytic ability of Pd coatings in the hydrogen dissociation process on surface-modified AB_5 -type alloys.

It was observed that sequential-deposition of Pd-Ag, irrespective of the order of deposition, did not facilitate high rates of hydrogenation on the surface-modified AB_5 -type alloy. In contrast, alloys surface-modified by Pd-Ag co-deposition exhibited slightly higher rates of hydrogenation, which were comparable to that exhibited by alloys surface-modified by N_2H_4 -derived crystalline Pd. It was also observed that an increase in the AgNO_3 concentration in the Pd-Ag mixed-metal bath facilitated a decrease in the Pd total loading on the AB_5 -type alloy resulting in a parallel decrease in the kinetics of hydrogenation. Ag addition was found to have no significant benefit on the catalytic ability of Pd surface coatings in the hydrogen dissociation process on surface-modified AB_5 -type alloys.

It was observed that co-deposition of Pd-Pt did not facilitate high rates of hydrogenation on the surface-modified AB_5 -type alloy as a result of the action of hydrazine to preferentially reduce more Pt ions than Pd ions in the mixed-metal bath solution. Alloys surface-modified by Pt-Pd sequential-deposition exhibited rates of

hydrogenation which were significantly better compared to that exhibited by alloys surface-modified by N_2H_4 -derived crystalline Pd. Deposition of Pt prior to Pd may have had the effect of enhancing the transport rate of hydrogen atoms into the core alloy, due to the high activity of Pt towards hydrogen exchange reactions, after hydrogen dissociation on the Pd catalyst at the exterior. Pt addition was found to have a significant benefit on the catalytic ability of Pd surface coatings in the hydrogen dissociation process on surface-modified AB_5 -type alloys.

4.5. INTRODUCTION OF A PLATINUM INTERFACIAL LAYER USING LIXIVIATION FOR ENHANCEMENT OF HYDROGEN TRANSPORT

The interfacial region between the core alloy surface and the encapsulation layer may play a significant role in the sorption characteristics of surface-modified AB_5 -type alloy materials. Logically, by introducing catalytic elements into the interfacial region it may be possible to increase the rate of hydrogen transport between the surface and the Pd surface layer.

Platinum has been known to be extremely active towards hydrogen exchange reactions and is known to be an excellent catalyst for the transport of hydrogen. It was also observed in the study of AB_5 -type alloys surface-modified using Pd-Pt mixed-metal layers that the sequential deposition of Pt-Pd resulted in rates of hydrogenation which were significantly better compared to that exhibited by alloys surface-modified by N_2H_4 -derived crystalline Pd. Enhancements may have been due to the Pt layer increasing the transport rate of hydrogen atoms from the surface, after dissociation of hydrogen molecules by the Pd layer, into the core alloy.

For these reasons, the deposition of Pt interfacial layers between the alloy surface and Pd surface layer might have the effect of increasing the rate of hydrogen transfer between the core and the encapsulation layer, leading to parallel improvements in the kinetics of hydrogenation, and therefore warranted further investigation.

4.5.1. Methodology in the introduction of a platinum interfacial layer

An approach was taken to introduce a Pt interfacial layer between the AB₅-type alloy surface and a Pd-P layer via lixiviation. By lixiviating the Pt interfacial layer onto the surface of the AB₅-type core material nickel atoms can be substituted with the result that the transport properties of the material may be altered. The Pt atoms may have the ability to substitute Ni atoms in the surface clusters as a result of their greater nobility. The process entailed suspending AB₅-type alloy powders in a 1.0 g/L solution of H₂PtCl₆ and agitating the suspension for measured periods (10 - 60 minutes), at room temperature, using sonication. The lixiviated alloy was washed, filtered, dried, and subjected to the standard Pd-P deposition procedure (NaH₂PO₂, 30 min, 50°C). The ratio of powder to solution was maintained at 200g AB₅-type alloy per litre H₂PtCl₆ solution. The filtrate was collected and analysed for Ni content to determine whether Pt atoms had substituted the Ni surface atoms of the alloy.

A schematic representation of the H₂PtCl₆ lixiviation process and the subsequent Pd deposition step can be illustrated in Figure 4.100. An increase in specific surface area of the alloy occurs upon lixiviation in H₂PtCl₆ solution as a result of the replacement of Ni surface atoms by Pt atoms ($\text{Ni}^0 + \text{Pt}^{2+} \rightarrow \text{Ni}^{2+} + \text{Pt}^0$).

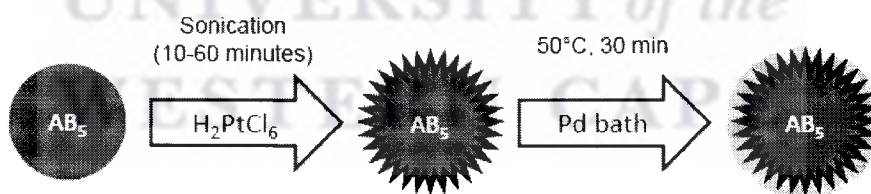


Figure 4.100. Schematic representation of H₂PtCl₆ lixiviation and subsequent Pd-P deposition using the standard Pd-P electroless plating bath (NaH₂PO₂, 50°C, 30 minutes)

4.5.2. Characterization of morphological and kinetic properties of AB₅-type alloys surface-modified using platinum interfacial layers

Elemental analysis of the Ni content in the H₂PtCl₆ solution after lixiviation was conducted using AAS to ascertain whether Pt atoms had successfully substituted the Ni surface atoms of the AB₅-type alloy. Results were presented in Table 4.20. Trace quantities of Ni were detectable in the H₂PtCl₆ solution, indicating that quantities of nickel had successfully been substituted by Pt atoms on the surface of the AB₅-type alloy. This deduction was verified by the detection of trace quantities of Pt on the AB₅-type alloy after EDS and AAS analyses (Table 4.21).

Table 4.20. Elemental analysis of H₂PtCl₆ solution after lixiviation of AB₅-type alloy

Lixiviation time (minutes)	Ni concentration (ppm)
10	2.0
30	2.4
60	2.7

An analysis of morphological features of the alloy after lixiviation in H₂PtCl₆ solution and subsequent Pd-P deposition was undertaken using FESEM (4.0 kV, 7.0 mm). The images were presented in Figures 4.101 - 4.103.

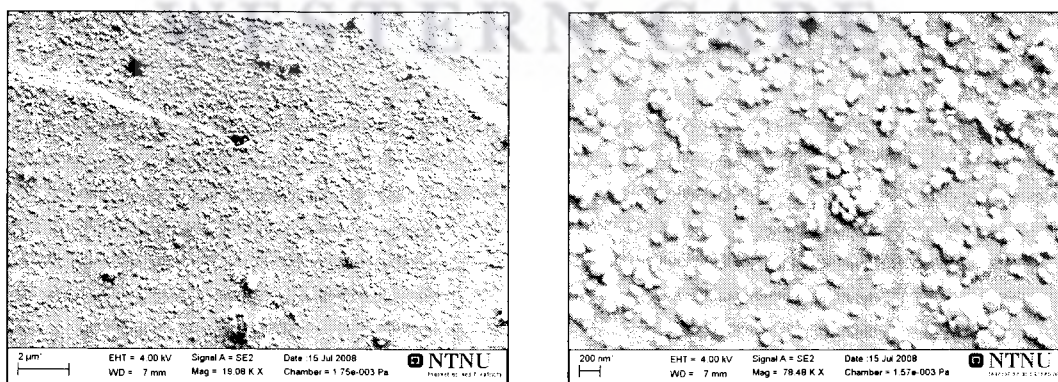


Figure 4.101. FESEM images of AB₅-type alloy lixiviated in 1.0 g/L H₂PtCl₆ (10 minutes) and encapsulated in Pd-P layer (NaH₂PO₂, 30 min, 50°C)

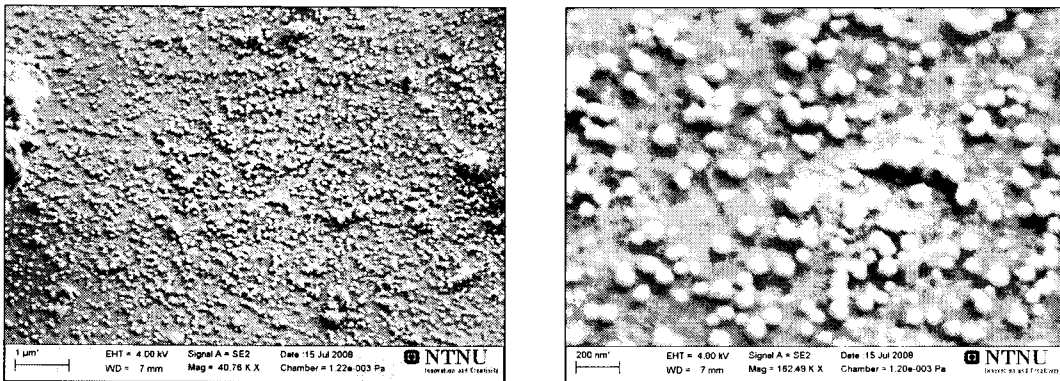


Figure 4.102. FESEM images of AB₅-type alloy lixiviated in 1.0 g/L H₂PtCl₆ (30 minutes) and encapsulated in Pd-P layer (NaH₂PO₂, 30 min, 50°C)

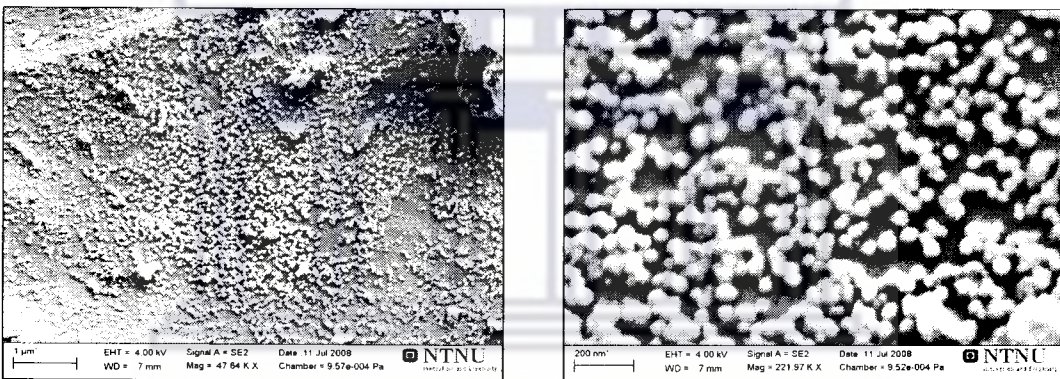


Figure 4.103. FESEM images of AB₅-type alloy lixiviated in 1.0 g/L H₂PtCl₆ (60 minutes) and encapsulated in Pd-P layer (NaH₂PO₂, 30 min, 50°C)

All three samples were observed to support fairly good dispersions of surface Pd-P particles after plating in NaH₂PO₂-based electroless plating baths. Elemental analysis of the surface and total Pd loadings of sample materials were conducted using EDS and AAS, respectively. The results were tabulated in Table 4.21.

Table 4.21. Elemental analysis results after lixiviation (1.0 g/L H_2PtCl_6) of AB_5 -type alloy and Pd-P surface modification (NaH_2PO_2 , 30 min, 50°C)

H_2PtCl_6 lixiviation time (minutes)	Pd surface loading (wt%)	Pd total loading (wt%)	Pt surface loading (wt%)	Pt total loading (wt%)
10	1.10	0.7	0.18	0.05
30	2.47	0.8	0.34	0.06
60	3.48	0.8	0.58	0.11

From Table 4.21 it was observed that the Pd surface loading increased with an increase in the lixiviation time. This may be in account of an increase of the surface roughness with an increase in the lixiviation time, which would promote physical adhesion of the Pd-P particles to the surface of the AB_5 -type alloy. Importantly, Pt surface and total loadings were observed to increase with increases in lixiviation time.

Measurements of the influence of the lixiviation time on the kinetics of hydrogenation by the Pd-P surface-modified AB_5 -type alloys were undertaken after ~ 2 week exposure of the samples to air, and without application of an activation procedure. The results were presented in Figure 4.104. The calculated rate constants were tabulated and presented in Table 4.22.

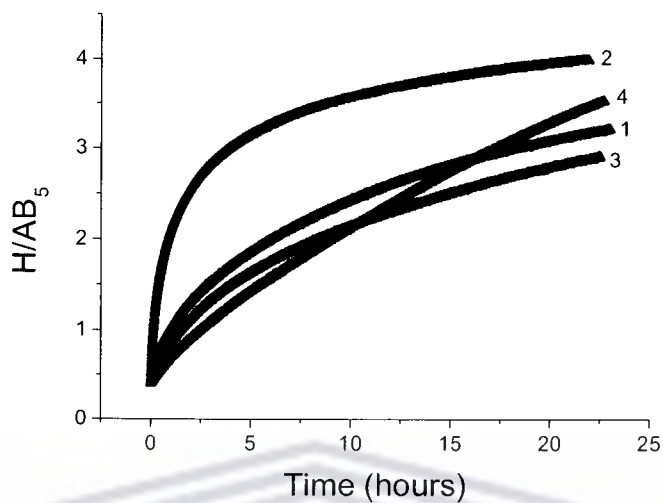


Figure 4.104. Influence of H_2PtCl_6 (1.0 g/L) lixiviation time on kinetics of hydrogenation of Pd-P surface-modified AB_5 -type alloys (NaH_2PO_2 , 30 min, 50°C), (1) no lixiviation; (2) 10 minutes; (3) 30 minutes; (4) 60 minutes

Table 4.22. Summary of kinetic properties of Pd-P surface-modified AB_5 -type alloys (NaH_2PO_2 , 30 min, 50°C) after lixiviation in H_2PtCl_6 (1.0 g/L)

Lixiviation time (minutes), including Pd-P deposition (NaH_2PO_2 , 30 min, 50°C)	Rate constant (k) / h^{-1}
0	3.8×10^{-3}
10	3.3×10^{-1}
30	5.6×10^{-3}
60	5.5×10^{-4}

It was observed that short lixiviation periods (~ 10 minutes) in dilute H_2PtCl_6 solution enhanced the hydrogenation rate, after subsequent Pd-P deposition, compared to that prepared without the introduction of the Pt interfacial layer. This observation may be due to increases in the hydrogen exchange rate between the AB_5 -type alloy surface and the Pd-P surface layer. Generally, longer lixiviation periods did not enhance

kinetic properties of the alloys, and the corresponding materials had similar characteristics to that prepared without the introduction of a Pt interfacial layer.

4.5.3. Summary

An approach was taken to introduce a Pt catalytic layer into the interface between the AB₅-type alloy surface and the Pd-P surface layer for the purpose of increasing the rate of hydrogen transport between the core and the encapsulation layer. The Pt interfacial layer was introduced through lixiviation in a dilute H₂PtCl₆ solution, to substitute surface Ni atoms of the AB₅-type core material.

Trace quantities of Ni in the H₂PtCl₆ solution and Pt on the AB₅-type alloy surface were detectable indicating that quantities of nickel had successfully been substituted by Pt atoms on the surface of the alloy.

The Pd surface loading was found to increase with an increase in the lixiviation time as a result of an increase of the surface roughness, which would promote physical adhesion of the Pd-P particles to the surface of the AB₅-type alloy.

Short lixiviation periods (~10 minutes) in dilute H₂PtCl₆ solution improved the transport of H atoms, compared to that prepared without the introduction of the Pt interfacial layer. Increases in the hydrogen exchange rate between the AB₅-type alloy surface and the Pd-P surface layer were assumed.

4.6. PALLADIUM SURFACE MODIFICATION OF FLUORINATED AB₅-TYPE HYDRIDE-FORMING ALLOYS

To fabricate more effective surface-modified AB₅-type alloys it was important to incorporate a high-surface area entity which may act as “scaffolding” for the deposition of the PGM catalyst layer, and at the same time participate in the surface protection of the alloy. Surface fluorination was identified as a potential method of

providing the “scaffolding” by increasing the specific surface area of the alloy prior to the deposition of the PGM layer, thereby facilitating the deposition of larger quantities of Pd. To date, no known attempts have been made to study the influence of the combination of Pd and fluoride layers on the hydrogenation performances of hydrogen sorption alloys. Separately, the encapsulation and fluorination techniques provide notable improvements in the performance of the alloy material, but combined these techniques may have the ability to produce high-performance materials, based on hydride-forming metal alloys, for the separation / purification / storage of hydrogen from impure feed streams. The incubation periods observed in fluoride-coated hydride-forming metal alloys can be suppressed by deposition of metal layers which act as excellent hydrogen dissociation catalysts. Also, the surface coverage of precious metals used in the encapsulation of the alloy surface can be improved by deposition of high-surface area fluoride layers on the surface of the alloy.

Surface treatment by fluorination is known to facilitate the generation of a Ni-rich sub-layer via the formation of fluorides with rare earth metals on AB₅-type alloys. In doing so, fluorination of metal hydride-forming alloys has been reported to improve performances in initial activation, reaction kinetics, durability, and sorption stability at the gas-solid interface of the alloy [49,69,97]. Other advantages of fluorination include: moderate cost of starting materials and simplicity of mechanism; the technique does not severely alter the integrity of sensitive alloy surfaces; increases gas selectivity [170].

Based on the review of the available methods, the fluorination of the AB₅-type metal-hydride forming alloy was conducted using a wet treatment technique in which the substrate material was stirred in a fluoride-containing solution under controlled conditions, with washing and drying. NiF₂ was included into the fluoride solution to replenish the extraction of surface Ni upon fluorination of the alloy surface by conversion to metallic Ni and self-impregnation into the LaF₃ shell [172].

4.6.1. Surface fluorination of AB₅-type alloys using wet treatment in fluoride-containing solutions

An investigation of the surface morphology of the AB₅-type alloy after chemical treatment in a fluorine-rich solution was conducted using high-resolution FESEM (Figure 4.105). The fluorinated alloy had a rough surface appearance after treatment, similar to the observations made by Wang *et al.* [173]. The observation of a rough surface, and the obvious change of colour, was indicative of the formation of a LaF₃ shell on the surface of the alloy. The fluoride layer was observed as large islands on the surface of the core material. Well-defined LaF₃ micro-channels were observed in the shell, with an average micro-channel size of about 79 nm. Therefore, the micro-channels were of sufficient size to be plugged by Pd particles deposited by electroless plating. Elemental analysis of the fluorinated alloy confirmed a F surface loading of 7.6 wt. %. The corresponding EDS spectrum can be seen in Figure 4.106. From the EDS spectra the presence of surface fluorides was easily detectable as two additional peaks in the low-energy region of the spectrum. Another interesting observation made in the elemental analysis of the surface-modified alloy was the increase in the oxygen content on the alloy surface with fluorination. This type of observation was shared by Hagenmuller [236], who proposed that dissolved oxygen atoms in solution have the ability to substitute fluorine atoms in fluoride layers.

Importantly, the treatment in the fluoride solution facilitated a significant increase in the specific surface area from 0.05 m²/g for the unmodified alloy to 3.9 m²/g after treatment.

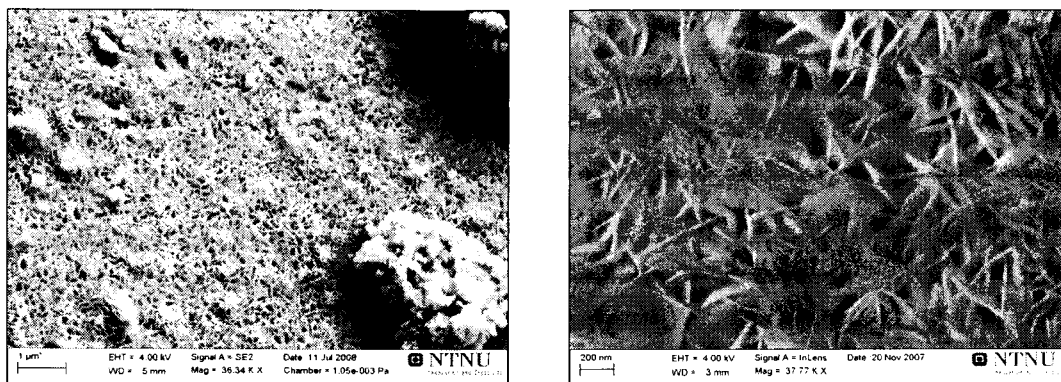


Figure 4.105. SEM images of AB₅-type alloys after treatment in fluoride solution (24 hours, 70°C)

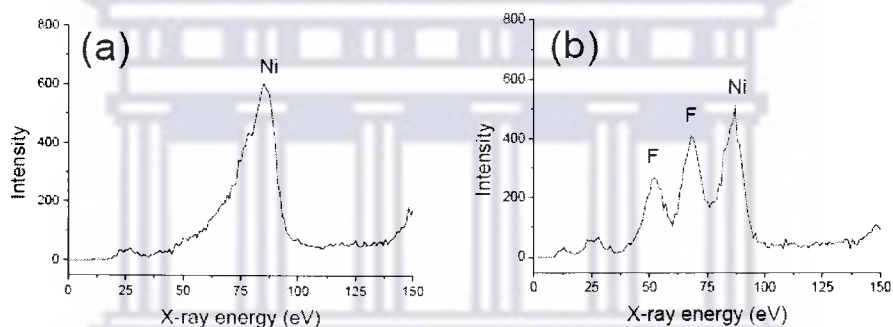


Figure 4.106. Elemental analysis of fluorinated AB₅-type alloy (24 hours, 70°C), (a) unmodified alloy; (b) fluorinated alloy

An XRD analysis was conducted on the fluorinated AB₅-type alloy to ascertain the changes in the material crystallinity with the deposition of a fluoride surface coating (Figure 4.107). Importantly, the nanocrystallinity of the LaF₃ fluoride layer was confirmed by the appearance of additional peaks. The emergence of twelve additional peaks were observed upon treatment in the fluoride solution: (100) at 14.3°; (002) at 24.2°; (110) at 24.9°; (111) at 27.7°; (112) at 34.9°; (022) at 37.9°; (121) at 40.4°; (300) at 43.8°; (113) at 44.8°; (004) at 49.5°; (302) at 50.7°; (220) at 51.0°. Minor peaks were omitted as they were insignificant and difficult to resolve from the background signal. The lattice parameters of the LaF₃ shell determined after

refinement ($a = 7.1817 \text{ \AA}$, $c = 7.3557 \text{ \AA}$) were similar to those determined by Zalkin *et al.* ($a = 7.1851 \text{ \AA}$, $c = 7.3511 \text{ \AA}$) [237].

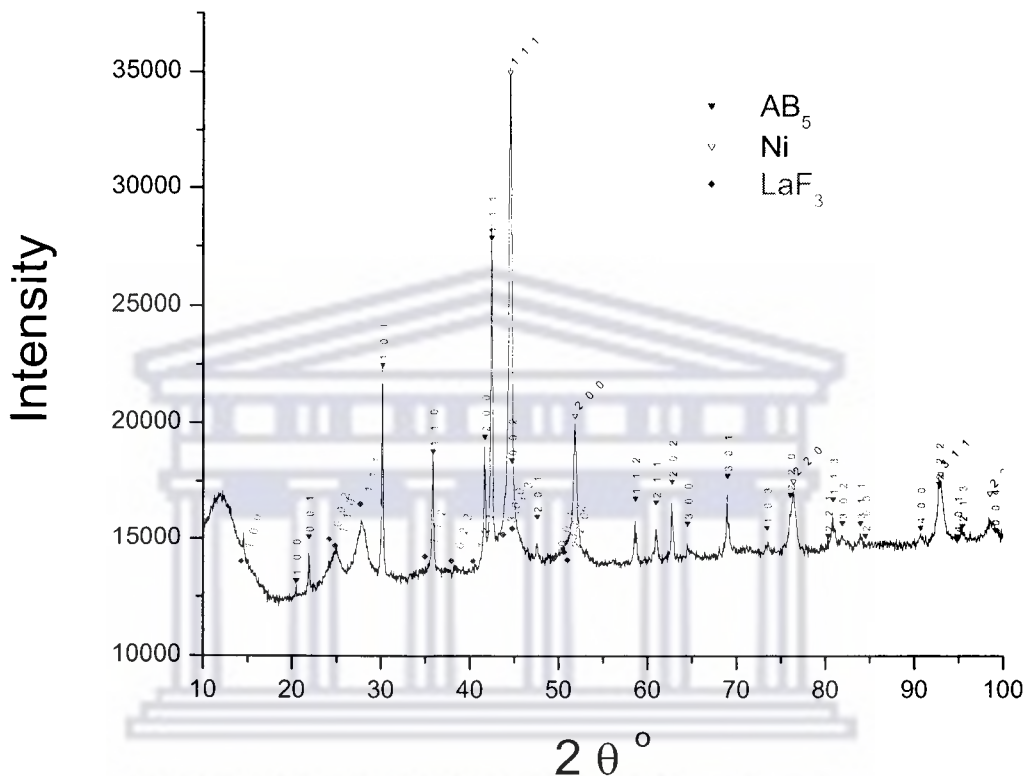


Figure 4.107. Fitted XRD diffractogram of the AB₅-type alloy after treatment in fluoride solution (24 hours, 70°C), (1) unfurinated alloy, (2) fluorinated alloy

An analysis of the influence of the Ni atom impregnation into the LaF₃ surface layer on the kinetics of hydrogenation of the surface-modified AB₅-type alloy was undertaken. Measurements of the kinetics of hydrogenation were undertaken after ~2 week exposure of the samples to air, and without application of an activation procedure. The results with respects to the kinetics of hydrogenation were compared and are presented as Figure 4.108. It was observed that the Ni impregnation into the fluoride layer slightly improved the kinetics of hydrogenation ($k = 3.0 \times 10^{-1} \text{ h}^{-1}$) compared to that prepared without the Ni impregnation ($k = 2.1 \times 10^{-1} \text{ h}^{-1}$). This

observation was a result of the replenishment of surface Ni atoms, by the inclusion of a NiF_2 salt into the fluoride solution, which had been removed in the surface treatment. For this reason, all subsequent fluorination treatments were conducted using the impregnation of Ni atoms into the fluoride layer. It was also observed that the Ni impregnation resulted in a noticeably shorter incubation period compared to that of the alloy which was fluorinated without the Ni impregnation.

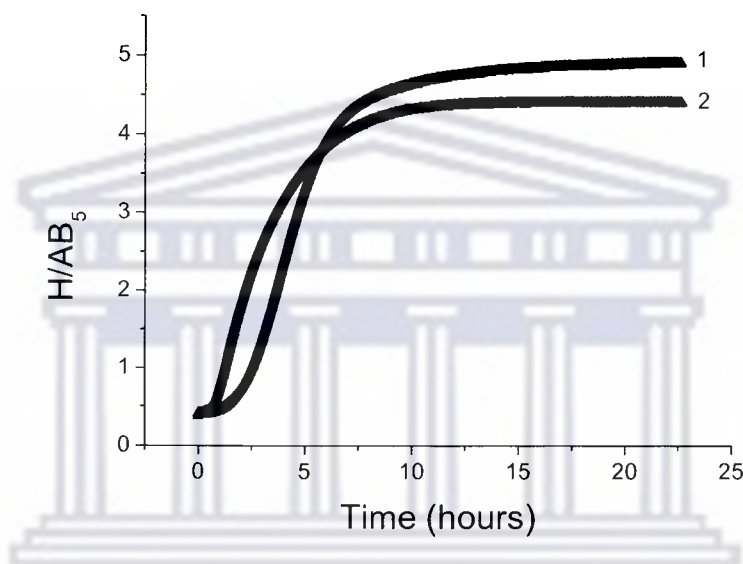


Figure 4.108. Influence of Ni impregnation into the surface LaF_3 layer on kinetics of hydrogenation of fluorinated AB_5 -type alloys (24 hours, 70°C), (1) without Ni impregnation; (2) Ni impregnation

The reproducibility of the enhanced kinetics of hydrogenation provided by the fluorination of the AB_5 -type alloy was analysed. Three samples were prepared by fluorination of the AB_5 -type alloy in the fluoride solution. Measurements of the kinetics of hydrogenation were undertaken after ~2 week exposure of the samples to air, and without application of an activation procedure (Figure 4.109). Good precision in the kinetics of hydrogenation was observed after fluorination, with the kinetic constant ranging between 2.8×10^{-1} and $3.0 \times 10^{-1} \text{ h}^{-1}$.

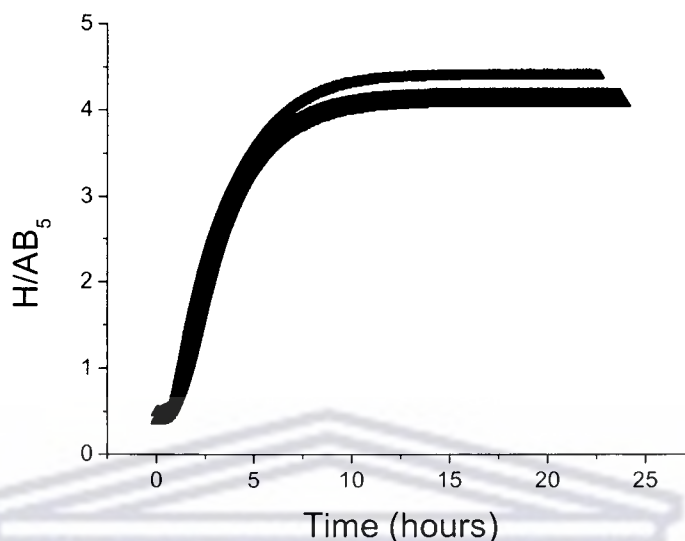


Figure 4.109. Reproducibility of activation dynamics ($P_{\text{H}_2} = 5.0$ bar, $T = 20^\circ\text{C}$, $t = 24$ hours) of non-activated AB₅-type alloys surface-modified using fluorination (24 hours, 70°C)

4.6.2. *Electroless plating of palladium on fluorinated AB₅-type alloys*

An attempt was made to study the morphology and kinetic properties of AB₅-type alloys surface-modified using a combination of Pd surface layer encapsulation and fluorination. The rationale behind this approach was the combination of the large increase in the specific surface area of the alloy with fluorination, and the enhanced activation kinetics observed with deposition of Pd catalytic layers, to form materials with exquisite hydrogen sorption properties.

The surface morphologies of the AB₅-type alloys surface modified using fluorination-encapsulation and encapsulation-fluorination approaches were investigated using FESEM. The results were recorded and are presented as Figures 4.110 and 4.111.

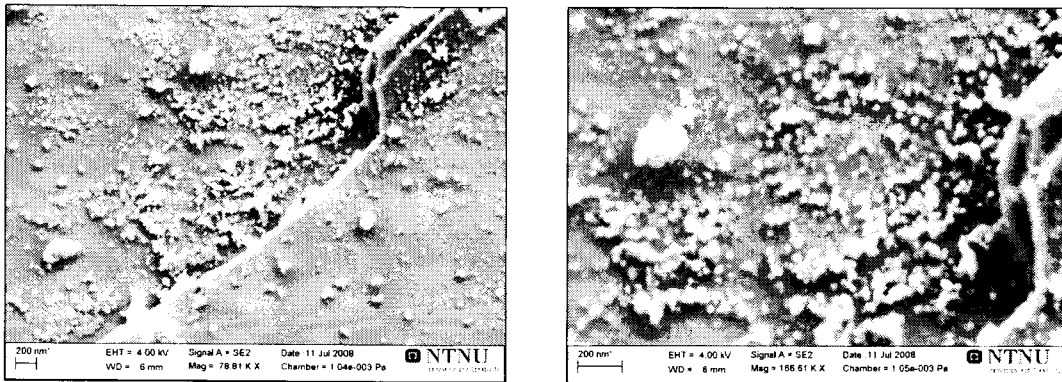


Figure 4.110. SEM images of the AB₅-type alloy surface-modified using a fluorination-encapsulation approach (NaH₂PO₂, 30 min)

From Figure 4.110, it was observed that fluorination-encapsulation facilitated the deposition of large agglomerates of the Pd-P particles on the surface. A parallel elemental analysis of the surface loading was undertaken. Moderate quantities of both Pd (3.0 wt.%) and F (1.9 wt.%) were detected on the surface of the alloy. The Pd total loading was determined as 0.54 wt.%.

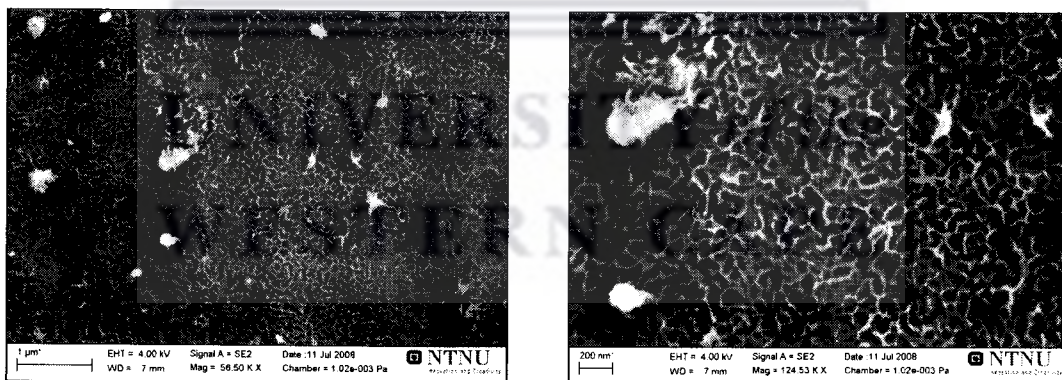


Figure 4.111. SEM images of the AB₅-type alloy surface-modified using an encapsulation-fluorination approach (NaH₂PO₂, 30 min)

From Figure 4.111, it was observed that encapsulation-fluorination facilitated the deposition of a network-like LaF₃ structure without the presence of large Pd-P agglomerates. A parallel elemental analysis of the surface loading was undertaken.

Moderate quantities of both Pd (1.8 wt.%) and F (3.8 wt.%) were detected on the surface of the alloy. The Pd total loading was determined as 0.48 wt%.

Following the analysis of the surface morphology of the AB₅-type alloys surface-modified using fluorination-encapsulation and encapsulation-fluorination approaches, an investigation of the corresponding kinetic properties was undertaken. Measurements of the kinetics of hydrogenation were undertaken after ~2 week exposure of the samples to air, and without application of an activation procedure. The results were compared in Figure 4.112.

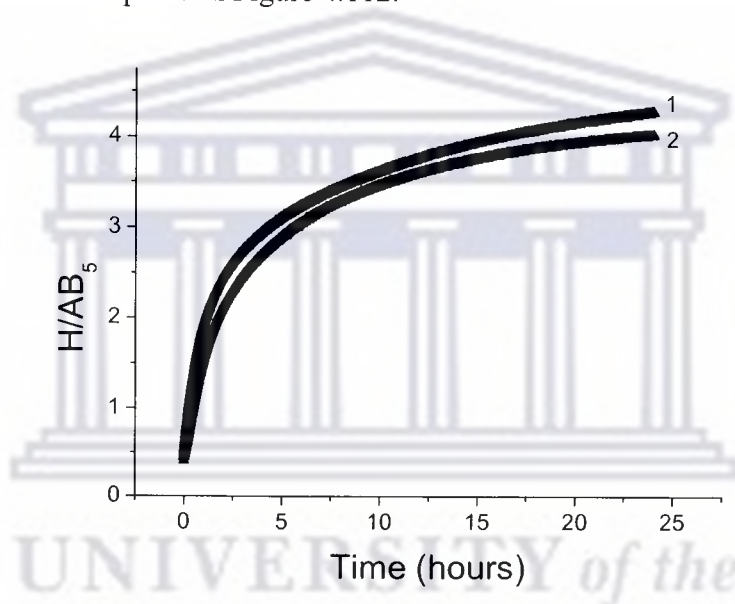


Figure 4.112. Comparison of activation dynamics of non-activated AB₅-type alloys surface-modified using fluorination-encapsulation and encapsulation-fluorination approaches ($P_{\text{H}_2} = 5.0$ bar, $T = 20^\circ\text{C}$, $t = 24$ hours), (1) fluorination-encapsulation; (2) encapsulation-fluorination

The kinetics of hydrogenation of the AB₅-type alloys surface-modified using fluorination-encapsulation ($k = 0.25 \text{ h}^{-1}$) and encapsulation-fluorination ($k = 0.19 \text{ h}^{-1}$) approaches were observed to be similar. The observation provided preliminary confirmation that the order of surface-modification did not have a significant influence on the kinetic properties of the sample materials. Further analysis of the influence of the order of surface-modification on the kinetic properties of AB₅-type

alloys was undertaken after an increase in the substrate-to-solution concentration (1:100). Measurements of the kinetics of hydrogenation were undertaken after ~2 week exposure of the samples to air, and without application of an activation procedure. The results were compared in Figure 4.113.

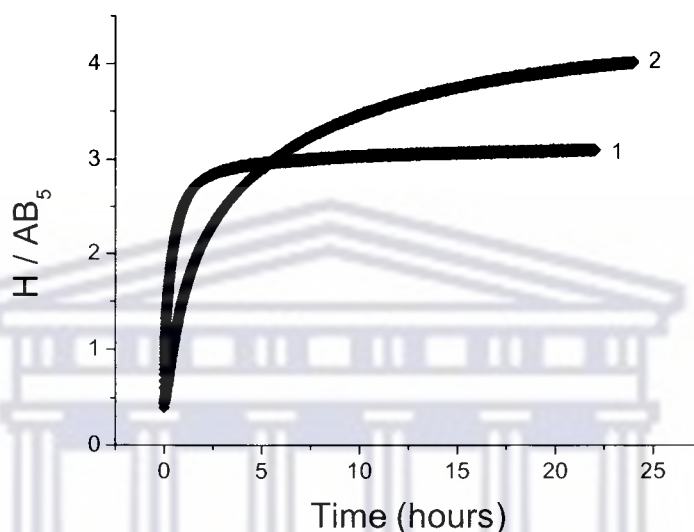


Figure 4.113. Comparison of activation dynamics of non-activated AB₅-type alloys surface-modified using fluorination-encapsulation and encapsulation-fluorination approaches after increasing the substrate-to-solution concentration ($P_{\text{H}_2} = 5.0$ bar, $T = 20^\circ\text{C}$, $t = 24$ hours), (1) fluorination-encapsulation (high-load); (2) encapsulation-fluorination (high-load)

It was observed from Figure 4.113 that the use of the fluorination-encapsulation approach in surface-modification facilitated enhanced kinetics of hydrogenation ($k = 2.9 \text{ h}^{-1}$) on the AB₅-type alloys compared to that prepared by the encapsulation-fluorination approach ($k = 0.31 \text{ h}^{-1}$), after increasing the substrate-to-solution concentration. This observation provided preliminary confirmation that the order of surface-modification had a significant influence on the kinetic properties of the sample materials.

The corresponding elemental analysis also confirmed that significantly large quantities of the active Pd-P catalyst was deposited on the AB₅-type alloy surface

after fluorination and “high-load” Pd-P deposition (total loading – 1.3 wt.% Pd; surface loading – 18 wt.% Pd, 0.9 wt.% F). In comparison, the sample prepared using the encapsulation-fluorination approach and “high-loading”, also exhibited appreciable quantities of the Pd-P catalyst (total loading – 1.1 wt.% Pd; surface loading – 12.2 wt.% Pd, 6.4 wt.% F).

4.6.3. *Electroless plating of palladium on fluorinated AB₅-type alloys after surface pre-treatment in γ -aminopropyltriethoxysilane*

Fluorination has been associated with formation of passive oxides on the surface of hydride-forming alloys [69]. It was observed that fluorination resulted in an increase in oxygen content on the AB₅-type alloy, as determined following EDS analyses. The increase in oxygen content may have been a result of the ability of the fluoride atoms to interchange with oxygen atoms in solution. Similar observations were made by Hagemuller [236]. Based on this observation, an approach was adopted to increase the quantity of Pd-P deposited on the surface of the alloy through the functionalization technique developed in this study (Section 4.3). It is known that surface (hydr)oxides have the capacity to assist the surface bonding of γ -APTES layers, which were found to immobilize large quantities of the Pd nuclei in electroless plating, thereby facilitating the deposition of continuous Pd layers. For this reason, fluorinated AB₅-type alloy were functionalized prior to deposition of the Pd-P layer.

An analysis of the Pd surface loading of the fluorinated and functionalized AB₅-type alloy was undertaken. The results were presented in Figure 4.114. Generally, an increase in the Pd surface loading was observed with an increase in the Pd-P deposition time.

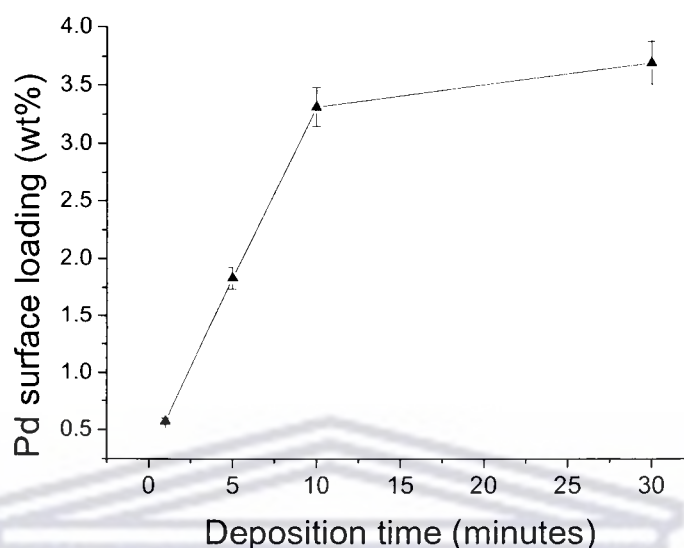


Figure 4.114. Influence of Pd-P deposition time on Pd surface loading on AB₅-type alloy after fluorination, γ -APTES functionalization, and Pd-P encapsulation (NaH_2PO_2 , 50°C)

An analysis of the specific surface area of the AB₅-type alloy surface-modified using fluorination, functionalization, and Pd-P encapsulation was undertaken to monitor the proposed plugging of the fluoride layer after encapsulation (Figure 4.115). It was observed that a consistent deterioration in the specific surface area of the surface-modified alloy occurs with an increase in the deposition time. A large decrease in the specific surface area was observed starting from the fluorinated alloy ($3.9 \text{ m}^2/\text{g}$) to the completion of the Pd-P encapsulation ($1.5 \text{ m}^2/\text{g}$). The result directly confirmed that the Pd-P surface layer, after functionalization, acted to plug the micro-channels of the LaF_3 surface layer of the fluorinated alloy.

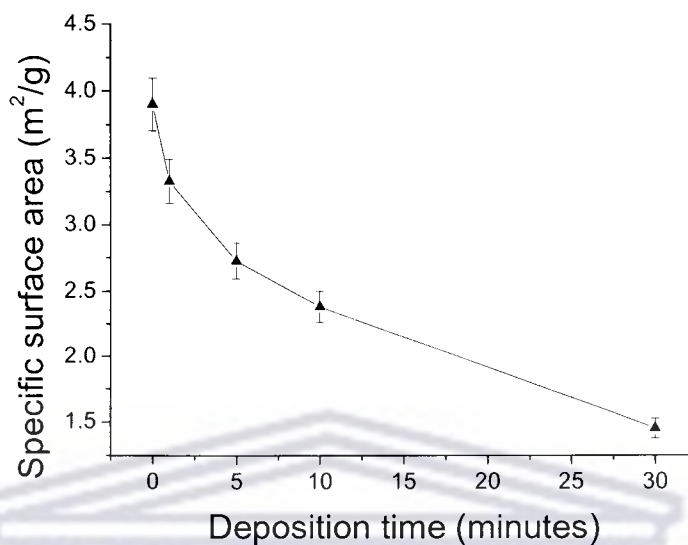


Figure 4.115. Influence of Pd-P deposition time on Pd specific surface area of AB₅-type alloy after fluorination (24 hours, 70°C), γ -APTES functionalization (1 hour, 90°C), and Pd-P encapsulation (NaH₂PO₂, 50°C)

Subsequent to the analysis of the Pd surface loading and specific surface area of the AB₅-type alloy after fluorination; functionalization; and Pd-P encapsulation, an analysis of the influence of the PdCl₂ concentration on the kinetics of hydrogenation was undertaken. Measurements of the kinetics of hydrogenation were undertaken after ~2 week exposure of the samples to air, and without application of an activation procedure. The results were compared in Figure 4.116. It was clearly observed that an increase in the PdCl₂ concentration facilitated a parallel increase in the kinetics of hydrogenation. Higher concentrations of deposited Pd-P were deduced to promote higher capacities for the catalysis of the hydrogen dissociation process on the surface of the fluorinated AB₅-type alloy.

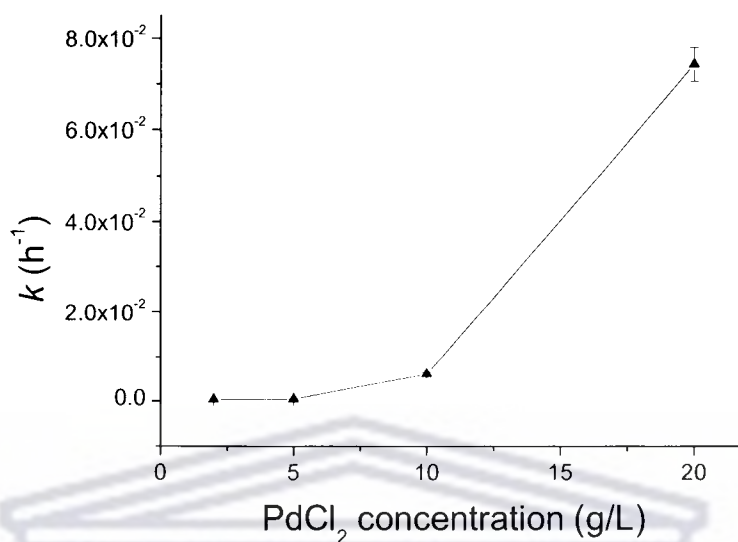


Figure 4.116. Influence of PdCl₂ concentration on kinetics of hydrogenation of the AB₅-type alloy surface-modified by fluorination (24 hours, 70°C), γ -APTES functionalization (1.0 vol.%, 1 hour, 90°C), and Pd-P encapsulation (NaH₂PO₂, 30 min, 50°C)

An approach was taken to increase the quantity of Pd-P deposited on the surface of the fluorinated-functionalized-encapsulated AB₅-type alloy through increasing the substrate-to-solution concentration. In doing so, it was assumed that significantly large quantities of Pd-P could be deposited into the micro-channels, thereby facilitating extremely fast kinetics of hydrogenation and superior hydrogen sorption stability. After preparation of the proposed sample materials the surface morphologies were investigated using high-resolution SEM. The results were recorded and are presented as Figure 4.117.

The surface coating of the AB₅-type alloy surface-modified by fluorination (24 hours, 70°C), γ -APTES functionalization (1.0 vol.%, 1 hour, 90°C), and Pd-P encapsulation (“high-load”, NaH₂PO₂, 30 min, 50°C) was described as a continuous layer exhibiting superior surface coverage. However, pinholes and cracks were still visible. Very close packing of the Pd-P particles could be observed, and these particles were

generally smaller than that observed without the surface pre-functionalization step (63 nm). A large increase in the specific surface area was observed ($0.62 \text{ m}^2/\text{g}$) compared to that observed for the parent alloy ($0.05 \text{ m}^2/\text{g}$). However, the specific surface area measured was significantly lower than that observed for the fluorinated alloy sample material ($3.9 \text{ m}^2/\text{g}$), indicating that the deposited Pd-P particles may have significantly plugged the micro-channels of the LaF_3 layer after functionalization and an increased substrate-to-solution concentration. The parallel AAS analysis confirmed that a Pd total loading of 1.4 wt.% was deposited on the AB_5 -type alloy, representing the largest loading achieved in the study.

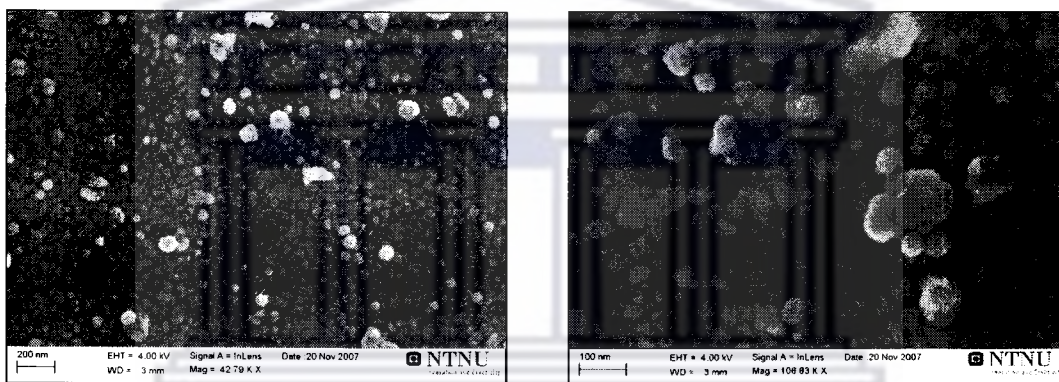


Figure 4.117. SEM images of the AB_5 -type alloy surface-modified by fluorination (24 hours, 70°C), γ -APTES functionalization (1.0 vol.%, 1 hour, 90°C), and Pd-P encapsulation (“high-load”, NaH_2PO_2 , 30 min, 50°C)

Measurement of the kinetics of hydrogenation by the surface-modified AB_5 alloy was carried out without pre-activation. Under the experimental conditions ($P_{\text{H}_2} = 5.0 \text{ bar}$, $T = 20^\circ\text{C}$, $t = 24 \text{ hours}$) the AB_5 -type alloy surface-modified by the fluorination (24 hours, 70°C), γ -APTES functionalization (1.0 vol.%, 1 hour, 90°C), and Pd-P encapsulation (“high-load”, NaH_2PO_2 , 30 min, 50°C) exhibited the best kinetics of hydrogenation observed in the study, reaching the maximum H/AB_5 molar ratio in $t_0 = 0.28 \text{ hours}$. A comparison of the kinetic behaviour was made to the alloy surface-modified by γ -APTES functionalization (1.0 vol.%, 1 hour, 90°C), and Pd-P

encapsulation (“high-load”, NaH_2PO_2 , 30 min, 50°C) (Figure 4.118). It was observed that the kinetics of the sample prepared by fluorination-functionalization-encapsulation and “high-loading” ($k = 3.6 \text{ h}^{-1}$) transcended that of the sample prepared by functionalization-encapsulation and “high-loading” ($k = 1.3 \text{ h}^{-1}$), and produced the best kinetics of hydrogenation in the study. Large increases in hydrogenation performances were observed with the introduction of Pd-P layers into the micro-channels of the LaF_3 shell after functionalization, and were associated with the promotion of the hydrogen spillover phenomenon.

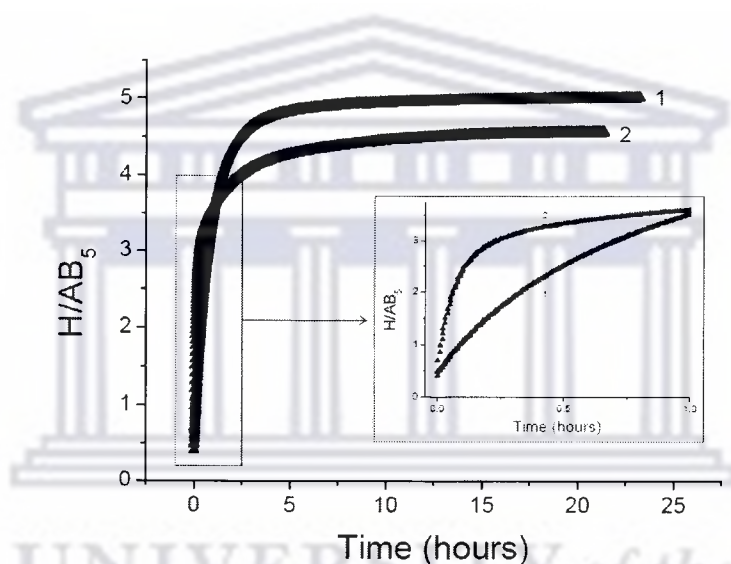


Figure 4.118. Comparison of activation dynamics of non-activated AB_5 -type alloys surface-modified using functionalization-encapsulation and fluorination-functionalization-encapsulation approaches ($P_{\text{H}_2} = 5.0 \text{ bar}$, $T = 20^\circ\text{C}$, $t = 24 \text{ hours}$), (1) functionalization-encapsulation (high-load); (2) fluorination-functionalization-encapsulation (high-load)

The combination of fluorination and Pd encapsulation, facilitated by surface functionalization of the AB_5 -type alloy using aqueous solutions of γ -APTES, was demonstrated to improve the subsequent process of the electroless plating of the alloys with Pd to yield more dense and uniform surface coatings on the high-surface area LaF_3 “scaffolding”, and in such a way resulted in superior kinetics of hydrogenation of the surface-modified alloys.

4.6.4. Summary

Treatment of the AB₅-type alloy in the fluoride solution facilitated a significant increase in the specific surface area, and based on this observation it was possible to further enhance the kinetics of hydrogenation using Pd-P encapsulation.

It was observed that Ni impregnation into the fluoride layer slightly improved the kinetics of hydrogenation compared to that without the Ni impregnation, as a result of the replenishment of surface Ni atoms lost in solution during the wet treatment.

The order of surface-modification (i.e. encapsulation / fluorination; fluorination-encapsulation) only significantly influenced the kinetic properties of the sample materials when appreciable amounts of Pd-P was deposited on the surface through an increase in the substrate-to-solution concentration. Also it was observed that an increase in the PdCl₂ concentration facilitated a parallel increase in the kinetics of hydrogenation on alloys surface-modified by fluorination and Pd-P encapsulation.

Continuous Pd-P layers, exhibiting superior surface coverage on the AB₅-type alloy, could be prepared by a combination of fluorination; functionalization; and encapsulation. It was deduced, based on the consistent reduction in the specific surface area that the Pd-P particles deposited during encapsulation, after γ -APTES functionalization, plugged the micro-channels of the LaF₃ shell generated after fluorination. The AB₅-type alloy surface-modified by fluorination; functionalization; and encapsulation exhibited the best kinetics observed in the study, attaining a rate constant of $k = 3.6 \text{ h}^{-1}$. The performance of the alloy surface-modified by fluorination-functionalization-encapsulation and “high-loading” was compared against other high-performance sample materials prepared in the study (Figure 4.119). A comparison of the kinetics of hydrogenation of the surface-modified materials can be summarised in Table 4.23. Large increases in hydrogenation performances was observed with the introduction of Pd-P layers into the micro-channels of the LaF₃

shell after functionalization, compared to that surface-modified using fluorination, Pd-P encapsulation, and Pd-P encapsulation after functionalization.

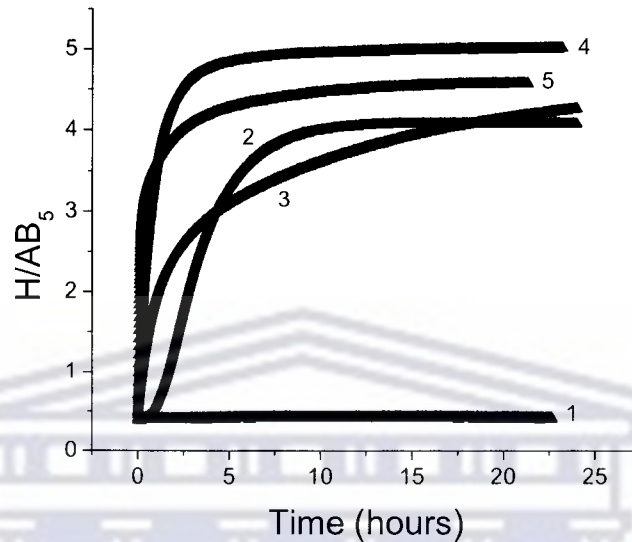


Figure 4.119. Dynamics of hydrogen absorption ($P_{\text{H}_2} = 5.0$ bar, $T = 20$ °C, $t = 24$ hours), (1) non-activated parent AB_5 -type alloy; (2) fluorinated AB_5 -type alloy ; (3) Pd-P (high-load) surface-modified AB_5 -type alloy; (4) Pd-P (high-load) surface-modified AB_5 -type alloy after functionalization in 1.0 vol. % aqueous solution of γ -APTES; and (5) Pd-P (high-load) surface-modified AB_5 -type alloy after surface fluorination and functionalization in 1.0 vol.% aqueous solution of γ -APTES

Table 4.23. Comparison of kinetics of hydrogenation of non-activated surface-modified AB_5 -type alloys ($P_{\text{H}_2} = 5.0$ bar, $T = 20$ °C, $t = 24$ hours)

Sample	Rate constant (k), h^{-1}	Incubation period
AB_5	9.8×10^{-6}	Yes
F(Ni) AB_5	0.3	Yes
AB_5 Pd-P (NaH_2PO_2 , high-load)	0.19	No
γ -APTES AB_5 Pd-P (NaH_2PO_2 , high-load)	1.3	No
F(Ni) γ -APTES AB_5 Pd-P (NaH_2PO_2 , high-load)	3.6	No

CHAPTER 5

CONCLUSIONS AND RECOMMENDATIONS

The ultimate scientific goal of the project was to successfully develop methodological approaches for the preparation of surface-modified hydrogen sorption materials that meet hydrogenation / dehydrogenation targets considered to be requirements for practical application of these materials in hydrogen separation / purification / storage systems. These requirements included easy activation; rapid hydrogen uptake rates, stable operation under conditions of mild temperature and pressure, and sorption stability in the presence of gaseous impurities. These targets were achievable through nano-engineering of Pd catalytic mantles onto the surface of the hydrogen sorbent materials, based on the unique interactions between Pd and hydrogen. Further, the hypothesis of the study was stated as follows:

“Development of surface modification techniques, based on electroless plating, for the preparation of advanced composite materials, based on rare earth metal hydride-forming alloys and platinum group metals, for the effective sorption of hydrogen from contaminated hydrogen feed streams. The fabricated materials should exhibit fast kinetics of hydrogenation, hydrogen sorption stability in the presence of gaseous impurities, and superior dynamics of activation in non-inert environments”.

In addressing the hypothesis the following sub-objectives were investigated:

1. Investigation of the best available parent AB₅-type hydride-forming alloy material for subsequent surface modification.
2. Investigation of the optimal preparation conditions in the encapsulation of AB₅-type hydride-forming alloys using the electroless plating of Pd.

3. Study of the influence of secondary metal additions (i.e. Ni-P, Cu-P, Ag, Pt) on hydrogenation properties after the electroless plating of Pd mixed-metal layers on AB₅-type hydride-forming alloys.
4. Investigation of optimal preparation conditions in the encapsulation of AB₅-type hydride-forming alloys using electroless plating of Pd mixed-metal layers.
5. Investigation of the influence of a Pt interfacial layer on the kinetics of hydrogenation.
6. Investigation of the influence of fluorination on hydrogenation properties of AB₅-type metal hydride-forming alloys.
7. Study of the influence of the combination of fluoride layers and Pd-based encapsulation layers on the hydrogenation properties of AB₅-type hydride-forming alloys.

The “layer-by-layer” approach used in this project allowed for the investigation of the morphological and kinetic properties of the materials as each layer was added. Experimental tasks and a detailed research work-plan were formulated to address the hypothesis and sub-objectives. A set of physico-chemical properties governing the applicability of the sample materials as hydrogen sorbents, due to the incentives they offer, were identified in a comprehensive literature review. The novelties of the formulated research work-plan were also highlighted. Standard characterization tools were reviewed and used in the investigation of this material, and included Scanning Electron Microscopy (SEM), Synchrotron Radiation X-ray Diffraction (SR-XRD), Surface Area and Porosity Analysis (BET), Energy Dispersive X-ray Spectroscopy (EDS), Atomic Absorption Spectroscopy (AAS), Particle-Induced X-ray Emission Spectroscopy (PIXE), Scanning X-ray Photo-Electron Spectroscopy (SXPS), and volumetric and kinetic measurements using a Sieverts-type installation.

Metal hydride-forming alloys were identified for application as the hydrogen sorption materials of interest due to their reversible interactions with hydrogen under mild conditions of pressure and temperature; minimal energy expenditure; simplicity in operation; high hydrogen selectivity, and release of high-pressure high-purity hydrogen at elevated temperature.

Of the classes of metal hydride-forming alloys under consideration for surface-modification, the rare earth metal AB₅-type alloys were found to be the most suitable for hydrogen separation / purification / storage from contaminated hydrogen admixtures based on their reasonable kinetics in hydrogenation, reasonable poisoning resistance, easy activation, and tuneable pressure-composition-temperature performances, confirmed by a comprehensive literature review. This combination of features demonstrated the technological flexibility of AB₅-type alloys and illustrates their potential benefit as a technology in hydrogen processing. However, susceptibility to aggressive poisons in hydrogen, such as CO and H₂S, and inadequate rates of hydrogen uptake limit the application of AB₅-type alloys in hydrogen separation / purification / storage systems. The susceptibility to surface deactivation was addressed by nano-engineering catalytic mantles onto the surface of the alloy to produce advanced composite hydride-forming materials. The nano-engineering of these composite materials was built upon a “layer-by-layer” approach.

Platinum group metals were considered as catalytic mantles as a result of their high affinity towards hydrogen, the ability to dissociate hydrogen molecules with no or very little activation energy required, and their wide applicability in hydrogen exchange reactions. Palladium, in particular, was considered for application as a hydrogen dissociation catalyst as a result of its ferocious affinity towards hydrogen and its high hydrogen selectivity.

Of the available deposition techniques, electroless plating was considered for the deposition of Pd-based catalytic surface layers on the AB₅-type alloys as a result of its ability to deposit most PGM's, ability to plate metal surface layers on materials

with irregular shape, ability to control the surface chemistry of the modified material on a molecular or atomic domain, and deposition of homogeneous coatings. Electroless plating also offered the possibility of depositing mixed-metal coatings on the surface of AB₅-type alloys, and to analyse the influences of crystalline and amorphous catalytic coatings on the hydrogen sorption performances of surface-modified AB₅-type alloys. In addition, no literature was found regarding the use of NaH₂PO₂-based electroless plating baths in the surface modification of metal hydride-forming alloys.

Results of the characterization of the surface-modified sample materials were collected and are summarized as follows:

1. The study was initiated by an investigation of the most suitable parent mischmetal AB₅-type alloy amongst three available samples prepared in collaboration with the Guangzhou Institute for Non-Ferrous Metals. The AB₅ (DL4) alloy, corresponding to the sample formula La_{0.40}Ce_{0.48}(Nd,Pr)_{0.16}Ni_{3.34}Co_{0.64}Al_{0.63}Mn_{0.58}, was identified as the most suitable parent alloy based on the criteria of highest cerium content and lowest thermal stability ($\Delta H = -39.8$ kJ/mole H₂), therefore greater ease in expelling absorbed hydrogen from the material due to a lower metal-hydrogen binding energy.

Following an investigation of the corresponding PCT isotherms the AB₅-type (DL4) alloy was concluded to exhibit typical AB₅-type alloy behaviour, with a maximum hydrogen absorption capacity of 1.27 wt.% H₂, maximum volume of 149 cm³/g H₂ (5.5×10^{22} H atoms/cm³), and maximum molar ratio of 5.60 formula units corresponding to a stoichiometry of AB₅H_{5.6}. Importantly, the maximum achievable molar ratios (T=30 °C) for AB₅ (DL4) alloy was equal to H/AB₅ = 5.6 and 5.0, at P_{H₂} = 50 and 5.0 bar, respectively. As a result, all subsequent kinetic investigations of hydrogen absorption by the non-activated surface-modified samples were conducted at 20°C with P_{H₂} ~ 5.0 bar.

The presence of a major CaCu₅-type intermetallic phase (95 wt.%), minor AB₅-type alloy phase (4.7 wt.%) characterized by the same structure, and mixed rare-earth – nickel oxide phase (RE₂NiO₄; 0.7 wt.%) possessing a perovskite complex oxide K₂NiF₄-type structure was detected on the parent AB₅-type alloy. The observation of the minor AB₅-type alloy may have been a direct result of inhomogeneity in the B-component of the parent AB₅-type alloy or presence the highly stable α -phase solid solution of the AB₅-type alloy as an artefact after preparation of the powdered alloy by ball-milling in NaH₂PO₂. Also, the presence of the RE₂NiO₄ phase may have originated from the surface oxidation of the material. A lattice expansion of merely 12.6% was observed for the β -hydride AB₅H_x phase as a result of the addition of Co to the mischmetal composition. Studies of the hydrogenation performances and kinetics of the parent AB₅-type alloy, under the standard experimental conditions, demonstrated extremely slow absorption of hydrogen ($k = 9.8 \times 10^{-6} \text{ h}^{-1}$) as a result of the passive RE₂NiO₄ phase on the surface behaving as a diffusion barrier towards hydrogen.

2. The deposition method of electroless plating was successfully applied in the surface modification of AB₅-type alloys for the purposes of enhancing the hydrogenation performance. The influence of the reducing agent on the activation kinetics and hydrogenation performance was analysed using N₂H₄- and NaH₂PO₂-based Pd electroless plating baths.

Importantly, an SR-XRD analysis confirmed that the RE₂NiO₄ phase observed in the parent alloy was completely removed after surface modification in both N₂H₄- and NaH₂PO₂-based Pd electroless plating baths. The Pd layers deposited after electroless plating of AB₅-type alloys in N₂H₄- and NaH₂PO₂-based Pd electroless plating baths were crystalline and amorphous, respectively. The amorphosity of the NaH₂PO₂-derived Pd layer was a result of the impregnation of P atoms into the Pd layer.

Surface coatings derived from N_2H_4 - and NaH_2PO_2 -based Pd electroless plating baths were found to be discontinuous in nature, with the Pd particles exhibiting high-dispersion; narrow particle size distribution ($\text{N}_2\text{H}_4 \approx 30\text{-}60$ nm, $\text{NaH}_2\text{PO}_2 \approx 80\text{-}110$ nm); and slightly irregular shape. Numerous other differences in the structural properties of the alloys surface-modified in N_2H_4 -based (specific surface area = $0.23 \text{ m}^2/\text{g}$; Pd total loading = 0.4 wt.%; Pd surface loading = 1.3 wt.%) and NaH_2PO_2 -based (specific surface area = $0.16 \text{ m}^2/\text{g}$; Pd total loading = 0.64 wt.%; Pd surface loading = 2.5 wt.%) Pd electroless plating baths were observed.

Initial studies of the hydrogenation performances and kinetics of the surface-modified alloys, under the standard experimental conditions, demonstrated significantly enhanced hydrogen absorption rates compared to the parent material and was initially not found to depend on the nature of the reducing agent, NaH_2PO_2 ($k = 3.8 \times 10^{-3}$) and N_2H_4 ($k = 3.7 \times 10^{-3}$). The enhanced kinetics was a result of the removal of the RE_2NiO_4 layer with surface-modification and the catalysis of the hydrogen dissociation process by the Pd catalytic layers. However, when surface modification was conducted using a larger substrate-to-solution concentration (1:100), it was found that the kinetics strongly depended on the nature of the reducing agent: N_2H_4 ($k = 5.9 \times 10^{-2} \text{ h}^{-1}$), and NaH_2PO_2 ($k = 1.9 \times 10^{-1} \text{ h}^{-1}$). For this reason NaH_2PO_2 -based electroless plating baths were used in all subsequent surface modification.

3. An investigation into the influence of preparation variables of the Pd-P electroless plating bath (e.g. deposition time, temperature, substrate-to-solution ratio, Pd precursor concentration, reducing agent concentration, plating solution pH) on the surface morphology, elemental composition, and hydrogenation performance of surface-modified hydride-forming alloys was undertaken. Significant influences of preparation variables on the morphology and kinetics of hydrogenation were observed. These preparation factors were optimised in all subsequent surface modification.

4. Based on previous observations of the presence of discontinuous Pd-P layers after electroless plating on the surface of AB₅-type alloys, an approach was adopted to deposit high-quality continuous Pd-P layers using an aminosilane functionalization method. The method used the existing surface (hydr)oxide layers of the AB₅-type alloy and aminosilane solutions to increase the chemical adhesion towards the Pd nuclei in electroless plating.

It was found that pre-treatment in dilute γ -aminopropyltriethoxysilane solutions (γ -APTES) facilitated large increases in Pd-P density, Pd total loading (1.0 – 1.2 wt.%), and surface loading (10 – 51 wt.%) on the alloy compared to that prepared without the functionalization step. Rapid coalescence of Pd-P particles was observed after γ -APTES pre-treatment, constituting the initial formation of continuous surface films. The Pd-P layer thickness corresponded to the deposition of ~10 layers of Pd-P particles (average thickness 550 nm) after functionalization. It was also observed that the functionalized sample exhibited a fairly wide particle size distribution (~40-170 nm) compared to that prepared without the functionalization step (~80-110 nm). The functionalized AB₅-type alloys exhibited significantly lower specific surface areas than the unfunctionalized alloys, after Pd-P deposition, which indirectly illustrated the attainment of continuous Pd-P layers with surface functionalization in γ -APTES.

A comparative study of the kinetics of hydrogenation of the γ -APTES functionalized AB₅-type alloys was conducted using the standard experimental procedure. It was observed that as the growth of the Pd-P particles was allowed to progress on the γ -APTES functionalized AB₅-type alloys, so the kinetics of hydrogenation began to deteriorate. This observation was indicative of a change in the mechanism of hydrogenation. It was deduced that functionalization increased the rate at which the Pd-P surface layer progressed from surface particles towards a continuous surface layer. The change in hydrogenation mechanism was also confirmed by comparison of the morphological dimensionalities of growth (n) of the functionalized alloys ($n = 0.4-0.5$), which

were different to that exhibited by the unfunctionalized alloy ($n = 0.6-0.7$). It was also observed that when the substrate-to-solution ratio of the Pd bath was increased for the alloy pre-treated in γ -APTES aqueous solution from 1:20 to 1:100, the kinetics of hydrogenation increased markedly from $k = 0.19 \text{ h}^{-1}$ to $k = 1.3 \text{ h}^{-1}$, illustrating the ability of the surface functionalization method in increasing the hydrogenation properties of surface-modified AB₅-type alloys.

Based on the observation that the oxide layer detected on the surface of the alloy facilitated the adhesion of the γ -APTES molecules, an attempt was made to completely pre-oxidize the surface of the alloy prior to functionalization to promote the adhesion of the maximum quantity of γ -APTES molecules onto the surface, and in that way promote the deposition of a continuous Pd-P layer. It was observed that the pre-oxidation of the alloy surface, and subsequent functionalization and Pd-P deposition, facilitated the deposition of a high density of Pd-P particles on the surface of the alloy (average Pd particle size = 137 nm; Pd total loading = 1.35 wt.%; specific surface area = 1.0 m²/g), resulting in better kinetics of hydrogenation ($k = 2.0 \text{ h}^{-1}$) compared to that prepared without the pre-oxidation step ($k = 1.3 \text{ h}^{-1}$).

5. Pre-complexation of Pd nuclei using aqueous solutions of γ -APTES, prior to electroless plating, improved the process of electroless deposition on the alloy surface to yield more dense and uniform coatings (Pd total loading = 0.8 wt.%) compared to that of the corresponding surface-modified alloy prepared without the Pd nuclei pre-complexation step (Pd total loading = 0.6 wt.%), and in such a way resulted in significantly better hydrogen sorption performances of the surface-modified alloys ($k = 1.1 \text{ h}^{-1}$), compared to that prepared using the standard sensitization / activation method in electroless plating ($k = 0.19 \text{ h}^{-1}$).
6. Based on the ability of the γ -APTES molecule to immobilize metal precursor cations onto substrate surfaces, an approach was adopted in which γ -APTES functionalization was used to immobilize trace quantities of PGM cations from

dilute solutions and fix them onto the surface of the AB₅-type alloy as a hydrogen dissociation catalyst. The kinetics of hydrogenation was generally observed to increase slightly with an increase in PdCl₂ concentration. Also, the kinetics of hydrogenation of NaH₂PO₂-reduced samples was generally better than that prepared using N₂H₄ and H₂.

A similar approach was adopted to immobilize Pt⁴⁺ precursor cations on the surface of the AB₅-type alloy. PtCl₄ was used in the Pt precursor solution due to its high solubility in water, and N₂H₄ was used exclusively as the reducing agent. The Pt surface loading was observed to increase with an increase in the PtCl₄ concentration. Under the standard experimental conditions, the kinetics of hydrogenation was generally observed to remain steady at very dilute PtCl₄ concentration. Higher PtCl₄ solution concentrations (> 0.1 g/L) were observed to facilitate a rapid increase in the kinetics of hydrogenation on the surface-modified AB₅-type alloy surface.

7. From a comprehensive review of the literature, it was established that Pd surface-modified AB₅-type alloys were still prone to low levels of surface poisoning after long periods of exposure to air (and particularly to CO and H₂S), manifesting in the gradual deterioration of hydrogen sorption capacity with repeated cycling. For this reason, Pd mixed metal layers, with secondary metals such as Ni; Cu; Ag; and Pt, were identified to overcome the deterioration in the hydrogen sorption properties of the alloys and to further enhance the kinetics of hydrogenation of the material. In addition, no works could be found into the use of co-deposition to coat the surface of metal hydride-forming alloys, although sequential-deposition was attempted.

Surface modification was conducted using the electroless plating of Pd(-P), Ni-P, Cu-P, Ag, and Pt either by single-metal, mixed-bath (co-deposition), or sequential-deposition, using N₂H₄ or NaH₂PO₂ as reducing agents.

Isolated clusters and large agglomerates of Pd(-P), Cu-P, Pt, and Ag were observed, illustrating the formation of discontinuous Pd mixed-metal layers on the surface of the AB₅-type alloy.

Surface modification by co-deposition of Pd-Ni-P ($k = 6.6 \times 10^{-2} \text{ h}^{-1}$) and Pd-Cu-P ($k = 2.9 \times 10^{-2} \text{ h}^{-1}$) onto the surface of the alloy resulted in significant improvements to the hydrogen sorption dynamics. The strongest influence of surface modification on H sorption properties was observed for the AB₅-type alloy modified by co-deposition of Pd-Ni, which exhibited the highest activity towards hydrogen transfer processes as a result of a synergistic effect observed between Pd and Ni atoms. Ni was found to have a significant benefit on the catalytic ability of Pd surface coatings in the hydrogen dissociation process on surface-modified AB₅-type alloys. In contrast, samples modified by sequential-deposition of Pd-Ni-P ($k = 5.3 \times 10^{-3} \text{ h}^{-1}$) and Pd-Cu-P ($k = 2.9 \times 10^{-3} \text{ h}^{-1}$) exhibited dynamics of hydrogenation which were worse than that observed for the unmodified alloy ($k = 9.7 \times 10^{-3} \text{ h}^{-1}$), and was a result of the secondary metal acting as a diffusion barrier towards the transport of hydrogen atoms to the core alloy.

An attempt was made to study the long-term hydrogen sorption stability after prolonged exposure of the surface-modified alloys to air. The kinetic properties of the sample prepared by co-deposition of Pd-Ni-P ($k = 6.6 \times 10^{-2} \text{ h}^{-1}$) did not change after 11-month exposure of the sample to air, illustrating the long-term hydrogen sorption stability of the material compared to the unmodified alloy, whose sorption stability deteriorates rapidly.

It was observed that sequential-deposition of Pd-Ag, irrespective of the order of deposition, did not facilitate high rates of hydrogenation on the surface-modified AB₅-type alloy. In contrast, alloys surface-modified by Pd-Ag co-deposition exhibited slightly higher rates of hydrogenation, which were comparable to that exhibited by alloys surface-modified by N₂H₄-derived crystalline Pd. Ag addition

was found to have no significant benefit on the catalytic ability of Pd surface coatings in the hydrogen dissociation process on surface-modified AB₅-type alloys.

It was observed that co-deposition of Pd-Pt did not facilitate high rates of hydrogenation on the surface-modified AB₅-type alloy as a result of the action of hydrazine to preferentially reduce more Pt ions than Pd ions in the mixed-metal bath solution. Alloys surface-modified by Pt-Pd sequential-deposition exhibited rates of hydrogenation which were significantly better compared to that exhibited by alloys surface-modified by N₂H₄-derived crystalline Pd. Deposition of Pt prior to Pd may have had the effect of enhancing the transport rate of hydrogen atoms into the core alloy, due to the high activity of Pt towards hydrogen exchange reactions, after hydrogen dissociation on the Pd catalyst at the exterior.

8. Based on an enhancement in the kinetics of hydrogenation observed with the sequential-deposition of Pt-Pd, an approach was taken to introduce a Pt interfacial layer between the AB₅-type alloy surface and a Pd-P layer for the purpose of increasing the rate of hydrogen transport between the core and Pd-P layer. The Pt interfacial layer was deposited, by substitution of surface Ni atoms, after immersion of alloy powders in dilute H₂PtCl₆ solution and sonication (i.e. lixiviation). Trace quantities of Ni in the H₂PtCl₆ solution and Pt on the AB₅-type alloy were detectable indicating that quantities of nickel had successfully been substituted by Pt atoms on the surface of the alloy. It was observed that short periods of lixiviation in dilute H₂PtCl₆ solution enhanced the hydrogenation rate compared to that prepared without the introduction of the Pt interfacial layer. This observation may have been in account of an increase in the hydrogen exchange rate of between the AB₅-type alloy surface and the Pd-P surface layer.
9. An approach was taken in which the AB₅-type alloys were treated with hydrogen-selective high-surface area fluoride and Pd-P surface layers to form advance composite materials for application in hydrogen separation / purification / storage

processes from impure feed streams. The advanced composite materials potentially have the capacity to exhibit fast activation kinetics, hydrogen selectivity, and hydrogen sorption stability. To date, no known attempts have been made to study the influence of the combination of Pd and fluoride layers on the hydrogenation performances of hydrogen sorption alloys.

Continuous Pd-P layers, exhibiting superior surface coverage on the AB₅-type alloy, could be prepared by a combination of fluorination; functionalization; and encapsulation. It was deduced, based on the consistent reduction in the specific surface area that the Pd-P particles deposited during encapsulation, after γ -APTES functionalization, plugged the micro-cavities of the oxygen-rich LaF₃ layer formed during fluorination. The AB₅-type alloy surface-modified by the fluorination; functionalization; and encapsulation exhibited the best kinetics observed in the study, attaining a rate constant of $k = 3.6 \text{ h}^{-1}$. Large increases in hydrogenation performances were observed with the introduction of Pd-P layers into the micro-cavities of the LaF₃ structure after functionalization, and were associated with the promotion of the hydrogen spillover phenomenon.

To summarize, the fabricated composite materials and Pd surface modification techniques have been observed to facilitate rapid hydrogen sorption under mild conditions of temperature and pressure, without prior activation, and without significant degradation of sorption efficiency. The kinetic performances of the fabricated materials can be comparatively summarized in Figure 5.1. Superior kinetics of hydrogenation were observed where γ -APTES surface functionalization, pre-complexation of Pd nuclei in electroless plating, increase substrate-to-solution ratio, and Pd mixed-metal co-deposition was utilized as a surface modification technique in the preparation of advanced composite hydrogen sorption materials based on AB₅-type alloys. Larger Pd total loadings on the AB₅-type alloys were also observed wherever γ -APTES surface functionalization was utilized in electroless plating. In addition, significant enhancements in the kinetics of hydrogenation were observed wherever the combined “layer-by-layer” fluorination-encapsulation

compared to N_2H_4 -based Pd plating baths; and sharp increases in kinetics of hydrogenation where the Pd total loading exceeded 1.0 wt.%

The developed materials and surface modification methods give the possibility of producing durable hydrogen sorption modules that can perform at near atmospheric pressure and room temperature with fast hydriding and dehydriding rates.

To conclude, in the course of addressing the hypothesis and sub-objectives, the morphological; sorption; and kinetic attributes of the fabricated composite materials have been analysed. Surface nano-engineering on the alloy surface was demonstrated to be a potentially promising approach for controlling kinetics of hydrogenation, activation, long-term sorption stability, and surface protection. The study has also aided in the understanding of the influence of the morphology of the deposited Pd surface layers on the kinetics of hydrogenation of the surface-modified materials. In addition, the scientific goals of improving the opportunities for a wider application of metal-hydride forming alloys in the future hydrogen economy were addressed. The knowledge emanating from this project is expected to allow the directed design of a new class of higher-efficiency; robust, recyclable hybrid hydrogen sorption materials based on metal hydride-forming alloys and Pd surface catalysts, as key elements of envisaged hydrogen separation / purification / storage systems.

Based on the analyses and conclusions of the study, a number of recommendations regarding future research directions of investigation were made:

- The aminosilane surface functionalization method is a powerful technique for preparing surface-modified metal hydride-forming alloys housing continuous catalytic surface layers. From a fundamental point of view, the method would find significant applicability in materials where the oxidation of sensitive surfaces is especially troublesome, such as in the case of low-cost TiFe intermetallic alloys.

-
- Efforts should be made to extend the novel laboratory-scale surface modification technologies, discussed in this work, to scaled-up pilot studies of hydrogen separation, purification, and storage. This can be done by loading the surface-modified materials into packed columns, rolling into composite membranes after the addition of high-temperature polymeric binders (e.g. polyimide), or by pressing into pellets.
 - Several combinations of Pd mixed-metal coatings can be prepared through electroless plating. Efforts should be made to incorporate new secondary metals into the Pd mixed-metal coatings and the influences on the kinetics of hydrogenation of the surface-modified metal hydride-forming alloys characterized.
 - The surface modification of AB, A₂B, AB₃, and A₂B₇ hydride-forming alloys or light metal hydrides (e.g. magnesium) using the novel methods of aminosilane surface functionalization, Pd mixed-metal coating, and fluoride-Pd combination coatings should be further investigated.
 - Investigation of the electrochemical properties of the surface-modified materials for battery applications should be undertaken.
 - The poisoning resistance of the surface-modified materials should be analysed using gaseous pre-exposure and sorption from hydrogen contaminated using controlled quantities of O₂, CO, CO₂, and H₂S.

REFERENCES

- [1] Yartys. V.A, Lototsky. M.V (2004) An Overview of Hydrogen Storage Methods, *Hydrogen Materials Science and Chemistry of Carbon Nanomaterials*, The Netherlands, Springer **172**: 75-104.
- [2] Hynek. S, Fuller. W, Bentley. J (1997) *International Journal of Hydrogen Energy*, **22**(6): 601-610.
- [3] Bénard. P, Chahine. R. (2001) *International Journal of Hydrogen Energy*, **26**: 849–855.
- [4] Zhou. L, Zhou. Y, Sun. Y. (2004) *International Journal of Hydrogen Energy*, **29**: 319-322.
- [5] Ma. Y, Xia. Y, Zhao. M, Ying. M, Liu. X, Liu. P (2001) *Physics Letters A*, **288**: 207–213.
- [6] Loutfy. R.O, Wexler. E.M. (2001) *Investigation of Hydrogen Storage in Fullerene Hydrides*, IEA Task 12: Metal Hydrides and Carbon for Hydrogen Storage.
- [7] Tarasov. B.P, Fokin. E.N, Moravsky. A.P, b and Yu. M. Shul'ga, (1998) *Russian Chemical Bulletin*, **47**: 2037-2040.
- [8] Jordá-Beneyto. M, Suárez-García. F, Lozano-Castelló. D, Cazorla-Amorós. D, Linares-Solano. A. (2007) *Carbon*, **45**: 293-303.
- [9] Cabasso. I, Yuan. Y. (2005) VI.C.4 Nanostructured Activated Carbon for Hydrogen Storage, DOE Hydrogen Program FY 2005 Progress Report.
- [10] Crabtree. G.W, Dresselhaus. M.S, Buchanan. M.V (2004) *Physics Today*, **57**: 39.
- [11] Zhou. L, Zhou. Y, Sun. Y. (2004) *International Journal of Hydrogen Energy*, **29**: 319 – 322.
- [12] Murphy. K. (2005) Not Hydrogen - Ammonia! [ONLINE] Available: <http://www.interocitor.com/archives/000659.html>.

References

- [13] Cooper. A.C, Campbell. K.M, Pez. G.P (2006) An Integrated Hydrogen Storage and Delivery Approach Using Organic Liquid-Phase Carriers, WHEC 16 / 13-16 June 2006 – Lyon France.
- [14] Hiyoshi. N, Osada. M, Rode. C.V, Sato. O, Shirai. M. (2007) *Applied Catalysis A: General*, **331**: 1–7.
- [15] Johnssen. W. (2000) U.S. Patent **6,074,769**.
- [16] Tarasov. B.P, Lototskii. M.V, Yartys. V.A. (2007) *Russian Journal of General Chemistry*, **77**: 694-711.
- [17] Weitkamp. J. (1996) Zeolites as Media for Hydrogen Storage [ONLINE] Available: http://www.uni-stuttgart.de/sfb270/B7_E.htm.
- [18] Yu. M, Li. S, Falconer. J.L, Noble. R.D. (2008) *Microporous and Mesoporous Materials*, **110**: 579–582.
- [19] Thomas. G.J, Gross K.J, Yang. N.Y.C, Jensen. C. (2002) *Journal of Alloys and Compounds*, **330-332**: 702–707.
- [20] Balogha. M.P, Tibbetts. G.G, Pinkerton. F.E, Meisner. G.P, Olk. C.H. (2003) *Journal of Alloys and Compounds*, **350**: 136–144.
- [21] Bogdanović. B, Schwickardi. M. (2001) *Applied Physics A: Materials Science & Processing*, **72**: 221–223.
- [22] Bogdanovic'. B, Felderhoff. M, Germann. M, Härtel. M, Pommerin. A, Schüth. F, Weidenthaler. C, Zibrowius. B. (2003) *Journal of Alloys and Compounds*, **350**: 246–255.
- [23] Huot. J, Liang. G, Schulz. R. (2001) *Applied Physics A: Materials Science & Processing*, **72**: 187–195.
- [24] Kim. J-H, Shim. J-H, Cho. Y.W. (2008) *Journal of Power Sources*, Article in Press, doi:10.1016/j.jpowsour.2008.02.094.
- [25] Vuk. A. Š, Jovanovski. V, Pollet-Villard. A, Jerman. I, Orel. B. (2008) *Solar Energy Materials & Solar Cells*, **92**: 126–135.
- [26] Hardacre. C, Mullan. E.A, Rooney. D.W, Thompson. J.M, Yablonsky. G.S. (2006) *Chemical Engineering Science*, **61**: 6995 – 7006.
- [27] Welch. G.C, Stephan. D.W. (2007) *Journal of the American Chemical Society*, **129**: 1880-1881
-

References

- [28] Schmitt M.L, Shelby J.E, Hall. M.M. (2006) *Journal of Non-Crystalline Solids*, **352**: 626–631.
- [29] Mueller. W.M, Blackledge. J.P, Libowitz. G.G. (1968) *Metal Hydrides*, New York, Academic Press.
- [30] Latroche. M (2004) *Journal of Physics and Chemistry of Solids*, **65**: 517-522.
- [31] Sakintuna. B, Lamari-Darkrim. F, Hirscher. M (2007) *International Journal of Hydrogen Energy*, **32**: 1121-1140.
- [32] Ivey. D.G, Northwood. D.O. (1983) *Journal of Materials Science*, **18**: 321-347.
- [33] Lasher. S, Stratonova. M, Thijssen. J. (2001) Hydrogen Technical Analysis, *Proceedings of the 2001 US DOE Hydrogen Program Review*, **NREL/CP-570-30535**.
- [34] Tarasov. B.P, Shilkin. S.P. (1995) *Russian Journal of Applied Chemistry*, **68**(1): 16-20.
- [35] Voløen. L.O (2000) *Metal Hydrides for Rechargeable Batteries*, **Published PhD Thesis**, Norway: Norwegian University of Science and Technology.
- [36] University of Oslo: Theoretical Activity in Solid State Chemistry and Material Science, *About Metal Hydrides*, [ONLINE], **Available:** http://folk.uio.no/ravi/activity/hydride/hyd_tutorial.html
- [37] Lewis. F.A. (1967) *The Palladium / Hydrogen System*, London, Academic Press, 1-12, 48-49
- [38] Sandrock. G.D, Goodell. P.D. (1980) *Journal of the Less-Common Metals*, **73**: 161-168.
- [39] Kleperis. J, Wójcik. G, Czerwinski. A, Skowronski. J, Kopczyk. M, Beltowska-Brzezinska. M. (2001) *Journal of Solid State Electrochemistry*, **5**: 229-249.
- [40] Jurezyk. M, Nowak. M, Jankowska. E. (2002) *Journal of Alloys and Compounds*, **340**: 281–285.
- [41] Schlapbach. L, Seiler. A, Stucki. F, Siegmann. H.C. (1980) *Journal of the Less-Common Metals*, **73**: 145 – 160.
-

References

- [42] Kurokawa. H, Nakayama. T, Kobayashi. Y, Suzuki. K, Takahashi. M, Takami. S, Kubo. M, Itoh. N, Selvam. P, Miyamoto. A. (2003) *Catalysis Today*, **82**: 233–240.
- [43] Snijder. E.D, Versteeg. G.F, van Swaaij. W.P.M. (1993) *AIChE Journal*, **39** (9): 1444-1454.
- [44] Carter. T.J, Cornish. L.A. (2001) *Engineering Failure Analysis*, **8**: 113-121.
- [45] Yartys. V.A, Denys. R.V, Hauback. B.C, Fjellvåg. H, Bulyk. I.I, Riabov. A.B, Kalychak. Ya.M. (2002) *Journal of Alloys and Compounds*, **330–332**: 132–140.
- [46] Piper. J. (1966) *Journal of Applied Physics*, **37**(2): 715-721.
- [47] Doyle. M.L, Harris. I.R, Pratt. A.S, Willey. D.B. (2000) U.S. Patent **6,165,643**.
- [48] Wu. H, Anani. A.A. (1995) U.S. Patent **5,451,474**.
- [49] Shan. X, Payer. J. H, Wainright. J.S. (2007) *Journal of Alloys and Compounds*, **430**: 262–268.
- [50] Schweppe. F, Martin. M, Fromm. E. (1997) *Journal of Alloys and Compounds*, **253-254**: 511-514.
- [51] Sandrock. G.D, Goodell. P.D. (1984) *Journal of the Less-Common Metals*, **104**: 159-173.
- [52] Ertl. G, Knözinger. H, Weitkamp. J. (1997) *Handbook of Heterogeneous Catalysis, Volume 1*, Wiley-VCH, France, **2**: 196-207.
- [53] Sakaguchi. H, Yagi. Y, Shiokawa. J, Adachi. G. (1989) *Journal of the Less-Common Metals*, **149**: 185-191.
- [54] Bratanich. T.I, Bulanov. V.N, Skorokhod. V.V, Klimenko. V.P. (2000) *Powder Metallurgy and Metal Ceramics*, **39** (11-12): 575-583.
- [55] Geng. M. (1994) *Journal of Alloys and Compounds*, **215**: 151-153.
- [56] Pratt. A.S, Willey. D.B, Harris. I.R. (1999) *Platinum Metals Review*, **43**(2): 50-58.
- [57] Wang. X.-L, Iwata. K, Suda. S. (1995) *Journal of Alloys and Compounds*, **231**: 829-834.

References

- [58] Chen. J, Dou. S.X, Liu. H.K. (1996) *Journal of Power Sources*, **63**: 267-270.
- [59] Chartouni. D, Kuriyama. N, Otto. A, Güther. V, Nützenadel. C, Züttel. A, Schlapbach. L. (1999) *Journal of Alloys and Compounds*, **285**: 292–297.
- [60] Zaluski. L, Zaluska. A, Tessier. P, Ström-Olsen. J.O, Schulz. R (1995) *Journal of Alloys and Compounds*, **217**: 295-300.
- [61] Gundiah. G, Govindaraj. A, Rajalakshmi. N, Dhathathreyan. K.S, Rao. C.N.R. (2003) *Journal of Materials Chemistry*, **13**: 209–213.
- [62] Dufour. J, Huot. J. (2007) *Journal of Alloys and Compounds*, **439**: L5-L7.
- [63] Feng. F, Northwood. D.O. (2003) *Surface and Coatings Technology*, **167**: 263–268.
- [64] Willey. D.B, Harris. I.R, Pratt. A.S. (1999) *Journal of Alloys and Compounds*, **293–295**: 613–620.
- [65] Jun. C, Yunshi. Z. (1995) *International Journal of Hydrogen Energy*, **20**: 235 – 237.
- [66] Chen. J, Bradhurst. D.H, Dou. S.X, Liu. H.K. (1998) *Journal of Materials Science*, **33**: 4671 – 4675.
- [67] Luo. J.L, Cui. N. (1998) *Journal of Alloys and Compounds*, **264**: 299–305.
- [68] Wang. X-L, Iwata. K, Suda. S. (1995) *Journal of Alloys and Compounds*, **231**: 860-864.
- [69] Park. H.Y, Cho. W.I, Cho. B.W, Lee. S.R, Yun. K.S. (2001) *Journal of Power Sources*, **92**: 149-156.
- [70] Yang. H, Yuan. H, Ji. J, Sun. H, Zhou. Z, Zhang. Y. (2002) *Journal of Alloys and Compounds*, **330–332**: 640–644.
- [71] Sun. Y-M, Suda. S. (2002) *Journal of Alloys and Compounds*, **330–332**: 627–631.
- [72] Higuchi. E, Toyoda. E, Li. Z.P, Suda. S, Inoue. H, Nohara. S, Iwakura. C. (2001) *Electrochimica Acta*, **46**: 1191–1194.
- [73] Rodriguez. D.S, Meyer. G. (1999) *Journal of Alloys and Compounds*, **293–295**: 374–378.

References

- [74] Uchida. H. (1999) *International Journal of Hydrogen Energy*, **24**: 861-869.
- [75] Xiao. L, Wang. Y, Liu. Y, Song. D, Jiao. L, Yuan. H. (2008) *International Journal of Hydrogen Energy*, Article in Press.
- [76] Zhao. X, Ding. Y, Yang. M, Ma. L. (2008) *International Journal of Hydrogen Energy*, **33**: 81 – 86.
- [77] Uchida. H, Yamashita. K, Goto. M. (2002) *Journal of Alloys and Compounds*, **330–332**: 622–626.
- [78] Ikoma. M, Komori. K, Kaida. S, Iwakura. C. (1999) *Journal of Alloys and Compounds*, **284**: 92–98.
- [79] Chen. W.X, Qi. J.Q, Chen. Y, Chen. C.P, Wang. Q.D, Zhou. J.M. (1999) *Journal of Alloys and Compounds*, **293–295**: 728–733.
- [80] Lin. H.C, Lin. K.M, Chou. H.T, Yeh. M.T. (2003) *Journal of Alloys and Compounds*, **358**: 281–287.
- [81] Liu. F.-J, Suda. S. (1995) *Journal of Alloys and Compounds*, **230**: 58-62.
- [82] Imoto. T, Kato. K, Higashiyama. N, Kimoto. M, Itoh. Y, Nishio. K. (1999) *Journal of Alloys and Compounds*, **282**: 274–278.
- [83] Ise. T, Murata. T, Hirota. Y, Imoto. T, Nogami. M, Nakahori. S. (2000) *Journal of Alloys and Compounds*, **307**: 324–332.
- [84] Imoto. T, Kato. K, Higashiyama. N, Kimoto. M, Itoh. Y, Nishio. K. (1999) *Journal of Alloys and Compounds*, **285**: 272–278.
- [85] Kaiya. H, Ookawa. T. (1995) *Journal of Alloys and Compounds*, **231**: 598-603.
- [86] Nan. J, Yang. Y, Lin. Z. (2001) *Journal of Alloys and Compounds*, **316**: 131–136.
- [87] Bakkar. A, Neubert. V. (2005) *Corrosion Science*, **47**: 1211–1225.
- [88] Wu. M-S, Wu. H-R, Wang. Y-Y, Wan. C-C. (2000) *Journal of Alloys and Compounds*, **302**: 248–257.
- [89] Wu. M-S, Wu. H-R, Wang. Y-Y, Wan. C-C. (2004) *International Journal of Hydrogen Energy*, **29**: 1263 – 1269.

References

- [90] Pan. H, Chen. Y, Wang. C, Wang. X, Chen. C, Wang. Q. (1999) *Journal of Alloys and Compounds*, **293–295**: 680–683.
- [91] Chen. W. (2001) *Journal of Power Sources*, **92**: 102-107.
- [92] Chen. W-X. (2001) *International Journal of Hydrogen Energy*, **26**: 603–608.
- [93] Chen. W.X, Xu. Z.D, Tu. J.P, Li. H.Y, Yuan. J, Chen. S, Bao. S.N. (2001) *International Journal of Hydrogen Energy*, **26**: 675– 681.
- [94] Lasher. S, Stratonova. M, Thijssen. J. (2002) Hydrogen Technical Analysis, *Proceedings of the 2002 US DOE Hydrogen Program Review*, **NREL/CP-610-32405**.
- [95] Lasher. S, Teagan. P. (2003) *Hydrogen Technical Analysis: Analysis of Metal Hydride Slurries, Hydrogen, Fuel Cells, and Infrastructure Technologies, FY2003 Progress Report*.
- [96] Mazej. Z, Lutar. K, Žemva. B. (1999) *Acta Chimica Slovenia*, **46(2)**: 229-238.
- [97] Liu. F-J, Sandrock. G, Suda. S. (1992) *Journal of Alloys and Compounds*, **190**: 57-60.
- [98] Wang. X.-L, Suda. S, (1995) *Journal of Alloys and Compounds*, **231**: 380-386.
- [99] Unger. E, Liebau. M, Duesberg. G.S, Graham. A.P, Kreupl. F, Seidel. R, Hoenlein. W. (2004) *Chemical Physics Letters*, **399**: 280-283.
- [100] Sun. Y-M, Iwata. K, Chiba. S, Matsuyama. Y, Suda. S, (1997) *Journal of Alloys and Compounds*, **253-254**: 520-524.
- [101] Xu. X, Song. C. (2006) *Applied Catalysis A: General*, **300**: 130–138.
- [102] Nakamura. K, Uchida. H, Fromm. E. (1981) *Journal of the Less-Common Metals*, **80**: 19-30.
- [103] Harris. I.R, Willey. D.B, Pederzollic. D, Pratt. A.S, Swift. J, Walton. A. (2002) *Journal of Alloys and Compounds*, **330-332**: 806–809.
- [104] Auto Industry (2006) *Bath University Scientists Devise New Rhodium Hydrogen Storage Material*, [ONLINE], Available: http://www.autoindustry.co.uk/news/04-12-06_17.

References

- [105] Royal Society of Chemistry (2006) *Catalysis Crucial for Hydrogen Storage*, [ONLINE], Available: <http://www.rsc.org/chemistryworld/News/2005/September>
- [106] Baudrand. D, Bengston. J. (1995) *Metal Finishing*, **September**: 55-57.
- [107] Sales. E, de Jesus Mendes. M, Bozon-Verduraz. F. (2000) *Journal of Catalysis*, **195**: 96-105.
- [108] Heinrichs. B, Schoebrechts. J-P, Pirard. J-P. (2001) *Journal of Catalysis*, **200**: 309-320.
- [109] Roa. F, Way. J.D, McCormick. R.L, Paglieri. S.N. (2003) *Chemical Engineering Journal*, **93**: 11-22.
- [110] Mao. T-F, Rempel. G.L. (2000) *Journal of Molecular Catalysis A: Chemical*, **153**: 63-73.
- [111] Jensen. C.M. (2000) U.S. Patent **6,074,447**.
- [112] Chen. W, Ermanoski. I, Madey. T.E. (2005) *Journal of the American Chemical Society*, **127**: 5014-5015.
- [113] Bratanich. T.I, Bulanov. V.N, Skorokhod. V.V. (2002) *Powder Metallurgy and Metal Ceramics*, **41** (5-6): 309-316.
- [114] Barsellini. D, Visintin. A, Triaca. W.E, Soriaga. M.P. (2003) *Journal of Power Sources*, **124**: 309-313.
- [115] Ambrosio. R.C, Ticianelli. E.A. (2005) *Surface and Coatings Technology*, **197**: 215-222.
- [116] Schober. T, Carl. A. (1979) *Journal of the Less-Common Metals*, **63**: 53-56.
- [117] Cuevas. F, Hirsher. M. (2000) *Journal of Alloys and Compounds*, **313**: 269-275.
- [118] Zheng. G, Popov. B.N, White. R.E. (1998) *Journal of Applied Electrochemistry*, **28**: 381-385.
- [119] Rivera M.A, Pal. U, Wang. X, Gonzalez-Rodriguez. J.G, Gamboa. S.A. (2006) *Journal of Power Sources*, **155**: 470-474.

References

- [120] Onyegbule. N. (2006) *Composite Low Temperature Hydrogen Storage Material on the Basis of Iron-Titanium Alloy: Synthesis and Structure*. Unpublished Masters Thesis. Bellville: University of the Western Cape.
- [121] Züchner. H, Barlag. H, Majer. G. (2002) *Journal of Alloys and Compounds*, **330–332**: 448–453.
- [122] Pandey. P, Chauhan. R.S. (2001) *Progress in Polymer Science*, **26**: 853 – 893.
- [123] R.M. De Vos. (1998) *High-Selectivity, High-Flux Silica Membranes for Gas Separation: Synthesis, Transport and Stability*, **Published PhD Thesis**, The Netherlands, 3-4: Twente University.
- [124] McLennan. K.D. (2005) *Structural Studies of the Palladium-Hydrogen System*, **Published PhD Thesis**, Australia, Griffith University.
- [125] Oriani, R.A. (1994) *A Brief Survey of Useful Information About Hydrogen in Metals*, International Symposium on Cold Fusion and Advanced Energy Sources. Belarusian State University, Minsk, Belarus: Fusion Information Center, Salt Lake City.
- [126] Züchner. H, Opara. L, Barlag. H. (2002) *Journal of Alloys and Compounds*, **330–332**: 434–437.
- [127] Lianos. L, Debauge. Y, Massardier. J, Jugnet. Y, Bertolini. J.C. (1997) *Catalysis Letters*, **44**: 211-216.
- [128] Schulz. R, Huot. J, Liang. G, Boily. S, Lalande. G, Denis. M.C, Dodelet. J.P. (1999) *Materials Science and Engineering*, **A267**: 240-245.
- [129] Abys. J.A. (2002) *Plating and Surface Finishing*, **8**: 42-43.
- [130] Im. J-S, Kwon. O, Kim. Y-H, Park. S-J, Lee. Y-S. (2008) *Microporous and Mesoporous Materials*, Article in Press.
- [131] Souza. E.C, Ticianelli. E.A. (2007) *International Journal of Hydrogen Energy*, **32**: 4917 – 4924.
- [132] Fazle Kibria. A.K.M, Sakamoto. Y. (1998) *Materials Science and Engineering*, **B53**: 256–261.
- [133] Szafránski, A.W. (2005) *Journal of Alloys and Compounds*, **395**: 36–40.
- [134] Heinze. S, Vuillemin. B, Colson. J-C, Giroux. P, Leterq. D. (1999) *Solid State Ionics*, **122**: 51–57.
-

References

- [135] Løvvik. O.M, Olsen. R.A. (2002) *Journal of Alloys and Compounds*: **330–332**: 332–337.
- [136] Zacharia. R, Kim. K-Y, Fazle Kibria. A.K.M, Nahm. K-S. (2005) *Chemical Physics Letters*, **412**: 369–375.
- [137] Ozaki. T, Zhang. Y, Komaki. M, Nishimura. C. (2003) *International Journal of Hydrogen Energy*, **28**: 297 – 302.
- [138] Friedrichs. O, Martínez-Martínez, Guilera. G, Sánchez López. G.C, Fernández. A. (2007) *Journal of Physical Chemistry C*, **111**: 10700-10706.
- [139] Laudahn. U, Pundt. A, Bicker. M, v. Hülsen. U, Geyer. U, Wagner. T, Kirchheim. R. (1999) *Journal of Alloys and Compounds*, **293–295**: 490–494.
- [140] Bulak. J, Jimenez. G, Millette. N, Rebeiz. K, Craft. A. (2007) *Journal of Phase Equilibria and Diffusion*, **28**: 422-426.
- [141] Kohler. U, Simon. G, Hofmann. G. (1992) U.S. Patent **5,128,219**.
- [142] Chen. H-I, Chu. C-Y, Huang. T-C. (2004) *Thin Solid Films*, **460**: 62-71.
- [143] Yasumatsu. T, Wan. J.L, Matsuyama. M, Watanabe. K. (1999) *Journal of Alloys and Compounds*, **293–295**: 900–907.
- [144] Baraton. M-I. *Synthesis, Functionalization and Surface Treatment of Nanoparticles*, American Scientific Publishers, California.
- [145] Rhoda. R.N, Vines. R.F. (1969) U.S. Patent **3,486,928**.
- [146] *Sputtering*, [ONLINE], Available: <http://en.wikipedia.org/wiki/Sputtering>.
- [147] McCool. B.A, Lin. Y.S (2001) *Journal of Materials Science*, **36**: 3221 – 3227.
- [148] Yeung K.L, Christiansen. S.C, Varma. A. (1999) *Journal of Membrane Science*, **159**: 107-122.
- [149] Xomeritakis. G, Lin Y.S. (1996) *Journal of Membrane Science*, **120**: 261-272.
- [150] Jun. C-S, Lee. K-H. (2000) *Journal of Membrane Science*, **176**: 121-130.
- [151] Lim. J, Lee. C. (2001) *Solid State Electronics*, **45**: 2083-2088.
- [152] Itoh. N, Tomura. N, Tsuji. T, Hongo. M. (2000) *Microporous and Mesoporous Materials*, **39**: 103-111.

References

- [153] Sakaguchi. H, Nagai. H, Adachi. G, Shiokawa. J. (1986) *Journal of the Less-Common Metals*, **126**: 83-88.
- [154] Rudman. P.S, Sandrock. G.D, Goodell. P.D. (1983) *Journal of the Less-Common Metals*, **89**: 437-446.
- [155] Charbonnier. M, Romand. M, Goepfert. Y, Léonard. D, Bessueille. F, Bouadi. M. (2006) *Thin Solid Films*, **515**: 1623–1633
- [156] Bindra. P, Light. D, Rath. D. (1984) *IBM Journal of Research and Development*, **28**: (6): 668-687.
- [157] Liu. Z, Gao. W. (2006) *Surface and Coatings Technology*, **200**: 3553-3560.
- [158] Keuler. J.N, Lorenzen. L, Sanderson. R.D, Linkov. V. (1997) *Plating and Surface Finishing*, **August**: 34-40.
- [159] Shafeev. G.A, Bellard. L, Themlin. J-M, Marine. W, Cros. A. (1995) *Applied Surface Science*, **86**: 387-391
- [160] Dressick. W.J, Dulcey. C.S, Georger. J.H, Calabrese. G.S, Calvert. J.M. (1994) *Journal of the Electrochemical Society*, **141**(1): 210-220.
- [161] Rao. C.R.K ., Trivedi. D.C. (2005) *Coordination Chemistry Reviews*, **249**: 613–631.
- [162] Keuler. J.N. (1997) *Preparation and Characterization of Palladium Composite Membranes*, **Published Masters Thesis**, Stellenbosch, Stellenbosch University.
- [163] Mallory. G.O, Hajdu. J.B. (1990) *Electroless Plating - Fundamentals and Applications*, New York, William Andrew Publishing/Noyes, **16**: 425-426.
- [164] Huang. T-C, Wei. M-C, Chen. H-I. (2003) *Separation and Purification Technology*, **32**: 239-245.
- [165] Cheng. D.H, Xu. W.Y, Zhang. Z.Y, Yiao. Z.H. (1997) *Metal Finishing*, **January**: 34-37.
- [166] Changrong. X, Xiaoxia. G, Fanqing. L, Dingkun. P, Guangyao. M. (2001) *Colloids and Surfaces A: Physicochemical and Engineering Aspects*, **179**: 229-235.
- [167] Hampel. C.A. (1961) *Rare Metals Handbook*, 2nd Edition, London, Reinhold Publishing Corporation, **17**: 317,318,321,326-328;**19**: 393,398,407,408.

References

- [168] Imori. T (2001) European Patent **EP1279750A1**.
- [169] Sakashita. M, Li. Z.P, Suda. S. (1997) *Journal of Alloys and Compounds*, **253-254**: 500-505.
- [170] Teplyakov. V.V, Syrtsova. D.A, *Modification of Polymeric Membranes for Effective Gas Separation*, Conference Proceedings, 23rd Summer School on Membranes: Smart Materials, Prague, Czech Republic, September 3-6, 2006.
- [171] Higuchi. E, Hidaka. K, Li. Z-P, Suda. S, Nohara. S, Inoue. H, Iwakura. C, (2002) *Journal of Alloys and Compounds*, **335**: 277-280
- [172] Wang. X-L, Hagiwara. H, Suda. S, (1996) *Vacuum*, **47(6-8)**: 899-902.
- [173] Wang. X.-L, Hagiwara. H, Suda. S, (1995) *Journal of Alloys and Compounds*, **231**: 376-379
- [174] Goldstein. J.I, Newbury. D.E, Echlin. P, Joy. D.C, Lyman. C.E, Lifshin. E, Sawyer. L, Michael. J.R. (2003) *Scanning Electron Microscopy and X-ray Microanalysis, 3rd Edition*, New York, Springer, **7,9**: 297-299, 346, 392.
- [175] *Handbook of Analytical Methods*, [ONLINE], Available: <http://www.mee-inc.com/eds.html>.
- [176] Robards. A.W, Wilson. A.J. (1993) *Procedures in Electron Microcopy*, Chichester, John Wiley and Sons, **2**.
- [177] Welz. B, Sperling. M. (1999) *Atomic Absorption spectroscopy, 3rd Completely Revised Edition*, Weinheim, Wiley-VCH Verlag GmbH, **1**: 1-3, **8**: 335, **9**: 537-540, 500-502, 553.
- [178] Lajunen. L.H.J. (1992) *Spectrochemical Analysis by Atomic Absorption and Emission*, Bath, Royal Society of Chemistry, **2**: 45-48.
- [179] Dean. J.R. (1997) *Atomic Absorption and Plasma Spectroscopy*, Chichester, John Wiley and Sons, **1**: 1; **2**: 27,28; **4**: 47.
- [180] Jenkins. R, de Vries. J.L, *An Introduction to X-Ray Powder Diffractometry*, Eindhoven, N.V. Phillips Gloeilampenfabrieken, **2**: 8-10.
- [181] Lipson. H, Steeple.H.(1970) *Interpretation of X-ray Powder Diffraction Patterns*, London, Macmillan and Company Ltd. **4**: 93-94, **5**: 113-114.
- [182] Cullity. B.D. (1978) *Elements of X-ray Diffraction, 2nd Edition*, Ontario, Addison-Wesley Publishing Company Inc. **7**: 188-226.

References

- [183] Von Dreele. R. B, Larson. A.C, *General Structure Analysis System*, Regents of the University of California (2001).
- [184] Cheetham. A.K, Day. P. (1987) *Solid State Chemistry Techniques*, New York, Oxford University Press, **2**: 56, 68-71, **10**: 372.
- [185] Poulsen. H.F. (2004) *Three-Dimensional X-ray Diffraction Microscopy: Mapping Polycrystals and their Dynamics*, Berlin, Springer-Verlag, **1**: 3,4.
- [186] Ferreira. J.G, Ramos. M.T. (1988) *X-ray Spectroscopy in Atomic and Solid State Physics*, New York, Plenum Press, 368.
- [187] Maehlen. J.P, Yartys. V.A, Denys. R.V, Fichtner. M, Frommen. C, Bulychev. B.M, Pattison. P, Emerich. H, Filinchuk. Y.E, Chernyshov. D. (2007) *Journal of Alloys and Compounds*, **446-447**: 280-289.
- [188] Liu. J. (2000) *Materials Characterization*, **44**: 353-363.
- [189] Goldstein. J.I, Newbury. D.E, Echlin. P, Joy. D.C, Fiori. C, Lifshin. E. (1981) *Scanning Electron Microscopy and X-ray Microanalysis: A Text for Biologists, Materials Scientists, and Geologists*, New York, Plenum Press, **1**: 1-3, **6**: 275-278.
- [190] Oatley. C.W. (1972) *The Scanning Electron Microscope, Part 1: the Instrument*, London, Cambridge University Press, **1**: 1-2.
- [191] Newbury. D.E, Joy. D.C, Echlin. P, Fiori. C.E, Goldstein. J.I (1986) *Advanced Scanning Electron Microscopy and X-ray Microanalysis*, New York, Plenum Press, **5**: 186, **7**: 295.
- [192] Fukatsugawa. S, Hatakeyama. S, Saitou. Y, Sera. K. (1996) *Nuclear Instruments and Methods in Physics Research B: Beam Interactions with Materials and Atoms*, **109-110**: 113-120.
- [193] Imaseki. H, Yukawa. M, Watt. F, Ishikawa. T, Iso. H, Hamano. T, Matsumoto. K, Yasuda. N. (2003) *Nuclear Instruments and Methods in Physics Research B: Beam Interactions with Materials and Atoms*, **210**: 42-47.
- [194] Johansson. S.A.E, Campbell. J.L, Malmqvist. K.G. (1995) *Particle-Induced X-ray Emission Spectroscopy (PIXE)*, Wiley, New York, 451.
- [195] Ryan. C.G, Jamieson. D.N, Churms. C.L, Pilcher. J.V. (1995) *Nuclear Instruments and Methods in Physics Research B: Beam Interactions with Materials and Atoms*, **104**: 157-165.
-

References

- [196] Prozesky. V.M, Pineda-Vargas. C.A, Mesjasz-Przybylowicz. J, Przybylowicz. W.J, Churms. C.L, Springhorn. K.A, Moretto. P, Michelet. C, Chikte. U, Wenzel. P. (2000) *Nuclear Instruments and Methods in Physics Research Section B: Beam Interactions with Materials and Atoms*, **161-163**: 852-859
- [197] Ryan. C.G, Cousens. D.R. (2002) *Geo-PIXE II Quantitative PIXE Trace Element Imaging and Analysis*, CSIRO Exploration and Mining, North Ryde, New South Wales, Australia.
- [198] Walker. C, *Surface Science Techniques*, [ONLINE], **Available:** <http://www.uksaf.org/tech/xps.html>
- [199] Briggs. D, Seah. M.P (1983) *Practical Surface Analysis by Auger and X-ray Photoelectron Spectroscopy*, Norwich, John Wiley and Sons Ltd., 17-18,112, 363.
- [200] Ross. S, Olivier. J.P. (1964) *On Physical Adsorption*, New York, John Wiley and Sons Inc., 2: 12, 29, 66-69, 75-76.
- [201] Wedler. G. (1976) *Chemisorption: An Experimental Approach*, London, Chapel River Press, 3: 29-31.
- [202] Webb. P.A, Orr. C, Camp. R.W, Olivier. J.P, Yunes. Y.S. (1997) *Analytical Methods in Fine Particle Technology*, Georgia, Micromeritics Instrument Corporation, 1: 11-14, 6: 219-268.
- [203] Atkins. P.W. (1979) *Physical Chemistry*, London, Oxford University Press, **28**: 942.
- [204] Schlapbach. L. (1988) *Hydrogen in Intermetallic Compounds, Volume I: Electronic, Thermodynamic, and Crystallographic Properties, Preparation*, Berlin, Springer-Verlag, 59-63.
- [205] Bliznakov. S, Lefterova. E, Bozukov. L, Popov. A, Andreev. P. *Techniques for Characterization of Hydrogen Absorption/Desorption in Metal Hydride Alloys*, Proceedings of the International Workshop "Advanced Techniques for Energy Sources Investigation and Testing" 4 – 9 Sept. 2004, Sofia, Bulgaria.
- [206] Fukai. Y. (1993) *The Metal Hydrogen System*, New York, Springer-Verlag.
- [207] McLennan. K.G, Mac.A.Gray. E. (2004) *Measurement Science and Technology*, **15**: 211–215.
- [208] Sastri. M.V.C, Viswanathan. B, Murthy. S.S. (1998) *Metal Hydrides: Fundamentals and Applications*, New Delhi, Narosa Publishing House, 11-13.

References

- [209] Wikipedia, [ONLINE], Available: <http://en.wikipedia.org/wiki/Air>.
- [210] Rudman. P.S. (1979) *Journal of Applied Physics*, **50**: 7195–7199.
- [211] Karty. A, Grunzweig-Genossar. J, Rudman. P.S. (1979) *Journal of Applied Physics*, **50**: 7200–7209.
- [212] Førde. T, Mæhlen. J.P, Yartys. V.A, Lototsky. M.V, Uchida. H. (2007) *International Journal of Hydrogen Energy*, **32**: 1041-1049.
- [213] Solonin. Yu.M, Kolomiets. L.L, Skorokhod. V.V. (1983) *Hydrogen storage alloys for Ni–MH batteries*. Preprint 93-5, Institute for Problems of Materials Science, Kiev, 54 (in Russian).
- [214] Kolachev. B.A, Shalin. R.E, Il'in. A.A. (1995) *Hydrogen Storage Alloys*.- Moscow: Metallurgy, 384 (in Russian).
- [215] Dantzer. P, Orgaz. E. (1986) *International Journal of Hydrogen Energy*, **11**: 797-806.
- [216] Yuan. X, Liu. H-S, Ma. Z-F, Xu. N. (2003) *Journal of Alloys and Compounds*, **359**: 300–306.
- [217] Lototsky. M.V. (2000) *Kharkov University Bulletin Chemical Series*, **477**: 45–53 (in Russian).
- [218] Lototsky. M.V, Yartys. V.A, Marinin. V.S, Lototsky. N.M. (2003) *Journal of Alloys and Compounds*, **356–357**: 27–31.
- [219] Holmberg. M, Lundström. I. (1996) *Applied Surface Science*, **93**: 67-76.
- [220] Huot. J, Swainson. I.P, Schulz. R. (1999) *Journal of Alloys and Compounds*, **292**: 292-295.
- [221] Williams. M, Pineda-Vargas. C.A, Khataibe. E.V, Bladergroen. B.J, Nechaev. A.N, Linkov. V.M. (2008) *Applied Surface Science*, **254** (10): 3211-3219.
- [222] Williams. M, Lototsky. M, Nechaev. A, Linkov. V, *Method of Surface Modification*, Provisional Patent Specification ZA 2007 / 099455 (October 31, 2007).
- [223] Williams. M, Nechaev. A.N, Lototsky. M.V, Yartys. V.A, Solberg. J.K, Denys. R.V, Pineda. C, Li. Q, Linkov. V.M, Accepted Manuscript, *Materials Chemistry and Physics*, Manuscript Number: MATCHEMPHYS-D-08-01343.

References

- [224] Charbonnier. M, Romand. M. (2003) *International Journal of Adhesion & Adhesives*, **23**: 277–285.
- [225] Paglieri. S.N, Way. J.D. (2002) *Separation and Purification Methods*, **31**:(1) 1-169.
- [226] Xu. L, Liao. J, Huang. L, Ou. D, Guo. Z, Zhang. H, Ge. C, Gu. N, Liu. J. (2003) *Thin Solid Films*, **434**: 121–125.
- [227] Brandow. S.L, Chen. M-S, Aggarwal. R, Dulcey. C.S, Calvert. J.M, Dressick. W.J. (1999) *Langmuir*, **15**: 5429-5432.
- [228] Yuan. W, van Ooij. W.J. (1997) *Journal of Colloid and Interface Science*, **185**: 197-209.
- [229] Demjén. Z, Pukánszky. B, Földes. E, Nagy. J. (1997) *Journal of Colloid and Interface Science*, **190**: 427-436.
- [230] Melashenko. N.F. (1987) *Galvanization of Dielectrics* [in Russian], Minsk, 51-53.
- [231] Dai. H, Li. H, Wang. F. (2006) *Applied Surface Science*, **253**: 2474–2480.
- [232] Jal. P.K, Patel. S, Mishra. B.K. (2004) *Talanta*, **62**: 1005-1028.
- [233] Briggs. D (1977) *Handbook of X-ray and Ultraviolet Photoelectron Spectroscopy*, Kent, Heyden and Son Ltd., 157-158, 198.
- [234] Schlappbach. L. (1992) *Hydrogen in Intermetallic Compounds, Volume II: Surface and Dynamic Properties, Applications*, New York, Springer-Verlag, 35, 36, 41, 50, 51, 55-56, 97, 169-171, 198-210.
- [235] Zhou. J, Zhou. R, Mo. L, Zhao. S, Zheng. X. (2002) *Journal of Molecular Catalysis A: Chemical*, **178**: 289–292.
- [236] Hagenmuller. P. (1985) *Inorganic Solid Fluorides*, London, Academic Press Inc., 5-8, 207, 208, 218-224.
- [237] Zalkin. A, Templeton. D.H. (1985) *Acta Crystallographica, Section B: Structural Science*, **41**: 91-93.